STRUCTURAL STUDIES OF PHOSPHATE AND GERMANATE GLASSES DOPED WITH La, Pr AND Nd IONS

Thesis submitted to

GOA UNIVERSITY

For the award of the degree of

DOCTOR OF PHILOSOPHY

IN

PHYSICS

By

BENEDICT PAULOS SOARES

Under the guidance of

PROF. J. A. ERWIN DESA

DEPARTMENT OF PHYSICS

FACULTY OF NATURAL SCIENCES

GOA UNIVERSITY

February 2020

DECLARATION

It is hereby declared that this thesis entitled "Structural Studies of Phosphate and Germanate Glasses Doped with La, Pr and Nd ions" submitted to Goa University for the award of the degree of **Doctor of Philosophy in Physics** is a record of original and independent work carried out by me during the period January 2013 – July 2019 at the **Department of Physics, Goa University**, under the supervision of Prof. J. A. Erwin Desa, Department of Physics, Goa University, and that it has not formed the basis for the award of any Degree or Diploma to me or any other candidate of this or any other University.

Benedict P. Soares

(Research Scholar)

Department of Physics,

Goa University.

CERTIFICATE

This is to certify that the thesis entitled "Structural Studies of Phosphate and Germanate Glasses Doped with La, Pr and Nd ions" submitted to Goa University for the award of the degree of **Doctor of Philosophy in Physics**, is a record of original and independent work carried out by **Mr. Benedict P. Soares** under my guidance and supervision during the period, January 2013 – July 2019 at the **Department of Physics, Goa University**, and that it has not previously formed the basis for the award of any Degree, Diploma or Fellowship or any other similar title to any candidate of this or any other University.

Prof. R. B. Tangsali — **CO-GUIDE**

Prof. J. A. Erwin Desa — **GUIDE**

DEPARTMENT OF PHYSICS

GOA UNIVERSITY

ABSTRACT

Structural studies of rare earth included alumino phosphate, alumino germanate and alumino germano-phosphate glasses are presented in this thesis. Several spectroscopic techniques -Raman, Fourier transform infrared (FTIR) and Ultra Violet-Visible (UV-Vis.) spectroscopy are used in understanding the type of basic structural units that form the glass network. In addition to X-ray and neutron diffraction techniques, Extended X-ray absorption Fine Structure (EXAFS) was used to estimate the correlation lengths and coordination numbers of oxygen around the host and modifier cations.

Rare earth alumino-phosphate glass has a basic structural unit consisting of a P atom doubly bonded to one oxygen atom and singly bonded to three other oxygen atoms and referred to as the PO_4 tetrahedron. The various ways in which the tetrahedra connect to each other define the different types of Q^n structural units, where n refers to the number of bridging oxygens i.e. oxygen atoms of each tetrahedron that are also bonded to atoms of neighbouring units or other included species. A set of ten rare-earth alumino-phosphate glasses were melt quenched in air and consisted of approximate percentages of 75 mole% P_2O_5 , 5 mole% Al_2O_3 , and 25 mole% rare-earth oxide being combinations of Nd, La, Pr either singly or in pairs. Raman studies indicate that the rare earth modified glasses are basically Q^1 and Q^2 connected while the host glass of alumino phosphate is mainly Q^2 connected. Neutron diffraction points out that the glasses consist of a tetrahedral network structure with the rare-earth to oxygen correlation length varying between 2.35Å to 2.38 Å. EXAFS study shows the Nd-O bond length of 2.36 Å and La-O bond length of 2.40Å in the single rare earth glass systems. The oxygen coordinations around the rare-earth being about 7 for the glasses and, 7 to 8.5 for the devitrified states. The devitrified samples also have similar Q^n structural units.

Rare-earth alumino-germanate glasses were prepared by the melt quenching process in air and consisting of 10 mole% alumina , 80 mole% germania and the remaining 10 mole% rare-earth oxides included either as Nd_2O_3 , Pr_6O_{11} or La_2O_3 separately or mixture of two rare earths. Raman studies showed that the structural units in these glasses are predominantly Q^2 and Q^3. The Pr included glasses have a maximum of Q^2 units indicative of a larger number of non-bridging oxygens and thus being less connected as compared to the other glasses which have a maximum of Q^3 units indicative of being better connected. EXAFS results show that in these glasses, the Ge-O distance is approximately 1.74 Å .The

Nd-O distance was found to be 2.53 Å with the coordination of Nd(O) of 8.8 while for the Pr containing glasses the Pr-O was 2.58 Å with the Pr(O) of 8.9. From neutron diffraction measurements the Ge-O bond length was found to be 1.75 Å with tetrahedral coordination. The rare-earth correlation length Nd-O was 2.47 Å with a Nd(O) coordination of 7.5 for the Nd included glass and Pr-O correlation length of 2.42 Å and a Pr(O) of about 10.

Rare earth ions neodymium (Nd) and lanthanum (La) have been included in alumino germano-phosphate glass both individually and in pairs. These glasses were studied along with alumino-phosphate and alumino-germanate host glassy networks. The La modifier increases the connectivity of the Nd-phosphate network. On adding GeO_2 to the Nd-phosphate the connectivity increases but on adding GeO_2 to the Nd-La-phosphate glass, its connectivity decreases. When phosphate is added to Nd-germanate glass or to Nd-La-germanate glass, the connectivity is substantially reduced.

Acknowledgement

I give thanks and praise to Almighty God-the Father-the Son Jesus Christ -the Holy Spirit for all the Blessings, Grace and Guidance received by me because of which this thesis was possible.

My sincere deep gratitude to my guide Prof. J. A. Erwin Desa, Former Head of the Department of Physics and Former Dean of the Faculty of Natural Sciences, Goa University for his competent guidance, encouragement, effort and time spent. Being associated with Prof. Desa helped me to understand the path to systematic research work. The interesting talks during tea breaks or waiting time at railway stations and airports during our trips for experiments or conferences always gave new dimensions to the thought process. I sincerely appreciate and thank Prof. Desa for his selfless service of being available for guidance even though he retired from his duties at the Goa University and inspite of his busy schedule and other family responsibilities so that I could complete my thesis.

I would like to gratefully acknowledge and thank the following persons and institutions for their help in various ways during my Ph.D. studies:

My co-guide Prof. R. B. Tangsali , former Head of the department of Physics for his valuable suggestions.

Prof. G. M. Naik, Dean of the Faculty of Natural sciences,Vice Chancellor's nominee, Prof. R. V. Pai former Head of the Department of Physics and the FRC committee for their valuable advice during FRC meetings.

Prof. K. R. Priolkar, Head of the Department of Phyics, Prof. Uma Subramanian and other U.G.C. recharge faculty for their support and contribution.

Dr. V. Siruguri, Centre Director, UGC-DAE Mumbai, for cooperation and financial assistance through the collaborative project CRS- M- 209.

Prof. M. Yusuf, Head of the Solid State Physics Division, B.A.R.C. for his generous help and cooperation in the use of the neutron beam facility viz. the High Q diffractometer, Dhruva Reactor, Bhabha Atomic Research Centre, Mumbai.

The UGC, Western regional office, Pune, for the award of the UGC –FIP teacher fellowship.

Dr. P.S. R. Krishna, Mr. A.B. Shinde and Mr. S. Wajhal , S.S.P.D., B.A.R.C., for their continuous and generous help in the neutron diffraction experiments and neutron data analysis at the High Q diffractometer, Dhruva Reactor, B.A.R.C., Mumbai.

Dr. Rekha Rao and Mr. S. Kesari, S.S.P.D., B.A.R.C. Mumbai for their help in the Raman Spectroscopy measurements on the glass samples of this study.

Dr. C. Nayak, Dr. D. Bhattacharrya and Dr. S. N. Jha for use of the BL-09 beam line and their help in EXAFS experiments at Raja Ramanna Centre for Advanced Technology, Indore.

Dr. P. U. Sastry for use of the XRD facility at B.A.R.C., Mumbai and Mr. G. Prabhu, N.I.O., Goa for help with the XRD measurements .

Dr. Reshma Raut Dessai for helpful suggestions and XRD measurements at St. Xavier's College, Mapusa and Ms. Priyanka Kambli for her assistance.

Mr. Manjunath T. Nayak - my companion - Ph.D. student working with the same guide – Prof. Desa, for all his valuable help, useful discussions and enthusiastic company in glass research at the Department of Physics and while travelling together for experiments and conferences.

Mr. M. Jeyakanthan -fellow Ph.D.student for his company and help, Mr. T. Suresh (from Prof. Desa's group) and all the current fellow Ph. D. students of the Department of Physics, Goa University for their company and time spent together in the research scholar's room, laboratories and canteen.

Mrs. Eva Baptista, Laboratory Assistant , Mr. S. Vaigankar and Mr. S. Salgaonkar , Laboratory Attendants and the Office staff and LDCs of the Department of Physics – Mrs Hermina, Mrs. Varsha Bhobhe - for their help and cooperation over the years.

Former principals of St. Xavier's college – late Fr. Antimo Gomes and late Prof. Newman Fernandes for their encouragement, Dr. (Fr.) Walter D'Sa, Dr. (Fr.) Jeronimo D' Silva and principal Dr (Mrs) Blanche Mascarenhas for their permission and support to complete my Ph.D. studies.

Fr. Zeferino D'Souza, President of Goa Diocesan Society of Education and administrator of St. Xavier's college, and Fr. Tony Salema, former administrator of St. Xavier's College for granting leave and permission to complete my Ph.D studies.

My colleagues- Rajendra Kanekar, Dr. Nelson Lobo, Pradeep Morajkar, late Andrew Dias, Manoj Salgaonkar, Dr. Bosco Lawrence, Dr. Reshma Raut Dessai, Priyanka Kambli, Abigail De Souza, Sheshgiri Shettigar, Remigio D'Souza, Ivan and students at the Department of Physics, St. Xavier's College, Mapusa for their good wishes and encouragement.

Sr. Cleris Fernandes BS and Sr. Moncia Cardozo BS for their constant prayerful support and motivation and other Bethany sisters, Priests, Religious and well-wishers for their prayers.

Family of Prof. Desa- Mrs Pramila Desa and children for having welcomed me every time I visited Prof. Desa at his residence for discussions and Mr. Rony Martins for his support.

My mother Mrs. Ritinha Soares for her everlasting love, constant prayers and encouragement that gave me the strength to complete the thesis, my father late Vicente Soares for his love, encouragement and blessings and my family- Manuel, late Herminia, Prisca, Felipe, Canviceo, Celestine and Mckinnon for shouldering my responsibilities at home and their constant support, motivation, love and prayers during my Ph.D. work.

All those persons who have been connected in one way or another with me during the years of my Ph. D. work but who have not been specially mentioned. My sincere Thanks to them all.

Dev Borem Corum.

Benedict P. Soares

To My Parents

CONTENTS

Title page			i
Declaration			ii
Certificate			iii
Abstract			iv
Acknowledgement			vi
List of figures			xiii
List of Tables			xxi
1		Introduction	1
	1.1	Origin of Glass	1
	1.2	Glass formation	1
	1.3	Theories of Glass formation	3
		1.3.1 Structural Theories Of Glass Formation	4
		1.3.2 The Kinetic Theories Of Glass Formation	6
	1.4	Devitrification	8
	1.5	Phosphate glasses	9
	1.6	Germanate Glass	11
	1.7	Germano-Phosphate Glasses	12
	1.8	Objectives Of This Study	13
		References	13
2		Theory	16
	2.1	Neutron scattering	16
	2.2	Total neutron diffraction	19
	2.3	Finite Q_{MAX}	21
	2.4	Correction for neutron static approximation	22
	2.5	The Corrections involved in the analysis of neutron data	25
		2.5.1 Sample container and background corrections	25
		2.5.2 Absorption correction and multiple scattering	25

	2.5.3	Normalization	26
	2.5.4	Renormalization	26
	2.5.5	Placzek corrections	27
2.6	Radial distribution function and Monte Carlo method		27
2.7	Extended X- ray Absorption Fine Structure (EXAFS)		28
2.8	Raman scattering		30
	2.8.1	Classical approach.	30
	2.8.2	Quantum approach	31
	References		33
3	Experimental Methods		35
3.1	Fourier Transform Infrared Spectroscopy		35
3.2	Ultra Violet-Visible Spectroscopy (UV- Visible)		38
3.3	Differential Thermal Analysis (DTA)		40
3.4	Raman spectroscopy		41
3.5	Extended X-ray Absorption Fine Structure (EXAFS)		43
	3.5.1	XANES – X-ray Absorption Near Edge Structure	43
	3.5.2	EXAFS –Extended X-ray Absorption Fine Structure	43
3.6	X-ray diffraction		45
3.7	Neutron diffraction		47
	References		49
4	Structural Studies of Alumino-Phosphate Glasses Doped with La, Pr and Nd ions and Respective Devitrified States		50
4.1	Introduction and literature survey		50
4.2	Sample preparation		51
4.3	Density and Glass Transition Temperature		56
4.4	X-ray Diffraction		60
4.5	Fourier Transform Infra Red Spectroscopy		64
4.6	UV-Visible Spectroscopy		68
4.7	Raman Spectroscopy		71
4.8	Extended X-ray Absorption fine structure		88
4.9	Neutron diffraction		92
5.0	Conclusions		100

		References	102
5		Structural Studies of Alumino Germanate Glasses Doped with La, Pr and Nd ions	105
	5.1	Introduction	105
	5.2	Sample preparation	106
	5.3	Differential thermal analysis and density	109
	5.4	X-Ray Diffraction	111
	5.5	Fourier Transform Infrared Spectroscopy	113
	5.6	Ultraviolet-Visible spectroscopy	115
		5.6.1 Tauc Plots	118
	5.7	Raman Spectroscopy	121
	5.8	Extended X-ray absorption fine structure	129
	5.9	Neutron diffraction	135
	5.10	Conclusions	142
		References	143
6		Structural Studies of Alumino-Germano-Phosphate Glasses Doped with La and Nd ions	147
	6.1	Introduction	147
	6.2	Sample preparation	148
	6.3	Differential thermal analysis and density	149
	6.4	X-Ray diffraction	151
	6.5	Fourier Transform Infrared Spectroscopy	152
	6.6	UV-Visible spectroscopy	156
		6.6.1 Tauc Plots	157
	6.7	Raman Spectroscopy	158
	6.8	Conclusions	167
		References	168
7		Conclusions	170
		Bibliography	174
		Appendix	183

LIST OF FIGURES

Figure No.	Title	Page No.
1.1	Volume v/s Temperature diagram (Jones (1956))	2
1.2(a)	Schematic representation of the structure of (i) Crystalline form and (ii)Glassy form	5
1.2(b)	Schematic representation of a complex glass	6
1.3	Dependence of homogeneous nucleation and crystal growth on temperature	7
1.4	Free energy – position diagram at the crystal- liquid interface	8
2.1	The scattering vector $\overline{Q}$	17
2.2	Raman stokes, Raman anti-Stokes and Rayleigh scattering representation on energy level diagram.	32
3.1	Schematic diagram of the FTIR-8900 spectrophotometer	37
3.2	UV- Visible spectrometer Optical system	39
3.3	The schematic diagram showing thermocouples in a DTA set up	40
3.4	Schematic diagram of a Raman spectrometer setup	41
3.5	Experimental set up of beam line BL-09 at RRCAT Indore	44
3.6	The Sample environment at the beam line BL-09	44
3.7	Schematic diagram of single crystal X-ray diffractometer	46

3.8	Schematic diagram of the high Q diffractometer at Dhruva reactor, BARC, Mumbai	47
4.1	Photograph of the glasses P1-G, P2-G and P3-G formed	56
4.2	X-Ray diffraction pattern of the glasses P1-G, P2-G and P3-G	60
4.3	X-Ray diffraction pattern of the devitrified samples P1-D, P2-D and P3-D	61
4.4	X ray diffraction spectrum of the glass samples P4-G, P5-G,P6-G and P7-G	62
4.5	Xray diffraction spectrum of glass samples P8-G and P9-G which got partially devitrified due to the absence of Al_2O_3 .	63
4.6	X-ray diffraction spectrum for the glass sample P10-G having only Al_2O_3 inclusions.	63
4.7	Comparative display of the Fourier Transform Infrared spectra of the glass P1-G, P2-G and P3-G and their respective devitrified samples P1-D, P2-D and P3-D	64
4.8	Fourier Transform Infrared spectra of glass samples P4-G, P5-G, P6-G and P7-G.	65
4.9	Fourier Transform Infrared spectra of glasses P1-G and P10-G and devitrified samples P8-D and P9-D	66
4.10	Comparative display of the Ultra Violet- Visible spectra of Glass and devitrified samples (a) P1-G and P1-D (b) P2-G and P2-D (c) P3-G and P3-D	69
4.11	Ultra Violet –Visible spectra of glass samples P4-G, P5-G, P6-G and P7-G	70
4.12	Ultra-Violet- Visible spectra of samples P8-G, P9-G and P10-G	71
4.13	Comparative display of Raman spectra of the glass P1-G and its devitrified sample P1-D	73
4.14	Comparative display of Raman spectra of the glass P2-G and its devitrified sample P2-D	74

4.15 Comparative display of Raman spectra of the glass P3-G and its devitrified sample P3-D 75

4.16 (a) Deconvoluted Raman peaks for glass P1-G 75

4.16 (b) Deconvoluted Raman peaks for P1-G along with the Raman peaks for P1-D 76

4.17 (a) Deconvoluted Raman peaks for glass P2-G 77

4.17 (b) Deconvoluted Raman peaks for P3-G along with the Raman peaks for P3-D 78

4.18 (a) Deconvoluted Raman peaks for glass P3-G 79

4.18 (b) Deconvoluted Raman peaks for P3-G along with the Raman peaks for P3-D 80

4.19 (a) Comparative display of the relative area of the different ^{Qn} for Glasses P1-G, P2-G and P3-G 82

4.19 (b) Comparative display of the relative area of the different Q^n for Glass P1-G and its devitrified sample P1-D 82

4.19 (c) Comparative display of the relative area of the different Q^n for Glass P2-G and its devitrified sample P2-D 83

4.19 (d) Comparative display of the relative area of the different Q^n for Glass P3-G and its devitrified sample P3-D 83

4.20 Deconvoluted Raman peaks for P4-G 84

4.21 Deconvoluted Raman peaks for P5-G 84

4.22 Deconvoluted Raman peaks for P6-G 85

4.23	Deconvoluted Raman peaks for P7-G	86
4.24	Comparative display of the relative area of the different Q^n for (a) Glasses P4-G, P6-G, P7-G and P10-G	87
4.25	Pictorial representation of the Q^n structural units.	87
4.26	XANES spectra at Nd L_3 edge for the Nd containing glass (P1-G, P3-G), devitrified samples (P1-D, P3-D) and the Nd_2O_3 standard	88
4.27	EXAFS $\mu(E)$ v/s E spectra for the Nd containing glasses P1-G, P3-G and devitrified samples P1-D, P3-D	89
4.28	$\chi(r)$ v/s r plots for the Nd containing glasses P1-G, P3-G and devitrified samples P1-D, P3-D	90
4.29	$\chi(r)$ v/s r plots for the La containing glass P2-G and devitrified sample P2-D	91
4.30	Neutron diffraction structure factor S(Q) for the glasses P1-G, P2-G, P3-G and their respective devitrified states P1-D, P2-D, P3-D	94
4.31	Total correlation function T(r) for the glasses P1-G, P2-G, P3-G and their respective devitrified states P1-D, P2-D, P3-D.	95
4.32	Peaks fitted to the radial distribution function N(r) of (a) P1-G (b) P1-D	96
4.33	Peaks fitted to the radial distribution function N(r)of (a) P2-G (b) P2-D	97
4.34	Peaks fitted to the radial distribution function N(r) of (a) P3-G (b) P3-D	98

5.1	Photographs of some germanate glass	109
5.2	Xray diffraction spectra of the glasses G1-G,G2-G,G3-G,G4-G and G5-G.	111
5.3	Xray diffraction spectra of the devitrified states G1-D, G2-D,G3-D, G4-D and G5-D.	112
5.4(a)	Fourier transform infrared spectra of the glasses G1-G, G2-G, G3-G, G4-G and G5-G.	113
5.4(b)	Fourier transform infrared spectra of the devitrified samples G1-D, G2-D, G3-D, G4-D and G5-D.	114
5.5	Absorbance spectra of the glasses G1-G, G2-G and G3-G.	116
5.6	Absorption spectra of the glasses G1-G, G4-G and G5-G	117
5.7	Absorption spectra of the Devitrified samples G1-D, G2-D, G3-D, G4-D and G5-D.	118
5.8(a)	Tauc plots plotted for the glass samples G1-G, G2-G, G3-G, G4-G and G5-G.	119
5.8(b)	Tauc plots plotted for the devitrified samples G1-D, G2-D, G3-D, G4-D and G5-D.	119
5.9	Comparative Raman spectra of glasses	121
5.10	Deconvoluted Raman peaks for glass G1-G.	123
5.11	Deconvoluted Raman peaks for glass G2-G.	124
5.12	Deconvoluted Raman peaks for glass G3-G.	125

5.13	Deconvoluted Raman peaks for glass G4-G.	126
5.14	Deconvoluted Raman peaks for glass G5-G.	127
5.15	Bar graph showing comparative area ratio of the different structural units in the glasses studied.	129
5.16	Experimental EXAFS spectra at the Ge-K edge	130
5.17	$\chi(r)$ versus r plots for the glasses G1-G, G2-G and G3-G.	131
5.18	XANES spectra of the glasses G1-G and G3-G at the Nd L_3 edge.	132
5.19	$\chi(r)$ versus r plots for the glass G1-G at the NdL_3 edge	133
5.20	$\chi(r)$ versus r plots for the glass G2-G at the PrL_3 edge	134
5.21	The structure factors S(Q) v/s the momentum transfer Q for the glasses G1-G, G2-G and G3-G.	136
5.22	The pair correlation functions g(r) for the glasses G1-G, G2-G and G3-G.	137
5.23	The comparative display of the total correlation function T(r) for the glasses G1-G, G2-G and G3-G.	138
5.24	The Gaussian peak fits to the radial distribution function N(r) of the glass G1-G.	139
5.25	The Gaussian peak fits to the radial distribution function N(r) of the glass G2-G.	140
5.26	The Gaussian peak fits to the radial distribution function N(r) of the glass G3-G .	141

6.1	X-ray diffraction spectra of the phosphate, germanate and germano-phosphate glasses	151
6.2:	Fourier Transform Infra-red Spectra of phosphate glasses NdAlP and NdLaAlP	152
6.3	Fourier Transform Infra-red Spectra of Germanate glasses NdAlGe and NdLaAlGe	153
6.4	Fourier Transform Infra-red Spectra of germano-phosphate glasses NdAlGeP and NdLaAlGeP	154
6.5	Comparative display of Fourier Transform Infra-red Spectra of phosphate, germanate and germano phosphate glass	155
6.6	Absorption spectra of NdAlGeP and NdLaAlGeP germano-phosphate glasses	156
6.7	Tauc plots for the germano-phosphate glasses (a) NdAlGeP (b) NdLaAlGeP	157
6.8	Comparative display of the Raman spectra of the phosphate, germante and germano-phosphate glasses	158
6.9	Comparison of the Raman spectra from the two samples having germano-phosphate host networks	159
6.10	Deconvoluted Raman peaks of vibrations of the basic structural units for NdAlP phosphate glass.	160
6.11	Deconvoluted Raman peaks of vibrations of the basic structural units for NdLaAlP phosphate glass.	161

6.12 Deconvoluted Raman peaks of vibrations of the basic structural units for NdAlG germanate glass 161

6.13 Deconvoluted Raman peaks of vibrations of the basic structural units for NdLaAlG germanate glass. 162

6.14 Deconvoluted Raman peaks of vibrations of the basic structural units for NdAlGeP germano-phosphate glass. 163

6.15 Deconvoluted Raman peaks of vibrations of the basic structural units for NdLaAlGeP germano phosphate glass. 164

6.16 Bar graph display of relative area ratios of Q^n of the phosphate, germanate and germano-phosphate glasses 165

List of Tables

Table No.	Title	Page No.
4.1	Composition of the prepared glass samples (P1-G, P2-G, P3-G) in mole %	52
4.2	Compositions of the glasses (P4-G – P10-G) in mole. %	53
4.3	Composition of the constituent oxide powders for glasses P1-G, P2-G and P3-G	54
4.4	Composition of the constituent oxide powders for glasses P4-G, P5-G and P6-G and P7-G.	55
4.5	Compositions of the constituent oxide powders for glasses P8-G, P9-G and P10-G.	56
4.6	Density and molar volume of the glass and devitrified samples.	58
4.7	Glass transition temperature and network connectivity of the rare earth glasses	58
4.8	FTIR peaks observed in the devitrified materials	67
4.9	Raman assignments for the fitted region	74
4.10	Relative areas of different Q^n tetrahedral units from the deconvoluted Raman spectra for the glasses P1-G, P2-G and P3-G and their respective devitrified states.	81
4.12	Correlation length and coordination number of the Nd contained glasses P1-G, P3-G and their respective devitrified states.	91
4.13	Correlation length and coordination number of the La containing glass P2-G and its corresponding devitrified state P2-D.	92
4.14	Correlation lengths (r(Å) $\pm$ 0.02) and coordination numbers (N) from neutron diffraction	99

5.1	Composition of the prepared glass samples in mole%	107
5.2	Calculations of the constituent powders of the respective glasses	108
5.3	Glass transition temperature, density and molar volume	110
5.4	Optical band gap energy, refractive index, dielectric constant and electronic polarizability .	120
5.5	Raman band assignments	128
5.6	Raman peak positions and relative areas of the deconvoluted peaks relating to the different Q^n vibrations.	128
5.7	Ge-O bond length and coordination numbers for the glasses G1-G, G2-G and G3-G.	131
5.8	Correlation length (Nd-O) and coordination number of O around Nd in glass G1-G.	134
5.9	Correlation length(Pr-O) and coordination number of O around Pr in glass G2-G	135
5.10	Correlation length (r) and coordination number (N) of the different correlations in the glases G1-G, G2-G and G3-G (Neutron diffraction)	141
6.1	Composition of the germano-phosphate glasses	149
6.2	Density and glass transition temperature	150
6.3	Relative area ratios of Q^n of the different structural units in the phosphate, germanate and germano-phosphate glasses	165

CHAPTER 1

INTRODUCTION

1.1. Origin of Glass

Glass is a non-crystalline solid whose properties can be altered to suit a particular application by changing the host or the dopants within it. Glass has numerous applications - in areas such as ; receptacles for liquids, optical fibers and telecommunications, radiation shielding, medical equipment, bioglass and ceramics, illumination, decoration, magnetic fields, electronics, etc. Natural glass probably originated since the creation of the solar system. Black obsidian glass of volcanic origin was the first kind of glass known to man and found good use in house hold objects and implements for hunting. Other natural glasses are Pumice – a glassy foam from lava, fulgurites- glass tubes formed from lightening and Libyan desert glass formed by meteoritic impact (Stocker and Cobean (1981), Weeks et al. (1980)).

The accidental method by which glass was first formed was investigated very secretly and modified by using various constituents resulting in the formation of different kinds of glasses by different civilizations. The Egyptians became the pioneers in glassmaking by preparing sodium glass which was subsequently modified by glass experts in Rome, Venice and other parts of Europe. Glass lovers in England were the first to prepare potassium glass from charcoal (burnt wood) and brilliant crystal glass using lead. Stable boro-silicate glasses, optical glasses and metallic glasses were made in the early years of the 20^{th} century. The exact composition of glasses was kept secret until about the end of the nineteenth century when several well-known researchers such as Zachariasen, Doremus, Navarro, Rawson, Vogel, Zarzycki and others made attempts to study the properties and structures of glasses which explained the process of glass formation (Scholze (1991).

1.2. Glass formation

Consider the Volume – Temperature diagram for a glass former shown in Figure 1.1. The volume of a molten liquid decreases steadily if it is allowed to cool. If the melt is allowed to cool at a sufficiently slow rate then there will be an abrupt decrease in volume at a temperature T_m accompanied by crystallisation. The volume of the crystalline material will decrease if it is allowed to cool further. However if the liquid is subjected to rapid cooling ,

it will bypass the process of crystallisation at the Temperature T_m , and the super cooled liquid will follow the curve with a change in the slope of the line which later becomes almost parallel to that of the crystalline material undergoing cooling.. Glass is formed below the temperature T_g called the glass transition temperature. In the region of high viscosity, the melt should be supercooled fast enough to bypass crystallisation and prevent nucleation, so that there is no driving force for crystallisation to occur (Debenedetti et al. (2001))

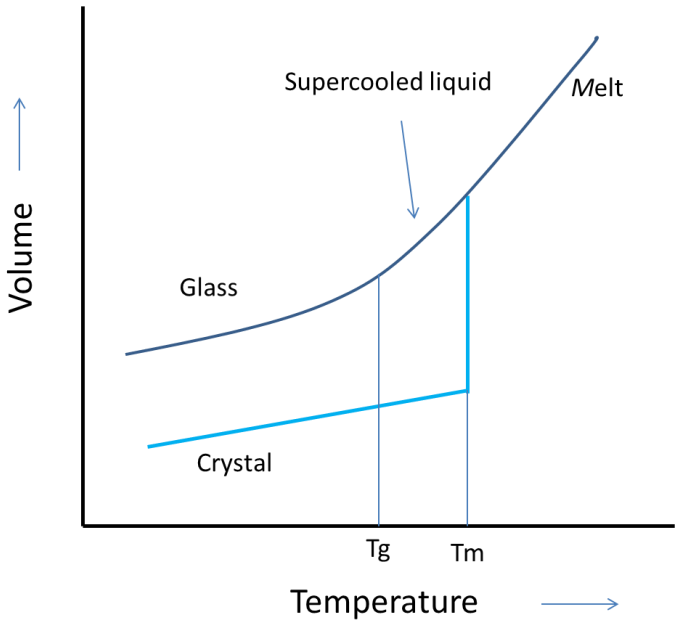

Figure1.1 : Volume v/s Temperature diagram (Jones (1956))

The glass transition temperature T_g is influenced by the rate of cooling. If the rate of cooling is slower then the glass transition temperature is lower. If this continues without any lower limit for T_g then at a particular point the entropy of the liquid will be lower than that of the crystal which is in violation of the third law of thermodynamics (Kauzmann (1948)). This is called as Kauzmann's Paradox. Hence there should be a lower limit of glass transition temperature called as the ideal glass transition temperature (Wong and Angell (1978))

The most general definition of glass was given by Tammann (1933) - a pioneer of glass research as "In the glassy state there are solid, uncrystallised materials". The American society of testing materials defined glass as "Glass is an inorganic product of fusion which

has been cooled to a rigid condition without crystallizing" (Scholes (1945)). Simon(2000) used the freezing in process to define glass as "In the physiochemical sense, glass is a frozen – in undercooled liquid". Zarzycki (1982) defined glass as a non – crystalline solid that presents the phenomena of glass transition while according to Zanotto and Cassar (2017) "Glass is a non-equilibrium, non-crystalline condensed state of matter that exhibits a glass transition. The structure of glass is similar to that of their parent super cooled liquids (SCL) and they spontaneously relax toward the SCL state. Their ultimate fate in the limit of infinite time is to crystallize".

In the preparation of oxide glasses the bond strength plays a very important role depending upon which it can be classified as (1) Glass former or network former (2) Intermediate or conditional formers and (3) Network modifier. Oxides which easily form a glass network by themselves are called as primary glass formers. These include SiO_2, GeO_2, B_2O_3, P_2O_5, V_2O_5 etc. In such glass formers or network formers, the bond strength between the cation and the oxygen anion is mostly higher than 80 Kcal/mol. Those oxides which cannot form the glass network by themselves even though the cation- oxygen bond strength is higher than 80 Kcal/mol are called as conditional formers. Al_2O_3, Ga_2O_3, Bi_2O_3 etc are examples of conditional glass formers and can form polyhedra which can replace that of the network forming oxide and connect with the network. Some oxides having Cation - Oxygen bond strengths about 60Kcal/ mol -80 Kcal/ mol can also become a part of the glass network and behave as intermediates between glass former and network modifier. Examples of such intermediates are ZnO, CdO, PbO, TiO_2, TbO_2, etc. Those oxides in which the Cation-Oxygen bond strength is generally lower than 60 Kcal/mol cannot become a part of the network and are called as network modifiers. Such cations do not form bonds with oxygen but occupy positions in the glass thereby modifying the structure and properties of the glass. Some examples of modifiers are Na_2O, K_2O, Li_2O, MgO, etc. Glass network modifiers can be chosen depending upon the applications for which a particular glass is prepared (Sun(1947)).

1.3. Theories of Glass formation

Glass formation has been explained on the basis of 1) Structural theories in which the structure of the glass forming material plays an important role. Features based on the way the constituent atoms are geometrically arranged, the type of inter atomic bonds and the stability of the bonds are stressed upon in this explanation and 2) Kinetic theories which

are based on the kinetics of crystallization of a liquid considering temperatures lower than the melting point. For glass formation the rate of crystallization has to be much slower than the rate of cooling and the limiting rates of processes such as crystal nucleation and crystal growth are to be set so that the liquid can form glass on cooling.

1.3.1. Structural Theories Of Glass Formation

Goldschmidt (1926) observed that the ability of an oxide having the general formula A_mO_n to form a glass is correlated to the relative sizes of the oxygen anion O and the cation A and found that the glass forming oxides would have the ratio of the ionic radius of the cation (R_A) to the ionic radius of the oxygen anion (R_O) in the range 0.2 to 0.4. This ratio controls the number of anions that can be packed around a given cation and has an important influence on the structure. Goldschmidt proposed a tetrahedral arrangement of oxygen anions around the cation A for glass formation. According to Smekal (1951) mixed bonding is essential for glass formation. Covalent and ionic bonds are formed by inorganic compounds while covalent bonds within chains with Van der Waals bonds between chains are being formed by organic compounds. Sun (1947) gave a criterion for glass formation based on the bond strength. Glass formers would require to have high bond strengths. The condition for glass formation as suggested by Rawson (1956) is that the ratio of bond strength to melting temperature should be high. He also discovered the fact that the liquidus temperature for compositions forming glass is lower than that for either constituent.

The conclusions of Zachariasen (1932) actually led to the random network theory. He considered a structure for glass in which the constituents are evenly placed forming the bulk of the material with the network modifying cations randomly situated in holes in the network close to non-bridging atoms. Zachariasen argued that glasses and crystals have similar inter atomic forces and the same type of basic structural units so that the internal energy of the glassy form is slightly higher than the internal energy of the crystalline form. The relative orientations of the adjacent tetrahedra in the vitreous state is variable as shown in Figure 1.2(a).

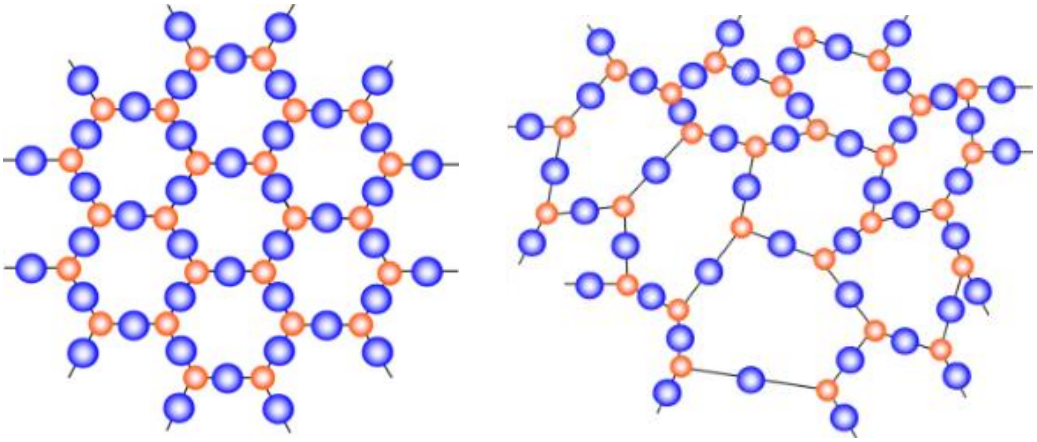

(i) (ii)

Figure 1.2(a): Schematic representation of the structure of (i) Crystalline form and (ii) Glassy form (Zachariasen (1932))

W. H. Zachariasen formulated that the following set of rules must be obeyed for an oxide to be a glass former:

1. No two oxygen atoms may be linked to more than two cation atoms A
2. The number of oxygen atoms surrounding cation A must be small
3. The oxygen polyhedra share corners with each other not edges or faces
4. For a three dimensional structure, at least three corners in each polyhedron must be shared.

Modification of these rules were allowed for the formation of more complex glasses involving the network forming oxides which form part of the network and the network modifying oxides which does not form any part of the network.

A schematic representation of a complex glass is shown in Figure 1.2(b). Any oxide glass can in general be represented as A_mB_nO where A is the modifying cation, B is the network forming cation, O is the oxygen, m and n are in general non-integers.

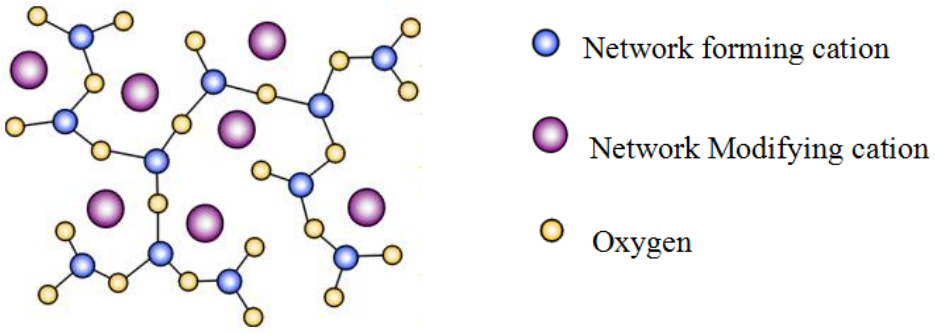

Figure 1.2(b): Schematic representation of a complex glass. (Ylanen(2000))

G. W. Morey (1934) showed that the internal energy in a glass can be appreciably higher than in the corresponding crystal. G. Hagg (1935) also criticised the random network theory and asserted that three dimensional random network was not essential for glass formation.

Randall et al. (1930) proposed the crystallite theory according to which glass is an assembly of very small crystals called crystallites. Later Warren (1937) opposed this idea by his X-ray diffraction studies on some glasses with the conclusion that crystallites do not exist in simple glasses. The Modern crystallite theory was actually formulated by Porai-Koshits (1953) who opined that the structure of glass is comprised of well-ordered regions (similar to crystallites) linked by relative disordered regions.

The difference between the Random network theory and the crystallite theory is the magnitude of fluctuations in the local order of the basic units. Wright et al. (1980) observed that the covalent random network is related to random close packing of spheres. Transformation from a random closed packed structure to a random network structure is possible.

1.3.2. The Kinetic Theories Of Glass Formation

The formation of nucleus (a very small volume of the crystalline phase) in a liquid involves the creation of a crystal-liquid interphase with an increase in free energy which may be greater than the decrease in free energy associated with crystallization. If this happens then the nucleus will be unstable.

The rate of nucleus formation measures the number of stable nuclei formed /cm^3 of the liquid/second and is expressed as

$$I = n\,\nu e^{\frac{-NW^*}{RT}} e^{\frac{-\Delta G'}{RT}} \qquad (1.3.1)$$

where n is the no. of atoms per cm^3 , ν is the vibrational frequency of atoms at the nucleus liquid interface.

$e^{\frac{-NW^*}{RT}}$ is the probabilty of formation of a nucleus larger than the critical size at the temperature T in which N is the Avogadro's number and W^* is the thermodynamic barrier to nucleation.

$e^{\frac{-\Delta G'}{RT}}$ is a factor controlling the rate of change of the structure of the material (liquid to crystal) during the formation of the nucleus in which ΔG' is the kinetic barrier to nucleation.

The relationship between the rate of nucleus formation and the temperature T is shown in the Figure 1.3 below.

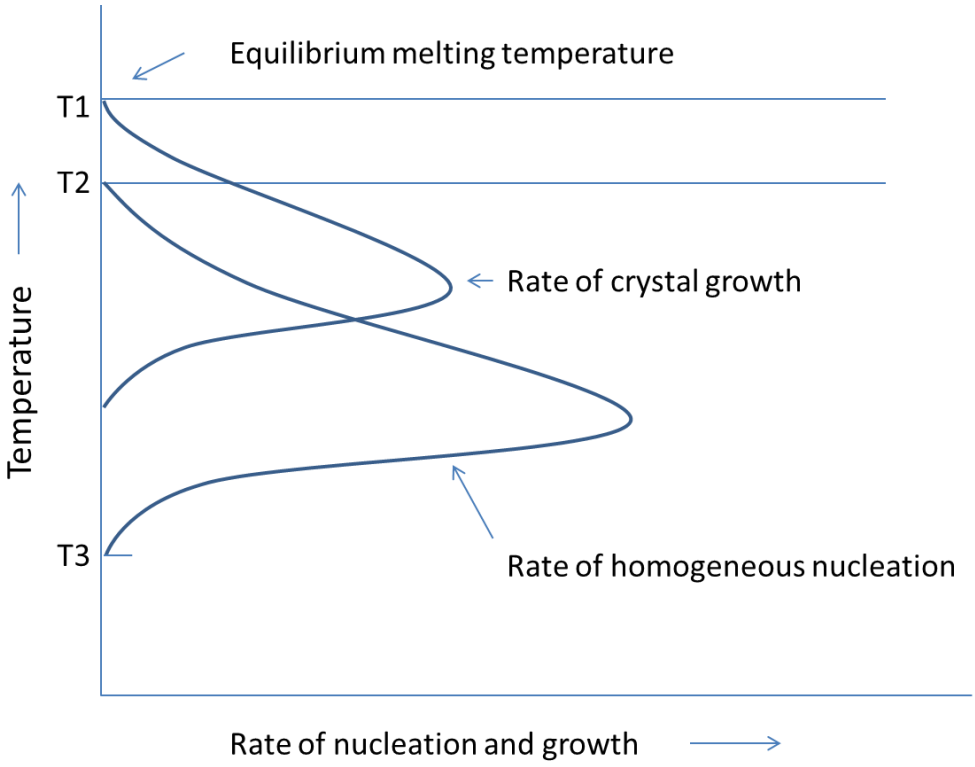

Figure 1.3: Dependence of homogeneous nucleation and crystal growth on temperature (Macmillan (1964))

The free energy – position relationship for atoms at the liquid – solid interface is shown in the Figure 1.4 below.

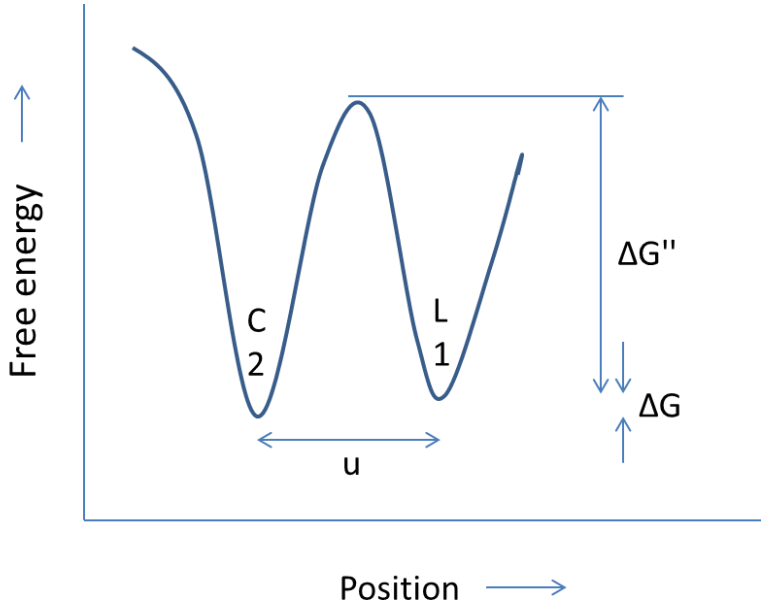

Figure 1.4: Free energy – position diagram at the crystal- liquid interface (Turnbull(1956))

An atom in the crystal (position 2) has a free energy lower than the atom in a liquid (position 1) by an amount ΔG called the bulk free energy of crystallization. At the inferface an atom would require a free energy of activation $\Delta G''$ to cross from the liquid to solid while a free energy of activation $\Delta G'' + \Delta G$ is required for the atom to cross from solid to liquid.

The rate of crystal growth can be expressed as

$$u = a_0 \nu \, (e^{\frac{-\Delta G''}{RT}})(1 - e^{\frac{\Delta G}{RT}}) \qquad (1.3.2)$$

Where ΔG is the bulk free energy of crystallization and ΔG" is the activation energy.

Glass formation is thus based on the strength of the bonds which need to be broken during crystallization and the thermal energy which is available to break these bonds.

For glass formation it is essential that the rates of crystal growth and nuclei formation are low below its melting point (Thomas and Staveley (1952), (Turnbull and Cohen (1958)).

1.4. Devitrification

Crystal nucleation and growth needs to be encouraged in the formation of a crystalline material. According to Rawson (1956) the energy available for breaking bonds was important in crystallisation. In order to develop crystalline phases in glass it must be heat treated to a temperature higher than the glass transition temperature and allowed to cool slowly (Holland (2003), Beveridge (2005)). During this process, structural relaxation occurs due to changes in viscosity and density. This is followed by either heterogeneous or homogeneous nucleation leading to crystallization. Heterogeneous nucleation occurs more often than homogeneous nucleation as it occurs at phase boundaries or impurities or container walls.

1.5. Phosphate glasses

Phosphate glasses are easily formed due to low melting temperature and good glass forming ability of Phosphorus Pentoxide (P_2O_5). These glasses have a wide range of applications; it finds the best use in medical field because of their bio compatibility and are considered to be important in temporary bone replacement due to its low chemical durability allowing natural bone to slowly replace it. Other applications of phosphate glasses includes use as nuclear waste host glasses, glass sealing, solid state electrolytic, LASER, opto magnetic and opto electronic applications (Sales (1987), Durville et al. (1986)).

Vitreous phosphorus pentoxide (v-P_2O_5) has a structure of interconnected PO_4 tetrahedra due to the phosphorous outer electrons forming sp^3 hybrid orbitals (Cruikshank (1961)). The number of tetrahedral linkages through the oxygen bridges depends on the ratio of oxygen to phosphorus (Van Vazer (1958)). P_2O_5 is one of the network formers identified by Zachariasen (1932) in his random network formulation using Q^3 tetrahedra forming a distorted network.

The tetrahedra can be classified on the basis of the Q^n terminology where n is the number of bridging oxygens per tetrahedron. Vitreous phosphate has a cross-linked network of Q^3 tetrahedra (three bridging oxygens and one terminal oxygen with a double bond). On addition of a modifier, this structure can change to a metaphosphate glass having chains of Q^2 or a pyrophosphate of Q^1 units and an orthophosphate of isolated Q^0 anions (Liebau et al. (1981)). Three different species of oxygen can exist in phosphate glasses - the shorter

double bonded oxygen (P=O), the terminal oxygen near a R modifier ($P\text{-}O^{-}R^{+}$) and bridging oxygen (P-O-P) (Martin (1991)).

Pure phosphate glasses are hygroscopic and have low chemical stability. However the durability can be improved by adding Iron oxide (Greaves (1990)). Addition of Al_2O_3 and B_2O_3 increases the chemical durability and stability as Al forms crosslinks (P-O-Al) in the network with Al having tetrahedral, penta coordinated and octahedral coordination (Takahashi (1962), Cole (1999)).

An X-ray photoelectron spectroscopic study on the effect of adding B_2O_3 to zinc phosphate glass by Brow (1996) shows the formation of B-O-P links, the concentration of which increases by reducing the P-O-Zn and P-O-P links.

Effect of introducing two cations Pb and Zn as network formers on the phosphate network by Shafi and Ibrahim (1998) showed differences in the links formed by these cations and the phosphate network which were correlated to the dissolution rate variations.

An EXAFS study on Nd and Er phosphate glasses by Karabulut et al. (2002) showed that in moving from the ultra-phosphate to the meta phosphate composition the rare earth-O coordination number decreases from 9.0 to 6.4 while the rare earth-O correlation length decreases from 2.40Å to 2.37Å for Nd and from 2.29 Å to 2.23Å for Er

Bionducci et al.(1981) performed neutron diffraction studies on zinc metaphosphate glasses by adding Europium and observed the P-O correlation length to be 1.53Å and O-O correlation length to be 2.47Å.

X-ray and neutron diffraction studies on a series of rare-earth alumina-phosphate glasses by Shikerkar et al. (2000) established the essential tetrahedral continuous random network of PO_4 tetrahedra with each of the rare-earth types in oxygen coordination ranging from 6 to 8 in these glasses and rare-earth to oxygen correlation lengths in keeping with the rare-earth ionic radius “contraction”.

Similarly, X-ray and neutron diffraction studies on Nd phosphate glass by U. Hoppe et al. (2001) indicates that the coordination number of oxygen around Nd equals the number of terminal oxygen atoms available for each Nd cation. Nd-O correlation length of 2.39Å and coordination number of 6.6 was obtained.

Neutron diffraction studies on rare earth alumino phosphate glass with rare earths such as Dy, Ho, La and Ce by Martin et al (2004) indicated that each of these rare earths and Al behave as network modifiers binding to the terminal oxygen. The coordination numbers of the smaller rare earth cations Dy or Ho were found to be 6.7 (1) while that of larger La or Ce cations to be 7.5 (2).

1.6. Germanate Glass

Germanate glasses are used in optical fibres and telecommunications. Germanate glass finds good use as an industrial glass as it has a refractive index higher than borate or silicate glass. It is also widely used in the construction of laser glasses because of its high transparency over a wide spectral range. The property of germanate glass to absorb X-rays makes these glasses useful in the manufacture of shield glasses (Margaryan (1993)).

Desa et al. (1988) in an X-ray and neutron diffraction study of pure GeO_2 glass established this to be a continuous random network of corner connected GeO_4 tetrahedra in close analogy with other oxide tetrahedral network glasses such as SiO_2.

In a study of Na germanate and Li germanate glasses, Murthy and Ip (1964) detected an anomaly in the density and refractive index related to compositional variation of the alkali in these glasses. This was attributed to the change in germanium coordination from GeO_4 to GeO_6. A similar anomaly was earlier reported by Ivanov (1962) in their study of Na and K glasses.

Yiannopoulos et al. (2001) in their study of density related to the structure of alkali germanate glass observed that the maximum value of density could not be reproduced by the change in the Ge- O coordination from 4 to 6 and suggested that a change in short and medium range order with the increase in alkali content could influence the germanate anomaly.

Henderson and Fleet (1991) studied the structure of germanate glass based on Na content using Raman spectroscopy and prepared a model to explain the observed anomaly. They proposed that the anomaly is based on the formation of 3 membered GeO_4 rings instead of GeO_4 getting converted to GeO_6.

In a thermal and a structural analysis of germanate glass by Carvalho (2016), it was indicated that the 3 membered rings of the GeO_4 gets altered on thermal treatment.

Koroleva et al. (2019) used Raman and Infra-Red spectroscopic methods to study the structure of potassium germanate glasses. Their results suggested the conversion of GeO_4 to GeO_6 units, the maximum of which occurs on addition of 20 mol% of potassium oxide. Further increase in the K content leads to depolymerisation of the network with a decrease in the Ge-O coordination number and formation of GeO_4 units.

1.7. Germano-Phosphate Glasses

Germano phosphate glass consists of two glass formers GeO_2 and P_2O_5. The glass network consists of separate areas of Ge-O-Ge and P-O-P structures linked together.

Sugiyama et al. (1991) used methods of diffraction to study the structures of germano-phosphate glasses by changing the P_2O_5 content. They observed that the coordination number of Ge-O increased with increase in P_2O_5 content.

In a Raman spectroscopic study of alkali germano-phosphate with different GeO2: P2O5 ratios doped with Na, K and Rb, Henderson and Amos (2003) observed that the alkali prefers to modify the phosphate part of the network in the glass network consisting of separate phosphate and germanate constituents , with the formation of Q^2 and $Q^1(PO_4)$ tetrahedra. Anomaly in density is observed at a higher Ge: P ratio attributed to three membered ring formation of GeO_4 tetrahedra.

Lithium ion transport properties were studied by Kumar and Rao (2004) by increasing the Li ion content. They proposed a model in which there will be formation of non-bridging oxygens (NBO) with increase in Li content. In the transport mechanism there is a change in the position of NBO and BO due to thermal fluctuations. This switching in the position of NBO helps the Li ion to jump close to the new NBO position.

In the study of Zwanziger et al. (2006) on germano-phosphates, they indicated that the Ge coordination number N(Ge-O) depends on the GeO_2 content defined by :
$N(Ge-O) = 4 + 2((1-x)/x)$ in the (1-x) P_2O_5- x(GeO_2) glass. According to their model this glass consists of a continuous network of (Ge-O-Ge) and (P-O-Ge) links with only bridging oxygens present. The network could also have (P-O-P) links provided that the P_2O_5 content is sufficient.

X-ray and neutron diffraction studies on potassium germano-phosphates (Hoppe et al. (2008)) suggest the presence of terminal oxygen probably of the PO_4 tetrahedra in

coordination with the K ion. Their results support the model that the Ge-O coordination number increases due to the conversion of GeO_4 to GeO_6 units.

1.8. Objectives Of This Study

The main objectives of this study are:

1) To study the structures of alumino-phosphate glass prepared using the melt quench technique by introducing the individual rare earth ions La, Pr and Nd and examine the related structural changes that take place on introducing these rare earth ions in pairs in the alumino-phosphate glass.
2) To study the structural changes that take place on devitrifying the alumina-phosphate glasses containing Nd and La singly and in pairs.
3) To study the structures of La, Nd and Pr doped germanate glass prepared using the melt quenched technique and the structural changes taking place when these rare earth ions are introduced in pairs.
4) To study the changes in the structure of the single host glass formers P_2O_5 and GeO_2 , on introduction of Nd and the pair Nd and La. In addition, the study of the structural changes that occur by preparing glass formed by mixing the two host networks viz. GeO_2 and P_2O_5 and introducing Nd as well as the pair of rare-earth types viz. Nd and La ions.

References:

1. Bionducci M., Bellisent R., Messa M. P., Piccaluga G., Pinna G., Bettinelli M., J. Non- Cryst. Solids 36 (1995) 192
2. Brow R. K., J. Non-Cryst. Solids 263&264 (2000) 1-28.
3. Brow R. K., J. Non-Cryst. Solids 194 (1996) 267
4. Carvalho E. A., Frietas A. M., Silva G. H,. Bell M. J. V. Kassab, L. R. P., Anjos V., Vibrational Spectroscopy 87 (2016) 147-148
5. Chakraborty I. N., Day D. E., Lapp J.C., Shelby J. E., J. Am. Ceram. Soc.,68 (1985) 368
6. Cole J. M., VanEck E.R.H., Mountjoy G., Newport R.J., Brennam T., Saunders G.A., J. Phys: Condens. Matter II (1999) 9165-9178.
7. Debenedetti P. G., Stillinger F. H., Nature 410 (2001) 259-267
8. Desa J. A. E., Wright A. C., Sinclair R. N., J. Non-Cryst. Solids, 99 (1988) 276-288

9. Durville F. M., Behrens E. G., Powell R. C., Phys. Rev. 34 (1986) 4213
10. Greaves G. N., Glass, Science and Technology, Academic Press London (1990)
11. Hagg G., J. Chem. Phys. 3 (1935) 42- 49
12. Hannon A. C., Sinclair R.N., Wright A.C., Physica A, 201 (1993) 375
13. Henderson G. S. and Amos R. T., J. Non- Cryst. Solids 328 (2003) 1-3
14. Henderson G. S. and Fleet M. E., J. of Non-Cryst. Solids 134 (1991) 259-269
15. Hoppe U., Heidepriem H. E., Neuefeind J., Bowron D. T., Z. Naturforsch 56a (2001) 237 – 243
16. Hoppe U., Brow R. K., Wyckoff N. P., Schops A., Hannon A. C., J. Non- Cryst. Solids 354 (2008) 3572-3579
17. Ivanov A.O., Evstropiev K. S., Dokl. Akad. Nauk. SSSR 145 (1962) 797
18. Jones G. O., Glass, Methuen, London (1956) 119
19. Karabulut M., Marasinghe G.K., Metwalli E.,.Witteenauer A.K, Brow R. K., Booth C. H., Shuk D. K., Phys. Rev. B, 65 (2002) 104206.
20. Kauzmann W., Chem. Rev. 43 (1948) 219
21. Koroleva O. N., Shtenberg M. V., Ivanova T. N., J. Non- Cryst. Solids 510 (2019) 143
22. Kumar S. and Rao K. J., Solid State ionics 170 (2004)191
23. Liebau F., Keefe M. O., Novrotsky A., Structure and Bonding in Crystals, Academic Press New York (1981) 197
24. Lorch E. A., J. Phys. C 2(1969) 229
25. Macmillan P. W., Glass Ceramics, Academic Press London, (1964) 229
26. Margaryan A., Pilavin M.A., Germanate glass: Structure ,Spectroscopy and Properties, Publisher Artech House Boston, London (1993)
27. Martin R. A., Salmon P. S., Fisher H. E., Cuello G. J., J. Non- Cryst. Solids 345 (2004) 208
28. Martin S. W., Eur. J. Solid State Chem. 28 (1991)163
29. Morey G. W., J. Am. Ceram. Soc 17 (1934) 315-328
30. Murthy M.K., Ip J., Nature 201(1964) 285
31. PoraiKoshits E. A., The structure of Glass Consultants Bureau, New York (1953) 25
32. Randall J. TRooksby., H. P., Cooper B. S., Nature 125 (1930) 458
33. Rawson H., Inorganic glass forming systems, University of Sheffield, Department of glass technology, Sheffield , England, (1967) Academic Press, London and New York
34. Scholes S. R., Glass. Ind. 26 (1945) 417,438

35. Scholes S. R., Glass Ind., 26 (1945) 417-438
36. Scholze H., Glass nature , Structure and Properties, Springer -Verlag, Berlin (1991)
37. Shelby J. E., J. Am. Ceram. Soc., 68 (1985) 368
38. Shikerkar A. G., Desa J. A. E., Krishna P. S. R., Chitra R., J. Non- Cryst. Solids 270 (2000) 234-246
39. Smekal A., J. Soc. Glass Technol. 35 (1951) 411-420
40. Stocker T.and Cobean R. C., National Geographic (1981)
41. Sugiyama K., Waseda Y., Ashizuka M., Mater. Trans. JIM 32(1991)1030
42. Sun K. H., J. Am. Ceram. Soc. 30 (1947) 277
43. Tammann G., Glaszustand Der, Leipzig: L. Vob (1933)
44. Thomas D. G., Staveley L. A. K., J. Chem. Soc. (1952) 4569
45. Turnbull D., Cohen M. H., J. Chem. Phys.29 (1958) 1049
46. Turnbull D., Seitz F., Solid State Physics,Academic Press, New York, 3 (1956) 223-306
47. VanWazer J. R., Phosphorus and its compounds, vol 1&2, Interscience, New York 1958
48. Warren B. E., J. Appl. Phys., 8 (1937) 645
49. Weeks R. A., Nastrallah M., Arafa S.and Bishay A., J. Non-Cryst. Solids 38,39 (1980) 129-134
50. Wong J. and Angell C. A., Glass: Structure by spectroscopy (1976)
51. Wright A. C., Conell G. A. N., Allen J. W., J. Non-Cryst. Solids 42 (1980) 69
52. Yiannopoulos Y. D., Varsamis C.P.E., Kamitsos E. I., J. Non-Cryst. Solids 293-295 (2001) 244-249
53. Ylanen H., Comb. And Mat. Chem. (2000)
54. Zachariasen W. H., J. Am. Chem. Soc. 54 (1932) 3841-3851
55. Zanotto E. D., Cassar D. R., Scientific reports (2017)
56. Zarzycki J., Glass structure, J. Non-Cryst. Solids 52 (1982) 31- 43
57. Zwanziger J., Shaw J .L., Zwanziger U. W., Aitken B. G., J. Phys. Chem. B 110 (2006) 20123

CHAPTER 2

THEORY

In this Chapter, we deal with the essential theoretical considerations pertaining to: neutron diffraction applied to the study of the disordered state; Monte Carlo based calculations of the radial distribution function; Extended Absorption Fine Structure (EXAFS); and an outline of the basic theory of Raman Scattering.

X-ray and neutron diffraction are complimentary tools in the structural study of condensed matter. X-rays scatter off the electronic clouds around atoms while neutrons scatter from the nuclei of atoms. Taken together, the two methods offer a powerful combination in the study of structures – particularly those of glasses and disordered materials. The theory of neutron diffraction applied to glasses and the various necessary experimental corrections that are outlined in this Chapter use the formalism of Wright (1974) and Fischer et al. (2006). The methods of extracting useful information from the correlation function and the techniques of isolating individual component correlation functions are also discussed.

2.1 Neutron scattering

According to Van Hove (1954), the scattering cross section of a system of particles interacting with each other can be expressed in terms of a generalised pair correlation function $G(\tilde{r},t)$ which represents the probability of finding another particle at a vector distance $\tilde{r}$ from a given particle at the origin at time t. $G(\tilde{r},t)$ can be split into self and distinct parts as

$$G(\tilde{r},t)=G^{S}(\tilde{r},t)+G^{D}(\tilde{r},t) \qquad (2.1)$$

where the self part $G^{S}(\tilde{r},t)$ refers to correlations of a particle with itself and the distinct part $G^{D}(\tilde{r},t)$ refers to correlations with any other particle.

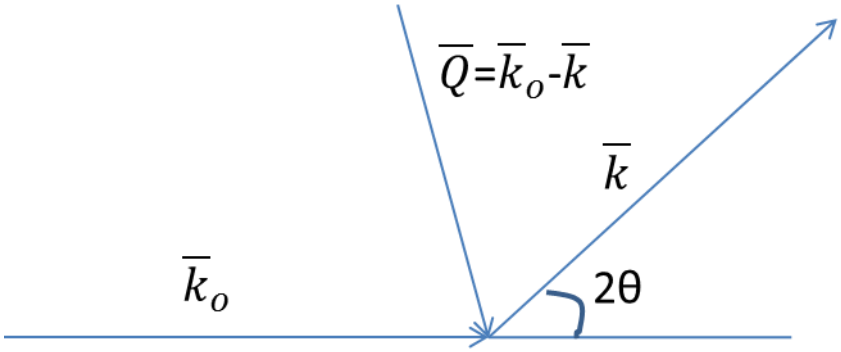

Figure 2.1: The scattering vector $\overline{Q}$

If E_0 is the energy and $\hbar\tilde{k}_0$ is the momentum of the incident neutrons scattered through an angle 2θ having energy E and momentum $\hbar\tilde{k}$ (Figure 2.1), the scattering event can be expressed in terms of the energy transfer as;

$$\hbar\omega = E_0 - E \qquad (2.2)$$

and momentum transfer as ;

$$\hbar\tilde{Q} = \hbar\tilde{k}_0 - \hbar\tilde{k} \qquad (2.3)$$

When a flux of neutrons is incident on a system of stationery particles to a first approximation, the probability of interaction is expressed by a cross section σ.

For a neutron of wavelength λ which is elastically scattered through an angle 2θ, the magnitude of the momentum transfer vector $\tilde{Q}_o$ is given by

$$Q_o = \frac{4\pi Sin\theta}{\lambda} \qquad (2.4)$$

The double differential cross section per unit solid angle Ω and energy interval ħω in terms of the self and distinct correlation functions as shown by Placzek (1952) is given by;

$$\frac{d^2\sigma}{d\Omega d\omega} = \frac{d^2\sigma^S}{d\Omega d\omega} + \frac{d^2\sigma^D}{d\Omega d\omega} \qquad (2.5)$$

Where the self-correlation function can be expressed as ;

$$\frac{d^2\sigma^S}{d\Omega d\Omega} = \frac{N_u}{2\pi}\frac{k}{k_0}\sum_j \overline{b_j^2}\int_0^\infty\int_{-\infty}^\infty G_j^S(\tilde{r},t)\, e^{i(\tilde{Q}\cdot\tilde{r}-\omega t)}d\tilde{r} \qquad (2.6)$$

and the distinct correlation function can be expressed as ;

$$\frac{d^2\sigma^{\mathrm{D}}}{\mathrm{d}\Omega\mathrm{d}\omega} = \frac{N_u}{2\pi}\frac{k}{k_0}\sum_j \sum_k \overline{b_j b_k} \int_0^{\infty} \int_{-\infty}^{\infty} G_{jk}^{D}(\tilde{\mathrm{r}},\mathrm{t})\mathrm{e}^{i(\tilde{\mathrm{Q}}\cdot\tilde{\mathrm{r}}-\omega\mathrm{t})}\mathrm{d}\tilde{\mathrm{r}}\mathrm{dt} \qquad (2.7)$$

Where $N_u$is the number of compositional units, the quantities $\overline{b_j}$, $\overline{b_k}$ and $\overline{b_j^2}$ are the isotopically averaged neutron scattering lengths in which *j* is the number of individual atoms in a given compositional unit and *k* is the number of atom types or elements in the unit.

These quantities represent the scattering amplitude due to the interaction of the neutron with a nucleus given as;

$$\mathrm{b}= -\frac{1}{4\pi}\int \frac{2m_n}{\hbar^2}\, V(r)dr \qquad (2.8)$$

where m_n is the mass of the neutron, $V(r)$ is the interaction potential. b can be positive, negative or complex. Its Q independence implies that for an isolated nucleus, dσ/dΩ is isotropic and the total scattering cross-section σ_{tot}^{s} is given by ;

$$\sigma_{tot}^{s} = \int \frac{d\sigma}{d\Omega}\, \mathrm{d}\Omega = 4\pi\overline{b^2} \qquad (2.9)$$

which can be either a free atom cross-section σ_f^s when a nucleus is free to recoil on scattering a neutron or bound atom cross-section σ_b^s when the nucleus remains stationary during the scattering event.

$\sigma_f^s \; and \; \sigma_b^s$ are related through $\mu = \frac{m_N}{m_n}$, which is the ratio of mass of nucleus to mass of neutron.

$$\frac{\sigma_b^s}{\sigma_f^s} = \left(\frac{\mu+1}{\mu}\right)^2 \qquad (2.10)$$

For an assembly of nuclei the differential scattering cross-section can be expressed as a sum of a phase dependent term – coherent scattering cross-section per atom written as

$$\sigma_{coh}^{s}=4\pi\bar{b}^2 \qquad (2.11)$$

and a phase independent term - incoherent scattering cross-section per atom written as

$$\sigma_{incoh}^{s}=4\pi(\overline{b^2}-\bar{b}^2) \qquad (2.12)$$

Hence the incoherent scattering cross-section is the difference between the total and coherent scattering cross-section.

In mono-isotropic materials having equal number of protons and neutrons in the nuclei, there is only one scattering length and so the incoherent scattering cross section is zero

The scattering laws $S(\tilde{Q}, \omega)$ may be defined as;

$$S_j^S(\tilde{Q}, \omega) = \frac{1}{2\pi}\int_0^\infty \int_{-\infty}^\infty G_j^S(\tilde{r}, t)\, e^{i(\tilde{Q}\cdot\tilde{r}-\omega t)} d\tilde{r}dt \quad (2.13)$$

$$S_{jk}^D(\tilde{Q}, \omega) = \frac{1}{2\pi}\int_0^\infty \int_{-\infty}^\infty G_{jk}^D(\tilde{r}, t)\, e^{i(\tilde{Q}\cdot\tilde{r}-\omega t)} d\tilde{r}dt \quad (2.14)$$

By performing a double Fourier transformation on the above scattering laws, its related correlation function can be obtained;

$$G(\tilde{r}, t) = \frac{1}{(2\pi)^3}\int_0^\infty \int_{-\infty}^\infty S(\tilde{Q}, \omega) e^{i(\omega t-\tilde{Q}\cdot\tilde{r})} d\tilde{Q}d\omega \quad (2.15)$$

2.2 Total neutron diffraction

Elastic or total scattering experiments can provide structural information based on the diffraction patterns. Total diffraction involves the detection of both elastically and inelastically scattered neutrons at a particular angle without any discrimination of energy. The differential total scattering cross-section measured is given by;

$$\frac{d\sigma}{d\Omega} = \int_{-\infty}^\infty \frac{\epsilon(E)}{\epsilon(E_0)} \frac{d^2\sigma}{d\Omega d\omega} d\omega \quad (2.16)$$

In this equation, $\epsilon(E)$ is the efficiency of the neutron detector and the upper limit of integration is $E_0/\hbar$ which is effectively infinity (∞) when E_0 is assumed to be large compared to vibrational energies.

Assuming that $\frac{\epsilon(E)}{\epsilon(E_0)} = \frac{k_0}{k}$ (2.17)

and that Q is constant and equal to the elastic value

$$Q_0 = \frac{4\pi}{\lambda_0}\sin\theta \text{ for all } \omega, \quad (2.18)$$

Integrating eqn. 2.5 with respect to ω gives;

$$\frac{d\sigma}{d\Omega} = \frac{d\sigma^S}{d\Omega} + \frac{d\sigma^D}{d\Omega} \quad (2.19)$$

in which $\frac{d\sigma^S}{d\Omega} = N_u \sum_j \overrightarrow{b_j^2} \int_0^\infty G_j^S(\tilde{r}, 0)\, e^{i\tilde{Q}\cdot\tilde{r}} d\tilde{r}$ (2.20)

and $\frac{d\sigma^D}{d\Omega} = N_u \sum_j \sum_k \overline{b_j}\,\overline{b_k} \int_0^\infty G_{jk}^D(\tilde{r}, 0)\, e^{i\widetilde{Q_0}\cdot\tilde{r}} d\tilde{r}$ (2.21)

$G_j^S(\tilde{r}, 0)$ is the instantaneous pair correlation function equal to a delta function δ(r) at the origin and $G_{jk}^D(\tilde{r}, 0)$ is the instantaneous pair correlation function equal to the number density $\rho_{jk}(\tilde{r})$ of k type atoms at a distance r̃ from the origin atom j.

Thus $\frac{1}{N_u}\frac{d\sigma}{d\Omega} = I_N(Q_0) = \sum_j \overrightarrow{b_j^2} + \sum_j \sum_k \overline{b_j}\,\overline{b_k} \int_0^\infty \rho_{jk}(\tilde{r})\, e^{i\widetilde{Q_0}\cdot\tilde{r}}\, d\tilde{r}$ (2.22)

Integration of equation (2.16) along a line of constant Q=Q_0 in the ω-Q space leads to the static approximation. Any deviation from this method leads to alterations in equation (2.22).

The average of $I_N(Q_0)$ over all relative orientations of r̃ with respect to Q_0 gives :

$$I_N(Q_0) = \sum_j \overline{b_j^2} + \sum_j \sum_k \overline{b_j}\,\overline{b_k} \int_0^\infty 4\pi r^2\, \rho_{jk}(\mathrm{t}) \frac{\sin Q_0 t}{Q_0 t}\, \mathrm{dr} \quad (2.23)$$

Defining correlation functions;

$$d_{jk}(r) = 4\pi r(\rho_{jk}(\mathrm{r}) - \rho_k^0 \quad (2.24)$$

and $d_k^0 = 4\pi r \rho_k^0$ (2.25)

where ρ_k^0 is the average number density of k type atoms contributing to the scattered intensity as a δ function at Q_0 =0 denoted as $I_N^0(Q_0)$.

The distinct intensity is defined as ;

$$i_N(Q_0) = I_N(Q_0) - \sum_j \overline{b_j^2} - I_N^0(Q_0) \quad (2.26)$$

Hence $Q_0 i_N(Q_0) = \sum_j \sum_k \overline{b_j}\,\overline{b_k} \int_0^\infty d_{jk}(r) \sin(Q_0 r) dr = \sum_j \sum_k Q_0\, i_{jk}^M(Q_0)$ (2.27)

where $Q_0 i_{jk}^N(Q_0) = \overline{b_j}\,\overline{b_k} \int_0^\infty d_{jk}(r) \sin Q_0 r\, dr$ (2.28)

which on Fourier transformation gives :

$$d_{jk}(r) = \frac{2}{\pi \overline{b_j} \overline{b_k}} \int_0^\infty Q_0 i_{jk}^N(Q_0) \sin rQ_0 \, dQ_0 \quad (2.29)$$

Defining the differential correlation function $D_N(r)$ as the Fourier transform of $Q_0 i_N(Q_0)$ gives;

$$D_N(r) = \frac{2}{\pi} \int_0^\infty Q_0 i_N(Q_0) \sin rQ_0 \, dQ_0 \quad (2.30)$$

Using equations 2.27and 2.29 gives;

$$D_N(r) = \sum_j \sum_k \overline{b_j} \, \overline{b_k} d_{jk}(r) \quad (2.31)$$

The total correlation function is defined as

$$T(r) = D(r) + T^0(r) \quad (2.32)$$

Where $T^0(r) = \sum_j \sum_k \overline{b_j} \, \overline{b_k} d_k^0(r) = \left(\sum_j \overline{b_j}\right)^2 4\pi r \rho^0$ (2.33)

The radial distribution function $N(r)$ can be expressed in terms of the differential correlation function $D_N(r)$ as;

$$N(r) = \sum_j \sum_k \overline{b_j} \, \overline{b_k} 4\pi r^2 \rho_{jk}(r) \quad = r(D_N(r) + T^0(r)) \quad (2.34)$$

Thus, N(r) = r T(r) (2.35)

2.3 Finite Q_{MAX}

The diffraction data can be measured only up to some maximum value of Q_0. The mathematical equivalent of this experimental limitation can be expressed by multiplying the intensity function $Q_0 i_N(Q_0)$ by a step modification function, $M(Q_0)$ which is unity for values of Q_0until Q_{MAX} and zero beyond.

The resulting correlation function $D'(r)$ can be expressed as;

$$D'(r) = \frac{2}{\pi} \int_0^{Qmax} Q_0 \, i'(Q_0) M(Q_0) \sin rQ_0 \, dQ_0 = \sum_j \sum_k d'_{jk}(r) \quad (2.36)$$

The Fourier transform of a step function appears as symmetrical satellite ripples around a central maximum.

The satellite maxima confuse the true features in the correlation functions and hence need to be reduced. This can be done by using a modification function $M(Q_0)$ such as Lorch Modification function (Lorch (1969)) which cuts off $Q_0 i_N(Q_0)$ more gradually and is of the form ;

$$M(Q_0) = \begin{cases} \frac{\sin \Delta r Q_0}{\Delta r Q_0} & Q_0 \leq Q_{max} \\ 0 & Q_0 \geq Q_{max} \end{cases} \quad (2.37)$$

In this the resolution in real space is upto length $\Delta r = \pi / Q_{max}$

The cosine transform of $M(Q_0)$ gives the peak shape function

$$P_{jk}^N(r) = \frac{\overline{b_j b_k}}{\pi} \int_0^{Q_{max}} \frac{\sin(\pi Q_0 / Q_{max})}{\pi Q_0 / Q_{max}} \cos r Q_0 \, dQ_0 \quad (2.38)$$

The use of $M(Q_0)$ leads to a convolution of the component correlation functions with $P_{jk}^N(r)$ and with the use of $P_{jk}^N(r)$, the height of the correlation function peaks get reduced with a simultaneous broadening which is symmetrical in D(r) and T(r) but asymmetrical in N(r). Hence the function N(r) needs to be avoided in accurate estimations of atomic separations, and T(r) used instead for correlation lengths.

2.4 Correction for neutron static approximation

In the integration of equation (2.16), any deviation from the static approximation (Assuming constant Q=Q_0 value) leads to distortions in I(Q_0) which affects only the term due to self scattering. These distortions can be corrected for, using the Placzek (1952) method.

Placzek gave the expansion of the scattering law S(Q, ω) in terms of a series in $Q^2 - Q_0^2$

$$\mathrm{S}(\mathrm{Q}, \omega) = \mathrm{S}(Q_0, \omega) + S'(Q_0, \omega)(Q^2 - Q_0^2) + \frac{S''(Q_0,\omega)(Q^2 - Q_0^2)^2}{2!} + \cdots \quad (2.39)$$

The prime superscript indicates that the differentiation is carried out with respect toQ^2. For a twin axis spectrometer $Q^2 - Q_0^2$ is expressed in terms of a power series in $\frac{\hbar\omega}{E_0}$ given as;

$$Q^2 - Q_0^2 = -\frac{Q_0^2}{2}\frac{\hbar\omega}{E_0} + \frac{1}{8}(2k_0^2 - Q_0^2)\left(\frac{\hbar\omega}{E_0}\right)^2 + \cdots \quad (2.40)$$

The efficiency $\epsilon(E)$of the detector can be expanded in terms of $k - k_0$

$$\epsilon(k) = \epsilon(k_0) + (k - k_0)\epsilon'(k) + \frac{(k-k_0)^2}{2}\epsilon''(k) + \ldots \quad (2.41)$$

In which the differentiation with respect to k is indicated by the prime superscript.

Since $E = \hbar\omega$ and $k^2 \propto E$;

$$k = k_o\left(1 - \frac{\hbar\omega}{E_0}\right)^{\frac{1}{2}} = k_o - \frac{k_o}{2}\left(\frac{\hbar\omega}{E_0}\right) - \frac{k_o}{8}\left(\frac{\hbar\omega}{E_0}\right)^2 - \cdots \quad (2.42)$$

Hence $\frac{k\epsilon(k)}{k_0\epsilon(k_0)} = 1 - B_1\left(\frac{\hbar\omega}{E_0}\right) - B_2\left(\frac{\hbar\omega}{E_0}\right)^2 \quad (2.43)$

The nth moment of scattering is given by

$$S_n(Q_0, \omega) = \int_{-\infty}^{\infty} \omega^n S(Q_0, \omega) d\omega \quad (2.44)$$

Using the scattering law , the expression for the intensity is given by ;

$$I_N(Q_0) = \frac{1}{N_u}\frac{d\sigma}{d\Omega} = \int_{-\infty}^{\infty} \frac{k\epsilon(k)}{k_o\epsilon(k_0)}\left(\sum_j \overline{b_j^2}\, S_j^S(Q, \omega) + \sum_j \sum_k \overline{b_j}\,\overline{b_k} S_{jk}^D(Q, \omega)\right) d\omega \quad (2.45)$$

Using equations (2.39) and (2.44) in (2.45), the self scattering part of the intensity considering terms up to the second moment of $S(Q_0, \omega)$can be written as ;

$$I_N{}^S(Q_0) = \sum_j \overline{b_j^2}\,\{S_{0,j}^S(Q_0, \omega) - B_1\frac{\hbar}{E_0}S_{1,j}^S(Q_0, \omega) - B_2\frac{\hbar^2}{{E_0}^2}S_{2,j}^S(Q_0, \omega) - \frac{\hbar {Q_0}^2}{2E_0}S_{1,j}^{S\prime}(Q_0, \omega) +$$

$$B_1\frac{\hbar {Q_0}^2}{2{E_0}^2}S_{2,j}^{S\prime}(Q_0, \omega) + \frac{\hbar^2}{8{E_0}^2}[(2{k_0}^2 - {Q_0}^2)S_{2,j}^{S\prime}(Q_0, \omega) + {Q_0}^4 S_{2,j}^{S\prime\prime}(Q_0, \omega)]\} \quad (2.46)$$

The initial moments given in (2.47) were obtained by Placzek

$$S_{0,j}^S(Q_0, \omega) = 1$$

$$S_{1,j}^S(Q_0, \omega) = \frac{\hbar Q_0^2}{2M_j}$$

$$S_{2,j}^S(Q_0, \omega) = \frac{\hbar^2 Q_0^4}{4M_j^2} + \frac{2}{2}\frac{\overline{\kappa_j} Q_0^2}{M_j} \quad (2.47)$$

where the average kinetic energy of a j atom of mass M_j is $\overline{\kappa_j}$. The distinct part of the intensity will have a similar expression but the moments of $S(Q_0, \omega)$ are very low with the zeroth moment unity (Lorch (1967)) and can therefore be neglected.

Using the equations (2.47) in equation (2.46) and introducing reductions (Wright (1981)) leads to the expression for $I_N(Q_0)$;

$$I_N(Q_0) = \sum_j \overline{b_j^2} \left\{ 1 - \frac{4C_1 Sin^2\theta}{\mu_j} + \frac{16C_2 Sin^4\theta}{{\mu_j}^2} - \frac{8}{3}\frac{C_3\overline{\kappa_j}}{E_0\mu_j} Sin^2\theta + \frac{1}{2\mu_j}\left[\frac{4Sin^2\theta}{\mu_j} + \frac{2\overline{\kappa_j}}{3E_0}\right]\right\} +$$

$$\sum_j \sum_k \overline{b_j}\,\overline{b_k} \int_0^\infty 4\pi r^2 \rho_{jk}(r) \frac{\sin Q_0 r}{Q_0 r} dr \qquad (2.48)$$

Where μ_j is the mass of the j atom to the mass of a neutron.

The errors in experimental intensity functions may be expressed as having additive (E(Q_0)) part and multiplicative part (e(Q_0)) hence

$$Q_0 i^{"}(Q_0) = [1 + e(Q_0)]Q_0 i'(Q_0) + (Q_0)\mathrm{E}(Q_0) \qquad (2.49)$$

The Fourier transformation of this equation gives

$$D^{"}(r) = \int_0^\infty D'(u)\, P"(r-u)du + R(r) \qquad (2.50)$$

P"(r) called the peak function is the cosine transform of [1+e(Q_0)]

and R(r)which is visible as a ripple at low r is the sine transform of $Q_0\mathrm{E}(Q_0)$.

The radial distribution function N(r) = r T(r), hence the ripple due to R(r) is visible to a lesser extent in the radial distribution function N(r) as compared to that in the total correlation function T(r). Error at a single point Q_p gives rise to a ripple R(r) of period

$2\pi / Q_p$

Hence R(r) =C sin $Q_p r$ (2.51)

where C is a constant.

M. Dixon et al. (1976) found that the statistical spread of data considered as high frequency noise actually results in noise in D(r) beyond the range of r $up\ to \sim 10$Å which is of importance for structural work.

2.5 The Corrections involved in the analysis of neutron data

Neutron diffraction data on the glass and devitrified samples of this work were obtained using the High Q neutron diffractometer at Dhruva Reactor, B.A.R.C., Mumbai. Each finely ground powdered sample was placed in a vanadium can and mounted at the sample position of the diffractometer so that it was symmetrically placed in the neutron beam. A copper monochromator was used, the orientation of which allowed the selection of the wavelength of the neutrons to be used. Several correction factors need to be considered in the analysis of the neutron data. The measured neutron data need to be corrected for absorption, multiple scattering and normalized to the corrected vanadium diffraction patterns to yield absolute intensities and structure factors S(Q).

2.5.1 Sample container and background corrections

Hollow cylindrical sample containers made of thin sheet vanadium were used in neutron diffraction experiments as vanadium has isotropic incoherent scattering. The height and diameter of the thin walled vanadium can be chosen such that the neutron beam is wider than the diameter and its height is less than the distance between the top and bottom ends of the can. The scattering due to the container has to be subtracted from the data. When the sample itself is prepared in the form of a solid cylinder for neutron diffraction, air background has to be subtracted from the data. The dimensions of the container and the packing density should be precisely known in order to calculate the number of scattering atoms in the neutron beam.

2.5.2 Absorption correction and multiple scattering

The corrections for absorption and multiple scattering are based on the geometric dimensions of the sample or sample container. The absorption coefficient gets modified due to the scattering from the sample as well as the container. Paalman and Pings (1962) have given the expressions for absorption corrections when containers of cylindrical geometries are used. Wright (1974) has given the expression for the absorption correction when the sample itself is of cylindrical shape. Soper and Egelstaff (1980) gave the modified expressions for multiple scattering corrections given by Blech and Averbach (1965) and were used for these data analyses.

For samples of cylindrical geometry the analytical expression is given by;

$$I_m = I_1 \left(\frac{\exp(2\delta)}{2\delta} - 1\right) \quad (2.52)$$

Where I_m is the multiply scattered intensity, I_1 is the singly scattered intensity, δ is the ratio of secondary to primary scattering.

2.5.3 Normalization

The experimental scattered intensities after correction must be normalised to a standard sample of known cross section. This also eliminates the systematic errors introduced during the use of the instrument. Vanadium scatters isotropically with a very low coherent scattering cross section (~0.03 barns) and a high incoherent scattering cross section (~ 5.13 barns) and is thus often used for normalization. Scattering lengths of the sample and the number of scattering atoms of the glass and the normalization standard should be correctly known. The normalized intensity of the sample is then given by;

$$I_N(Q) = \frac{I_{s(c)}(Q) C_R}{I_{v(c)}/S_v(Q)} \quad (2.53)$$

Where $I_{s(c)}$ and $I_{v(c)}$ are the corrected intensities (for background, absorption and multiple scattering) of the sample and vanadium standard respectively. $S_v(Q)$is the vanadium self scattering and C_R is the ratio of the compositional units of the glass sample to the vanadium standard per unit volume.

2.5.4 Renormalization

Despite a well applied normalization procedure, there are instances when the normalized intensity does not oscillate about the self scattering level perfectly. In such cases, "renormalization" must to be done. The incomplete normalization may be caused by errors in the scattering length of the constituents and compositions. The uncertainty in normalization could also occur due to errors in sample density, and cross section of the neutron beam.

Krogh- Moe (1956) and Norman (1957) used the integration method considering errors in the self as well as distinct parts. The renormalized intensity function $I_R(Q)$ is given by

$$I_R(Q) = \alpha I(Q) - \beta S(Q) \quad (2.54)$$

Where α and β are constants, each of which is evaluated separately , assuming that the other is unity, $S(Q)$ is the corrected self scattering (Placzek(1952)), $I(Q)$ is the normalised and corrected intensity function.

2.5.5 Placzek corrections

Neutron static approximation is an assumption made in neutron data analysis that the atoms are stationary during the scattering event. Thus the intensity is integrated at a constant value of Q in $\omega - Q$ space thereby leading to distortions of the self-scattering level which can be eliminated by using the Placzek method given in section 2.4.

For a detector having an energy dependent efficiency, the effective integrated cross section is given by;

$$\frac{d\sigma}{d\Omega} = Nb^2 \int_{-\infty}^{+\infty} \frac{|k|}{|k_o|} \epsilon(k) S(\overline{Q}, \omega) d\omega \qquad (2.55)$$

If M is the mass of the scattering atom which is much greater than the non-negligible mass m of the neutrons, then corrections of the order of m/M at large scattering angles arise due to values of $|k/k_o|$ deviating from the value of 1 (Yarnel et al.(1973)).

2.6 Radial distribution function and Monte Carlo method

The total structure factor S(Q) obtained from neutron data analysis is expressed in terms of partial structure factors $S_{ij}(Q)$;

$$S(Q) = a + \frac{1}{\langle \bar{b} \rangle^2} \sum_{i,j} (c_i c_j)^{1/2} \bar{b_i} \bar{b_j} \left[S_{ij}(Q) - \delta_{ij} \right] \qquad (2.56)$$

Where c_i are the concentration and b_i is the coherent scattering length of the i^{th} component, $\langle \bar{b} \rangle = \left| \sum c_i \bar{b_i} \right|$ and Q = momentum transfer vector.

The pair distribution functions g(r) are obtained by the Fourier transformation of the total structure factor;

$$g(r) = 1 + \frac{1}{2\pi^2 r \rho} \int_0^\infty Q(S(Q) - 1) SinQr dQ \qquad (2.57)$$

Peak positions are obtained from the total correlation function T(r) given by ;

$$T(r) = 4\pi r \rho + \frac{2}{\pi} \int_0^\infty Q(S(Q) - 1) SinQr \, dQ \qquad (2.58)$$

where ρ is the bulk number density of the scattering matrix.

The radial distribution function N(r) given by;

$N(r) = r\,T(r) = 4\pi r^2 \boldsymbol{\rho}\, g(r)$ (2.59)

N(r) is used to derive the average number of atoms lying within a range r to r+dr of a given atom.

After Fourier transformation of S(Q), the T(r) and N(r) functions were used in obtaining correlation distances and coordination numbers.

The numerical radial density function g(r) was also generated by using a MCGR program in an inverse method called the Monte Carlo method. This method is preferred as it helps in reducing the truncation errors that occur in conventional methods such as those that arise while using the Lorch modification function. In this method a trial g(r) having an analytically known S(Q) is taken and modified randomly for a chosen r . For every change in g(r), its corresponding interference structure factor $S^{exp}(Q)$ gets modified at every point analytically. The deviation of the obtained interference function from the experimental value can be computed from the expression

$$\chi^2 = \frac{1}{n}\sum\{\left(S^{exp}(Q) - S^{cal}(Q)\right)^2/\sigma^2\} \quad (2.60)$$

Where σ is the statistical error and n is is the number of experimental data.

This move is accepted if the value of χ^2 reduces, where χ is a function related to the difference between experimental and calculated structure factors. However if it increases then the move is accepted with a probability of $\exp(-\Delta\chi^2/T)$. This process is repeated until a suitable value of $\chi^2$is reached at which point the experimental and calculated structure factor matches for the investigated glass.The T(r) and N(r) functions obtained from g(r) derived by this method are fitted to obtain bond lengths and coordination numbers. In particular, the areas of the first few peaks in N(r) were related to coordination numbers of the constituent atoms of the composition unit (Mc Greevy et al (1988), Pusztai (1999), Rao et al. (1998)).

2.7 Extended X- ray Absorption Fine Structure (EXAFS)

For measurements in the transmission mode, the sample is placed between two ionization chamber detectors at room temperature.

The measured absorbance of the sample is obtained as;

$$\mu x = -\ln(\frac{I_t}{I_0}) \quad (2.61)$$

Where *x* is the thickness of the sample, I_0 is the incident flux and I_t is the transmitted intensity. The conversion of the measured absorption spectra to energy dependent absorption coefficient $\mu(E)$ was done.

The absorption function $\chi(E)$was found as given by Konigsberger and Prince (1988);

$$\chi(E) = (\mu(E) - \mu_0(E_0))/\Delta\,\mu_0(E_0) \quad (2.62)$$

where E_0 is the energy of the absorption edge, $\mu_0(E_0)$ is the background of the bare atom and $\Delta\,\mu_0(E_0)$ is the rise in the $\mu(E)$ value at the absorption edge
The energy scale was converted to the photoelectron wave number scale (k) as per the equation

$$k = \sqrt{\frac{2m(E-Eo)}{\hbar^2}} \quad (2.63)$$

Where m is the mass of the electron and E_o is the absorption edge energy. The conversion of the energy dependent absorption coefficient $\mu(E)$ to wave number dependent $\mu(k)$ and the energy dependent absorption function $\chi(E)$ to wavenumber dependent $\chi(k)$ was done. The k^3 weighted (k) functions were Fourier transformed to r space so as to generate $\chi(r)$ v/s r in terms of real distances to the absorbing atom.

The analysis of the EXAFS data is carried out following the standard procedure (Sharaf El-Deen (2008), Kelly(2008)) using the IFEFFIT software package (Newville(1995)) in which background correction and normalisation is done using ATHENA while modelling and fitting was done using ARTHEMIS. This also includes data reduction and Fourier transform to derive the $\chi(R)$ versus R plots from the absorption spectra, generation of the theoretical EXAFS spectra starting from an assumed crystallographic structure and finally fitting of the experimental $\chi(R)$ versus R data with the theoretical ones using the FEFF 6.0 code.

The bond distances, co-ordination numbers (including scattering amplitudes) and disorder (Debye-Waller) factors (σ^2), which give the mean-square fluctuations in the distances, have been used as fitting parameters. The k range for Fourier transform and the R range

for data fitting have been chosen in such a way that in each case during fitting, the number of free variables were always kept below the upper limit set by the Nyquist theorem (N_{free}= $2\Delta k\Delta r/\pi + 1$) (Kelly et al. (2008)).

The goodness of the fit in the above process is generally expressed by the R_{factor} which is defined as:

$$R_{factor} = \sum \frac{[\mathrm{Im}(\chi_{dat}(r_i) - \chi_{th}(r_i)]^2 + [\mathrm{Re}(\chi_{dat}(r_i) - \chi_{th}(r_i)]^2}{[\mathrm{Im}(\chi_{dat}(r_i)]^2 + [\mathrm{Re}(\chi_{dat}(r_i)]^2} \qquad (2.64)$$

where, χ_{dat} and χ_{th} refer to the experimental and theoretical $\chi(r)$ values respectively and Im and Re refer to the imaginary and real parts of the respective quantities. The R_{factor} of all the fitting are less than 0.01 which assures good fitting of the data.
The coordination number and the correlation lengths are then obtained.

2.8 Raman scattering

When an a light beam passes through matter, the oscillatory electric field induces polarization in its molecule. The induced dipole will then radiate scattered light. If light undergoes elastic scattering, it is called Rayleigh scattering while if it undergoes inelastic scattering then it is called Raman scattering.

2.8.1 Classical approach.

The dipole moment μ of a molecule having no excitations placed in an electric field E depends on the polarizability α of the molecule given as ;

$$\mu = \alpha E \qquad (2.65)$$

The induced polarization of such a molecule in terms of electric susceptibility will be given by

$$P = \varepsilon_o \chi E \qquad (2.66)$$

If the electric field is given by given by

$$\mathrm{E} = \mathrm{Eo\ Cos\ \omega t} \qquad (2.67)$$

The induced dipole will be

$$\mu = \alpha\ \mathrm{Eo\ Cos\ \omega t} \qquad (2.68)$$

and will radiate with the same frequency ω giving rise to Rayleigh scattering.

However if excitations are present in the molecule, then the electric susceptibility and the induced polarization will be modulated due to fluctuations of dynamical variables ξ.

The polarization will now have an additional term due to the fluctuations and is given by

$$P = \varepsilon_o \chi E + \varepsilon_o \chi' \xi E \qquad (2.69)$$

where $\chi' = \frac{d\chi}{d\xi}$

The first term in this equation gives rise to simple elastic scattering while the second term contributes to inelastic features to the scattering.

As most of the excitations are vibrations, the vibrational displacement q will be the dynamical variable. The polarizability of the molecule can be expressed in a Taylor series

$$\alpha = \alpha_o + \left[\frac{\partial \alpha}{\partial q_k}\right]_o q_k + \left[\frac{\partial^2 \alpha}{\partial {q_k}^2}\right] \frac{{q_k}^2}{2} + \ldots\ldots\ldots\ldots \qquad (2.70)$$

where k represents different normal modes of the molecule.

For a molecule oscillating with frequency ω_m , neglecting higher powers we can write

$$P = \alpha_o \text{Eo Cos } \omega t + \left[\frac{\partial \alpha}{\partial q_k}\right]_o E_o {q^o}_k \frac{1}{2}(Cos(\omega + \omega_m)t + (Cos(\omega - \omega_m)t) \qquad (2.71)$$

in which the first term describes the Rayleigh scattering and the second term relates to Raman Stokes and anti-Stokes lines (B. Schrader(1995).

2.8.2 Quantum approach

In this the transitions between vibrational states involves second order time dependent perturbation theory using which an expression for the Raman transition probability in terms of time dependent wave functions can be obtained .

The Raman transition probability is equal to;

$$\sum_k \frac{\int {\psi_j}^* e\, E_o r\, \psi_k \, d\tau . \int {\psi_k}^* e\, E_o r\, \psi_G \, d\tau}{\omega_{jk} + \omega} \qquad (2.72)$$

Here ψ_j,ψ_k are orthonormal stationary state wave functions, ω_{jk} is the frequency corresponding to transition from k state (considered to be a state of higher energy) to the first excited vibrational j state (considered to be near the ground state G) and τ is the life time of the system between fluctuations (Howrath (1973)).

Considering j to be the first excited vibrational state, then for the Raman stokes line the intensity would be proportional to the product of the above expression for Raman transition probability and the fraction of ground state vibrators. The excitation is from the G state to the higher excited state shown in green and then transition from the excited state to the j state shown in red in Figure 2.2.

The anti-Stokes line can be also visualised by just reversing j and G states. In this the excitation is from the j state (less populated initially) to the higher excited state shown in green and then transition from the excited state to the G state giving lesser intensity than the stokes line shown in red (Boyd (1992)).

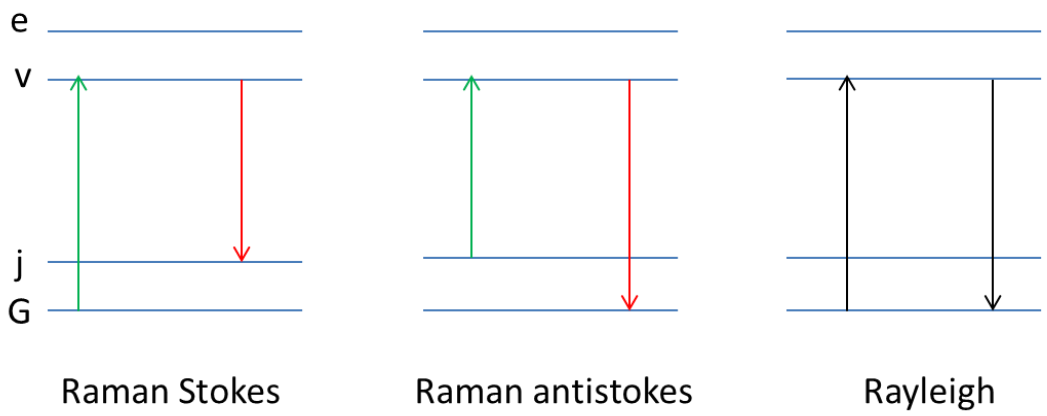

Figure 2.2: Raman stokes, Raman anti-Stokes and Rayleigh scattering representation on energy level diagram.

Raman scattering differential cross section due to an elementary excitation is given by Long (2002) as;

$$\frac{d^2\sigma}{d\Omega d\omega_s} = \frac{V\,\omega_1\omega^3 s}{(4\pi\varepsilon_0)^2 c^4 |E_1|^2}\langle \hat{\varepsilon}_s . P_s^{*} \hat{\varepsilon}_s . P_s \rangle_{\omega_s} \qquad (2.73)$$

where c is the speed of light, ε_s is the polarization of the scattered light, V is the light scattering volume, $\langle \hat{\varepsilon}_s . P_s^{*} \hat{\varepsilon}_s . P_s \rangle_{\omega_s}$ is the spectral density of fluctuations in polarization.

Spontaneous Raman scattering is an incoherent and a weak process having a low scattering cross section (~ 10^{-6}cm^{-1}) for Raman Stokes scattering. Stimulated Raman scattering is a better process in which a strong laser pump beam transfers energy to the propagating signal beam and excites vibrational modes.

Hellwarth (1963) related the spontaneous Raman scattering and Stimulated Raman scattering process and obtained an expression for the Raman gain coefficient g given by

$$g\ (\text{cm/W}) = \frac{4\pi^2 N c^2}{\hbar \omega_s^2 \omega_p n_s^2}\left(\frac{\partial^2\sigma}{\partial_\omega \partial_\Omega}\right) \qquad (2.74)$$

where ω_s is the Stokes frequency, ω_p is the laser pump frequency, n_s is the refractive index at the Stokes wavelength and $\left(\frac{\partial^2\sigma}{\partial_\omega \partial_\Omega}\right)$ is the differential Raman cross section.

References

1. Basu S., Nayak C., Yadav A. K., Agrawal A., Poswal A. K., Bhattacharyya D., Jha S. N. and Sahoo N. K., J. Phys.: Conf. Ser. 493 (2014) 012032.
2. Blech L.A. and Averbach B. L., Phys. Rev. 137 (1965) 1113
3. Boyd R. W., Non linear Optics, Academic press (1992).
4. Dixon M., Wright A. C., P. Hutchinson, U.K.A.E.A. Harwell report R 8619 (1976)
5. Fisher H.E., Barnes A. C., Salmon P. S., Rep. Prog.Phys.69 (2006) 233
6. Hellwarth R. W., Phys. Rev. 130 (1963) 1850
7. Howrath O., Theory of spectroscopy, Halsted printing press (1973)
8. Kelly S.D., Hesterberg D.and Ravel B., Analysis of soils and minerals using X-ray absorption spectroscopy (2008) 387-464; Methods of Soil Analysis - Part 5. Mineralogical Methods
9. Konigsberger D.C., and Prince R., X ray Absorption: Principles, Applications, Techniques of EXAFS, SEXAFS and XANES. Wiley, New York, 1988.
10. Krogh-Moe J., ActaCryst. 9 (1956) 551
11. Long D. A., The Raman effect, John Wiley and Sons Press (2002)
12. Lorch E. A., Thesis, Univ. of Birmingham (1967)
13. Lorch E. A., J. Phys. C 2(1969) 229
14. McGreeevy R. L., Pusztai L., Mol. Simu. Vol.1 (1988) 359-367.
15. Newville M., Ravel B., Haskel D., Rehr J.J., Stern E.A. and Yacoby Y., Physica B 154 (1995) 208.

16. Norman N., Actacryst. 10 (1957) 370
17. Paalman N. H. and Pings C. J., J. Appl. Phys. 33 (1962) 2635
18. Placzek G., Phys. Rev. 86(3) (1952) 377-388
19. Poswal A. K., Agrawal A., Yadav A. K., Nayak C., Basu S., Kane S. R., Garg C. K., Bhattachryya D., Jha S. N. and. Sahoo N. K., AIP Conf. Proc. 1591 (2014) 649.
20. Pusztai L., McGreevy R. L., J. Neutron Research, 8 (1999) 17-35.
21. Rao N. R., Krishna P.S.R., Basu S., Dasannacharya B.A., Sangunni K.S., Gopal E.S.R., J. Non-Cryst. Sol., 240 (1998) 221-231.
22. Rawson H., Inorganic Glass-Forming Systems, Academic Press (1967).
23. Schrader B., Infrared and Raman Spectroscopy: Methods and applications VCH (1995)
24. Sharaf El-Deen L. M., Al Salhi M. S., Elkholy M. M., J. of Alloys and Compounds 465 (2008) 333-339
25. Soper A. K.and Egelstaff P. A., Nucl. Instrum. Meth. (1980) 415
26. Van Hove L., Phys. Rev. 95 (1954)249
27. Wright A. C., Advances in Structure Research by Diffraction Methods, 5 (1974) 1-84
28. Wright A. C., University of Reading publication (1981)
29. Yarnel J. L., Kartz M. J., Wenzel R. G., Koenig S. H., Phys. Rev. A7 (1973) 2130
30. Zachariasen W. H., J. Am. Chem. Soc. 54 (1932) 3841-3851

CHAPTER 3

EXPERIMENTAL METHODS

The principles and essential features of the various experimental techniques that were used in this work are described in this Chapter.

3.1 Fourier Transform Infrared Spectroscopy

The Infra-Red (IR) range is from 12500 cm^{-1} to 10 cm^{-1} and can be divided into the following three regions:

NIR - Near Infra-Red region 12500 cm^{-1}- 4000 cm^{-1}

MIR - Mid Infra-Red region 4000 cm^{-1} - 400 cm^{-1}

FIR - Far Infra-Red region 1000 cm^{-1} - 50 cm^{-1}

A Fourier Transform Infra-Red (FTIR) spectrometer consists of source, interferometer, detector and computer. The beam of Infra-Red radiation is split by the beam splitter of the interferometer. The partly reflected beam strikes the movable mirror and is reflected back while the partly transmitted beam strikes the stationary mirror and is reflected back. Both these beams recombine at the beam splitter. When the distance travelled by the two beams is different, an optical path difference is introduced between the two beams. The spectral resolution in an FTIR depends on the maximum value of achievable optical path difference. The beam is then guided through the sample and the detected signal is called as interferogram which is a function of the mirror position or time. These raw data are Fourier transformed to obtain the Fourier transformed infrared spectrum which is a function of infrared frequency or wavelength. A schematic diagram of an FTIR spectrophotometer is shown in the Figure 3.1.

When a vibrational mode is excited due to change in the dipole moment associated with it, IR absorption takes place. Alben and Boutron (1975) gave the expression for the dipole moment M in terms of the displacement vectors u_i as

$$M = \sum_{i(j,k)}[(r_{ik} - r_{ij})(u_i - u_j).r_{ij} - (u_i - u_k).r_{ik}] \qquad (3.1.1)$$

The bond compressions are $C_{ij} = (u_i - u_j).r_{ij}$

where r_{ij} ia a unit vector from a site i to a site j.

Thus $M = 2\sum_i(\sum_j C_{ij})(\sum_k r_{ik})$

An asymmetrical charge distribution gives rise to dipole moment, hence for a material having perfect tetrahedral symmetry $\sum_{ij} r_{ij} = 0$ and the induced dipole moment is also zero.

The Absorbance in a sample is given by the relation:

$$A = \log(I_0/I) \qquad (3.1.2)$$

where I_0 is the intensity of the background spectrum

I is the intensity of the sample spectrum

Absorbance is also given in terms of the Beer-Lambert's law as ;

$$A = C\,l\,\varepsilon \qquad (3.1.3)$$

where 'C' is the concentration of molecules in the sample, l is the path length and ε is the absorptivity.

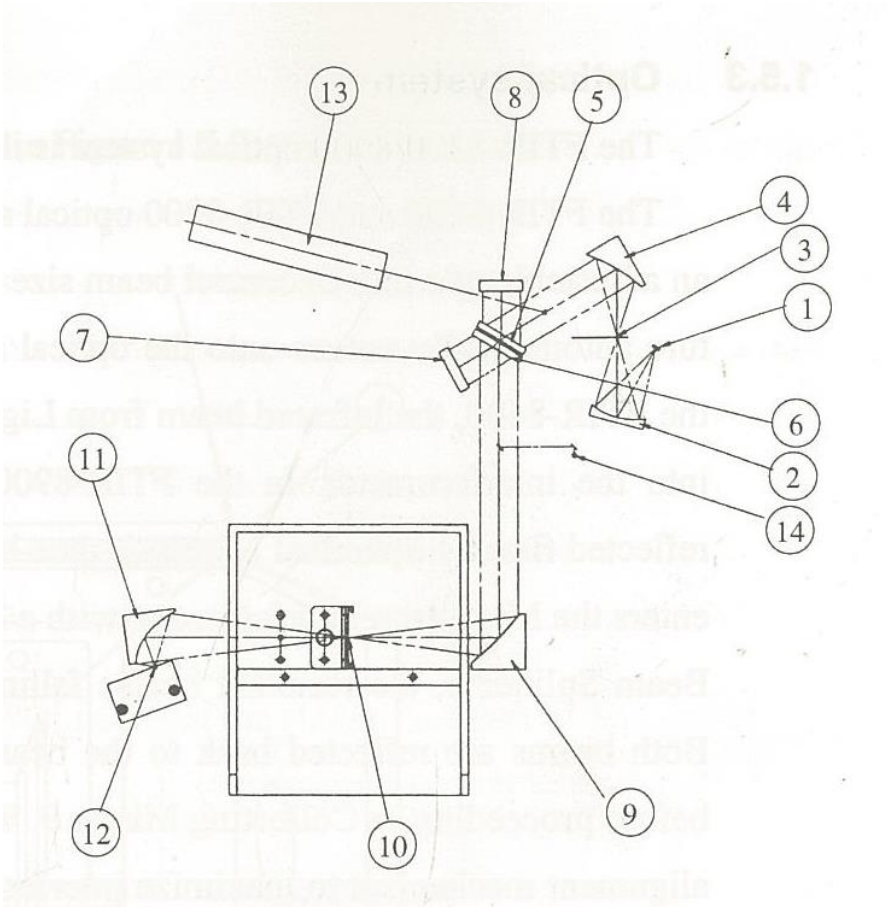

1. Source
2. Spherical mirror
3. Aperture
4. Collimator mirror
5. Beam splitter
6. Compensator
7. Fixed Mirror
8. Moving mirror
9. Paraboloidal mirror
10. Collecting mirror
11. Highly sensitive pyroelectric detector
12 He- Ne- Laser
13. 1/8 wavelength plate
14. He-Ne Laser half mirror
15. Polarised beam splitter
16. He-Ne Laser detector
17. He-Ne Laser beam introducing mirror

Figure 3.1 : Schematic diagram of the FTIR-8900 spectrophotometer (From Shimadzu manual of FTIR-8900)

Fourier Transform Infra-Red spectroscopic data on all the samples in this study are collected using Shimadzu 8900 FTIR spectrometer in the 4000-200 cm^{-1} range at ambient temperature. Sample pellets were prepared by pressing finely ground and well mixed

powder consisting of 2mg of each type of glass powder with 200 mg of Potassium Bromide (KBr) under 6 tons pressure.

3.2 Ultra Violet-Visible Spectroscopy (UV- Visible)

UV-Visible absorption spectroscopy (Banwell (1983)) is an important and useful method for studying the structure of materials and their electronic states. In atoms and molecules absorption of visible and ultra-violet radiation leads to excitation of electrons from lower to higher energy levels. The UV-Visible range of wavelength is from about 200nm to 800nm. Figure 3.2 shows Shimadzu (UV-2401) UV- Visible spectrophotometer optical system.

In the transmittance mode, the UV-Visible spectrophotometer compares the intensity of the light going through the sample to the incident intensity of light striking the sample.

$$\text{Transmittance} = (I/I_o) \tag{3.2.1}$$

In the reflectance mode the intensity of sample material reflected light is compared with the reference material reflected light and absorbance is obtained. From the graph of absorbance versus wavelength, the extrapolation of the linear portion of the measured function cuts the wavelength axis from which the cut off wavelength is obtained and the band gap energy can be calculated using the formula

$$E = \frac{hc}{\lambda} \tag{3.2.2}$$

where $h = 6.626 * 10^{-34}$ Joules second is the Planks constant, $c = 3.0*10^{8}$ meter/second is the speed of light and λ is the cut off wavelength.

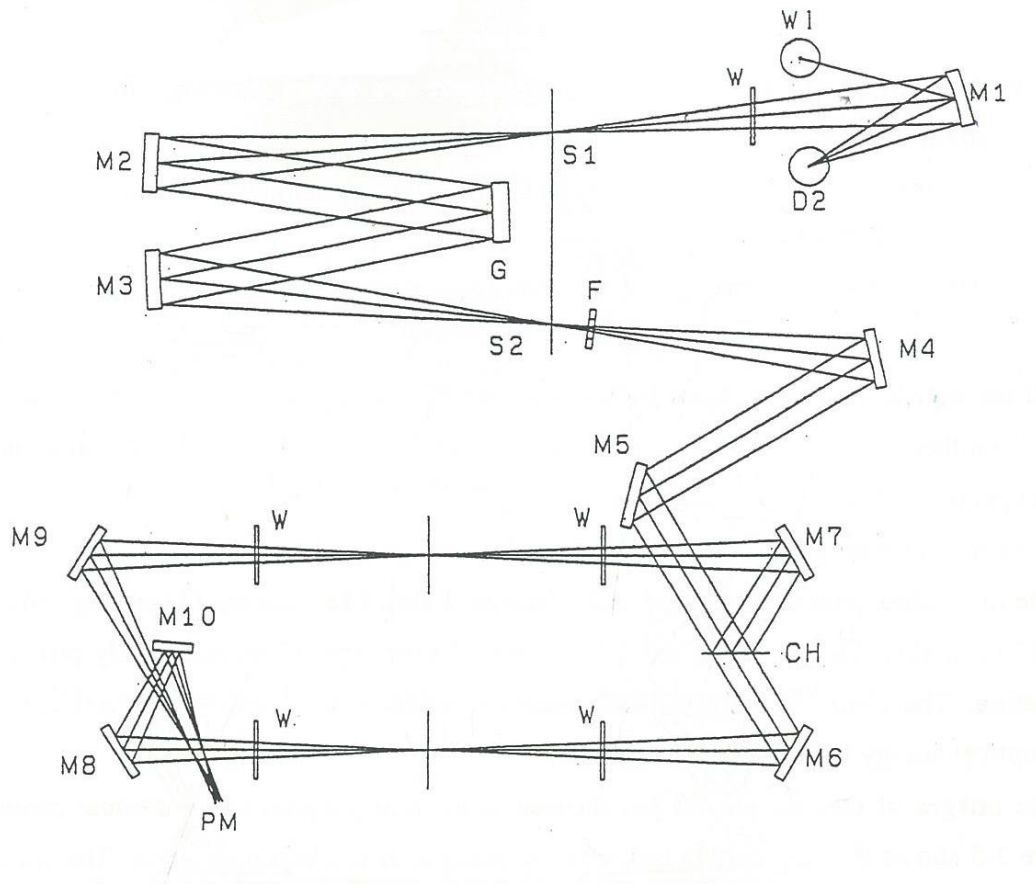

D2 Deuterium lamp	G diffraction grating
W1 Halogen lamp	S2 Exit slit
S1 Entrance slit	F Filters
W Quartz window	CH Beam choppers
M1-M10 Mirrors	PM Photo multiplier

Figure 3.2: UV- Visible spectrometer Optical system (From Shimadzu UV-2401 Manual)

UV-Visible spectroscopic studies on all the glasses in this study were performed using Shimadzu UV-2401 PC spectrophotometer in the range of 200 -800 nm at room temperature .

3.3 Differential Thermal Analysis (DTA)

Differential thermal analysis (Shriver and Atkins.(2006) , West (2001)) is a thermo-analytic technique in which the change in physical property of the sample is measured relative to an imposed change in temperature. The same amount of heat is allowed to flow in the sample and the reference. During an endothermic event (eg. melting), the temperature of the sample will be lower than that of the reference showing a ‘ dip ‘ or minimum in the DTA curve, while during an exothermic event (eg. crystallization) the temperature of the sample will be higher than that of the reference resulting in a maximum in the DTA curve. The area under the DTA curve is a measure of the enthalpy of the sample and is independent of the heat capacity of the sample.

The peak area can be written as

$$A = \frac{mq}{Kg} \qquad 3.3.1$$

where m is the mass of the sample, q is the change in enthalpy per unit mass, K is the thermal conductivity of the sample and g is the measured shape factor.

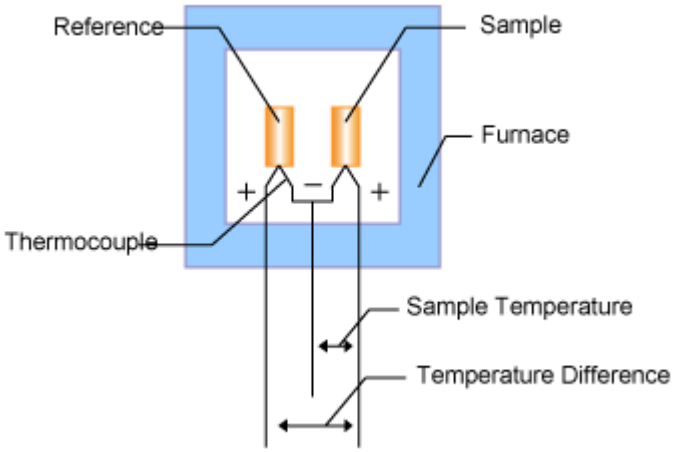

Figure 3.3 : The schematic diagram showing thermocouples in a DTA set up (From Hitachi manual)

The DTA setup consists of a furnace assembly, sample crucibles, temperature programmer and recording system. The temperature programmer is programmed to obtain constant heating rates in the furnace and the recording system records the corresponding temperature variation with respect to time or temperature. Two thermocouples -one for the sample and the other for the reference are surrounded by a ceramic or metallic block to ensure uniform heat distribution in the furnace. For the measurements in this work, the sample was held in a platinum crucible placed over the flat bead top of the thermocouple in a snug fit. The schematic diagram in Figure 3.3 shows the use of thermocouples to measure the temperatures of the reference and the sample.

In Differential Scanning Calorimetry (DSC), the temperatures of the reference and the sample are both increased at a constant rate. In DSC the heat flowing to the sample and the heat flowing to reference material are recorded at a given temperature.

In thermogravimetric analysis (DTG), changes in the mass of the sample as a function of time or temperature are measured under a controlled atmosphere.

Differential thermal analyses of all the glasses studied was done using Shimadzu DTG-60 analyser at a rate of 10^{o}C /min from 30^{o}C to 1000^{o}C

3.4 Raman spectroscopy

Raman spectroscopy depends on the principle of interaction of light with matter. It is a light scattering process which can provide information about molecular vibrations as well as those of the crystal lattice. During the interaction of light with matter most of the photons undergo elastic scattering or Rayleigh scattering in which the photons are scattered at the same energy as that of the incident photons. Some photons undergo inelastic or Raman scattering in which the photons are scattered at a different energy or frequency than that of the incident photon. Raman shift is a measure of the change in energy between the scattered photon and that of the incident photon. Stokes lines have a longer wavelength or lower energy than that of the incident radiation while the anti-Stokes lines have shorter wavelengths or higher energies than the incident radiation.

Raman spectroscopy is based on the changes in molecular polarizability which can occur due to the deformation of the electron cloud of a molecule on interaction with light. Bonds between homo-nuclear atoms can undergo a change in polarizability on interaction with

photons and hence become Raman active even though such bonds are unresponsive to infrared radiation.

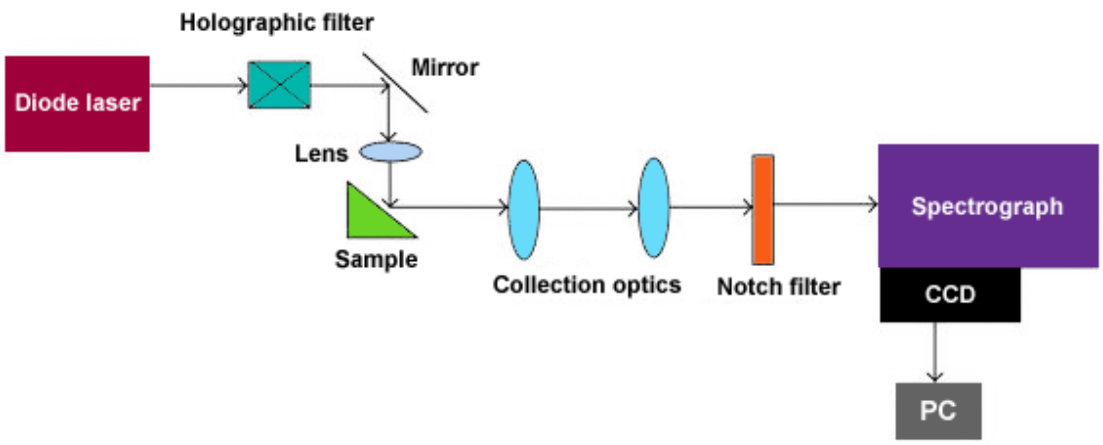

Figure 3.4: Schematic diagram of a Raman spectrometer setup (From Princeton manual)

A Raman spectrometer consists of an excitation source such as a solid state laser. Shorter wavelengths have a better Raman scattering cross-section. However, in order to overcome the incidence of fluorescence that increases at shorter wavelengths a laser of 785 nm is preferred. Fiber optic cables collect the laser energy from the sample and an edge or notch filter removes the Rayleigh lines and the anti-Stokes lines. A CCD detector is used to capture the Stokes scattered light through a grating to give the Raman spectrum. A schematic diagram of a Raman spectrometer setup is shown in Figure 3.4.

The Raman scattering intensity is plotted against the Raman shift which is the difference between the frequency of scattered light and the incident beam and is expressed as wave number in cm^{-1} (inversely proportional to wavelength).

A Linkam TS 1500 spectrometer at SSPD, BARC, and Mumbai was used to collect the Raman spectroscopic data on all the glass samples in this study. The sample was taken in the form of a small piece and scanned from 80 to 3000 cm^{-1} at room temperature. A 532 nm emission from a frequency doubled solid state laser (diode pumped) of power 15mW was used to excite the Raman spectra (Roy et al. (1992).

3.5 Extended X-ray Absorption Fine Structure (EXAFS)

EXAFS is an excellent method used to extract information about short range order and local structure around the investigated element. The extended absorption spectrum can be considered in terms of the energy range as :

3.5.1 XANES – X-ray Absorption Near Edge Structure

The energy range from -50 eV to +50 eV around the absorption edge is the range of XANES . It gives information about the oxidation state of an atom, bond angles and energy bandwidth.

3.5.2 EXAFS –Extended X-ray Absorption Fine Structure

The range of EXAFS is from 50 eV to an upper limit in the range 700 eV to 1000 eV above the absorption edge. The bond length, coordination number and the disorder factor can be obtained from EXAFS.

XANES can be obtained in: 1) Transmission mode 2) Fluorescence mode in which X-rays are detected and 3) The total electron yield count mode in which the secondary conversion electrons are detected. XANES arises due to the excitation of an inner shell electron to a higher shell by an incident photon, thereby involving an electronic transition. Hence the absorption coefficient μ(E) can be written in terms of a transition matrix element coupling the initial state |I > to the final state < f| .

If ε is the polarization vector due to the photon and r is the position vector of the photoelectron, we can write;

$$\mu(E) = |< f| \varepsilon.r|I>|^2 \qquad (3.5.1)$$

The allowable final state is governed by selection rules as the electric dipole operator governs the coupling of the two states. For Example, in a K edge absorption process a 1s level electron is excited to occupy the lowest p state.

EXAFS is caused by the absorption of the incident X-ray photonic waves by the interference pattern caused by the interaction of the inner core photoelectrons ejected by the resonant radiation and the electrons which are backscattered from the close neighbour atoms. The absorbing atom's final state wave function gets modulated and is related to the radial distribution function of the central absorbing atom.

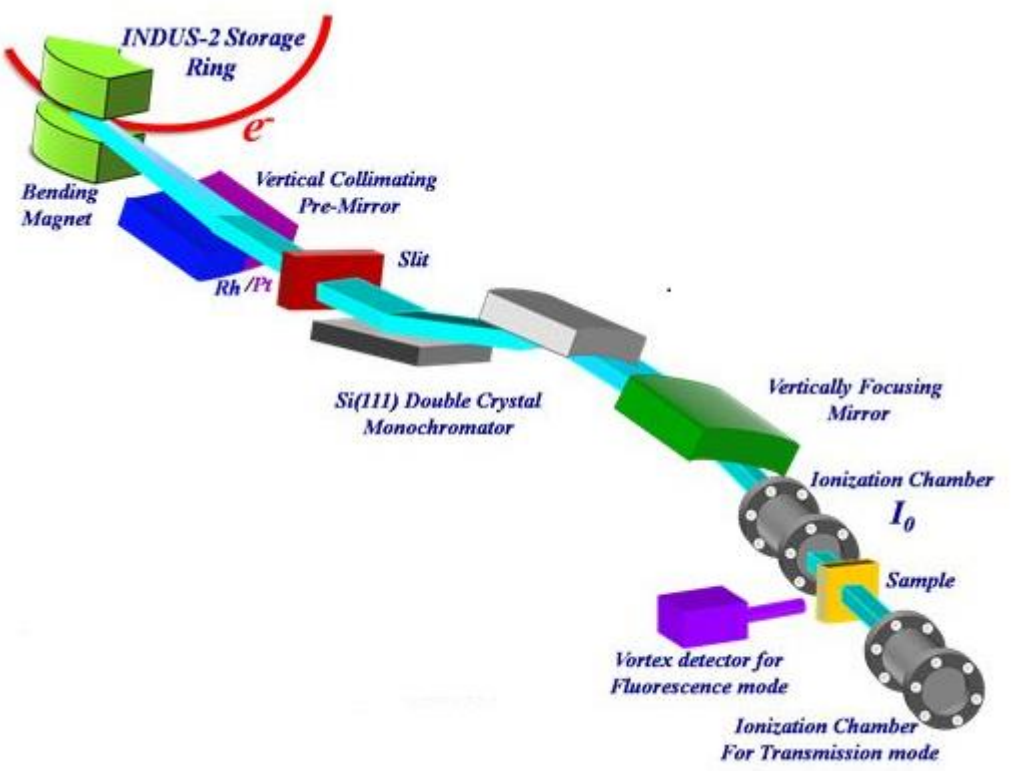

Figure 3.5: Experimental set up of beam line BL-09 at RRCAT Indore (From website of RRCAT)

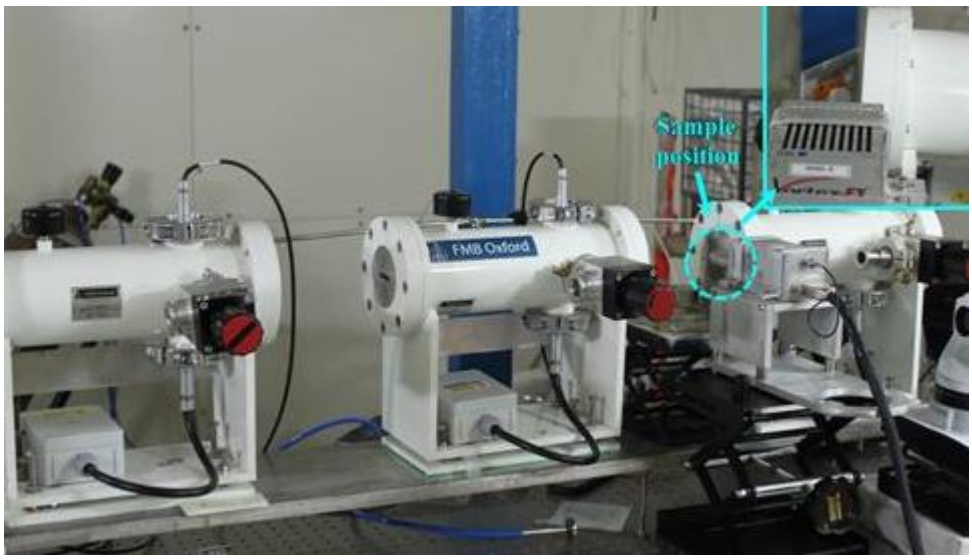

Figure 3.6: The Sample environment at the beam line BL-09, RRCAT, Indore (From website of RRCAT).

The X-ray Absorption Spectroscopy **(**XAS) measurements on the glass samples have been carried out at Ge K edge, LaL_3 edge, Pr L_3 edge and NdL_3 edge with the Scanning EXAFS Beamline (BL-09) at the INDUS-2 Synchrotron Source (2.5 GeV, 100 mA) at the Raja Ramanna Centre for Advanced Technology (RRCAT), Indore, India (Poswal et al. (2014), Basu et al. (2014)). Finely ground mixture of appropriate weight (~ 25mg) of glass powder and cellulose were pressed to form the sample pellets. The experimental set up of the beam line BL-09 at RRCAT, Indore is shown in Figure 3.5 and the sample environment in this facility is shown in Figure 3.6.

3.6 X-ray diffraction

X-rays consist of high energy electromagnetic radiation having short wavelength (~ 0.01nm to 10nm) which are produced from the collision of high energy electrons with a metal target. X-rays have been widely used for structure determinations of crystalline materials as their wavelength is comparable to the interatomic distance. However it is not especially favoured for structure determination of disordered materials. The reasons for this are that the scattered intensities are low at higher scattering angles with a consequent lower limit of the maximum momentum transfer (Q_{max}).

For the production of X-ray photons the filament in a cathode ray tube is heated to produce electrons which are accelerated by a high voltage (~50 kV) and bombarded on to a metallic target (such as Cu, Mo, Fe or Ag). The kinetic energy of the electrons gets converted to the energy of X-ray radiation due to the rapid deceleration of the electrons within the target. When an incident electron knocks off an inner shell electron from the atom of the target material, an outer shell electron occupies the vacancy created by the emitted electron. The difference in energy is released in the form of X-rays. Thus we have a characteristic line spectrum superimposed on a continuous background due to bremsstrahlung. The most preferred material for use as a target in the production of X-rays is copper giving Cu(K_α) radiation of wavelength of 1.5418 Å. Monochromatic X-rays are produced for X-ray diffraction experiments by using filter foils or crystal monochromators.

The basic elements of an X-ray diffractometer are X-ray tube, goniometer, sample holder, and X-ray detector. X-ray diffraction is a non-destructive technique used to determine the structural properties and crystalline phases.

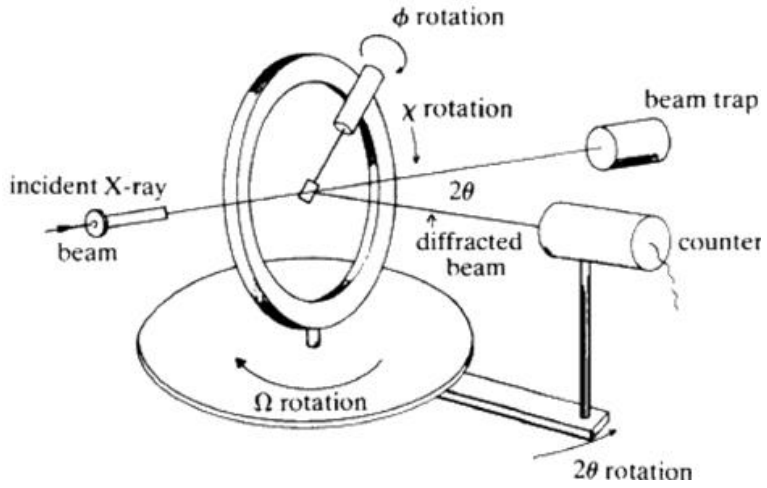

Figure 3.7 : Schematic diagram of single crystal X-ray diffractometer (From Clark and Dutrow)

In an atom, X-rays are scattered by electrons in all directions. The scattered intensity depends on the angle between the incident beam and the scattering direction (2θ). The diffraction pattern of a material is a plot of diffraction intensity I versus 2θ angle and shows several intensity peaks at different 2θ values. Each peak arises due to diffraction from a specific crystallographic plane when the scattered wave satisfies the Bragg's law

$$2\,d\,sin\theta = n\lambda \qquad (3.6.1)$$

where d is the interplanar spacing, 2θ is the scattering angle, n is the order of the diffraction and λ is the wavelength of X-rays (Bragg (1913)).

A schematic diagram of an XRD experimental set up is shown in Figure 3.7. For the measurement of Xray diffraction spectrum, finely ground sample powder is pressed into a shallow depression of a glass plate which is mounted onto a sample holder. The collimated X-rays are focussed on the sample. An instrument called a goniometer rotates the sample and the detector by the appropriate angles. The sample rotates at an angle θ while the detector rotates at an angle 2θ to detect the diffracted X-rays and record the intensity of the reflected X-rays. When the Braggs law is satisfied, constructive interference takes place and a peak in intensity is observed. The recorded X-ray signal is processed and converted to a count rate using a scintillation detector or a proportional counter.

Crystalline phases in a material can be identified by matching the obtained spectrum with a standard spectrum. The crystallite size can be obtained from the line broadening using the Debye-Scherer's formula (C. Kittel (1976)).

$$D = \frac{K\lambda}{\beta \, Cos\theta} \qquad (3.6.2)$$

Where K = 0.89, λ is the wavelength of X-rays, β is full width at half maximum (FWHM) and 2θ is the scattering angle for a Bragg reflection.

The XRD data on all the glass samples are collected using Rigaku Ultima IV X-Ray Diffractometer. X-rays of incident wavelength 1.54Å from a Cu K_α target are used for diffraction. Data on the samples were measured with a 2θ scattering angular range from 10^o to 80^o.

3.7 Neutron diffraction

Neutron were discovered by J. Chadwick in 1932, Neutron has a mass 1.67 * 10^{-27} kg and ½ spin .Thermal neutron of energy 25MeV has a velocity of 2200 m/s. Neutrons being neutral in charge can penetrate deep and interact with matter, it has a magnetic moment and thus can also interact with magnetic materials.

Neutron diffraction or elastic neutron scattering is based on Bragg's law and can be used to study ordered systems or crystalline materials as well as short-range order in disordered systems or amorphous materials. Neutron diffraction can be used to obtain the atomic structure from its interaction with atomic nuclei and information such as the bond length and coordination numbers or the magnetic structure from the interaction of the magnetic moments of neutrons with the magnetic moments of the atoms.

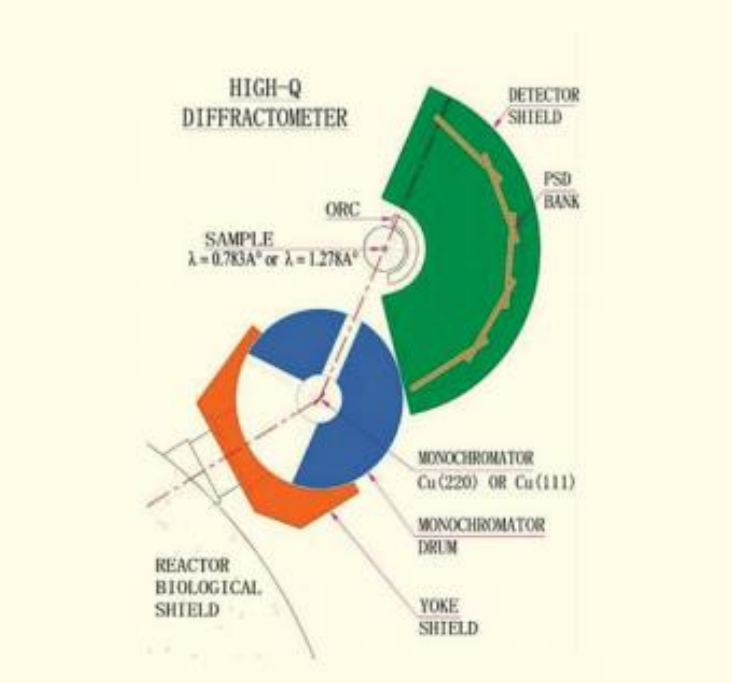

Figure 3.8 : Schematic diagram of the high Q diffractometer at Dhruva reactor, BARC, Mumbai, India (From Neutron Beam Research Facility manual, BARC website).

Neutron diffraction experiments on the glass samples studied were performed on the high Q diffractometer in the reactor hall at the Dhruva Reactor, Bhabha Atomic Research Centre, Mumbai . A schematic layout of this facility is shown in the Figure 3.8. It uses a Copper (2,2,0) monochromator of wavelength $\lambda = 0.783$Å and 10 detectors (PSDs) at 5 positions, the flux at the sample is $3* 10^5$ n/cm^2 /sec. The sample size is 5- 10 mm diameter, 40 mm high. The scattering angle is $3^o < 2\theta < 140^o$ with Q range 0.3Å^{-1} - 15Å^{-1}.

References

1. Alben R. and Boutron P., Science, 187 (1975) 430
2. Banwell C. N., Fundamentals of molecular spectroscopy, 3rd edition, May 1983 University of Sussex
3. Basu S., Nayak C., Yadav A. K., Agrawal A., Poswal A. K., Bhattacharyya D., Jha S. N. and Sahoo N. K., J. Phys.: Conf. Ser. 493 (2014) 012032.
4. Bragg W. L., Proceedings of the Cambridge Philosophical society, 17 (1913) 43-57
5. Clark C. M., Dutrow B. L. (Geochemical Instrumentation)
6. Hitachi high Technologies, America, manual.
7. Kittel C., Introduction to Solid State Physics, New York, John Wiley and Sons (1976)

8. Neutron Beam Research Facility manual, B.A.R.C.
9. Neutron beam research facilty, BARC,website.
10. Poswal A. K., Agrawal A., Yadav A. K., Nayak C., Basu S., Kane S. R., Garg C. K., Bhattachryya D., Jha S. N. and Sahoo N. K.. AIP Conf. Proc. 1591 (2014) 649.
11. Roy A.P., Dev S. K.,. Rekha M. A, and Sinha A. K., J. Pure and Appl. Phys. 30 (1992) 724
12. RRCAT, Indore, BL-09 facility, website.
13. Shimadzu FTIR-8900 manual
14. Shimadzu UV-2401 manual
15. Shriver D. F., Atkins P. W., Inorganic Chemistry, 4th edition, Oxford University Press, Oxford (2006) 189-190
16. Teledyne Princeton instrument manual.
17. West A. R., Basic Solid State Chemistry, 2nd Edition, Wiley, London (2001) 203-210

CHAPTER 4

STRUCTURAL STUDIES OF ALUMINO-PHOSPHATE GLASSES DOPED WITH La, Pr AND Nd IONS AND RESPECTIVE DEVITRIFIED STATES

A set of alumino- phosphate glasses were prepared and studied. The rare earth elements Lanthanum (La), Praseodymium (Pr) and Neodymium (Nd) were included in the glasses both singly and in pairs. The glasses were prepared using the melt quenching technique and the effects of adding a single rare earth and two rare earths together were studied using Raman spectroscopy, Fourier Transform Infrared (FTIR) spectroscopy, Ultra Violet-Visible (UV-Vis) spectroscopy , neutron diffraction and Extended X-ray absorption fine structure (EXAFS). Structural parameters such as correlation lengths and coordination numbers were obtained using both EXAFS and neutron diffraction.

4.1 Introduction and literature survey

Rare earth doped phosphate glasses are found to exhibit good magnetic and optical properties and thus have a variety of applications in science and technology (Sales (1987)).These applications depend upon the local structure around the rare-earth ions in the glass making such information important in the synthesis of rare-earth included phosphate glasses for particular applications (Cole et al. (2001)). Hoppe et al. (1998)) performed X-ray and neutron diffraction experiments on lanthanum phosphate glass and observed that the P-O correlations consist of two overlapping peaks, one at a shorter distance of 1.48 Å having a terminal oxygen atom and the other at 1.60Å having a bridging oxygen atom. X-ray and neutron diffraction studies on a series of rare-earth doped phosphate glasses indicated that the the average P-O distance is approximately 1.54Å (Shikerkar et al. (2000)). Addition of Al in phosphate glass creates cross-links in the phosphate glass network making it stronger and more durable (Brow et al. (1993). Various phosphate anions are formed as tetrahedra link together using covalent bridging oxygens and can be understood using the Q^n terminology, where n is number of bridging oxygens per tetrahedron. The basic building block of phosphate glass is the Q^3 tetrahedron of the PO_4 unit (Vanwazer (1958), Brow (2000)). Rare earth oxides such as Lanthanum oxide and Neodymium oxide modify the glass network by increasing the number of non-bridging oxygens in the glass (Liang et al. (2011), Campbell and Suratwala (2000)). Crystalline phases can be allowed to develop in the glass matrix by subjecting the glass to heat

treatment above the glass transition temperature and then letting it to cool very slowly (Holland et al. (2003), Beveridge et al. (2005)).The strength and thermal stability of the devitrified material is improved due to the presence of the crystalline phases (Mollazadeh et al (2013)), Luo et al (2013)). Few of the stable correlations present in the crystalline state also survive in the glass as the crystallization temperature is bypassed during the melt quenching process (Zarzycki (1991)). Study of the devitrified material is useful to understand the local structure of the corresponding glass (Leadbetter and Wright (1972)). Raman spectroscopy is a preferred non-destructive method to study changes in the glass structure through its vibrational spectra (Baert et al (2011), Colomban et al (2004)). EXAFS and Neutron were used to study the coordination of oxygen around the rare earth ion Nd, La and, Nd and La together in alumino-phosphate glass and their respective devitrified states. Study of the change in structure of glass on devitrification has not been reported much. In this work we have obtained the devitrified samples from the glass itself and have studied its structure along with that of the glass. Raman spectroscopic measurements have been made on all the phosphate glasses discussed in this Chapter. In particular, the three glasses having Nd, La and Nd plus La were carefully compared in going from the glass to the crystalline or devitrified states. This was done in order to gain insight into the vibrational states of each glass as compared to its devitrified state and so permit a discussion of some prominent structural features of each glass in comparison to its corresponding crystalline state from which it is derived.

4.2 Sample preparation:

The method of Melt-quench was employed for the preparation of the glasses in this study. The molar percentages of ammonium dihydrogen orthophosphate (as the source of P_2O_5 shown in equation 4.1), aluminium oxide and rare earth oxide for each sample in this study were first calculated. Constituent compositions of these glass samples are shown in Table 4.1 and Table 4.2. In order to achieve these molar values in the dry mixture of oxide powders (and consequently in the glass) , the constituent weights in each batch of 25 gm of the mixture were calculated as shown in Tables 4.3, 4.4 and 4.5 and weighed out using a Mettler (Toledo) balance.

Ammonium dihydrogen orthophosphate (ADP) or Monoammonium Phosphate (MAP) was used as a source of P_2O_5. It has a molar mass of 115.03 g/mol and can be represented by the formula $NH_4H_2PO_4$ or H_6NO_4P or NH_6PO_4. It has a density of 1.80 gm/cc and a

melting point of 190^{o}C (Lide (1998)). It may be noted that 2 gm mole of NH4H2PO4 decomposes into one gram mole of P_2O_5 by the following reaction

$$2NH_4H_2PO_4 \longrightarrow P_2O_5 + 2NH_3 + 3H_2O \quad (4.1)$$

The powder mixtures for each sample were finely ground in an agate pestle and mortar and transferred to an alumina crucible which was then placed in a high temperature furnace (Carbolite 1600).

The powders in the crucible were melted by increasing the temperature of the furnace from room temperature up to 1450^{o}C over a period of 5 hours very slowly initially to allow slow decomposition of ammonium dihydrogen orthophosphate. The melt was kept at 1450^{o}C for about 30 minutes after which it was poured out onto a metal plate in air. Homogeneous and transparent bubble free clear glass beads were formed. For annealing, these glass beads were immediately transferred to a pre-heated furnace at 400^{o}C and kept for one hour. The furnace was then put off and the glass beads were allowed to cool with the furnace over night. Some of the glasses formed are shown in Figure 4.1. Some of the glass beads of each type of glass were devitrified so as to allow a crystalline structure to develop. These glass beads were placed in an annealing furnace and the temperature increased to 1050^{o}C at which it was held for 1 hour. The sample was then allowed to cool slowly to room temperature with the furnace. Fully opaque and coloured crystalline materials were formed.

Table 4.1: Composition of the prepared glass samples (P1-G, P2-G, P3-G) in mole %

Rare earth oxide content	Glass code	P_2O_5	Al_2O_3	Nd_2O_3	La_2O_3
20% Nd_2O_3	P1-G	75	05	20	00
20% La_2O_3	P2-G	75	05	00	20
20 % Nd_2O_3 5% La_2O_3	P3-G	70	05	20	05

Some of the glass beads of the glasses P1-G, P2-G and P3-G prepared were subjected to heat treatment to yield the devitrified samples P1-D, P2-D and P3-D.

Table 4.2: Compositions of the glasses (P4-G – P10-G) in mole. %

Rare earth oxide content	Glass code	P_2O_5	Al_2O_3	Nd_2O_3	La_2O_3	Pr_6O_{11}
7.69% Pr_6O_{11}	P4-G	86.54	05.77	00	00	07.69
10% Nd_2O_3 10% La_2O_3	P5-G	75	05	10	10	00
10.71% Nd_2O_3 3.57% Pr_6O_{11}	P6-G	80.36	05.36	10.71	00	03.57
10.71% La_2O_3 3.57% Pr_6O_{11}	P7-G	80.36	05.36	00	10.71	03.57
25% La_2O_3	P8-G	75	00	00	25	00
25% Nd_2O_3	P9-G	75	00	25	00	00
NIL	P10-G	75	25	00	00	00

Table 4.3: Composition of the constituent oxide powders for glasses P1-G, P2-G and P3-G (Powders from Thomas Baker , 99.9%). * (2 moles of ADOP yield 1 mole of P_2O_5

Glass sample	Compound	Mol. Wt. (gram-mole)	Mole %	Corresponding weight	For 1 gm ± 0.0005 gm	For 25 gm ± 0.0005 gm
P1-G	Nd_2O_3	336.48	20	67.296	0.2747	6.8686
	Al_2O_3	101.96	05	05.098	0.0208	0.5203
	$NH_4H_2PO_4$*	115.03	150*	172.545	0.7044	17.6110
				244.939	1	25
P2-G	La_2O_3	325.81	20	65.162	0.2683	6.7093
	Al_2O_3	101.96	05	05.098	0.0210	0.5249
	$NH_4H_2PO_4$*	115.03	150*	172.545	0.7106	17.7658
				242.805	1	25
P3-G	Nd_2O_3	336.48	20	67.296	0.2695	6.7370
	La_2O_3	325.81	05	16.291	0.0652	1.6308
	Al_2O_3	101.96	05	05.098	0.0204	0.5103
	$NH_4H_2PO_4$*	115.03	140*	161.042	0.6449	16.1218
				247.727	1	25

Table 4.4: Composition of the constituent oxide powders for glasses P4-G, P5-G and P6-G and P7-G. * (2 moles of ADOP yield 1 mole of P_2O_5)

Glass sample	Compound	Mol. Wt. (gram-mole)	Mole %	Correspon-ding weight	For 1gm $\pm$ 0.0005 gm	For 25 gm $\pm$ 0.0005 gm
P4-G	Pr_6O_{11}	1021.44	07.69	78.573	0.2771	6.9277
	Al_2O_3	101.96	05.77	05.882	0.0207	0.5186
	$NH_4H_2PO_4$*	115.03	173.08*	199.090	0.7021	17.5538
				283.545	1	25
P5-G	Nd_2O_3	336.48	10	33.648	0.1380	3.4494
	La_2O_3	325.81	10	32.581	0.1336	3.3400
	Al_2O_3	101.96	05	05.098	0.0209	0.5226
	$NH_4H_2PO_4$*	115.03	150*	172.545	0.7075	17.6881
				243.872	1	25
P6-G	Nd_2O_3	336.48	10.71	36.051	0.1371	3.4287
	Pr_6O_{11}	1021.44	03.57	36.480	0.1388	3.4695
	Al_2O_3	101.96	05.36	05.462	0.0208	0.5195
	$NH_4H_2PO_4$*	115.03	160.71*	184.870	0.7033	17.5823
				262.863	1	25
P7-G	La_2O_3	325.81	10.71	34.908	0.1334	3.3345
	Pr_6O_{11}	1021.44	03.57	36.480	0.1394	3.4846
	Al_2O_3	101.96	05.36	05.462	0.0209	0.5218
	$NH_4H_2PO_4$*	115.03	160.71*	184.870	0.7064	17.6591
				261.72	1	25

Table 4.5: Compositions of the constituent oxide powders for glasses P8-G, P9-G and P10-G. * (2 moles of ADOP yield 1 mole of P_2O_5)

Glass sample	Compound	Mol. Wt. (gram-mole)	Mole %	Corresponding weight	For 1 gm ± 0.0005 gm	For 25 gm ± 0.0005 gm
P8-G	La_2O_3	325.81	25	81.453	0.3207	8.0171
	$NH_4H_2PO_4$*	115.03	150*	172.545	0.6793	16.9829
				253.998	1	25
P9-G	Nd_2O_3	336.48	25	84.120	0.3277	8.1936
	$NH_4H_2PO_4$*	115.03	150*	172.545	0.6723	16.8064
				256.665	1	25
P10-G	Al_2O_3	101.96	25	25.490	0.1287	3.2178
	$NH_4H_2PO_4$*	115.03	150*	172.545	0.8713	21.7821
				198.035	1	25

Glass P1 -G Glass P2-G Glass P3-G

Figure 4.1: Photograph of the glasses P1-G, P2-G and P3-G formed

4.3 Density and Glass Transition Temperature

Bulk densities (ρ) of the glass and devitrified samples were measured using the the fluid displacement method with xylene as the buoyant fluid (Besancon et al. (1974), Gibbons (2008)). Densities were found using equation (4.2) and are listed in Table 4.6.

$$\rho = \rho_x(\frac{W_a}{W_a - W_x}) \quad (4.2)$$

Where ρ_x is the density of xylene, W_a is the weight of the sample in air and W_x is the weight of the sample in xylene. The density of the devitrified samples P1-D, P2-D and P3-D are found to be higher than the corresponding glasses P1-G, P2-G and P3-G. Nucleation and crystal growth during the devitrification process increases the density of the devitrified samples. Also the competition between the stable and metastable phases leads to the evolution of dominant phases of the crystalline structure. The neodymium containing glass P1-G has a higher density than the lanthanum containing glass P2-G. However the mixed neodymium and lanthanum containing glass P3-G is found to have a density higher than both P1-G and P2-G. In the mixed rare earth glasses with Pr as a common constituent it is seen that the mixed Pr and Nd containing glass P6-G is denser than the mixed Pr and La containing glass P7-G. The presence of rare earth encourages the formation of cross links in the network through the formation of RE-O-P bonds thereby making the phosphate chains shorter and hence more denser. The cationic field strength (CFS) given by equation (4.3) is calculated for the glasses (Q. Shi et al. (2018)) and listed in Table 4.7.

$$\text{CFS} = \frac{Z}{r^2} \quad (4.3)$$

where Z is the atomic number, r is the ionic radius.

The molar volume V_m (Chanshetti et al (2011)) is calculated for all the glass samples using the equation (4.4)

$$V_m = \frac{\sum(n_x M_x)}{\rho} \quad (4.4)$$

Where n_x is the molar fraction and M_x is the molecular weight of the x^{th} component of the sample. The molar volume for the prepared glasses is higher than that for the corresponding devitrified samples and are listed in Table 4.6

Table 4.6: Density and molar volume of the glass and devitrified samples.

Glass/Devitrified sample	Density ρ in g/cc ($\pm$ 0.0005)	Molar Volume V_m in cc
P1-G	3.2182	55.5742
P1-D	3.3102	54.0297
P2-G	3.0764	57.4421
P2-D	3.1077	56.8636
P3-G	3.3856	55.5420
P3-D	3.4800	54.0353
P4-G	3.1719	65.3511
P5-G	3.1362	56.6871
P6-G	3.1622	60.7340
P7-G	3.1328	60.9388
P8-D	3.4972	53.7310
P9-D	3.4491	55.2535
P10-G	2.5068	52.6348

Table 4.7: Glass transition temperature and network connectivity of the rare earth glasses

Glass sample	Glass Transition temperature $T_g(^oC)$ ± 2 ^oC	Network connectivity $2 + \frac{(BO-NBO)}{G}$	Cationic field strength Z/r^2 ($Å^{-2}$)
P1-G	697	4	10.52
P2-G	677	4	8.99
P3-G	706	3.86	12.73
P4-G	688	3.91	14.53
P5-G	688	4	9.72
P6-G	680	3.96	12.40
P7-G	673	3.96	11.19

The kinetic slowdown at the glass transition leads to the super-cooling of the melt and hence the formation of glass. Differential thermal analysis was used to obtain the glass transition temperatures of the glasses which are listed in Table 3. The glass transition (T_g) and crystallization (T_c) temperatures were observed for all the three glass samples while the melting temperatures (T_m) were not observed on account of the limitation of measurement upto 1000^{o}C. Hence the melting temperature is expected to be greater than 1000^{o}C. The presence of Al in the glass breaks down the P=O bonds thereby forming P-O-Al cross links through the glass network thus strengthening the glass structure. The glass transition temperature of the phosphate glass with only aluminium (P10-G) is 813^{o}C and is the highest. Modifiers Nd and La included in the glass encourages the formation of Nd-O-P or La-O-P linkages in the respective glasses as a result of which the glass becomes more compact with shorter phosphate chains. The glass P1-G has a glass transition temperature (697^{o}C) which is higher as compared to P2-G (677^{o}C). The molar mass of Nd is higher than that of La, hence the melt containing Nd becomes more viscous at a temperature higher than that containing La and hence exhibits a higher glass transition temperature. In the glass P3-G , some amount of phosphorous has been also been replaced by La and so there are fewer P-O-Al bonds but more RE-O linkages making the melt still more viscous at a still higher temperature and thus a higher glass transition temperature (706^{o}C). Network connectivity is a measure of the average number of bonds connecting the glass forming tetrahedral units (Q^n) for the entire network where n is the number of bridging oxygen ions in each PO_4 tetrahedron. It is defined by the relative number of network forming (bridging) and network modifying (non-bridging) ions in the glass. The network connectivity (NC) for the glasses studied were calculated by considering the molar compositions of the formed glasses (Hill (1996)) using equation (4.5) and is listed in Table 4.7.

$$NC = 2 + \frac{(BO - NBO)}{G} \qquad (4.5)$$

where BO is the total fractional number of bridging oxygens per network forming ion (Five per P_2O_5). NBO represents the total fractional number of non-bridging oxygen ions per network modifier ion (Three per Nd^{3+} or La^{3+} or Al^{3+}) and G is the total number of glass forming units (Two per P_2O_5).

The network connectivity is found to be lower for the mixed Nd and La glass P3-G as compared to that for the single Nd containing P1-G or single La containing P2-G. Also,

the network connectivity is found to be lower for the mixed rare-earth glass. This is justified by the Raman analysis discussed later.

4.4 X-ray Diffraction

The X-ray diffraction data on the glass samples P1-G, P2-G and P3-G are shown in Figure 4.2 below. The absence of Bragg reflections and the presence of a broad hump in the X-ray diffraction spectrum of all three glass samples confirm that the glass samples prepared are amorphous in nature.

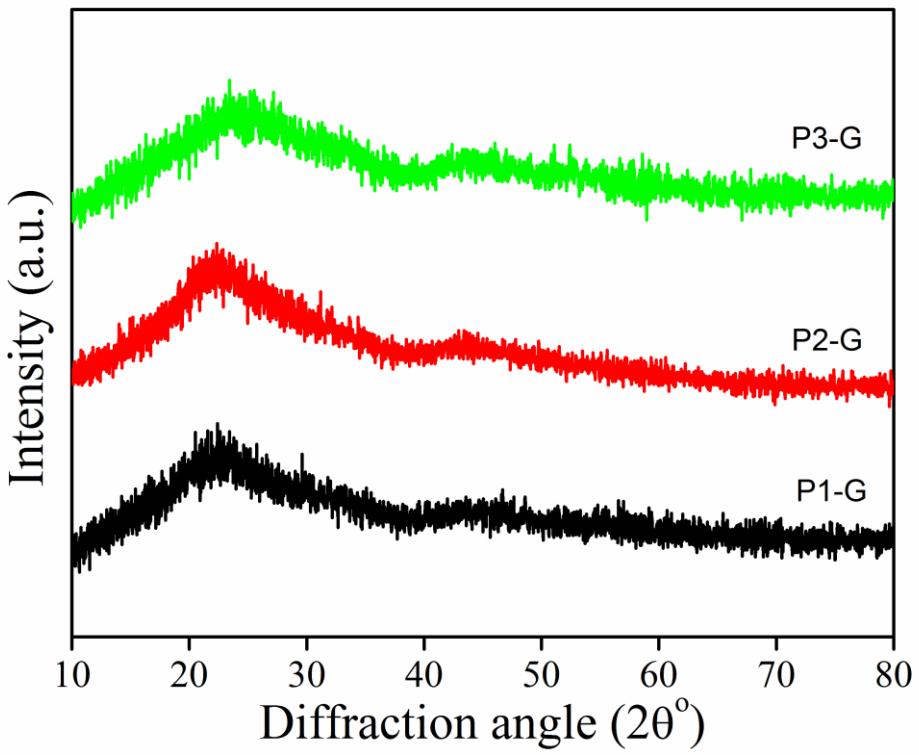

Figure 4.2 : X ray diffraction spectrum of glasses P1-G, P2-G and P3-G

The X-ray diffraction spectrum of the devitrified forms obtained from the prepared glasses is shown in Figure 4.3. The presence of well-defined Bragg diffraction peaks confirms the crystalline nature of the devitrified samples. The respective glasses were subjected to heat treatment at 1050^{o}C and allowed to cool slowly with the furnace. This slow cooling provided the constituent atoms sufficient energy and time to reorganise and develop their crystalline structures. The crystallinity in the devitrified material P1-D is due to the

orthorhombic phase of NdP_3O_9 (PDF No.-96-210-6694) with space group C 2 2 21. The structure of the devitrified material P2-D is the orthorhombic phase of LaP_3O_9 (PDF No.-96-153-0370) with space group C 2 2 21. In the case of the devitrified material P3-D, the crystalline reflections are due to NdP_3O_9 (PDF No.-96-210-6694) and LaP_3O_9 (PDF No.-96-153-0370) both with space group C 2 2 21 (Hong (1982), Matuszewski et al (1988), Jouini et el (2003), Muraoka and Kihara (1997)). Thus when both Nd and La are included together in the glass, the structure appears to be similar to that for an intermediate sized ion such as Pr.

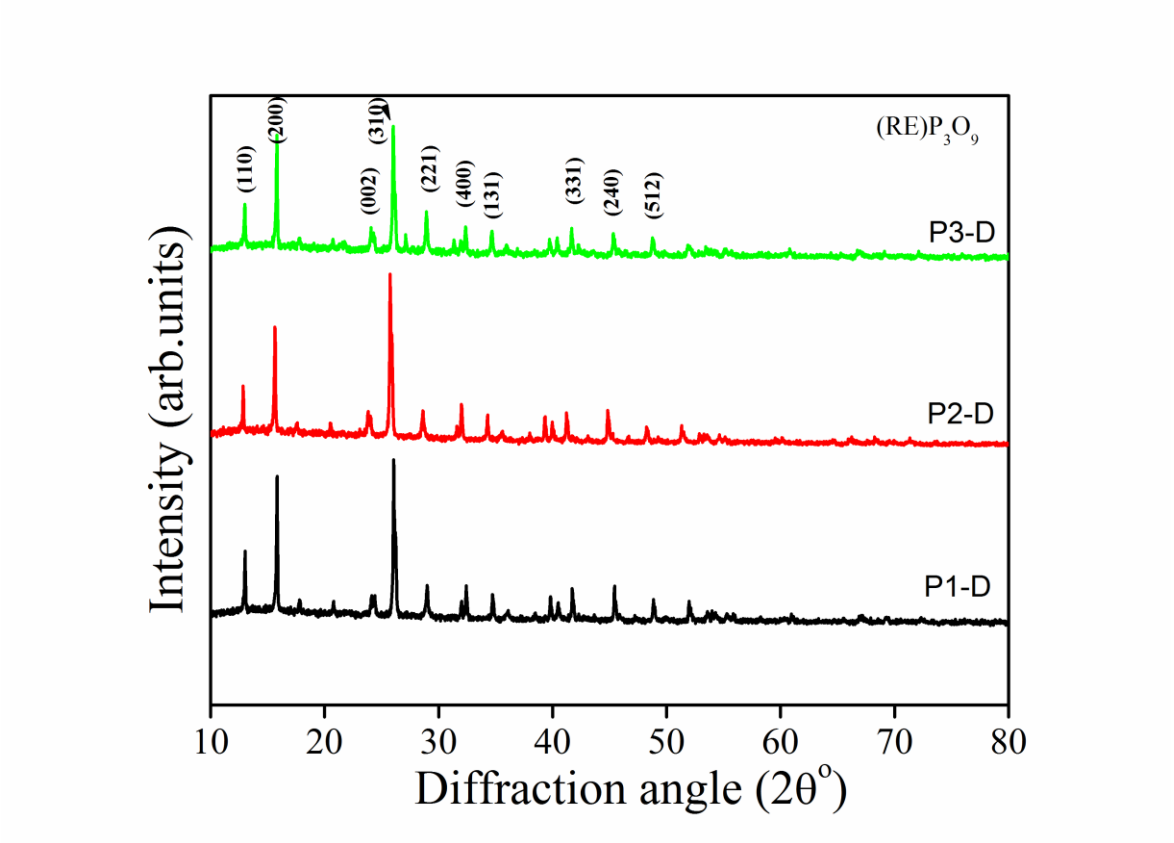

Figure 4.3: X ray diffraction spectrum of the devitrified samples P1-D, P2-D and P3-D

The X-ray diffraction data on the samples P4-G, P5-G, P6-G and P7-G are shown in the Figure 4.4 also confirms the amorphous nature of these glasses.

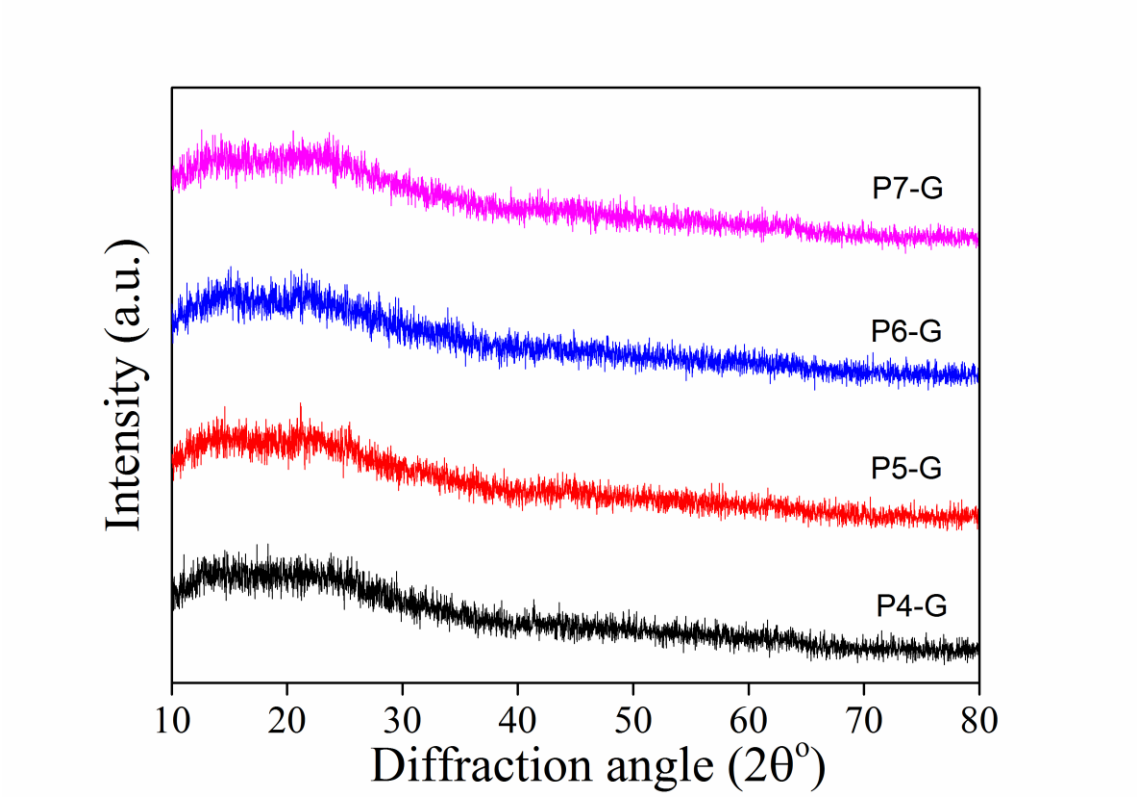

Figure 4.4: X ray diffraction spectrum of the glass samples P4-G, P5-G, P6-G and P7-G

The glasses prepared with higher percentages (25%) of only rare earth inclusions La_2O_3 (P8-G) or Nd_2O_3 (P9-G) without adding Al_2O_3were found to be partially devitrified (Figure 4.5) while the glass prepared with the same higher percentage (25%) of only Al_2O_3 (P10-G) is found to form a clear, homogeneous glass (Figure 4.6).

X ray diffraction spectra of these glasses showed the presence of crystalline peaks due the orthorhombic phase LaP_3O_9 in sample P8-G and due to orthorhombic phase NdP3O9 in sample P9-G. The Neodymium containing glass (P9-G) showed better developed crystalline peaks than the lanthanum containing glass (P8-G). However, the effect of replacing the rare-earth oxide by aluminium oxide was the formation of a stable glass (P10-G). This confirmed that the presence of aluminium oxide as an intermediate helps in glass formation. Thus, 5% Al_2O_3 was included in all the phosphate glasses prepared in this study.

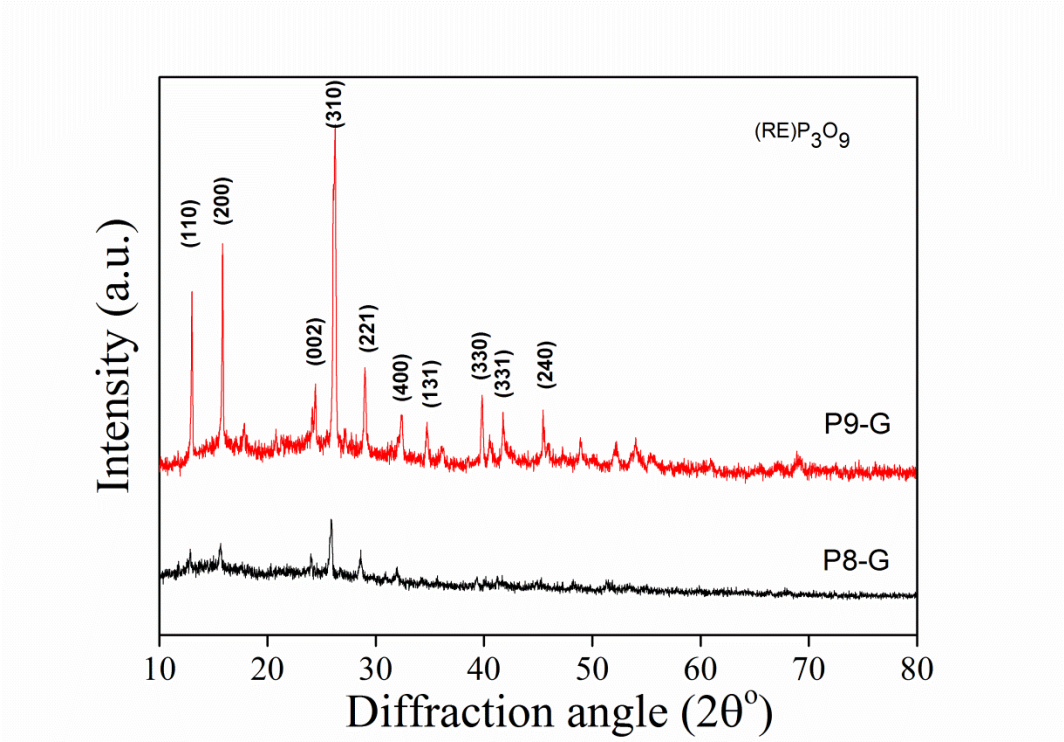

Figure 4.5: Xray diffraction spectrum of glass samples P8-G and P9-G which got partially devitrified due to the absence of Al_2O_3 .

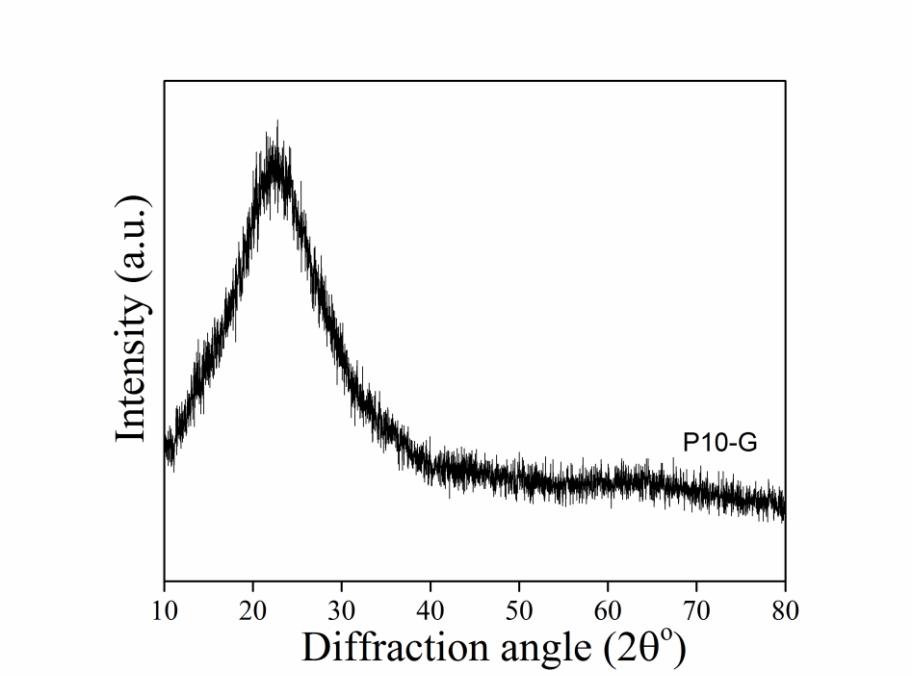

Figure 4.6: X-ray diffraction spectrum for the glass sample P10-G having only Al_2O_3 inclusions.

4.5 Fourier Transform Infra Red Spectroscopy

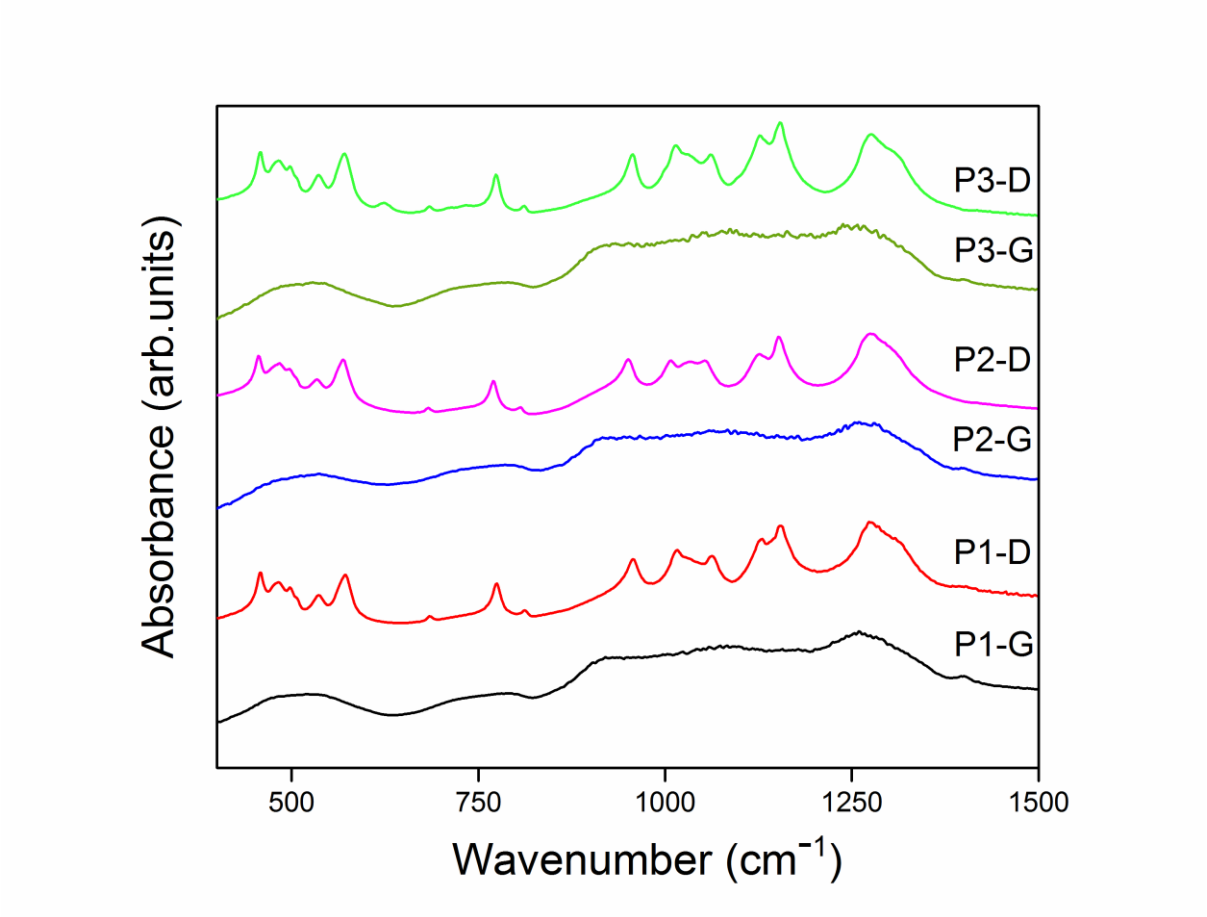

Figure 4.7: Comparative display of the Fourier Transform Infrared spectra of the glass P1-G, P2-G and P3-G and their respective devitrified samples P1-D, P2-D and P3-D

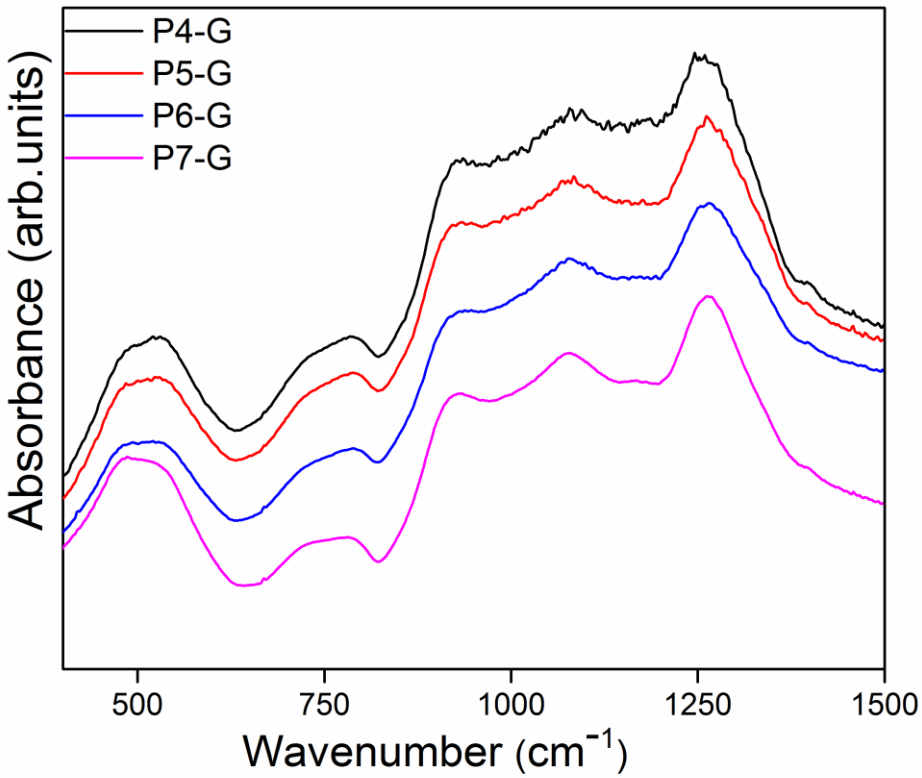

Fig 4.8: Fourier Transform Infrared spectra of glass samples P4-G, P5-G, P6-G and P7-G.

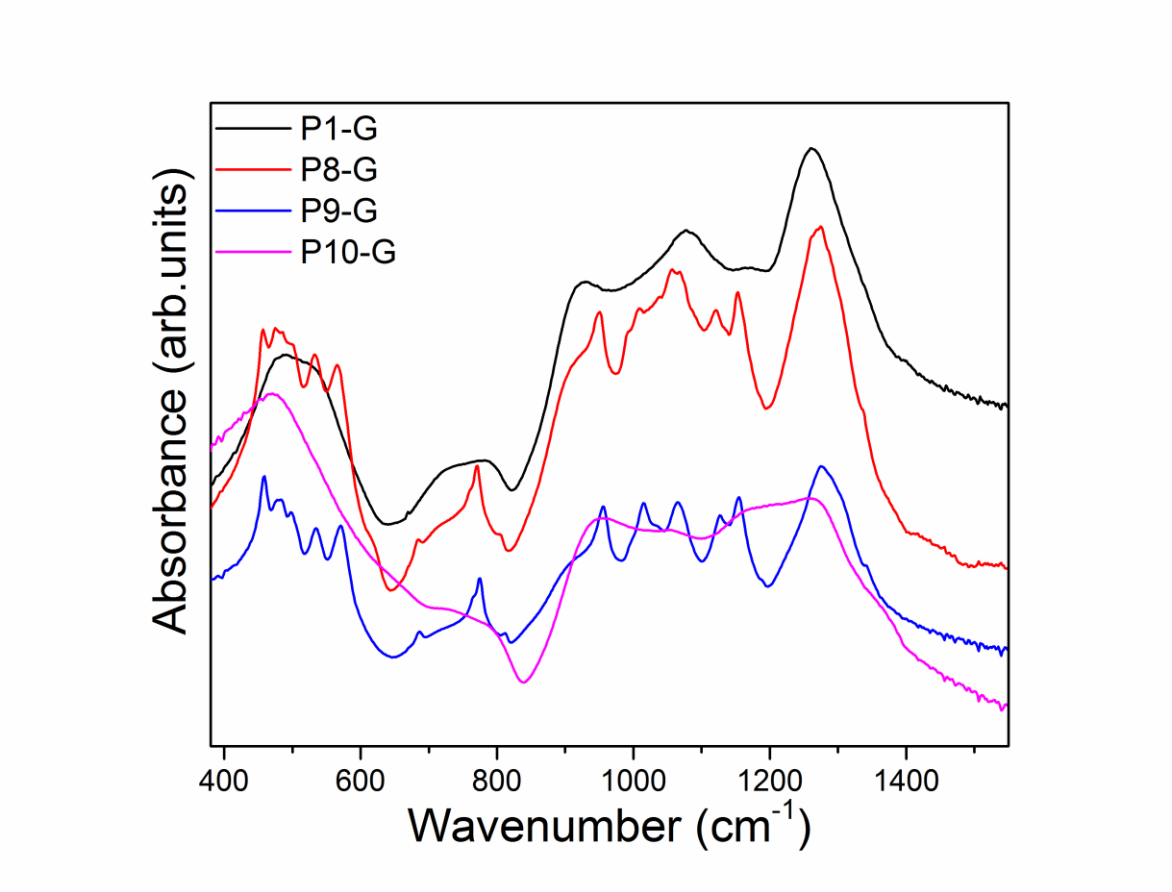

Figure 4.9: Fourier Transform Infrared spectra of glasses P1-G and P10-G and devitrified samples P8-G and P9-G

The FTIR bands of the three glasses P1-G, P2-G and P3-G and their corresponding devitrified states P1-D, P2-D and P3-D are shown in Figure 4.7. The FTIR spectra of the other glasses P4-G, P5-G, P6-G and P7-G are shown in Figure 4.8. The FTIR data for the samples P8-G and P9-G (with rare-earths but without Al_2O_3 and unstable) along with the glass samples P1-G and P10-G (with Al_2O_3 but without rare-earths) and stable are shown in Figure 4.9. The tetrahedral units are better linked in the devitrified materials which have relatively fewer non-bridging oxygen atoms as compared to the glasses. Thus the FTIR spectra of the devitrified materials show sharper and better resolved features than the corresponding vitreous states.

The broad bands observed for the glass and centered at around 500cm^{-1} are due to O-P-O vibrations, while the feature between 650 cm^{-1} and 840 cm^{-1} is due to the vibrations in P-O-P connectivities. The vibrations in the range between 840 cm^{-1} and 1400 cm^{-1} are due to the distribution in numbers of structural units having different non-bridging oxygen atoms i.e. spread of Q^n units (Abdel-Kader et al. (1991)).

Several authors have assigned the peak positions for the various modes of vibrations. The band and peak positions for the devitrified samples are listed in the Table.4.8

Table 4.8 FTIR peaks observed in the devitrified materials

FTIR peak positions (cm^{-1})			Assignments of peaks	References
P1-D	P2-D	P3-D		
469	464	467	O-P-O bending vibrations	Kader et al.(1991)
492	492	492	Harmonics O=P-O bending	Abo-Naf et al. (2008)
517	517	517	δ(P=O) modes	Kader et al.(1991
549	546	549	P-O-P stretching modes	Sammons et al. (2007)
638	665	660	δ(O-P-O) modes	Kader et al.(1991
697	693	695	ν_s(P-O-P) vibrations in Q^2	Saout Le et al. (2002)
		722	ν_s(P-O-P) linkages in between Q^1 and Q^2 units	Yifen et al.(1986)
		745	ν_s(P-O-P) vibrations in Q^1	Yifen et al.(1986)
800	795	800	ν_s(P-O-P) vibrations in Q^1	Yifen et al.(1986)
823	823	823	ν_{as}(P-O-P)	Shaim et al.(2003)
983	976	978	Symmetric stretching mode of NBO's in Q^o tetrahedral	Pavic et al.(2014)
	1017	1021	Vibrations due to P-O-La	Rai et al.(2011)
1049		1049	Vibrations due to P-O-Nd	Rai et al.(2011)
1090	1084	1085	Symmetric vibrations of NBO's in Q^1 tetrahedra	Pavic et al.(2014
1138	1138	1138	ν_s(O-P-O) vibrations in Q^2 tetrahedra	Saout Le et al.(2002)
1209	1204	1215	ν_s(P=O) vibrations in Q^2	Chahine et al. (2004)

4.6 UV-Visible Spectroscopy

The comparative display of the absorption spectra of the glasses P1-G, P2G and P3-G along with their respective devitrified samples are shown in the Figures 4.10 (a), 4.10 (b) and 4.10 (c) respectively. Above the UV edge (~ 325 nm) the spectra due to the rare earths La, Pr or Nd are the same in the glass and devitrified states, but with the intensities of absorption peaks for the devitrified samples being reduced as compared to those of the glasses. The absorption spectra of the glasses containing Pr (P4-G), mixed Nd and La (P5-G), mixed Nd and Pr (P6-G) and mixed La and Pr (P7-G) are shown in Figure 4.11. The absorption spectra for the phosphate glasses containing only La (P8-G), only Nd (P9-G) and only Al (P10-G) are shown in Figure 4.12. While La and Al show absorptions in the UV region, they do not contribute to absorption in the visible range. The absorption peaks due to the optical absorption in the Nd contained glass (Carnall (1968), Karunakaran (2010)) and the Pr containing glasses (Harani (1984), Khan (1985), Smith (1963)) were identified spectroscopically to be due to the 4f electronic levels and are shown in the optical spectra displayed. These transitions due to the 4f configurations interact only very weakly with the host phosphate glass network as earlier reported by Shikerkar et al (2000). In the mixed rare earth containing glasses, the observed spectra are the superposition of the individual rare earth ions. The relative transition probabilities and the theory of such transitions involving rare earth elements have been analysed by Judd and Offelt (1962). Detailed analysis of these glasses involving the Judd-Ofelt parameters would explain the effect of the interaction between two optically active rare earths on these electronic transitions.

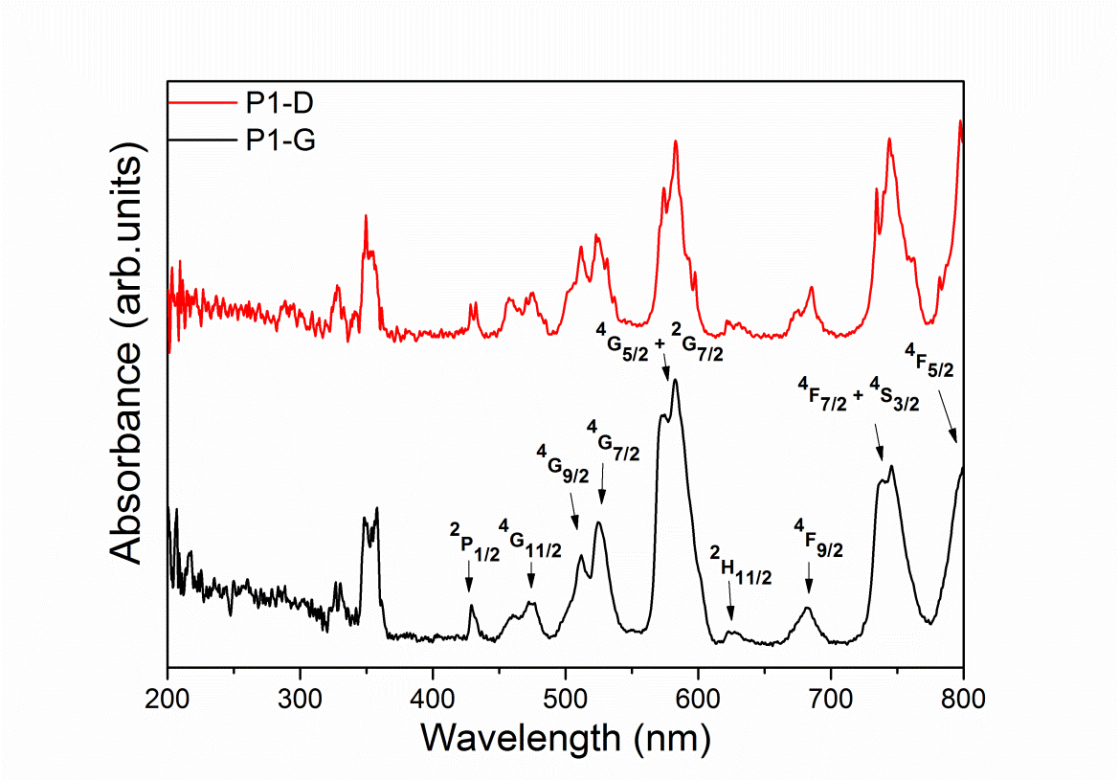

Figure 4.10 (a)

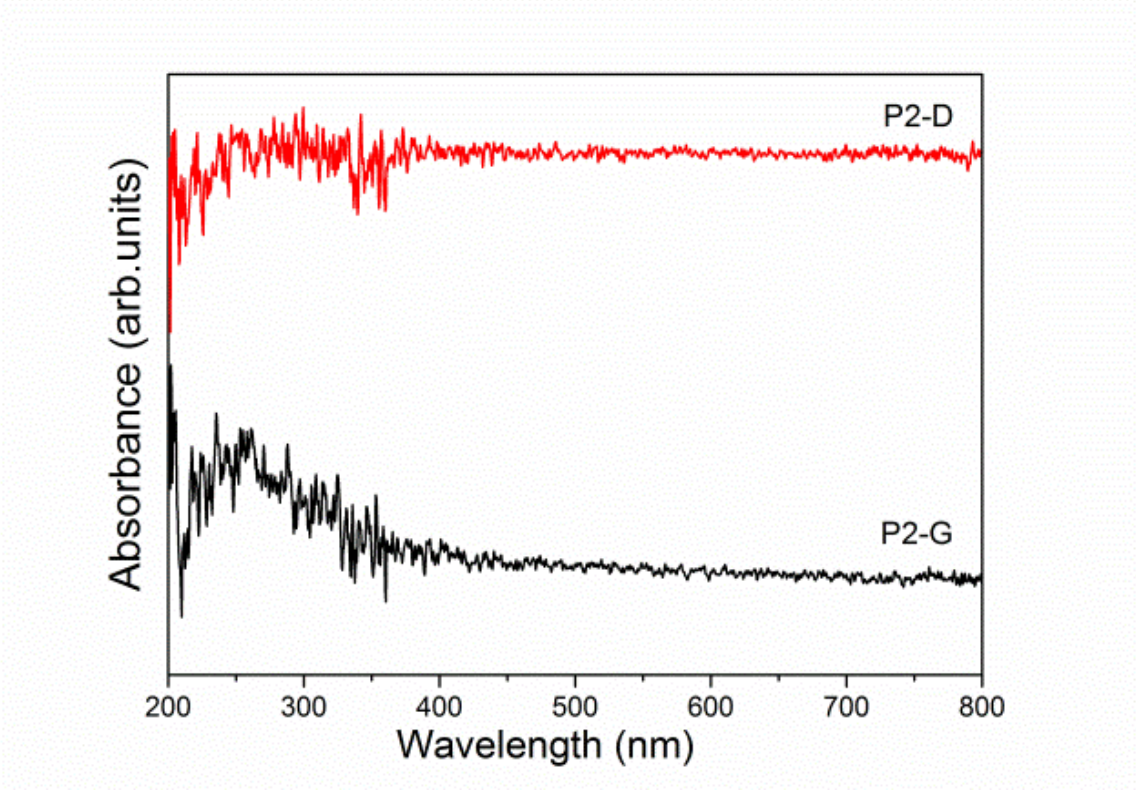

Figure 4.10 (b)

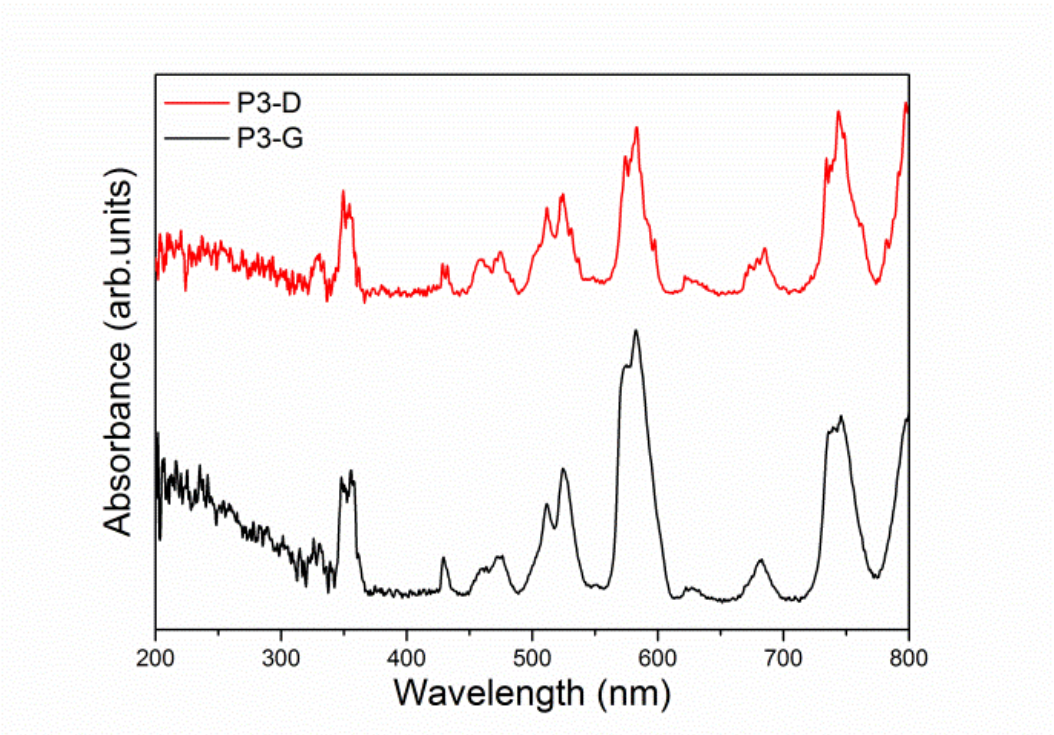

Figure 4.10 (c)

Figure 4.10: Comparative display of the Ultra Violet- Visible spectra of Glass and devitrified samples (a) P1-G and P1-D (b) P2-G and P2-D (c) P3-G and P3-D

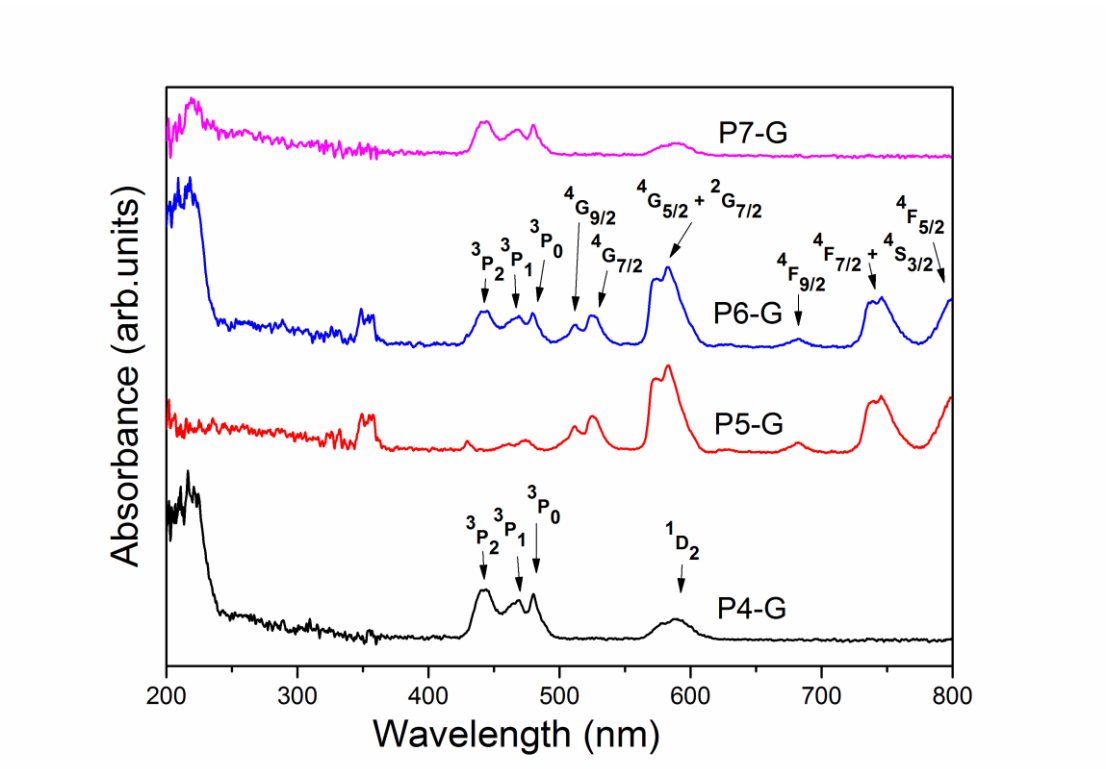

Figure 4.11: Ultra Violet –Visible spectra of glass samples P4-G, P5-G, P6-G and P7-G

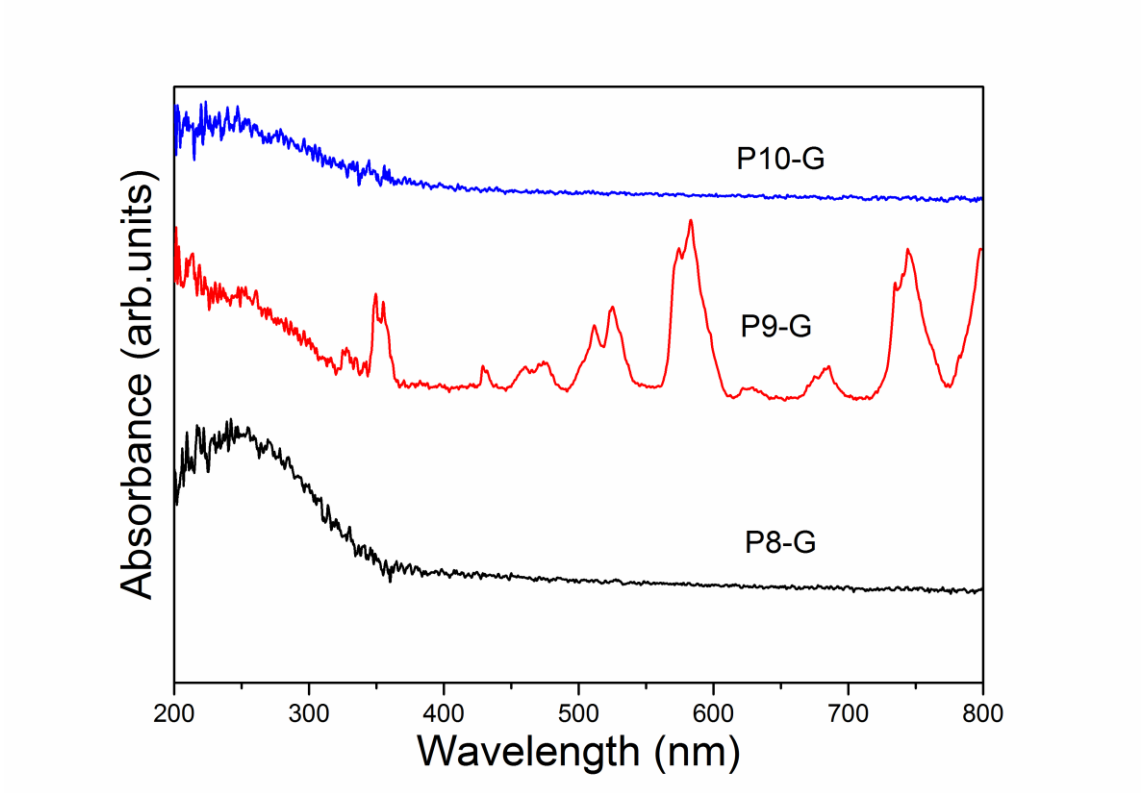

Figure 4.12: Ultra-Violet- Visible spectra of samples P8-G, P9-G and P10-G

4.7 Raman Spectroscopy

The Raman spectra in the range 200 cm^{-1} to 1400 cm^{-1} for each of the glasses P1-G, P2-G, and P3-G and their corresponding devitrified samples P1-D, P2-D and P3-D are shown in Figures 4.13, 4.14 and 4.15 respectively.

Raman spectra relate to the vibrations of molecules in a bonded molecular structure. They arise from the energy interactions between the incident photons and these vibrational energies. Sharper peaks are observed for the samples P1-D, P2-D and P3-D as the lattices of these crystalline materials have long range periodic order while broad bands are observed for the glass samples P1-G, P2-G and P3-G for which the continuous random networks have only short range periodic order. The most prominent peaks in the devitrified samples are found to be positioned at around the maxima in the Raman bands of the corresponding glasses. The main Raman vibrations present in the devitrified samples are found to still exist in the glasses suggesting similarity in the interatomic bonding forces in the glass and its corresponding devitrified states. The energy content of the lattice in the glass is higher as compared to that in the corresponding devitrified state.

The Raman band between 625cm^{-1} to 850cm^{-1} gives information about the P-O-P stretch in the chain. If the network modifier cation size is small or the length of the phosphate chain is shorter, then the P-O-P bond angle will be smaller and the band will appear at a larger wavenumber (Nelson et al (1979), Rouse Jr. et al (1978)). The vibrations of the Q^n structural units in the glass samples P1-G, P2-G and P3-G give rise to the Raman band between 860 cm^{-1} to 1400 cm^{-1} (Pemberton et al. (1991), Koo (1997), Lai (2011)). This Raman band is deconvoluted into several peaks to obtain the Raman modes arising from specific molecular vibrations as shown in Figures 4.16, 4.17, and 4.18.

Several authors have assigned the peak positions for the Q^n structural units as listed below.

Q^0 ~940 cm^{-1} - Velli et al. (2005) and J. J. Hudgens et al. (1998),

Q^1 ~1010-1190 cm^{-1} - Chakraborty et al. (1995), Hee (2014),

Q^2 ~1150-1240 cm^{-1}- Pemberton et al. (1991), Magdas et al. (2008), Morgan et al. (1987) and Brow (2000)

Q^3~1305 cm^{-1}- Koo et al. (1997)

These assignments for the fitted Raman bands in the deconvoluted region are shown in the Table 4.9

Table 4.9: Assignmed peak positions for the Q^n structural units in the fitted region

P1-G	P2-G	P3-G	Assignments
925	945	958	Symmetric stretching vibrations of PO_4^{3-} (Q^0units)
1003	1005	1022	Symmetric vibration of PO_3^{2-} (Q^1 units)
1105	1100	1088	Asymmetric vibrations of PO_3^{2-} (Q^1 units)
1172	1175	1144	Symmetric vibrations of PO_2 (Q^2units)
1192	1196	1181	$\nu_s(PO_2)$ vibrations (Q^2 units)
1234	1246	1210	ν_{as} (PO_2) vibrations (Q^2 units)
1300	1313	1310	Vibrations due to Q^3 units

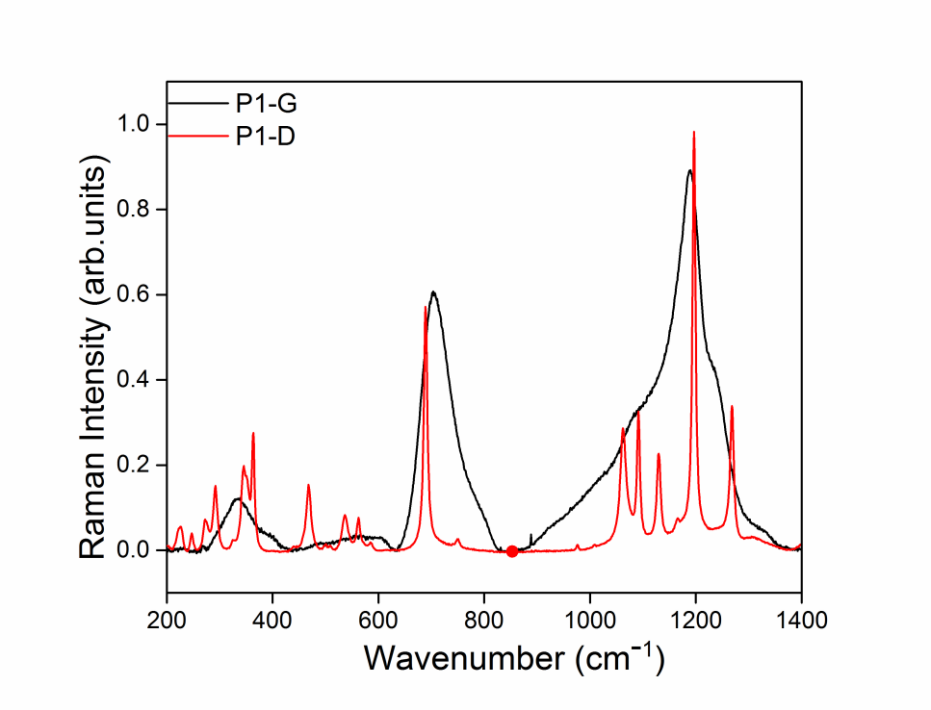

Figure 4.13: Comparative display of Raman spectra of the glass P1-G and its devitrified sample P1-D

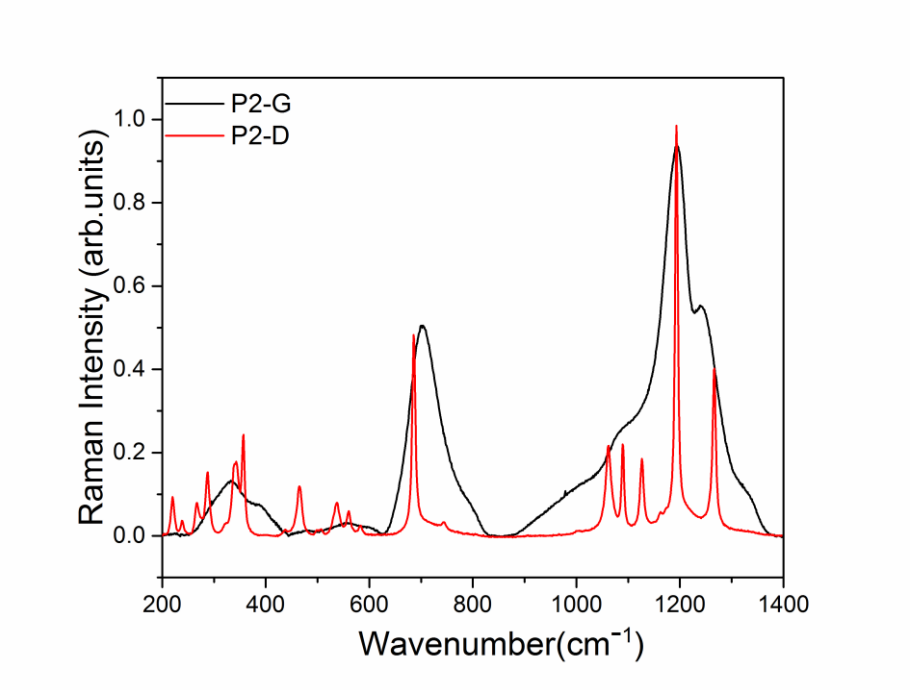

Figure 4.14: Comparative display of Raman spectra of the glass P2-G and its devitrified sample P2-D

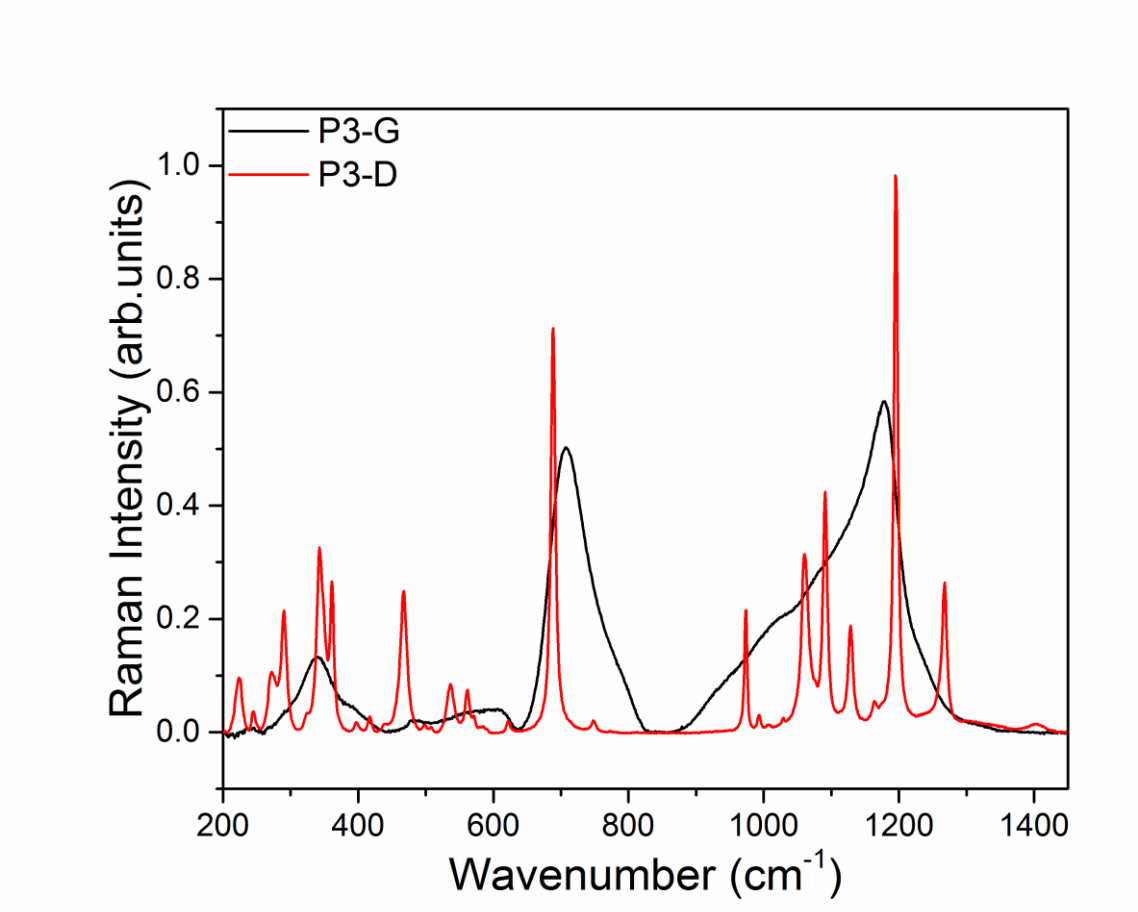

Figure 4.15: Comparative display of Raman spectra of the glass P3-G and its devitrified sample P3-D

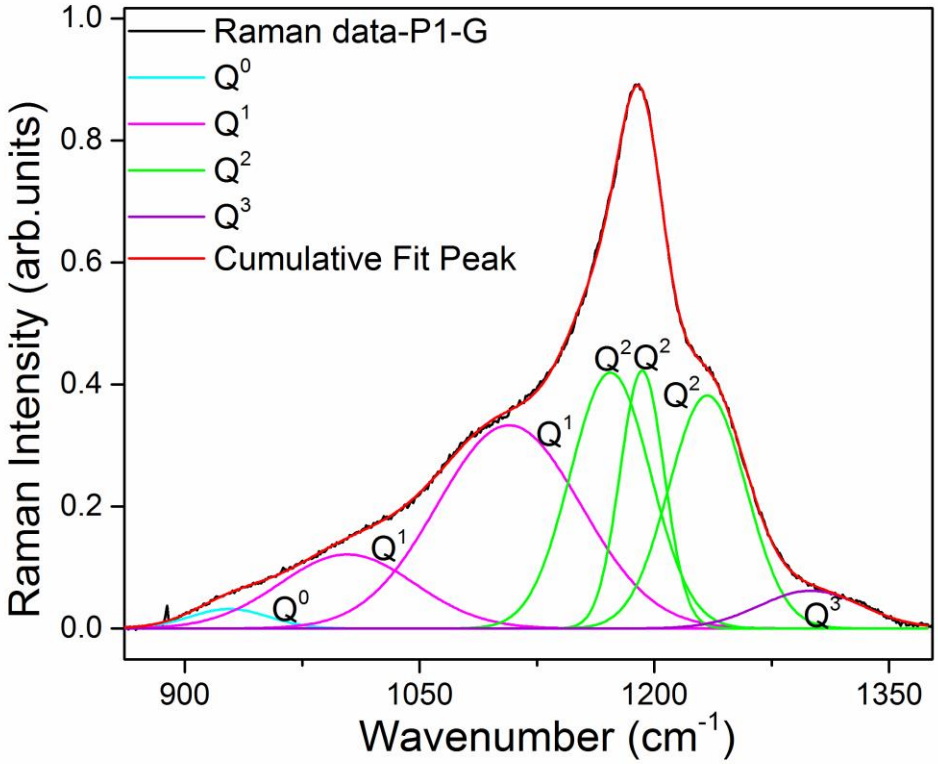

Figure 4.16 (a): Deconvoluted Raman peaks for glass P1-G

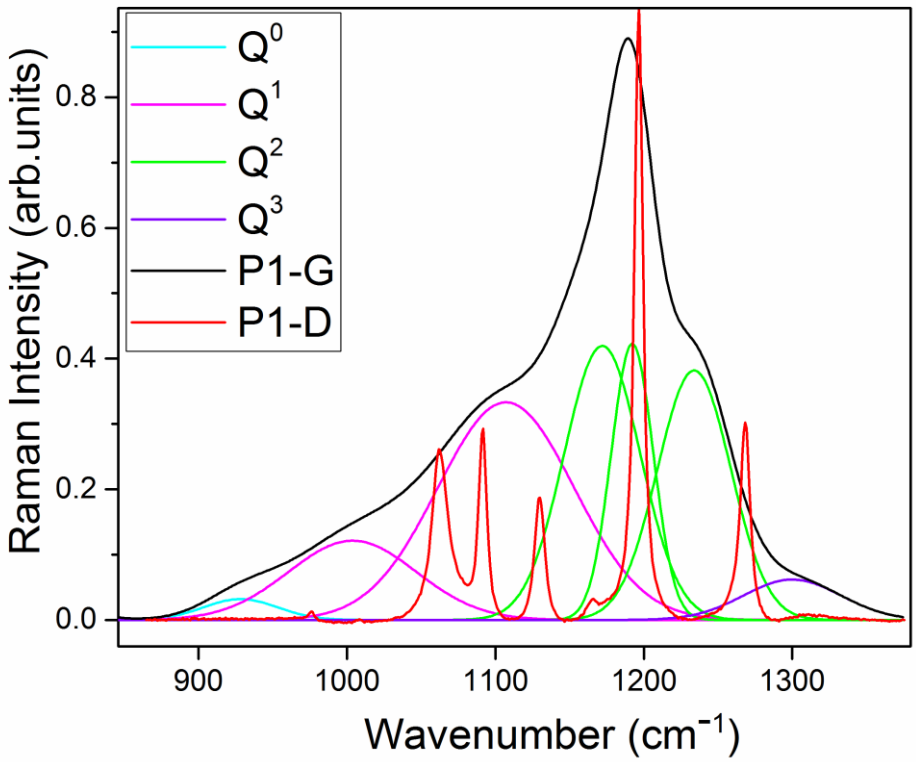

Figure 4.16 (b): Deconvoluted Raman peaks for P1-G along with the Raman peaks for P1-D

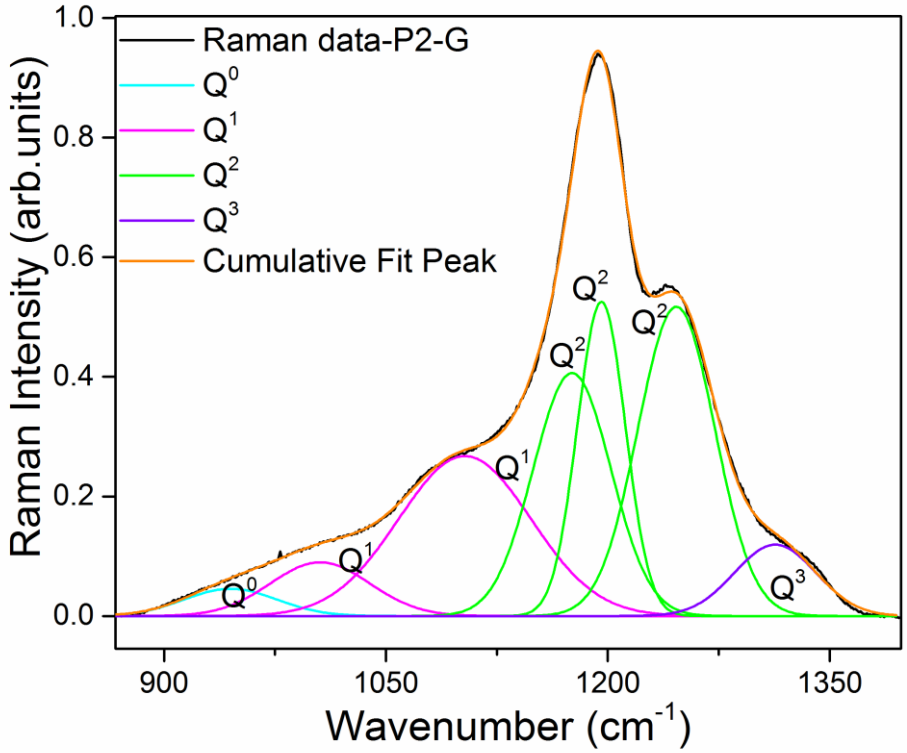

Figure 4.17 (a): Deconvoluted Raman peaks for glass P2-G

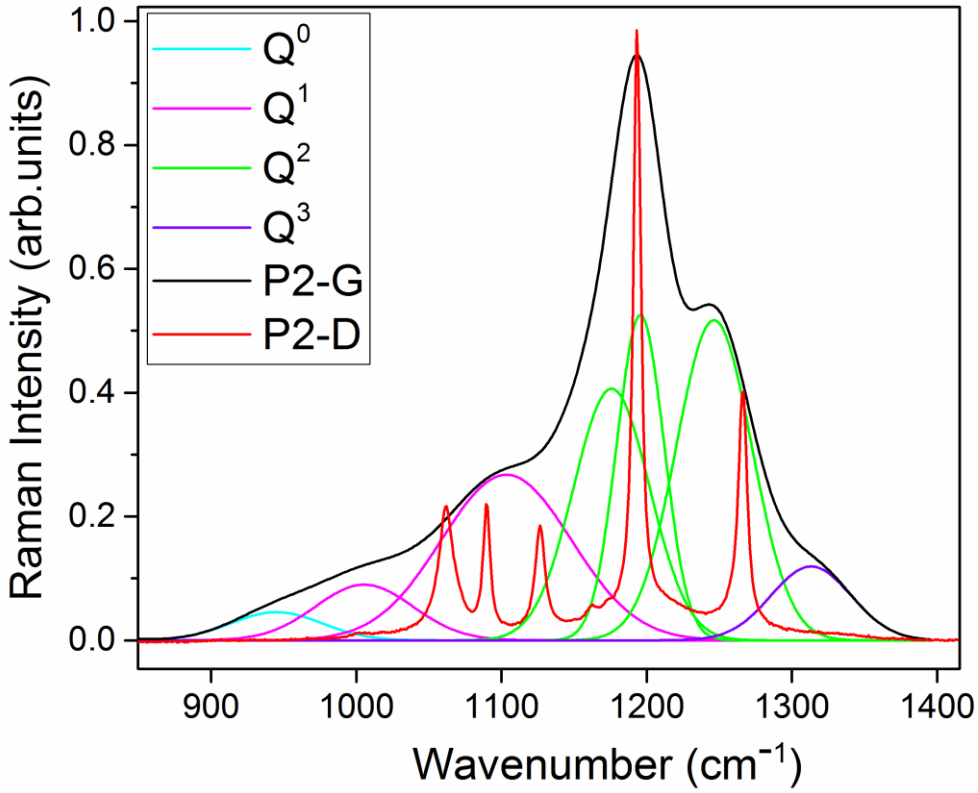

Figure 4.17 (b):Deconvoluted Raman peaks for P2-G along with the Raman peaks for P2-D

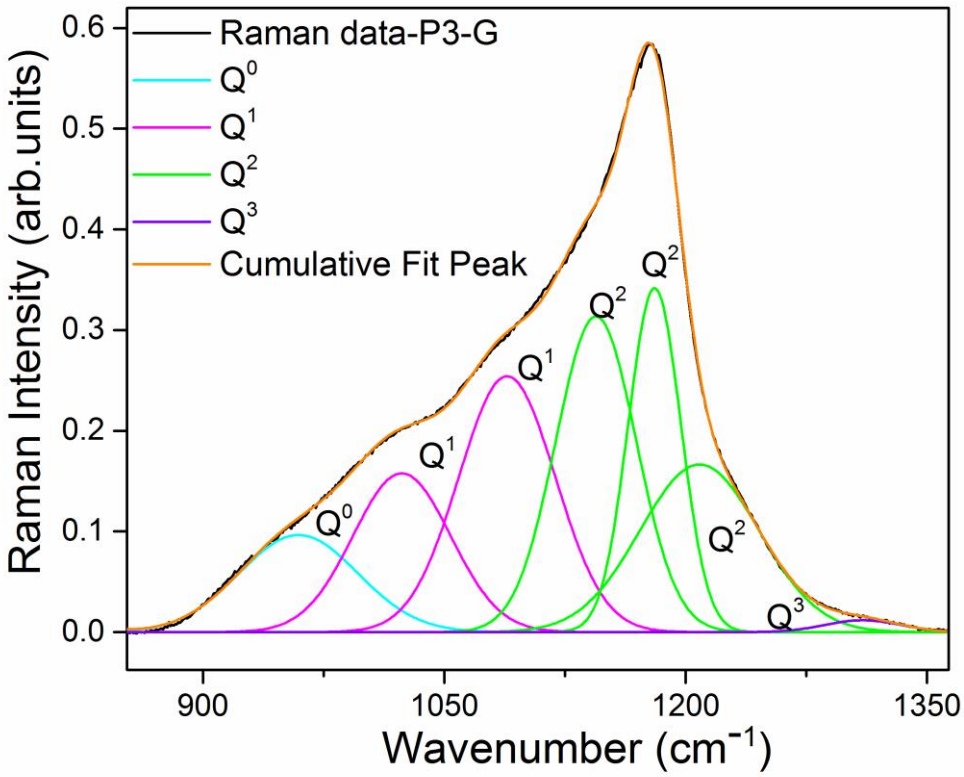

Figure 4.18 (a): Deconvoluted Raman peaks for glass P3-G

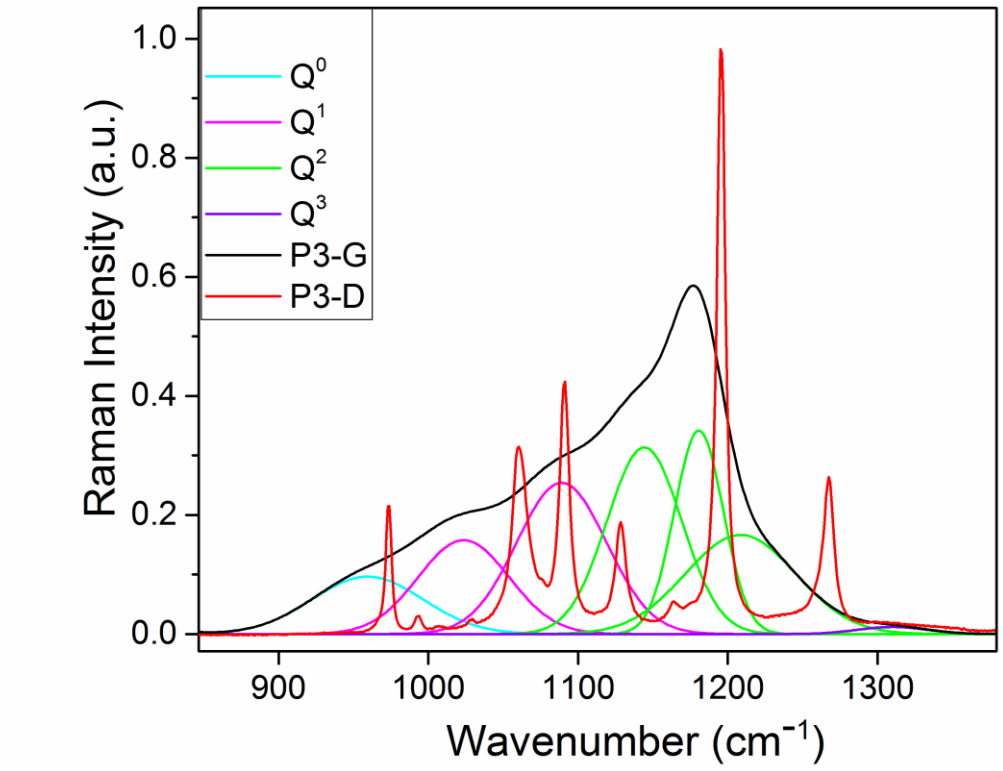

Figure 4.18 (b): Deconvoluted Raman peaks for P3-G along with the Raman peaks for P3-D

Table 4.10: Relative areas of different Q^n tetrahedral units from the deconvoluted Raman spectra for the glasses P1-G, P2-G and P3-G and their respective devitrified states.

	P1-G	P1-D	P2-G	P2-D	P3-G	P3-D
Q^0	0.016108	0	0.027206	0	0.099543	0.053302
Q^1	0.414948	0.344041	0.286313	0.261790	0.346287	0.375472
Q^2	0.528028	0.648187	0.623609	0.738210	0.546487	0.571226
Q^3	0.040915	0.007772	0.062872	0	0.007683	0
Q^4	0	0	0	0	0	0
	1	1	1	1	1	1

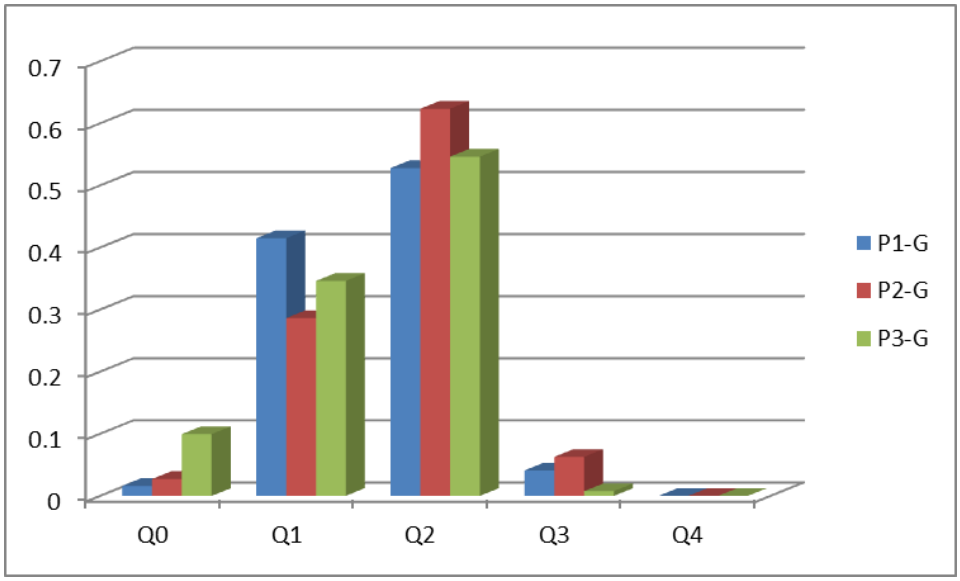

Figure 4.19 (a): Comparative display of the relative area of the different Q^n for Glasses P1-G, P2-G and P3-G

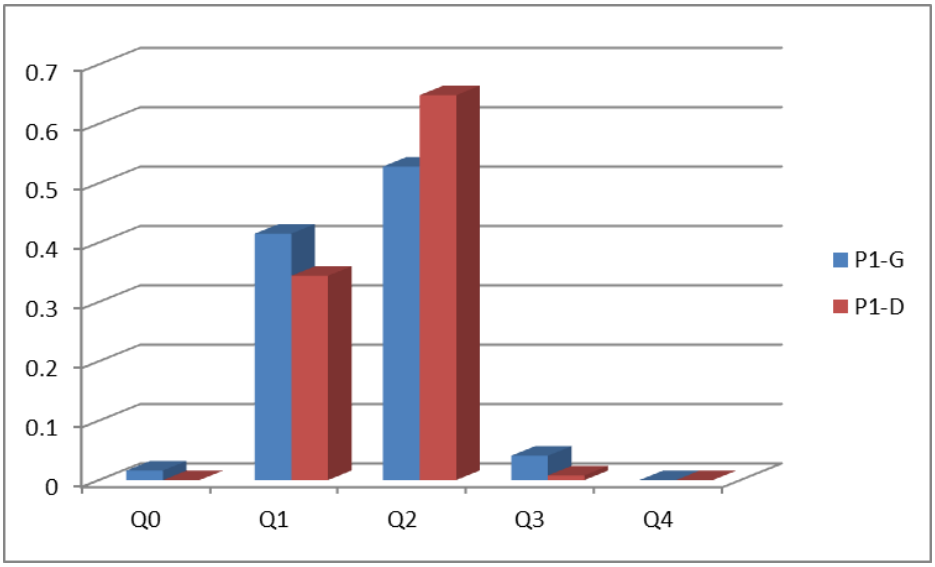

Figure 4.19 (b): Comparative display of the relative area of the different Q^n for Glass P1-G and its devitrified sample P1-D

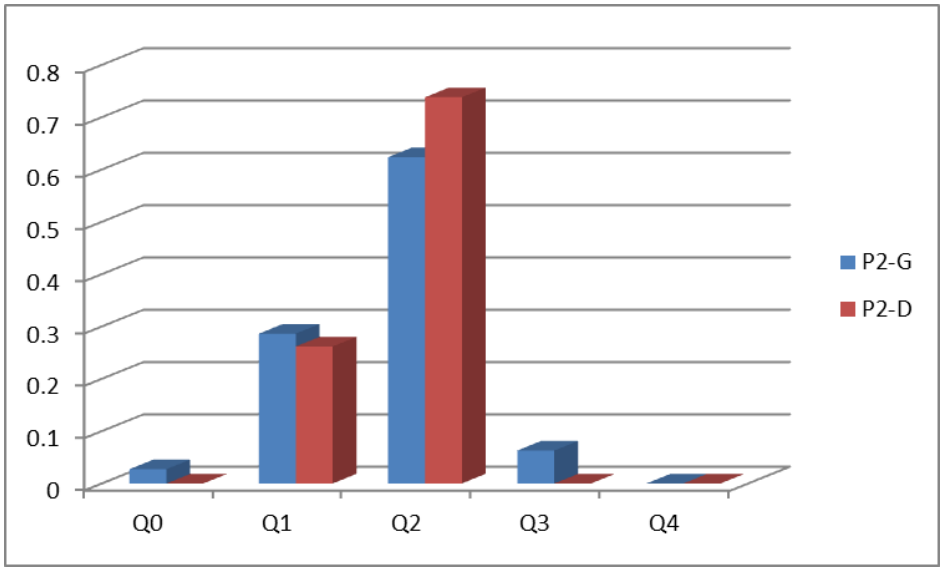

Figure 4.19 (c): Comparative display of the relative area of the different Q^n for Glass P2-G and its devitrified sample P2-D

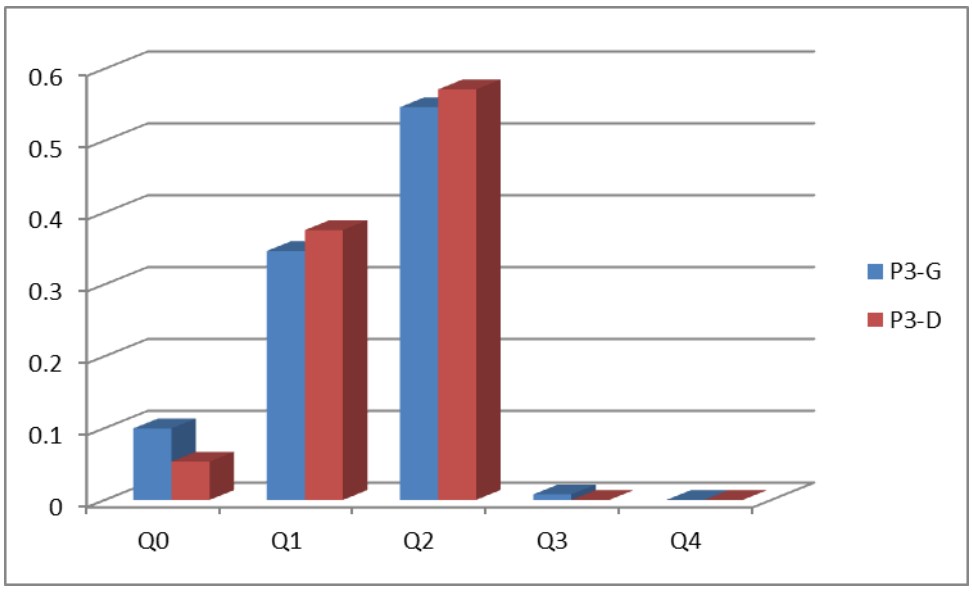

Figure 4.18 (d):

Figure 4.19 (d): Comparative display of the relative area of the different Q^n for Glass P3-G and its devitrified sample P3-D

Deconvolution of the Raman spectra in the 840 cm^{-1} to 1400 cm^{-1} region shows that the network of the three glasses P1-G, P2-G and P3-G of this study comprises mainly Q^1 and Q^2 structural units. The relative fractions of these structural units for the glass P3-G containing both Nd and La is found to be approximately an average of that for the Nd containing glass P1-G and La containing glass P2-G. This indicates that the Nd and La ions are homogeneously placed in the glass network of P3-G. Also, the number of isolated tetrahedral units Q^0 in the mixed Nd and La glass P3-G is substantially more (~ 10%) as compared to (~ 1%) in the Nd or La containing glasses. The relative number of three-connected Q^3units in this glass is negligibly small (Figure 4.19 (a)).

The connectivities in the devitrified samples are also found to be mainly Q^1 and Q^2 with the presence of Q^0 structures only in the mixed Nd and La devitrified sample (P3-D) just as the Q^0 structures also appeared in a higher percentage in the P3-G samples. Figures 4.19 (b), 4.19 (c) and 4.19 (d) show the comparison of the relative numbers of Q^n units for each glass and its corresponding devitrified state. This fact that glass and its devitrified state are similar in Q^n suggests that any detailed discussion of any glass structure can begin from the detailed study of its devitrified structure.

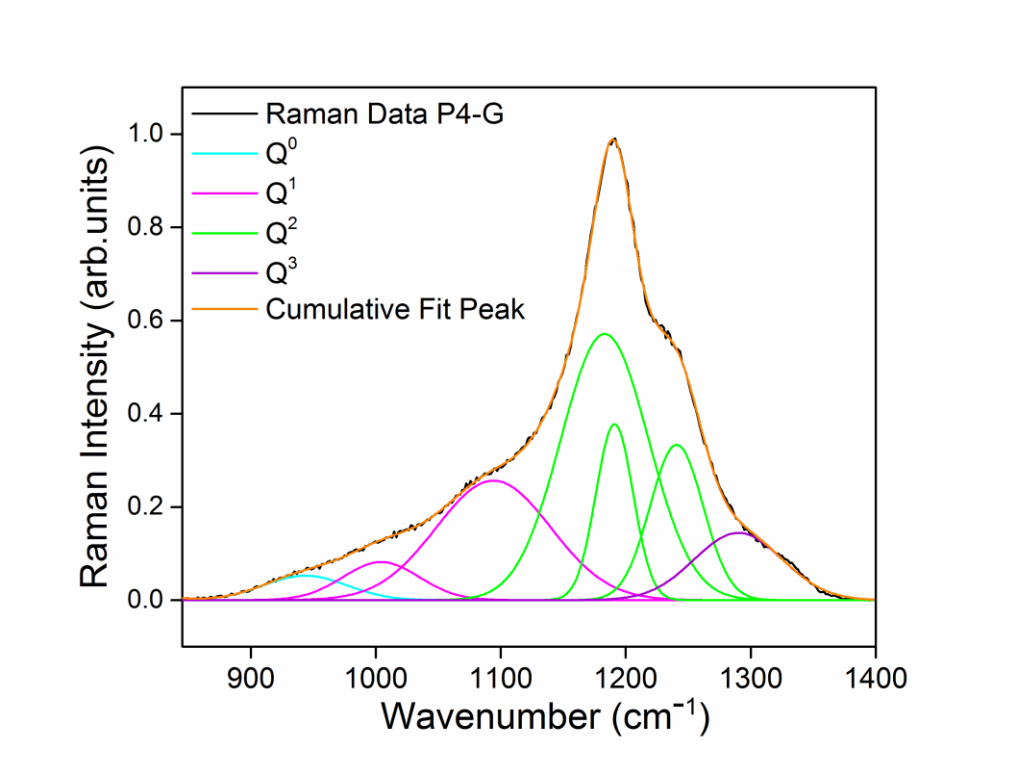

Figure 4.20: Deconvoluted Raman peaks for P4-G

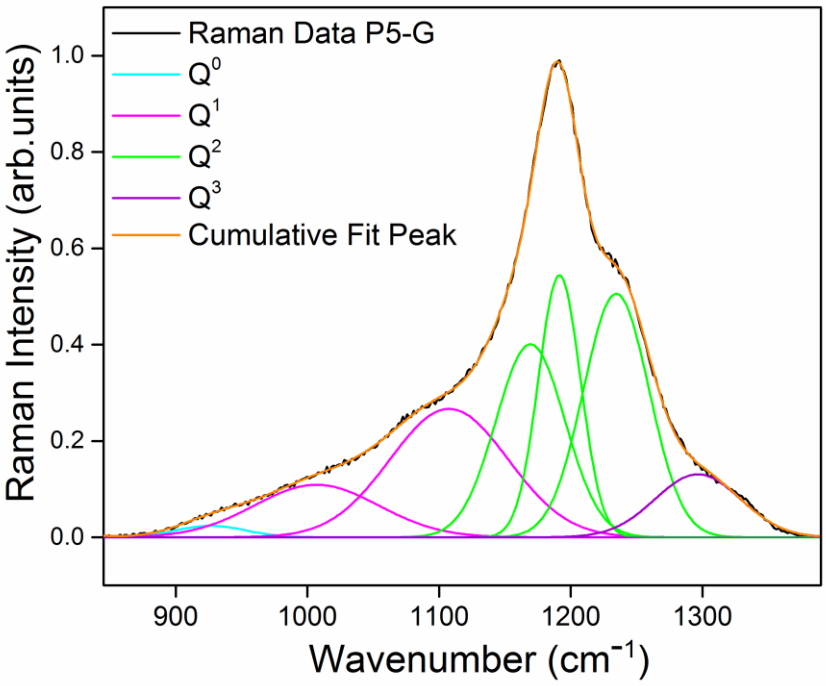

Figure 4.21: Deconvoluted Raman peaks for P5-G

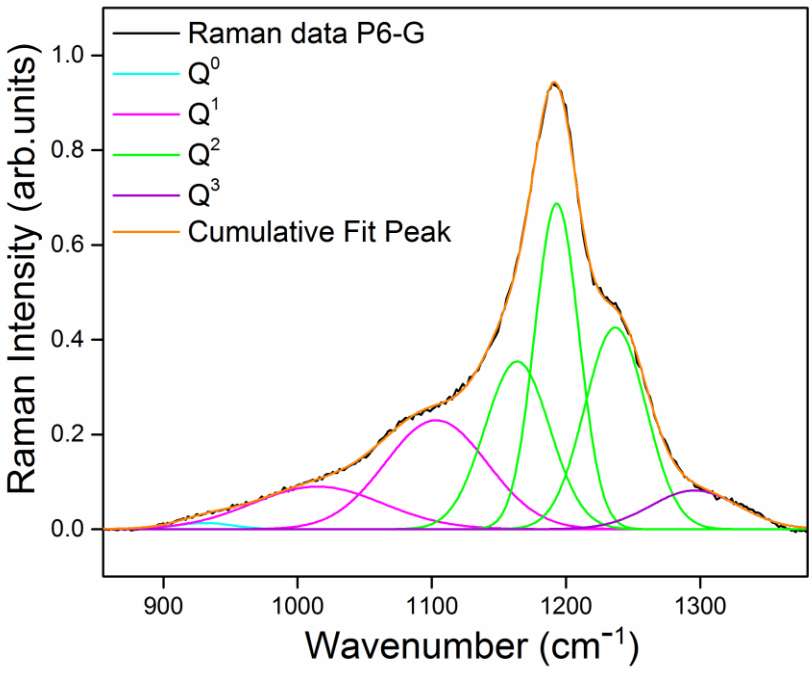

Figure 4.22 : Deconvoluted Raman peaks for P6-G

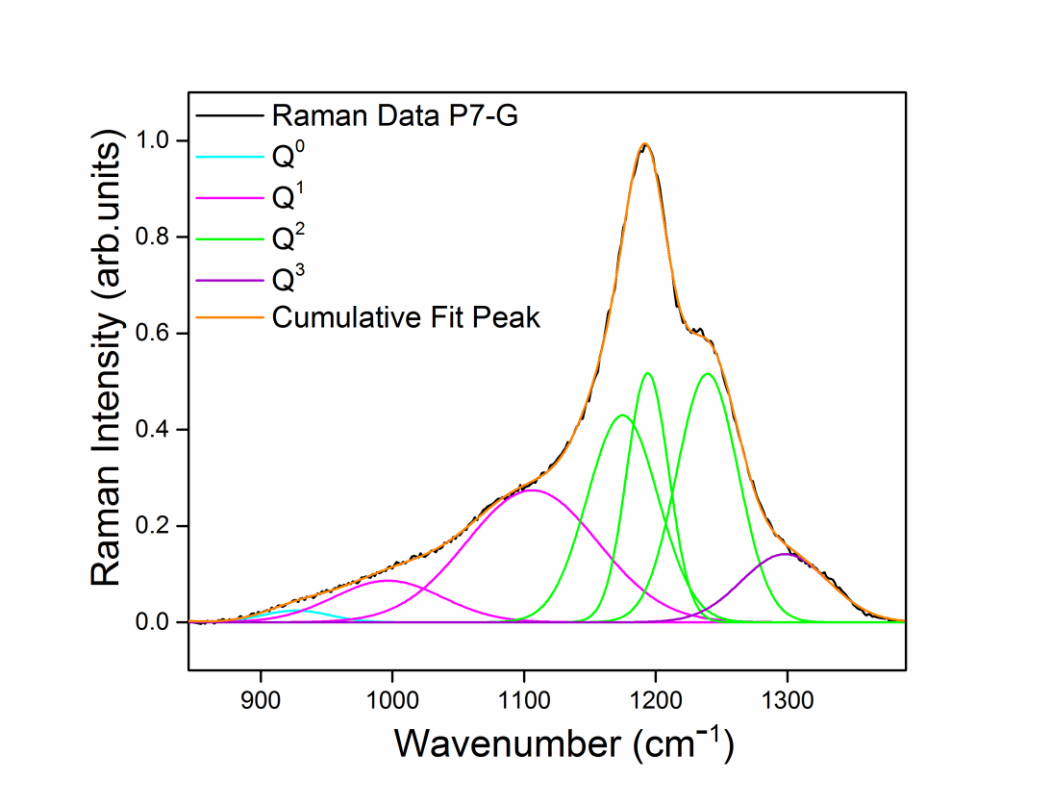

Figure 4.23: Deconvoluted Raman peaks for P7-G

Table 4.11 : Relative areas of the Q^n relating to their relative fractions.

	P4-G	P5-G	P6-G	P7-G	P10-G
Q0	0.032536	0.011743	0.00607	0.011415	0.009169
Q1	0.265117	0.318326	0.287581	0.316999	0.129804
Q2	0.607817	0.590963	0.647952	0.586101	0.779722
Q3	0.09453	0.078967	0.058397	0.085485	0.081305
Q4	0	0	0	0	0
	1	1	1	1	1

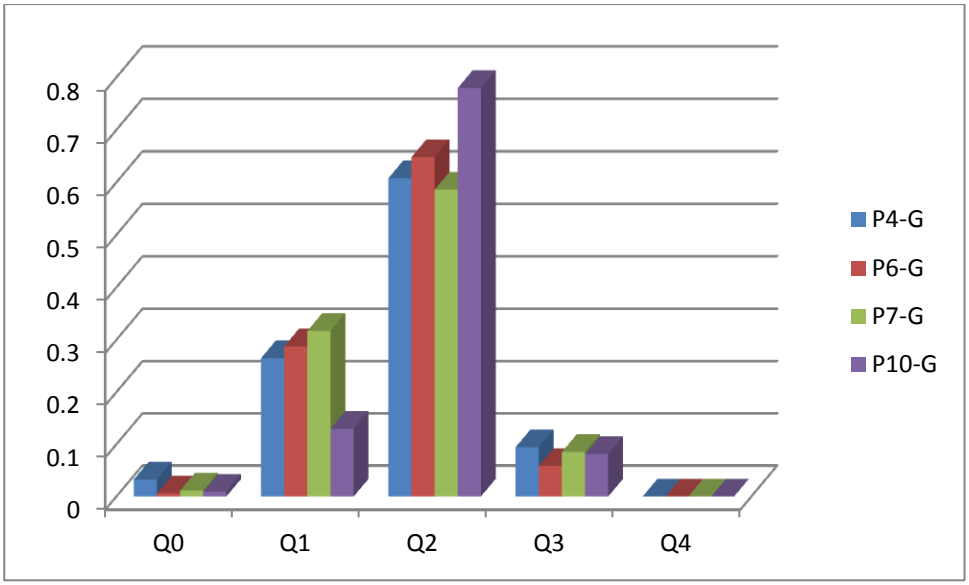

Figure 4.24 : Comparative display of the relative area of the different Q^n for (a) Glasses P4-G, P6-G, P7-G and P10-G

Deconvolution of the Raman spectra in the 840 cm^{-1} to 1400 cm^{-1} region for the glasses P4-G, P5-G, P6-G and P7-G are shown in Figures 4.20, 4.21, 4.22 and 4.23 respectively. Table 4.11 shows the relative areas of the Q^n connectivities in these glasses. The comparison of the relative number of these connectivities for the Pr containing glasses along with the alumino phosphate glass P10-G without any rare earth inclusions are shown in the figure 4.24. The connectivities in these glasses are also found to be predominantly in Q^1 and Q^2 with the non-rare earth glass having the maximum number of Q^2 connectivities and is better connected. Thus on adding the rare earth modifier Pr to this alumino phosphate glass there are more number of non-bridging oxygens formed which can be seen from the increase in the number of Q^1 connectivities and the glasses becomes less connected. The figure 4.25 shows a pictorial representation of the different Q^n structural units in the glasses in this study.

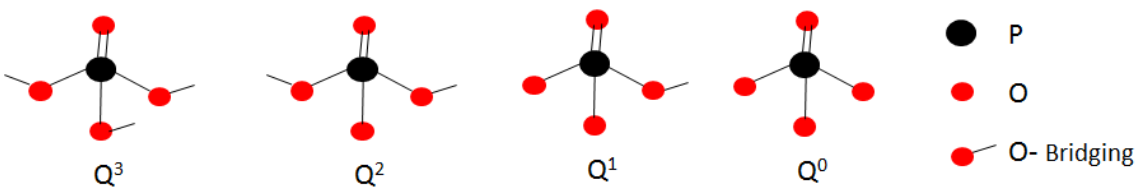

Figure 4.25: Pictorial representation of the Q^n structural units.

4.8 Extended X-ray Absorption fine structure

Figure 4.26 shows the XANES spectra at the Nd L_3 edge of the Nd doped phosphate glass and devitrified samples along with the Nd_2O_3 standard. It has been observed that the absorption edges of the samples lie close to the Nd_2O_3 standard. This suggests that the oxidation states of Nd cations in the samples are the same as that in the Nd_2O_3 standard (i.e. +3). All the samples show a white line at ~ 6210 eV that occurs due to the $2p_{3/2}$ to 5d transition. The Nd_2O_3 standard has intensity higher than the white line intensity of the samples.

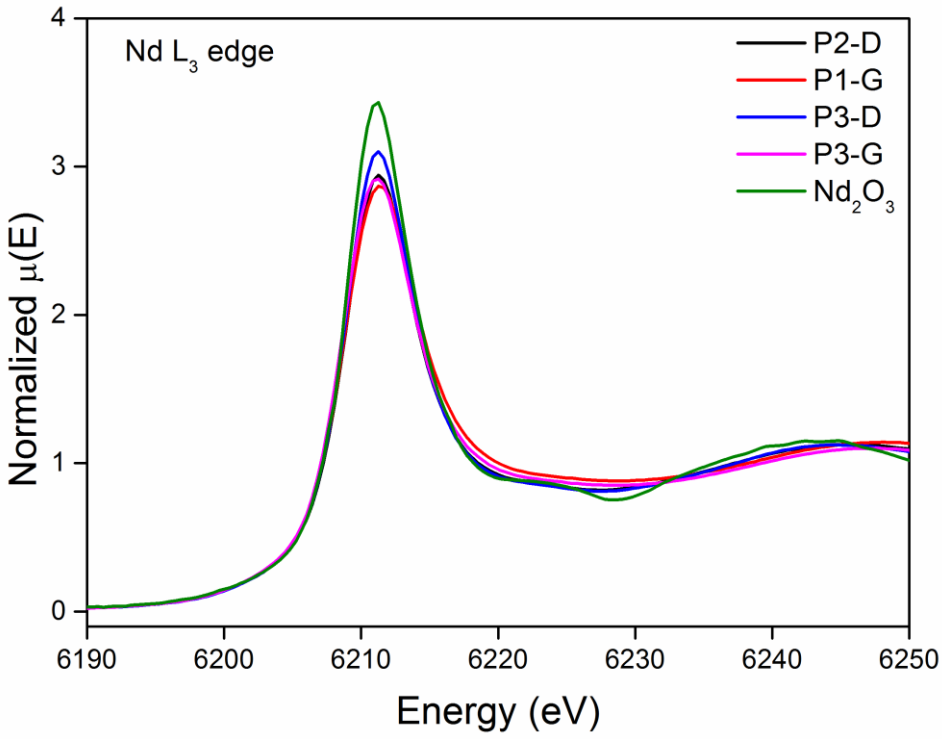

Figure 4.26: XANES spectra at Nd L_3 edge for the Nd containing glass (P1-G, P3-G), devitrified samples (P1-D, P3-D) and the Nd_2O_3 standard

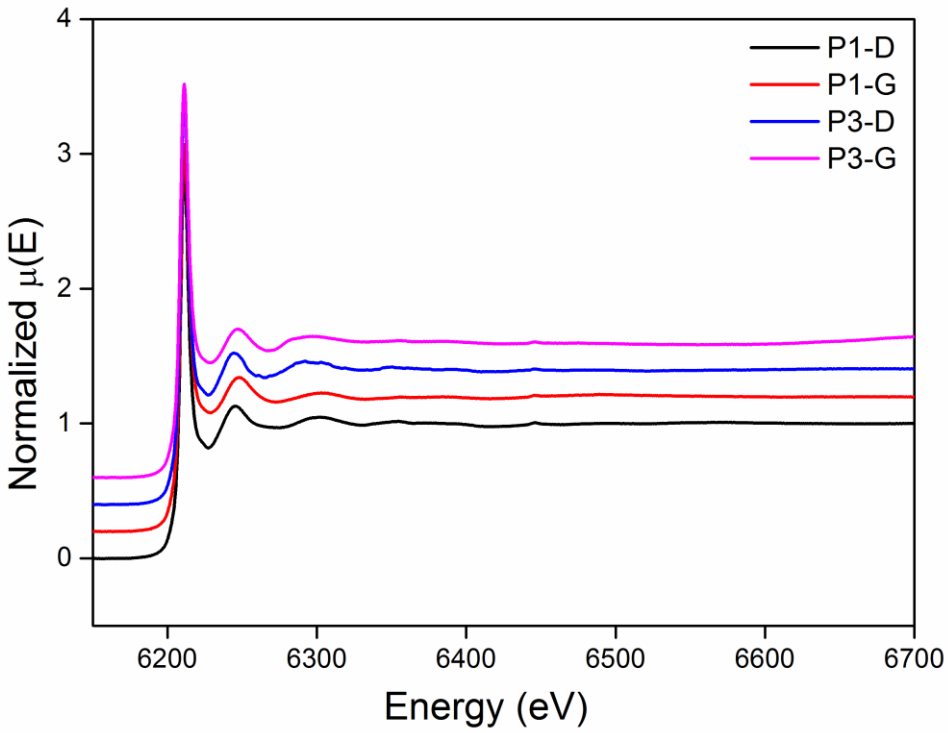

Figure 4.27: EXAFS $\mu(E)$ v/s E spectra for the Nd containing glasses P1-G, P3-G and devitrified samples P1-D, P3-D

The experimental EXAFS spectra of the Nd doped phosphate glass and devitrified samples measured at the Nd L_3 edge are shown in Figure 4.27. The analyses of the EXAFS data have been carried out following the standard procedure (Konigsberger et al. (1988), Kelly (2008)). This includes data reduction and Fourier transformation to derive the $\chi(r)$ v/s r plots from the absorption spectra, generation of the theoretical EXAFS spectra starting from an assumed crystallographic structure and final fitting of the experimental $\chi(r)$ v/s r data with the theoretical ones using the FEFF 6.0 code of the IFEFFIT software package (Newville et al. (1995)).

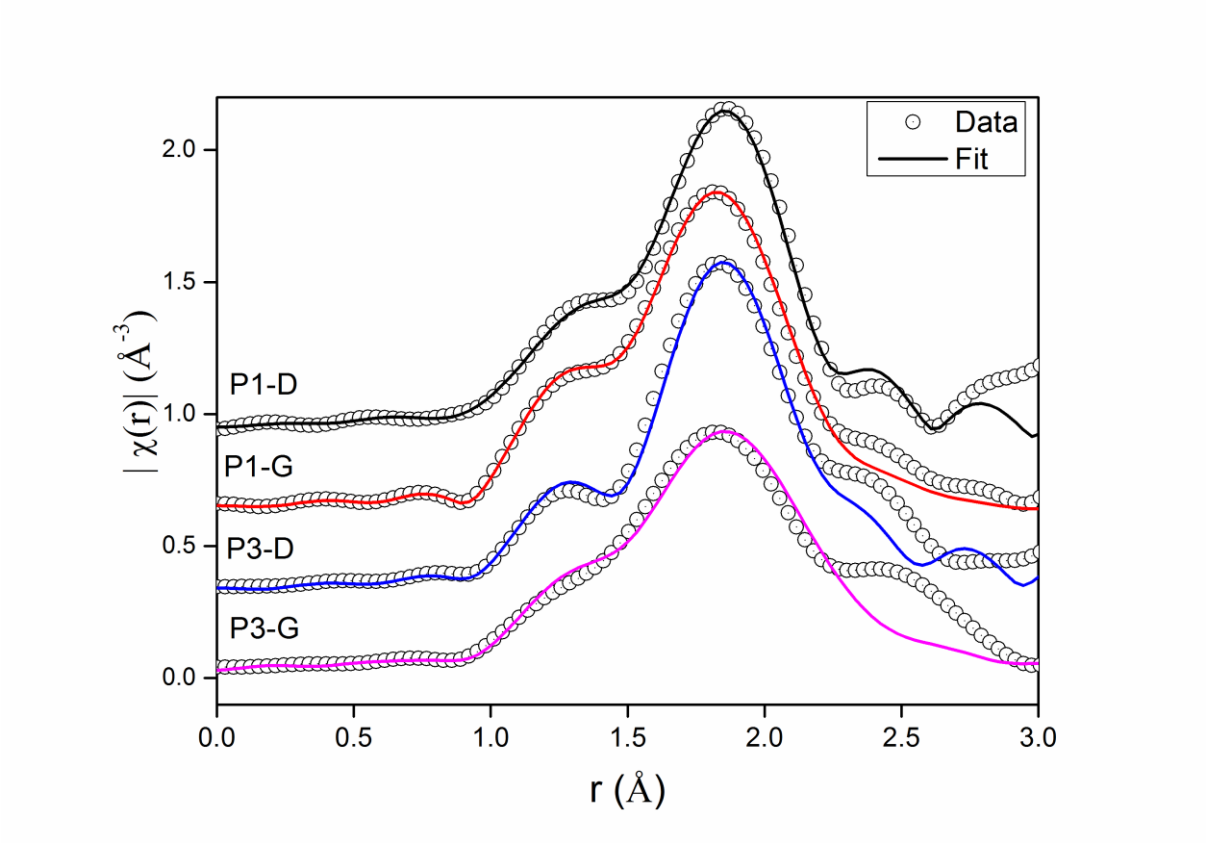

Figure 4.28: $\chi(r)$ v/s r plots for the Nd containing glasses P1-G, P3-G and devitrified samples P1-D, P3-D

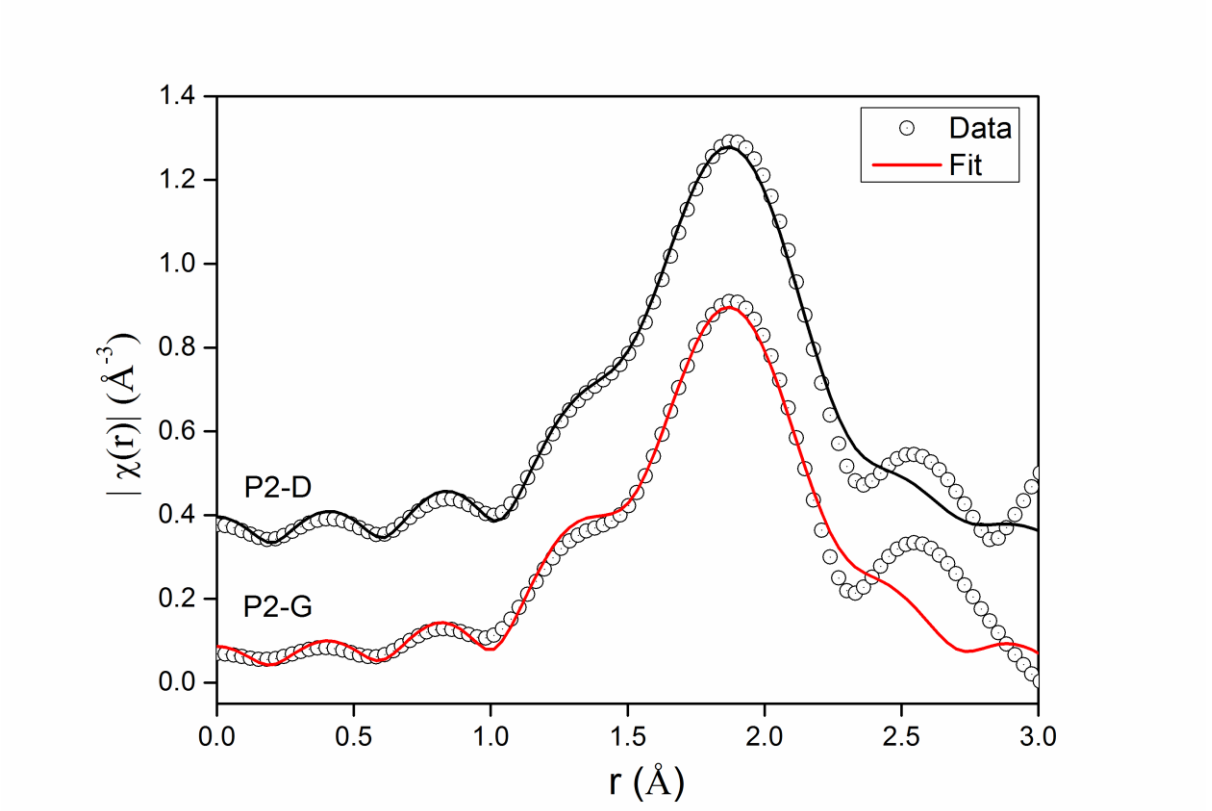

Figure 4.29: $\chi(r)$ v/s r plots for the La containing glass P2-G and devitrified sample P2-D

The experimental $\chi(r)$ versus r plots of the Nd contained glasses and devitrified samples at the Nd L_3 edge are shown in Figure 4.28 along with best fit theoretical plots fitted from 1Å to 2.5Å assuming an Nd-O shell at 2.3Å (Bowron et al. (1996)). The fitting results are listed in Table 4.12.

Table 4.12 : Correlation length and coordination number of the Nd contained glasses P1-G, P3-G and their respective devitrified states.

Correlation	P1-G		P1-D		P3-G		P3-D	
	r (Å) ± 0.01	N	r (Å) ± 0.01	N	r (Å) ± 0.01	N	r (Å) ± 0.01	N
Nd-O	2.36	7.7	2.37	8.1	2.40	7.1	2.39	7.6

Figure 4.29 shows the experimental $\chi(r)$ versus r plots of La containing glass and devitrified samples at the La L_3 edge with the best fits from 1Å to 2.2 Å assuming a La-O shell at 2.4 Å. The fitting results are tabulated in Table 4.13.

Table 4.13: Correlation length and coordination number of the La containing glass P2-G and its corresponding devitrified state P2-D.

Correlation	P2-G		P2-D	
	r (Å) $\pm$ 0.01	N	r (Å) $\pm$ 0.01	N
La-O	2.41	7.4	2.42	7.7

EXAFS results indicates that in comparing the glass to the devitrified samples, the coordination number of oxygen around Nd increases from 7.7 to 8.1 for P1-G and P2-G while it changes from 7.1 to 7.6 for P3-G and P3-D (mixed Nd and La). The La-O coordination number changes from 7.4 to 7.7 for the La included glass and devitrified states respectively. A decrease in the coordination number of oxygen around Nd is observed from 7.7 in a single rare earth (Nd) containing glass P1-G to 7.1 in the mixed rare earth containing glass P3-G i.e., on adding La along with Nd . A similar decrease is also seen in the respective devitrified material. Thus, a slightly lower than octahedral coordination is present in the glassy states which increases to approximately octahedral when the glass becomes predominantly crystalline as during devitrification.

4.9 Neutron diffraction

The measured neutron intensities of both glasses and devitrified samples were corrected for the usual experimental corrections and normalized to vanadium to obtain the structure factors S(Q) shown in Fig.4.30. The devitrified scattering intensity patterns show crystalline reflections superimposed on a glassy background.
The total correlation functions T(r) for the glasses and their devitrified states are shown in Figure 4.31. The first peaks in T(r) for the P1-D are significantly sharper and better resolved than for P2-D and P3-D samples, both at lower and at higher values of ‘r’. The total correlation functions T(r) and the radial distribution functions N(r) were calculated from the S(Q) functions by the usual method of multiplying this function by the Lorch

modification function and then Fourier transforming (referred to as the “Lorch” correlations) as well as by the method of MCGR (referred to as the “MCGR” functions). The peaks in the MCGR function are clearly narrower and better resolved as expected. The calculated and measured S(Q) functions were in excellent agreement up to the measured maximum value of Q.

Since the peak positions in T(r) and N(r) are closely similar , all Gaussian fits were made to the maxima in N(r) in order to relate to structural parameters as shown in Figure 4.32(a) for P1-G, 4.32 (b) for P1-D, Fig.4.33(a) for P2-G , 4.33 (b) for P2-D and Figure 4.34 (a) for P3-G, 4.34 (b) P3-D. A summary of the fitting to the MCGR radial distribution functions up to about 3 Å for all the samples is given in Table 4.14.

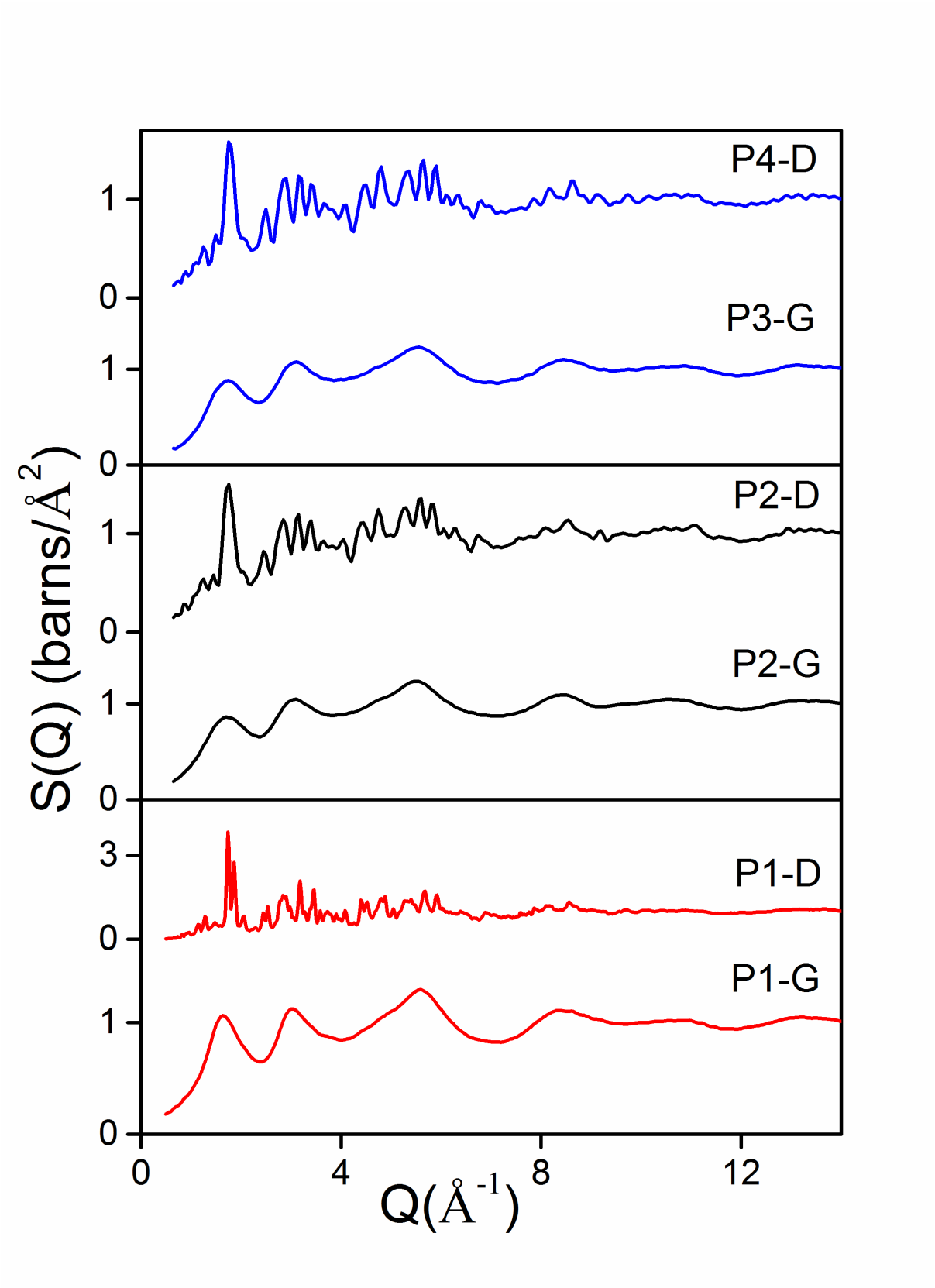

Figure 4.30: Neutron diffraction structure factor S(Q) for the glasses P1-G, P2-G, P3-G and their respective devitrified states P1-D, P2-D, P3-D

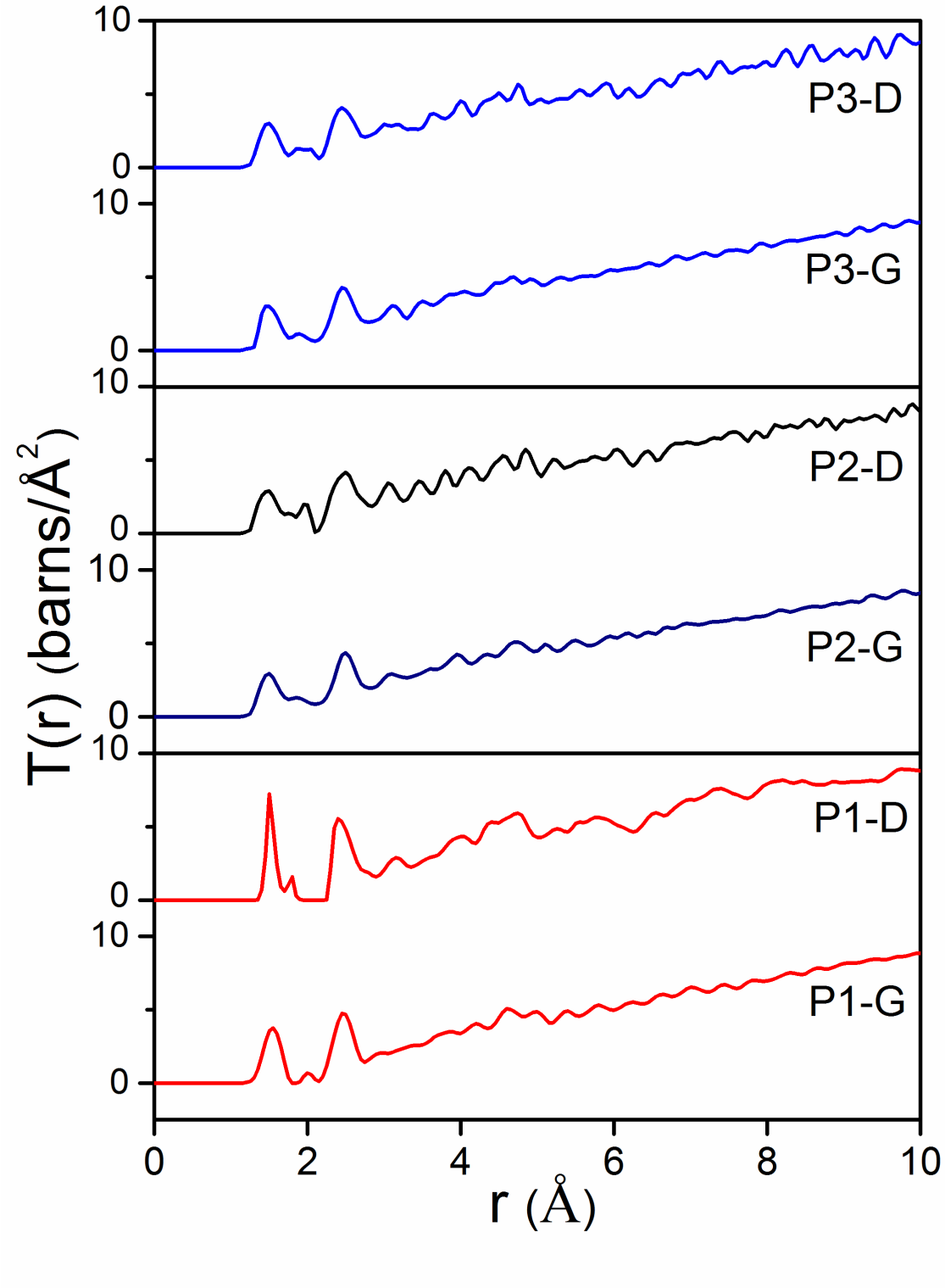

Figure 4.31: Total correlation function T(r) for the glasses P1-G, P2-G, P3-G and their respective devitrified states P1-D, P2-D, P3-D.

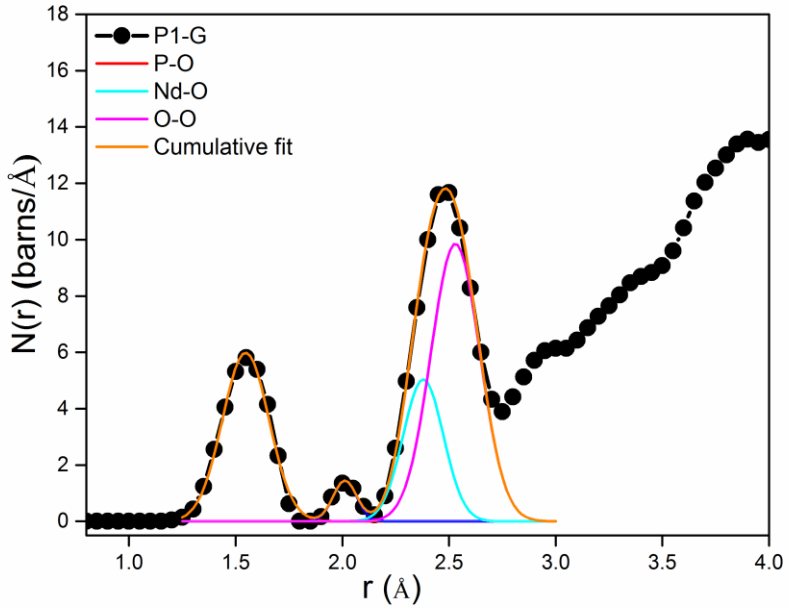

4.32 (a)

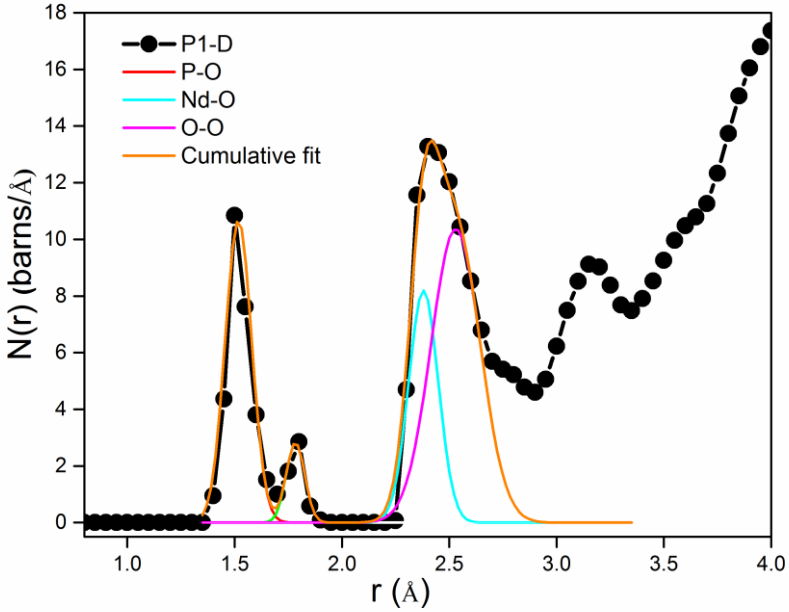

4.32 (b)

Figure 4.32: Peaks fitted to the radial distribution function N(r) of (a) P1-G (b) P1-D

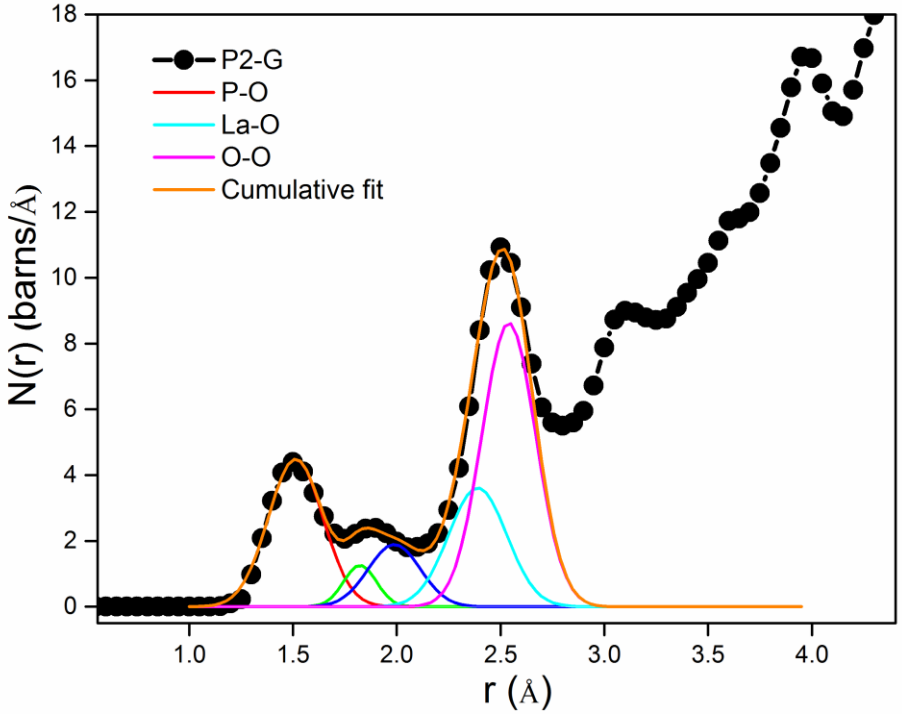
P2-G
P-O
La-O
O-O
Cumulative fit
N(r) (barns/Å)
r (Å)

4.33 (a)

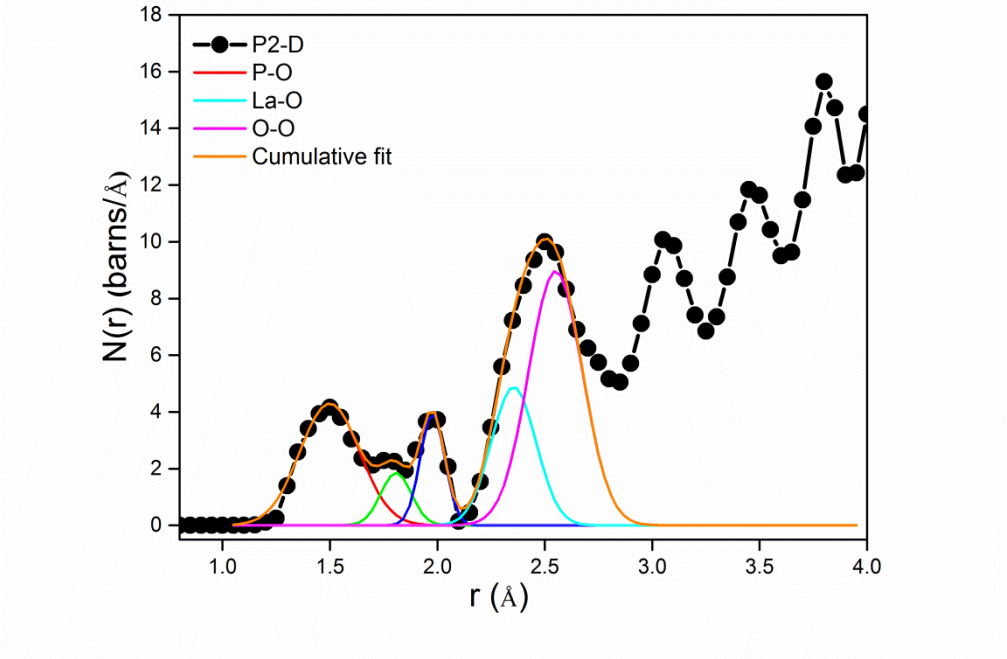
P2-D
P-O
La-O
O-O
Cumulative fit
N(r) (barns/Å)
r (Å)

4.33 (b)

Figure 4.33 : Peaks fitted to the radial distribution function N(r)of (a) P2-G (b) P2-D

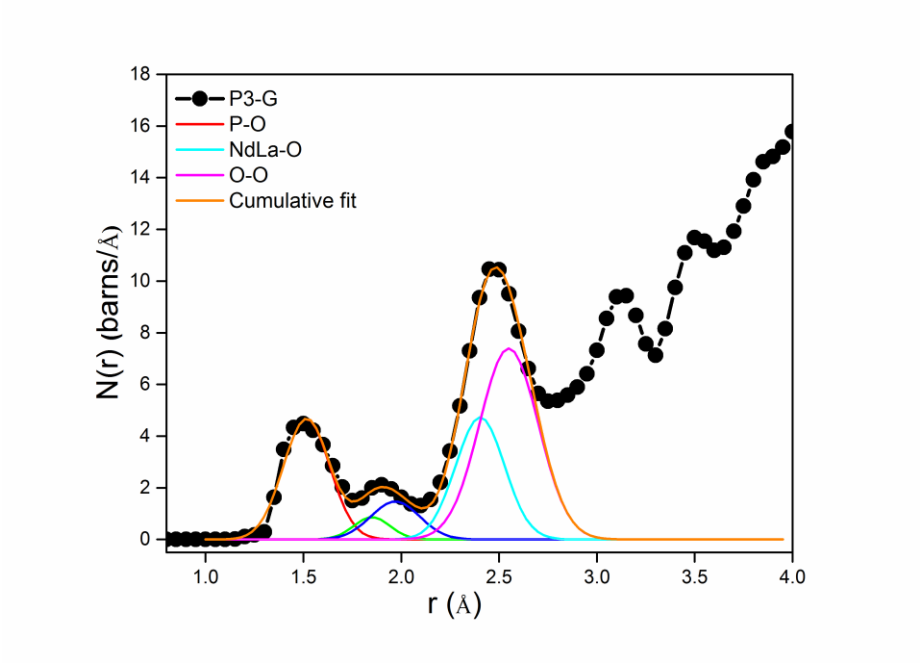

4.34 (a)

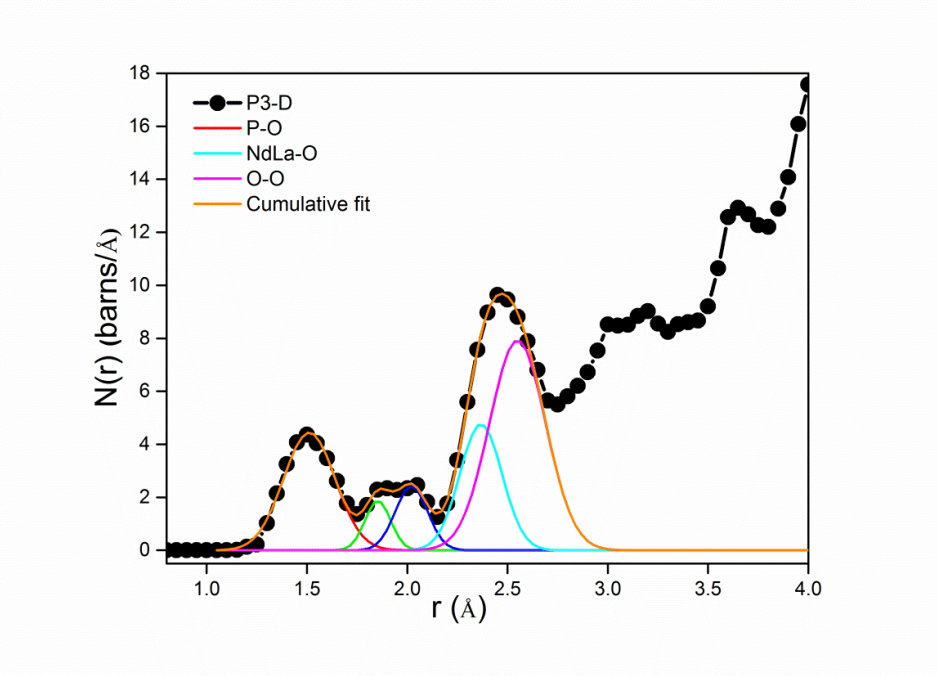

4.34 (b)

Figure 4.34 : Peaks fitted to the radial distribution function N(r) of (a) P3-G (b) P3-D

Table 4.14: Correlation lengths (r(Å) $\pm$ 0.02) and coordination numbers (N) from neutron diffraction.

Corrl.	P1-G		P1-D		P2-G		P2-D		P3-G		P3-D	
Type	r(Å)	N	r(Å)	N	r(Å)	N	r(Å)	N	r(Å)	N	r(Å)	N
P-O	1.54	3.89	1.51	3.94	1.51	3.58	1.49	3.62	1.51	3.53	1.51	3.69
RE-O	2.37	7.11	2.38	8.48	2.39	7.11	2.35	7.16	2.40	6.98	2.36	5.90
O-O	2.53	4.00	2.53	4.21	2.54	4.00	2.55	4.00	2.55	4.00	2.55	4.00

The first peak is due to the P-O correlation which is also the average bond length within the PO_4 tetrahedron. The coordination number of oxygen around phosphorous is found to slightly increase from the glass to its devitrified form along with a slight decrease in the correlation length. Thus the devitrified state is more compacted than the glass. The slight departure of this value from 4 is due to the presence of some 3-fold coordination of O around P.

The two small peaks after the P-O correlation were considered to be due to Al-O and Al-P in all the samples. The peak at around 1.8Å is taken to be due to the Al-O correlation. The feature at about 2.093 Å in the devitrified samples P2-D and P3-D was taken to be resulting from the Al-P correlation. This correlation was also assumed to be present – though unresolved - in the fitting of peaks for samples P2-G and P3-G.

The second large peak in N(r) was assumed to be composed of RE-O and O-O. The O-O correlation length was taken to be about 2.55 Å and its calculated coordination was taken to be around 4 for metaphosphate glass. The remainder area of the second large peak was considered to be due to RE-O.The area of this peak is also found to be slightly more in the devitrified samples and a slight shift towards lower r(Å) has been observed. The neodymium to oxygen coordination number in P1-G is found to increase on devitrification (P1-D). From the glass P2-G to its devitrified state P2-D, the coordination number of oxygen around lanthanum remains almost unaltered. The average mixed rare earth to oxygen coordination number is found to slightly decrease from glass P3-G to its devitrified state P3-D.

5.0 Conclusions

Several glasses (13 samples) of rare-earth oxides (Nd, La, Pr and combinations of these) included in alumino-phosphate host networks were prepared by the melt-quenching method. The rare-earth oxide percentages were mostly between 20 to 25 mol % of the mixture with three of these glasses being made to devitrify.

The X-ray diffraction patterns of the glass samples confirmed their vitreous nature while for the devitrified samples the crystalline phases were identified. Density measurements of the samples showed the devitrified ones to have a 3% higher value than the glasses from which they were formed.

Fourier Transform Infra-red Spectroscopy showed the glass samples to all have the main features associated with the basic tetrahedral vibrational modes of the PO_4 tetrahedra. As expected, the spectra for the devitrified samples displayed sharper, better resolved features pertaining to the PO_4 tetrahedral bond bending and stretching modes in the 460 cm^{-1} to 1200 cm^{-1} region of the absorption spectrum. The fact that there are no major differences between these spectra of the glasses is indicative that the rare-earth ions are not likely to be bound to the host network but have a modifier role in the structure.

UV-Visible spectroscopy data show the absorption peaks due to both the Pr and Nd ions in those systems in which both these ions were included. The implication of this is that most of these rare-earth ions would be occupying sites in the host network without being necessarily bonded to the phosphate units and hence would permit the transitions of the 4f electronic states (responsible for the observed transitions in the spectra) to be less affected by their immediate structural environments.

Raman vibrational spectra of these glasses and some of their devitrified states have focussed on the P-O-P related bending/stretching modes from 650 to 850 cm^{-1} and the PO_4 vibrational modes in the 850 to 1400 cm^{-1} range. As expected, the modes of the devitrified states are better defined than those of the corresponding glasses. From the assessment of the relative ratios of the different Q^n modes of these glasses, the main linkages for the Nd, La and Nd-La included glasses were found to be Q^1 and Q^2. The devitrified states of these glasses also showed the Q^1 and Q^2 to dominate but with higher percentages than their vitreous counterparts. By comparing the deconvoluted spectra (into constituent Q^n) of these three glasses with the measured spectra of their devitrified states, it was observed that for the Nd-La containing system, neither glass nor devitrified had Q^3 or Q^4 linkages and that Q^0 was present in this glass and its crystalline state. As expected, the calculated

connectivity was seen to be lower than when only Nd or La was present – in keeping with larger fractions of Q^0 and lower fractions of Q^3 and Q^4 - all indicative of a more open structure of the Nd-La containing glass. However, this more open structure has a slightly higher bulk density than the other two glasses in this series – due to the higher content of rare-earth (25 mole% compared with 20 mole %).

In the comparison of the Pr containing glasses, it has been observed that when there is no rare-earth (i.e. a simple alumino-phosphate) the main linkage is Q^2 with some Q^1 and Q^3 which remains when the Pr is added but with the Q^1 fraction being enhanced while the Q^3 fraction remains unaffected. This increase in a less well connected or more open network for the Pr glasses is in keeping with the view that the Pr_6O_{11} which was used in the preparation had components of both Pr^{2+} (network former) and Pr^{3+} (network modifier). Hence the resultant connectivity of the alumino-phosphate gets modified with the addition of Pr ions.

EXAFS data taken at the Nd and La edges for the three glasses containing Nd and La have found the coordination of oxygen around Nd to be slightly less than octahedral in the glass with this coordination increasing to approximately 8 in the devitrified states. The Nd-O and La-O bond lengths vary in the range 2.36 Å to 2.40Å in these systems.

The neutron diffraction data on the glasses containing Nd, La and Nd-La show the basic PO_4 structural unit to have a P-O bond length in the range of 1.51 Å to 1.54 Å with coordination numbers typically in the range 3.53 for the glass to about 3.89 for the devitrified state. The rare-earth to oxygen correlation length was seen to vary between 2.35Å to 2.38 Å with coordination numbers of oxygen around the rare-earth ion in the range of about 6 to 8.5. These values are in good agreement with those obtained with from EXAFS and serve to confirm the role of rare-earth ions as modifiers in the continuous random network of PO_4 tetrahedra. A feature in the total correlation function in the range 1.8Å to 2Å in the three glasses and devitrified systems that were measured by neutron diffraction is likely to relate to the Al-O correlation. This feature was not further analysed and was excluded in the aforementioned fittings to the P-O and rare-earth to oxygen correlations. The O-O correlation in the second major peak in T(r) was ascribed a coordination number of 4 at a length in the range of 2.53Å to 2.55Å.

References

1. Abo-Naf S.M.,.El-Amiry M.S, Abdul-Khalik A.A.,Opt.Mater.30(2008)900
2. Baert K., Meulebroeck W., Wouters H., Cosyns P, Nys K., Thienponttb H. and Terryna G., J. Raman Spect.42 (2011) 1789
3. Besancon R. M., The encyclopedia of Physics, (second edition) Van Nostrand Reinhold (1974)
4. Beveridge P., Domènech I. and Pascual E., Warm Glass, Lark Books (2005) 66
5. Bowron D. T., Saunders G. A., Newport R. J., Rainford B. D. and Senin H. B., Phys. Rev. B 53 (1996) 5268.
6. Brow R. K., Kirkpatrick R. J. and Turner G. L., J. Amer. Cer. Soc 76 (1993) 919-928
7. Brow R. K., J. Non-Cryst. Sol., 263 & 264 (2000) 1.
8. Brow R. K., J. Non-Cryst. Solids, 263 (2000) 1-28
9. Campbell J. H., Suratwala T. I., J. Non-cryst. Sol., 263 & 264 (2000) 318-341.
10. Carnall W. T., Fields P. R.and Rajnak K., J. Chem. Phys.49 (1968) 4412-4423
11. Chahine A., Et-Tabirou M., Pascal J. L.,Mater.Lett.58 (2004) 2776-2778
12. Chakraborty I. N., Condrate Sr R .A., Phys. Chem. Glasses 26 (1985) 68
13. Chanshetti U.B., Shelke V..A., Jadhav S. M., Shankarwar S.G., Chondhekar T. K., Shankarwar A. G., Sudarshan V., Jogad M. S., Phys., Chem. and Tech.Vol.9, 1 (2011) 29-36
14. Cole J. M., VanEck E. R. H., Mountjoy G., Anderson R.,Brennam T., B-Wye G., Newport R. J. and Saunders G. A., J. Physics; condens. matter 13 (2001) 4105-4122.
15. Colomban P., Milande V. and Lucas H., J. Raman Spect. 35 (2004) 68
16. Gibbons P. C., Physics, Barron Educational Series (2008)
17. Harani R., Hograth C. A., Ahmed M.M., J. Mater. Sci. Lett. 3 (1984) 843
18. Hee P., Christensen R., Ledemi Y., Wren J. E. C., Dussauze M., Cardinal T., Fargin E., Kroekar S., Messaddeq Y., J. Mater. Chem. C 2 (2014) 7906
19. Holand W., Rheinberger V. and Schweiger M., Phil. Trans. R. Soc. Lond. A 361 (2003) 575-589
20. Hong H Y P , Act. Crysta. B ,(24 (1968) 38, 30 (1974) 468-474)
21. Hoppe U., Walter G., Kranold R., Stachel D., Z. Naturforsch, 53a, (1998) 93-104.

22. Hudgens J. J., Brow R. K., Tallant D. R., Martin S. W., J. Non-Cryst. Solids 223 (1998) 21-31
23. Jouni A., Ferid M., Gacon J.C., Grosvalet L., Thozet A., TrabelsiAyadi M., Mat. Res. Bull., 38 (2003) 1613-1622
24. Judd B. R., Phys. Rev. 127 (1962) 750
25. Kader A.A., Higazy A.A., Elkholy M.M., J. Mater.Sci.: Mater. Electron. 2 (3) (1991) 157-163
26. Karunakaran R .T ., Marimuthu K., Arumugam S., Babu S. S., Leon-Luis S. F. and Jayasankar C. K., Opt. Mater.32 (2010) 1035-1041
27. Kelly S.D., Hesterberg D.and Ravel B., Analysis of soils and minerals using X-ray absorption spectroscopy ch. 14 (2008) 387-464; in Methods of Soil Analysis - Part 5. Mineralogical Methods (Soil Sci. Soc. Am. Books series 5)
28. Khan M.N., Harani R., M.M. Ahmed, Hograth C. A., J. Mater. Sci. 20 (1985) 2207
29. Konigsberger D.C., and Prince R., X ray Absorption: Principles, Applications, Techniques of EXAFS, SEXAFS and XANES. Wiley, New York, 1988.
30. Koo J., Bae Byeong-Soo, Na Hoon-Kyun, J. Non-Cryst. Solids 212 (1997) 173-179
31. Lai Y.M., Liang X. F., Yang S. Y., Wang J. X., Cao L. H., Dai B., 992 (2011) 84-88
32. Leadbetter A. J., Wright A. C., J. Non-Cryst. Sol., 7, (1972) 23-36
33. Liang X., Yin G., Yang S, Lai Y. and Wang J., Spectroscopy letters 44 (2011) 418-423.
34. Lide D. R., Hand book of chemistry and Physics (87ed), Boca Raton, Florida; CRC Press(1998) pp 4-40
35. Luo Z., Lu A., Hu X. and Liu W., J. Non-Cryst. Solids 368 (2013) 79-85
36. Magdas D. A., Cozar O., Chis V., Ardelean I., Vedeanu N., Vib. Spectrosc. 48 (2008) 251-25
37. Matuszewski J., Kropiwnicka J., Znamierowska T., Jour. of Sol. State Chem., 75 (1988) 285-290
38. Mollazadeh S., Yekta B. E., Javadpour J., Yusefi A. and Jafarzadeh T. S., J.Non-cryst. Solids 361 (2013) 70-77
39. Morgan S. H., Magruder R. H., Silberman E., J. Am. Ceram. Soc. 70 (1987) 70
40. Muraoka Y., Kihara K., Phys. and Chem. of Minerals 24 (1997) 243-253
41. Nelson B. N. and Exarhos G. J., J.Chem. Phys. 71 (1979) 2739

42. Newville M., Ravel B., Haskel D., Rehr J.J., Stern E.A. and Yacoby Y., Physica B 154 (1995) 208.
43. Ofelt G. S., J. Chem. Phys. 37 (1962) 511
44. Pavic L., Milankovic A.M., Rao P.R., Santic A., Kumar V.R., Veeraiah N., J.Alloys Comp. 604 (2014) 352-362
45. Pemberton J. E., Latifzadeh L., Fletcher J.P., Rishbud S.H., Chem. Mater. 3 (1991) 195-200
46. R. Hill, J. Mater. Sci.Lett. 15 (1996) 1122-1125
47. Rai V.N., Rajasekhar B. N., Tiwari P., Kshirsagar R. J., Deb S. K., J.Non-Cryst. Solids 357 (2011) 3757-3764
48. Rouse Jr G. B., Miller P. J. and Risen W.M., J. Non-Cryst. Solids 28 (1978) 193
49. Sales B.C., Mater. Res. Soc. Bull. 12 (1987)32
50. Sammons R. L., Thackray A. C., Ledo H. M., Marquis P. M., Jones I. P., Yong P.and Macaskie L. E., J. Physics: Conference series 93(2007) 012048 :1-7)
51. Saout L.G., Simon P., Fayon F., Blin A., Vaills Y., J.Raman Spec. 33(2002)740-746
52. Shaim A., Et-Tabirou M., Pascal J.L., Mater. Chem. Phys. 80 (2003) 63-67
53. Shi Q., Kang J., Qu Y., Liu S., Khater G. A., Li S., Wang Y. and Yue Y., J. Non-Cryst. Solids 491 (2018) 71-78
54. Shikerkar A. G., Desa J. A. E, Krishna P. S. R., Chitra R., J. Non-Cryst. Solids., 270 (2000) 234-246.
55. Smith H., Cohen H., Phys. Chem. Glasses 4 (1963) 173
56. VanWazer J. R., Phosphorus and its compounds, vol. 1&2, Interscience, New York (1958).
57. Velli L. L., Varsamis P. E., Kamitsos E. I., Moncke D., Ehrt D., Phys. Chem. Glasses, 46 (2005) 178-181
58. Yifen J., Dehua J., Xiangsheng C., Behya B., Xihuai H., J.Non-Cryst.Solids 80(1-3) (1986)147-151
59. Zarzycki J., Glass And The Vitreous State, Cambridge Univ. Press 220 (1991)

CHAPTER 5

STRUCTURAL STUDIES OF ALUMINO GERMANATE GLASSES DOPED WITH La, Pr AND Nd IONS

Rare earth ions such as Lanthanum(La) , Praseodymium(Pr) and Neodymium(Nd) - both as single type and duo - were incorporated in alumino-germanate glass. These glasses were prepared by using the melt quenched technique. Their structures and dynamics were studied using Extended X-ray Absorption Fine Structure (EXAFS), spectroscopic techniques such as Fourier Transform Infra-Red spectroscopy, UltraViolet -Visible spectroscopy and Raman spectroscopy, Differential Thermal Analysis (DTA), X-ray and neutron diffraction.

5.1 Introduction

Germanate glasses are considered to be very important in technological applications in telecommunications and optical industries because of better transmission in the infra-red region (Margaryan and Pilavin(1993)). Rare earth germanate glasses have important applications in laser devices, opto-electronic devices and glasses for protection against radiation such as X-rays or Gamma rays (Rachkovskaya and Zakharevich (2007), Polukhin and Khim (1982), Balda et al (2000)). In addition, rare-earth alumino-germanate glasses being transparent, having good thermal stability, water resistance and chemical durability find use in solar energy tapping and spectroscopic applications (Rao (2002), Sahnounet al. (2005)).

An early study of germania using X-ray diffraction (Zarzycki (1957)) showed that GeO2 is of tetrahedral nature. Later a neutron diffraction study by Lorch (1969) confirmed that germanium is four-fold coordinated to oxygen. Germanium dioxide has two polymorphs - hexagonal GeO2 which has a structure similar to β-quartz with germanium having a coordination number of 4 and tetragonal GeO2 which has a rutile-like structure with germanium having a coordination number of 6 (Greenwood, Earnshaw (1997)).

Neutron diffraction studies showed that GeO_2 glass forms a continuous random network of corner linked GeO_4 tetrahedra (Leadbetter and Wright (1972), Desa et al. (1988), Stone et

al. (2001). The basic building block of vitreous germania is the germanium Q^4 structural unit (Shelby (2005))

Murthy and Kirby (1964) observed that by increasing the alkali content in a germanate glass there is a simultaneous increase in the coordination of oxygen around Ge which reaches a maximum for a composition having 20 mol% alkali oxide. During this process octahedral GeO_6 gets developed from tetrahedral GeO_4 structural units depending on the number of oxygen ions made available by the modifier alkali oxide. With further increase in alkali content, GeO_6 structural units get reconverted to GeO_4. A Raman spectroscopic study of germanate glass with Na_2O (Henderson and Fleet (1991)) found evidence that three-membered rings of GeO_4 tetrahedral units are formed rather than the formation of GeO_6 units, while a high resolution neutron diffraction study of PbO-GeO_2 glasses by Umesaki et al. (1995) supports the formation of GeO_6 units.

In a study of cesium germanate glasses using neutron diffraction, Hannon et al. (2007) developed a model to study the Ge-O coordination. They concluded that the increase in the number of oxygen ions around Ge is due to the formation of GeO_5 structural units instead of GeO_6. Rada et al. (2010) in their FTIR and UV-Visible studies of lead germanate glasses suggested the formation of GeO_5 structural units as a transitional phase during which GeO_4 structural units get transformed to GeO_6.

Desa et al. (1982) used the anomalous dispersion technique in their study of samarium aluminium germanate glasses by neutron diffraction and found the coordination of oxygen around samarium to be ~ 6.5. Structural studies of germanate glass included with promising rare earth ions such as neodymium and praseodymium suitable for laser applications have not been extensively reported. In the present study, alumino-germanate glasses have been prepared containing La, Pr and Nd ions both singly and together. Raman spectroscopic techniques have been used in addition to FTIR and UV-Visible spectroscopy in order to examine the structures of the glasses and the effect of including two rare earths together on the structure of the host alumino-germanate glass. EXAFS and neutron diffraction studies were made on the Nd, Pr and mixed Nd –Pr glasses to examine the structural and dynamical effects of inclusion of both Nd and Pr on the glass.

5.2 Sample preparation

The melt-quenched technique was used to prepare all the glasses in this study. The calculated values of the constituent oxide powders were weighed as per the respective molar percentages shown in Table 5.1. Batches of 12 gm of each composition were made up using constituent weights as shown in Table 5.2. Germanium dioxide (germania) was used in preparing these germanate glasses. After being thoroughly mixed and finely ground in an agate mortar and pestle, the mixture was transferred to an alumina crucible and placed in a high temperature furnace (Carbolite 1600). The temperature of the furnace was controlled and increased from room temperature gradually to a target temperature of 1400^{o}C. After this process of melting the powders over a period of four hours, the melt was held at 1400^{o}C for 20 minutes in the furnace. The crucible was then removed from the furnace and its contents were poured on to a metal plate. The clear, homogeneous but coloured glass beads (Figure 5.1) that formed on quenching from the melt were then kept for annealing in a pre-heated furnace at 400^{o}C and held for 60 minutes. The furnace was then switched off and the glass was allowed to cool slowly (overnight). Some of these glass beads of each type were placed in an annealing furnace for devitrification and the temperature was increased to 1000^{o}C. The temperature was held constant for about 1 hour and the furnace was put off and allowed to cool to room temperature. The transparency of the glass beads was lost and opaque devitrified coloured samples were formed as a result of this heat treatment.

Table 5.1: Composition of the prepared glass samples in mole%

Rare earth oxide content	Glass code	GeO_2	Al_2O_3	Nd_2O_3	Pr_6O_{11}	La_2O_3
10% Nd_2O_3	G1-G	80	10	10	00	00
10% Pr_6O_{11}	G2-G	80	10	00	10	00
05% Nd_2O_3 05% Pr_6O_{11}	G3-G	80	10	05	05	00
10% La_2O_3	G4-G	80	10	00	00	10
05% Nd_2O_3 05% La_2O_3	G5-G	80	10	05	00	05

Table 5.2: Calculations of the constituent powders of the respective glasses

Glass sample	Compound	Molecular weight (gm-Mole)	Mole %	Corresponding weight	For 1gm ± 0.0005	For 12 gm ± 0.0005
G1-G	Nd_2O_3	336.48	10	33.648	0.2638	3.1654
	Al_2O_3	101.96	10	10.196	0.0799	0.9592
	GeO_2	104.64	80	83.712	0.6563	7.8753
			100	127.556	1	12
G2-G	Pr_6O_{11}	1021.44	10	102.144	0.5210	6.2520
	Al_2O_3	101.96	10	10.196	0.0520	0.6241
	GeO_2	104.64	80	83.712	0.4270	5.1239
			100	196.052	1	12
G3-G	Nd_2O_3	336.48	05	16.824	0.1040	1.2477
	Pr_6O_{11}	1021.44	05	51.072	0.3156	3.7877
	Al_2O_3	101.96	10	10.196	0.0630	0.7562
	GeO_2	104.64	80	83.712	0.5174	6.2084
			100	161.804	1	12
G4-G	La_2O_3	325.81	10	32.581	0.2576	3.0910
	Al_2O_3	101.96	10	10.196	0.0806	0.9673
	GeO_2	104.64	80	83.712	0.6618	7.9417
			100	126.489	1	12
G5-G	Nd_2O_3	336.48	05	16.824	0.1324	1.5894
	La_2O_3	325.81	05	16.2905	0.1282	1.5390
	Al_2O_3	101.96	10	10.196	0.0803	0.9632
	GeO_2	104.64	80	83.712	0.6590	7.9084
			100	127.0225	1	12

PrAlGe NdPrAlGe LaAlPrGe

Figure 5.1: Photographs of some germanate glass

5.3 Differential thermal analysis and density

The glass G2-G which contains only Pr shows the highest glass transition temperature T_g of 867^oC and the glass G4-G containing only La shows the lowest glass transition temperature T_g at 812^oC. The fluid displacement method with xylene as the buoyant medium was used to measure the density of the glass samples. The glass transition temperatures, molar volume and measured densities are listed in the Table 5.3. In the praseodymium included glasses G2-G and G3-G, both Pr^{2+} and Pr^{3+} cations are present thereby increasing the mobility of oxygen in the melt (Rossignol (2001)). This leads to a higher value of viscosity of the melt resulting in the density (ρ) of the melt and the glass transition temperature (T_g) being higher. Density of glass also gives an estimate of the compactness of the glass structure, higher the density more compact is the glass structure.The molar volume for the glasses was obtained (Chanshetti et al. (2011)) using equation 5.1 :

$$V_m = \frac{\Sigma(n_i M_i)}{\rho} \qquad (5.1)$$

Where, n_i is the molar fraction, M_i is the molecular weight of the i^{th}component of the sample and ρ is the density.

The network connectivity (NC) (Hill (1996)) was calculated for the above glasses using equation 5.2 :

$$NC=2+[(BO-NBO)/G] \quad (5.2)$$

Where BO is the total number of bridging oxygens, NBO is the total number of non-bridging oxygens and G is the number of glass forming units.
The network connectivity is found to be the highest at 3.25 for the Glass G1-G, G4-G and G5-G, intermediate at 2.75 for G3-G while it is the lowest for the glass G2-G at 2.25. This is also supported by FTIR and Raman spectroscopy.

Table 5.3 : Glass transition temperature, density and molar volume

Glass sample	Glass transition temperature $T_g(\pm 2^{O}C)$	Density ρ (±0.01 gm/cc)	Molar volume $V_m(\pm 0.05$ cc)
G1-G	830	4.33	29.46
G2-G	867	4.88	40.15
G3-G	858	4.71	34.33
G4-G	812	4.19	30.16
G5-G	817	4.26	29.83

5.4 X-Ray Diffraction

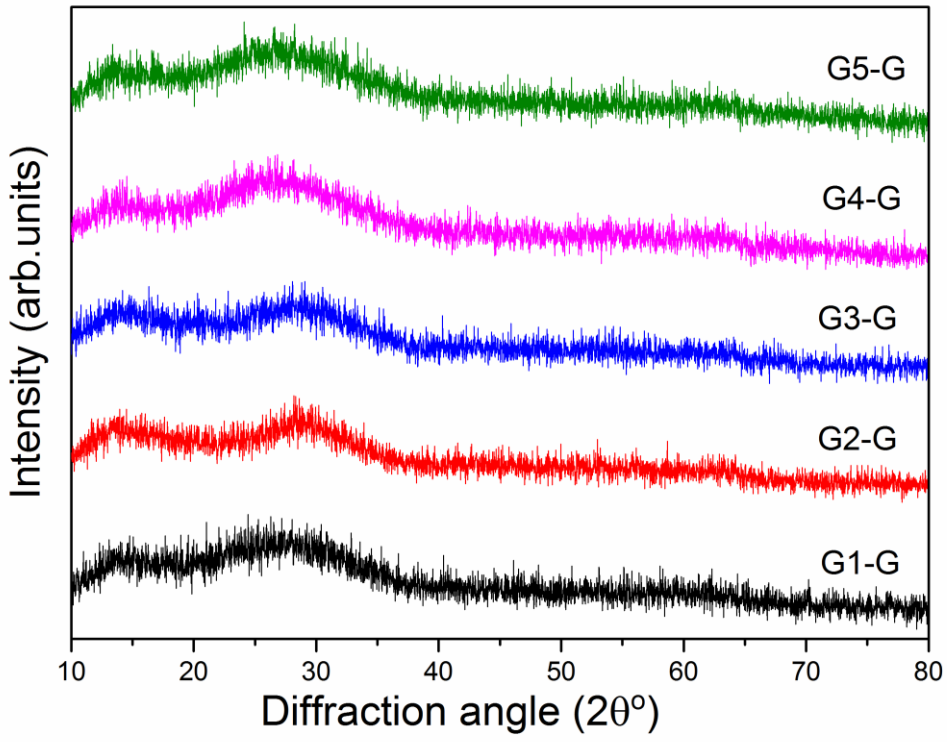

Figure 5.2 : Xray diffraction spectra of the glasses G1-G ,G2-G, G3-G, G4-G and G5-G.

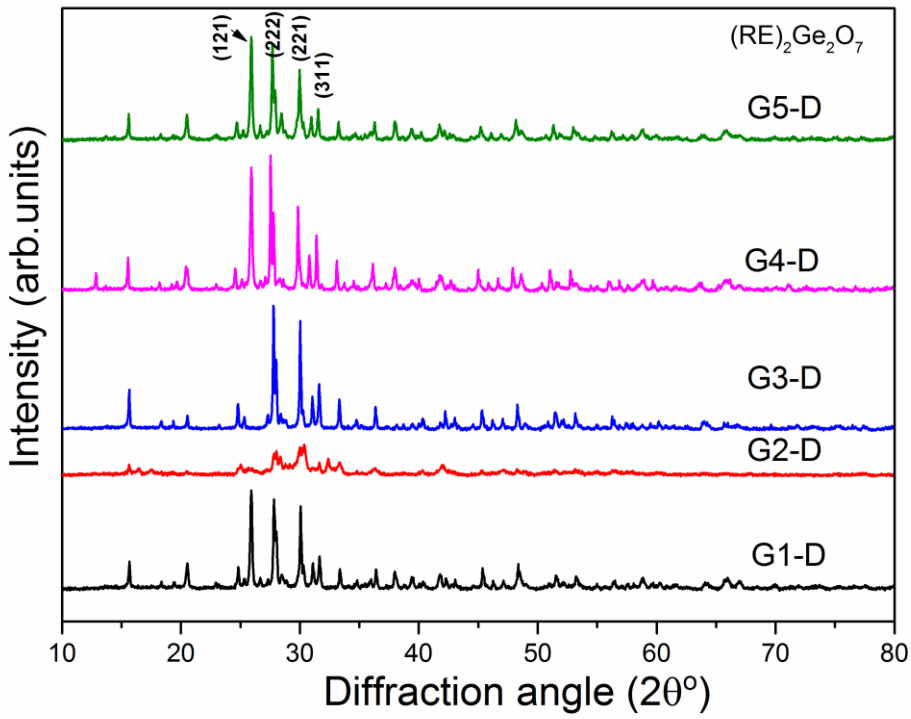

Figure 5.3: Xray diffraction spectra of the devitrified states G1-D, G2-D,G3-D, G4-D and G5-D.

The X-ray diffraction pattern for the glasses G1-G, G2-G, G3-G, G4-G and G5-G are shown in Figure 5.2. The absence of Bragg reflection peaks indicates the amorphous nature of these glasses and the presence of broad maxima arises from the amorphous nature of the glasses prepared. In the Figure 5.3 the presence of sharp Bragg peaks in the diffraction patterns of the devitrified states confirms their crystalline natures. The crystallinity in these samples is due to the $(RE)_2Ge_2O_7$ phase with space group P1 in the respective rare earth (RE) alumino germanate devitrified states (Denisova (2018)).

5.5 Fourier Transform Infrared Spectroscopy

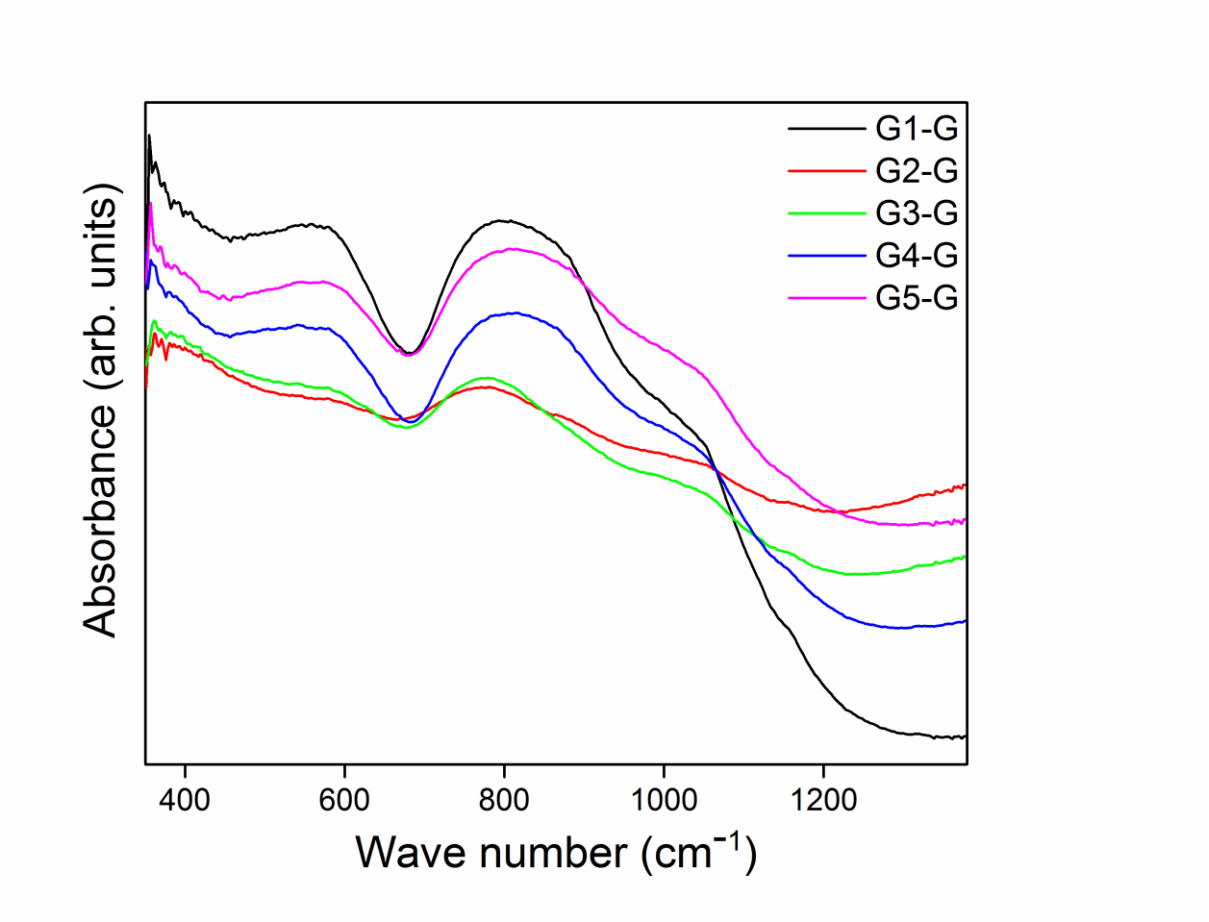

Figure 5.4(a) : Fourier transform infrared spectra of the glasses G1-G, G2-G, G3-G, G4-G and G5-G.

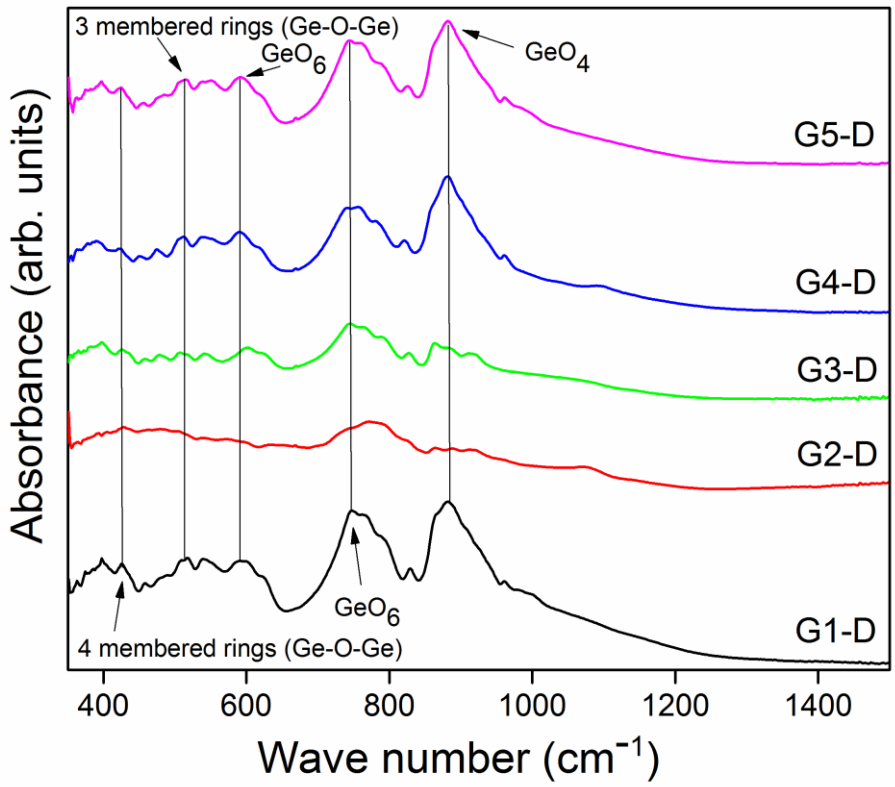

Figure 5.4(b): Fourier transform infrared spectra of the devitrified samples G1-D, G2-D, G3-D, G4-D.

From the FTIR absorbance spectra of the devitrified samples shown in Figure 5.4(b), it is found that there is presence of both GeO_4 structural units at ~ 880 cm^{-1}(Rachkovskaya et al. (2007) and GeO_6 structural units at ~ 745 cm^{-1} (Simon et al. (2000)) in the Nd containing G1-D, La containing G4-D. and both Nd and La containing G5-D samples. Both these structural units are also present in the mixed Nd and Pr containing G3-D sample but to a much lesser extent. However, it is noted that both these structural units appear to be missing in the Pr containing sample G2-D. In this sample G2-D it appears that the intermediate GeO_5 structural transitional unit could have been present (Rada et al. (2010)). The structure seems to have been distorted due to the presence of Pr in these G2-D and G3-D samples. Also the stretching of GeO_4 related to 3 membered rings appear at 513 cm^{-1} and those related to the 4 membered rings appear at 425 cm^{-1} (Henderson and Fleet (1991)) in the Nd and La contained glasses but are seen to have been distorted in the Pr containing glass G2-G.

In the FTIR spectra for the glass samples shown in Figure 5.4(a), the band at about 590 cm^{-1} in the glass samples G1-G, G3-G and G4-G is due to the symmetric stretching vibrations of germanium atom in six coordination (Martino et al. (2001)). This band appears to be reduced in bandwidth and intensity in the mixed Nd and Pr containing glass G3-G and almost flattened in the Pr containing glasses G2-G probably due to Pr^{2+} taking part in network formation. This band also shows the GeO_4 vibrations of three and four membered rings. The band in the range 680 cm^{-1} to 1100 cm^{-1} is associated with the vibrations of the Ge-O-Ge and O-Ge-O bonds (Xiao et al.(2009)) The region at about 800 cm^{-1} to 850 cm^{-1} is due to vibrations of Ge ions in combination of 4 and 6 coordination structural units. This band is seen in the glasses G1-G, G4-G and G5-G which do not contain Pr but appears reduced and narrowed in the Nd-Pr glass G3-D and flattened in the Pr glass G2-G (Kim (2005), Murthy (1964), Culea (2010), Alvarado-Rivera (2014))

There is formation of more of GeO_6 in the glasses G1-G, G4-G and G5-G which do not contain any Pr, while for those containing Pr there is probable formation of less of GeO_4 and more of non-bridging oxygens which is also seen in the Raman spectra with the existence of Q^0 structures in the glasses G2-G and G3-G.

5.6 Ultraviolet-Visible spectroscopy

The Optical absorption spectra of the glasses in this study originates from the 4f electronic levels of the rare earth ions Nd and Pr as shown in Figure 5.5 without any contribution from La ions in the visible range as the latter do not have any f shell electrons for absorptions in the visible region (see G4-G of Figure 5.6). The absorption edge is found to occur in the near-ultraviolet region. The absorption peaks of Nd in the G1-G glass were identified to be from the following ground to excited states : $^2P_{1/2}$, $^4G_{11/2}$, $^2G_{9/2}$, $^4G_{9/2}$, $^4G_{7/2}$, $^4G_{5/2}$, $^2H_{11/2}$, $^4F_{9/2}$, $^4S_{3/2}$ and $^4F_{7/2}$. In the G2-G glass, the transitions are due to Pr : $^3P_2$, $^3P_1$, $^3P_0$ and $^1D_2$ (Carnall et al. (1968),.Kutub et al. (1986) and Karunakaran (2010)). The absorption spectrum of the mixed Nd and Pr glass G3-G is a linear superposition of the spectrum due to Nd in G1-G glass with that due to Pr in the G2-G glass. The optical absorption spectra of the devitrified samples are similar to that of the respective glasses but with a reduced intensity as shown in the Figure 5.7.

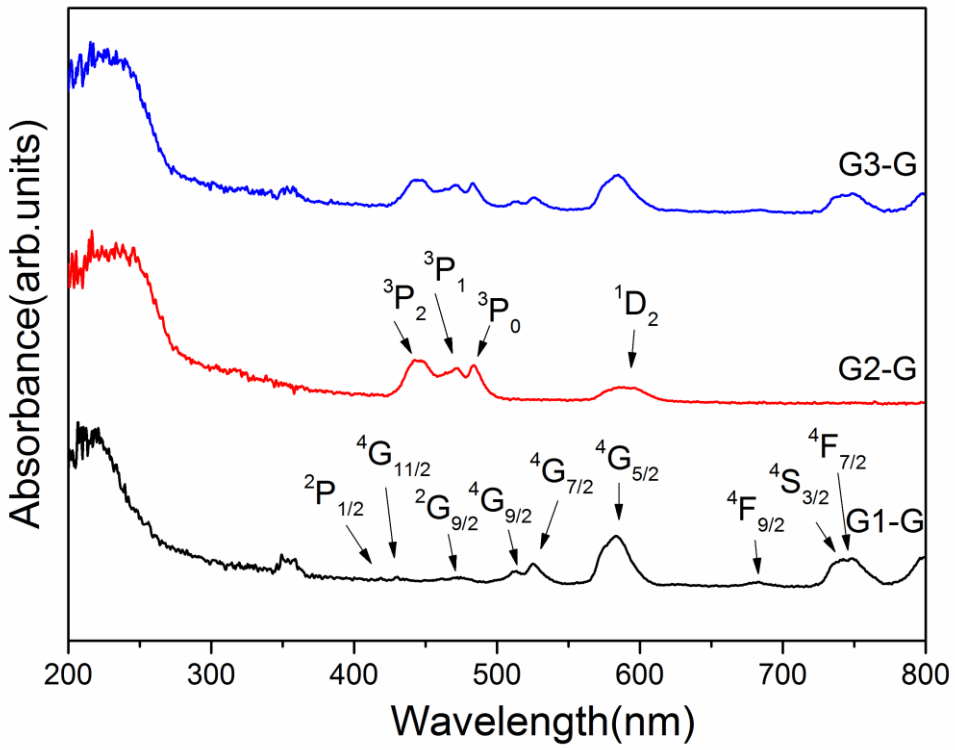

Figure 5.5: Absorbance spectra of the glasses G1-G, G2-G and G3-G.

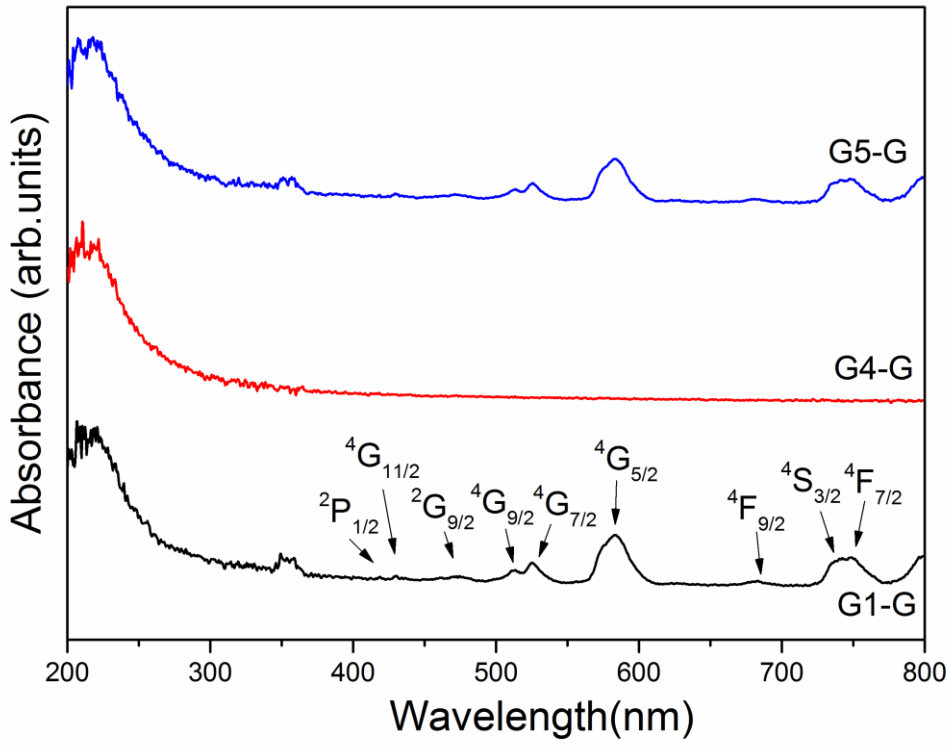

Figure 5.6 :Absorption spectra of the glasses G1-G, G4-G and G5-G

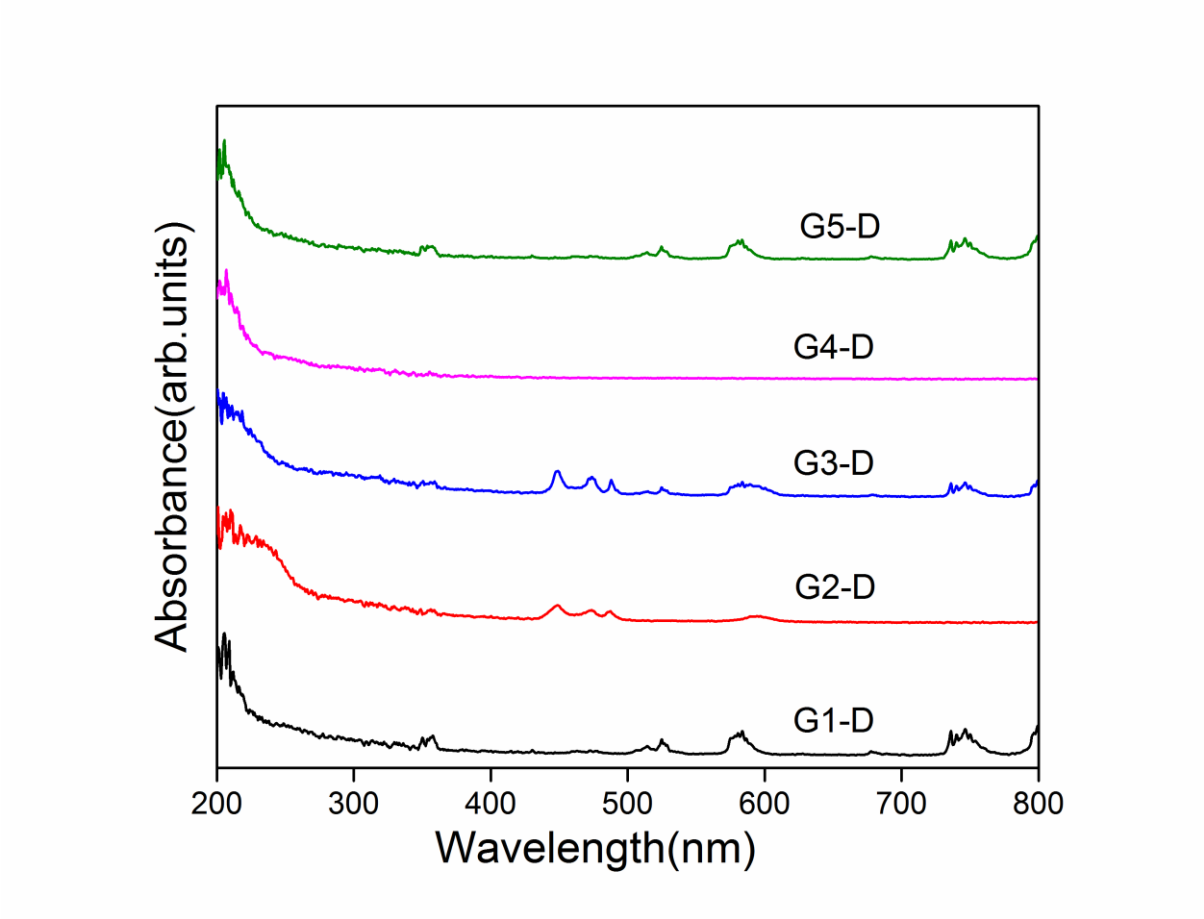

Figure 5.7: Absorption spectra of the Devitrified samples G1-D, G2-D, G3-D, G4-D and G5-D.

5.6.1 Tauc plots

Tauc plots ($(\alpha h\nu)^2$ v/s $h\nu$) were plotted for each glass considering direct allowed transitions from valence to free states. The linear portion of the curve was extrapolated to the photon energy axis to obtain the optical band gap energy E_g as shown in Figure 5.8.

This follows from the Davis-Mott relation (Davis and Mott (1970));

$$\alpha h\nu = B^2(h\nu - E_g)^r \qquad (5.3)$$

where α is the absorption coefficient, $h\nu$ is the incident photon energy, B is a constant known as the band tailing parameter, E_g is the optical band gap energy and r is an index which takes a value 2 for indirect allowed, 1/2 for direct allowed, 3 for indirect forbidden and 1/3 for direct forbidden transitions. The electronic band gap energy is found to be the lowest (4.55 eV) for the Pr containing glass G2-G, and the highest in the La containing

glass G4-G. The latter trend might be the result of the structural rearrangement of the glass network in the glasses G2-G and G3-G having Pr which exists in the divalent and trivalent states as Pr^{2+} and Pr^{3+}. In these two glasses Pr^{3+} plays the role of network modifier similar to the network modifier role of Nd^{3+} and La^{3+} while Pr^{2+} acts as a network former.

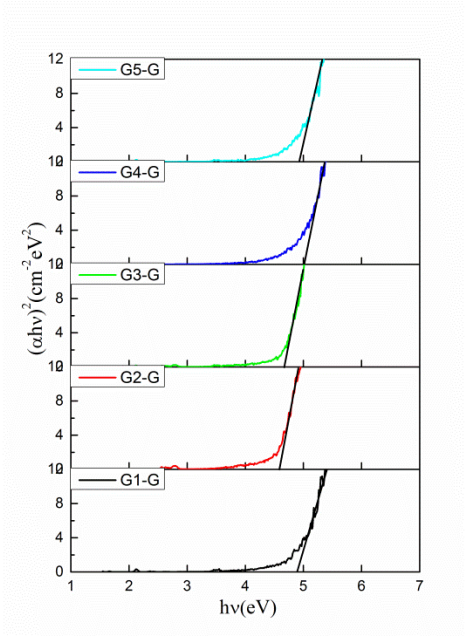

(a)

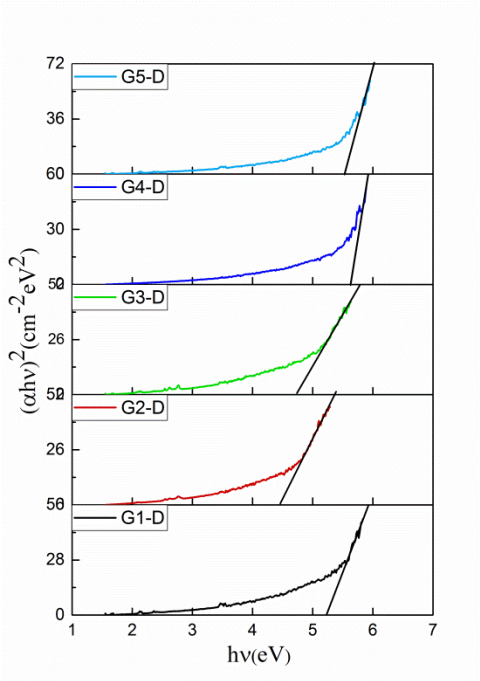

(b)

Figure 5.8 : Tauc plots plotted for the (a) Glass samples G1-G, G2-G, G3-G, G4-G and G5-G and (b) Devitrified samples G1-D, G2-D, G3-D, G4-D and G5-D .

The refractive index 'n' was calculated for these glasses (Dimitrov and Sakka (1996)) using the relation 5.4 :

$$\frac{n^2-1}{n^2+2} = 1 - \sqrt{\frac{E_g}{20}} \qquad (5.4)$$

The refractive index n is found to be the highest for the Pr containing glass P2-G. This could be due to the additional presence of Pr^{2+}ions in the glass network and the presence of non-bridging oxygens which have a higher polarity as compared to that of the bridging oxygens (Chen et al. (2008)).The dielectric constant ϵ was calculated using equation (5.5) ;

$$\epsilon = n^2 \qquad (5.5)$$

and the molar electronic polarizability α_m was found as given by Klonkowski (1985) from the relation (5.6) ;

$$\propto_m = \left(\frac{3}{4\pi N}\right)\left(\frac{n^2-1}{n^2+2}\right)V_m \qquad (5.6)$$

Where, N is Avogadro's number, n is the refractive index and V_m is the molar volume. Electronic polarizability is also found to be the highest in Pr containing glass G2-G as it has more non-bridging oxygens as compared to that of the other glasses in this study. These parameters are summarised in the Table 5.4. The E_g values (eV) for the devitrified samples (G1-D~5.29, G2-D~4.56, G3-D~4.73, G4-D~5.63 and G5-D~5.54) are ~ 0.4 eV – 0.6 eV higher than the E_g of the glasses except that for the Pr containing sample for which the values of E_g are similar.

Table 5.4 : Optical band gap energy, refractive index, dielectric constant and electronic polarizability .

Glass samples	Optical band gap energy E_g(±0.02eV)	Refractive index n (±0.01)	Dielectric constant ϵ(±0.01)	Electronic polarizability α_m ((±0.02Å)^3
G1-G	4.87	2.019	4.08	5.92
G2-G	4.55	2.071	4.29	8.33
G3-G	4.66	2.053	4.22	7.04
G4-G	4.97	2.004	4.02	5.99
G5-G	4.89	2.016	4.07	5.97

5.7 Raman Spectroscopy

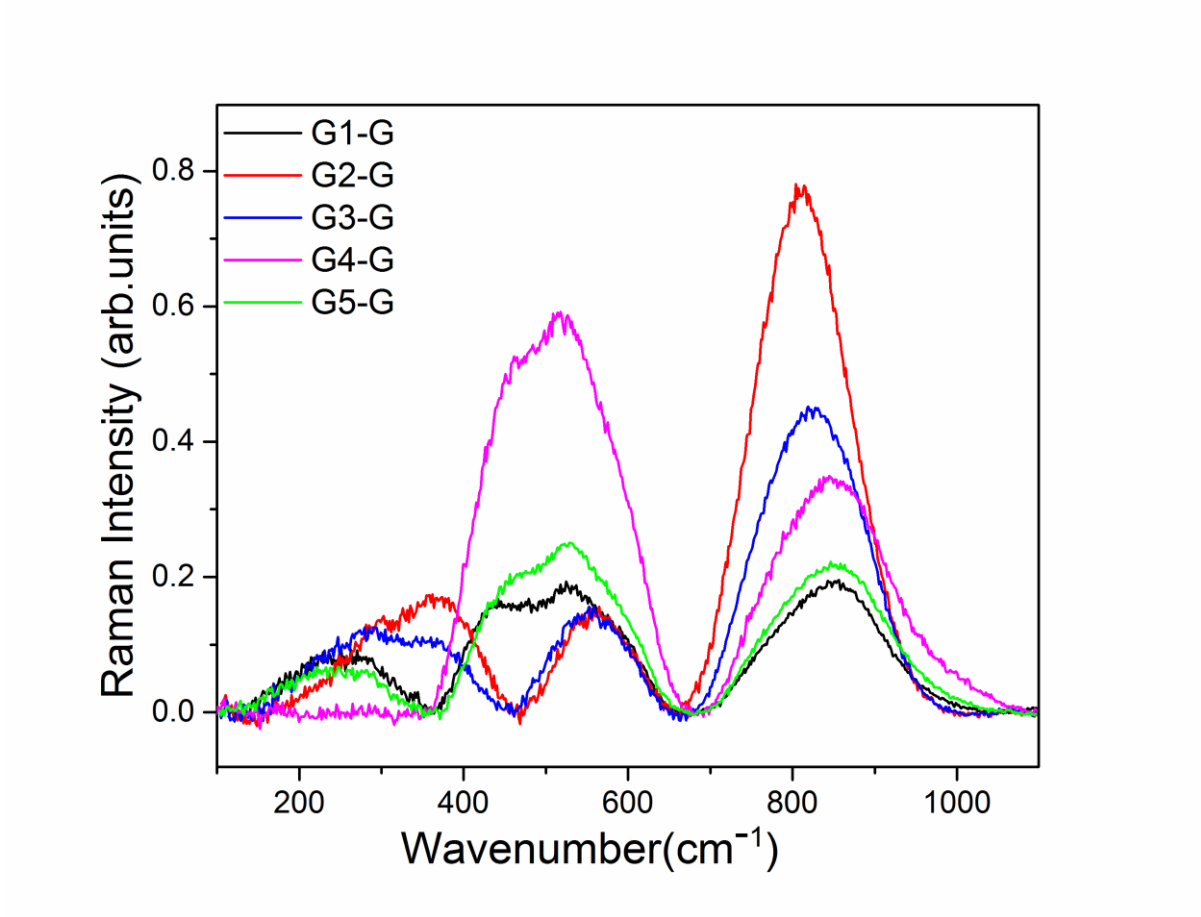

Figure 5.9 : Comparative Raman spectra of glasses

The Raman spectra for all the glasses studied are shown in Figure 5.9 and can be divided into three main groups. The region below 400 cm^{-1} arises due to the vibrations of the network modifying cations La, Pr and Nd that modify the network structure. The region between 400 cm^{-1} to about 700 cm^{-1} is due to the intra-tetrahedral Ge-O-Ge vibrational modes. It is worth noting that in the Pr containing glasses G2 and G3, the band due to the Ge-O-Ge symmetric stretching vibration associated with three membered rings of GeO_4 appears at 550 cm^{-1}, while in the glasses G1-G (Nd), G4-G (La) and G5-G(Nd-La) which do not contain Pr, there is formation of both four membered GeO_4 rings for which the symmetric stretching vibration of Ge-O-Ge is shown by a peak at about 440 cm^{-1} and three membered rings of GeO_4 due to which the symmetric stretching vibration of Ge-O-Ge is shown by a peak at about 525 cm^{-1}. The conversion of 4 membered rings to 3 membered rings (Henderson and Amos (2003)) also contribute to the increase in density of the Pr included glasses.

The region from about 700 cm^{-1} to 1100 cm^{-1} is due to the vibrations of the different GeO_4 structural units that form the network structure (Henderson and Fleet (1991), Kamitsos et al. (1996), Martino et al. (2001) and Sigaev (2001). These structural units are represented as Q^n where n refers to the number of bridging oxygen ions. Gaussian fitting was employed to deconvolute the Raman band in the region from around 650 cm^{-1} to 1100 cm^{-1} for all the glasses studied and is shown in Figure 5.10 for G1-G, Figure 5.11 for G2-G, Figure 5.12 for G3-G, Figure 5.13 for G4-G and Figure 5.14 for G5-G. The Raman band assignments for the deconvoluted Raman band are shown in Table 5.5 .The relative ratios of the areas of the Q^n were calculated as displayed in Table 5.6 and represented in the form of a comparative bar graph shown in the Figure 5.15. The structural units of these glasses studied are predominantly Q^2 and Q^3. The distribution of Q^n for the Nd glass (G1-G), Nd-Pr glass (G3-G), La glass (G4-G) and Nd-La glass (G5-G) has a maximum for the Q^3 linkages having three bridging oxygens and one non-bridging oxygen, while for the Pr glass G2-G, the distribution shows a maximum in Q^2 structural units having two bridging and two non-bridging oxygen ions in the GeO_4 unit. Isolated tetrahedra or Q^0 are seen mainly in the Pr containing glasses G2-G and G3-G. The Pr containing glass is thus likely to consist of a less well-connected network of basic GeO_4 tetrahedral units as compared to the Nd and NdPr containing glasses. On the other hand, the La contained glasses G4-G show the presence of Q^4 structural units.

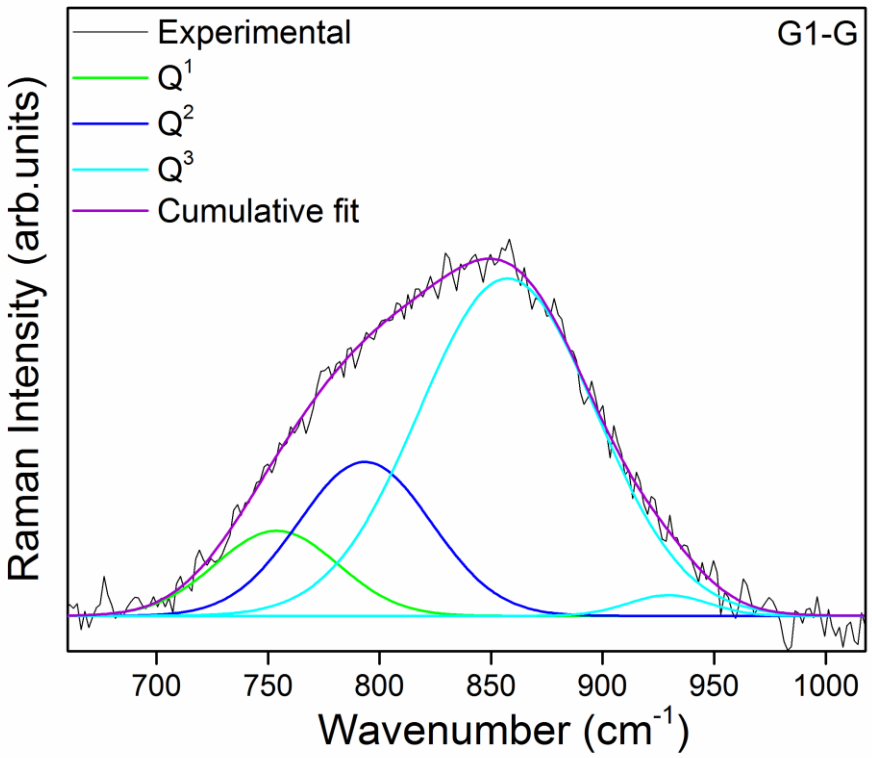

Figure 5.10 : Deconvoluted Raman band for glass G1-G.

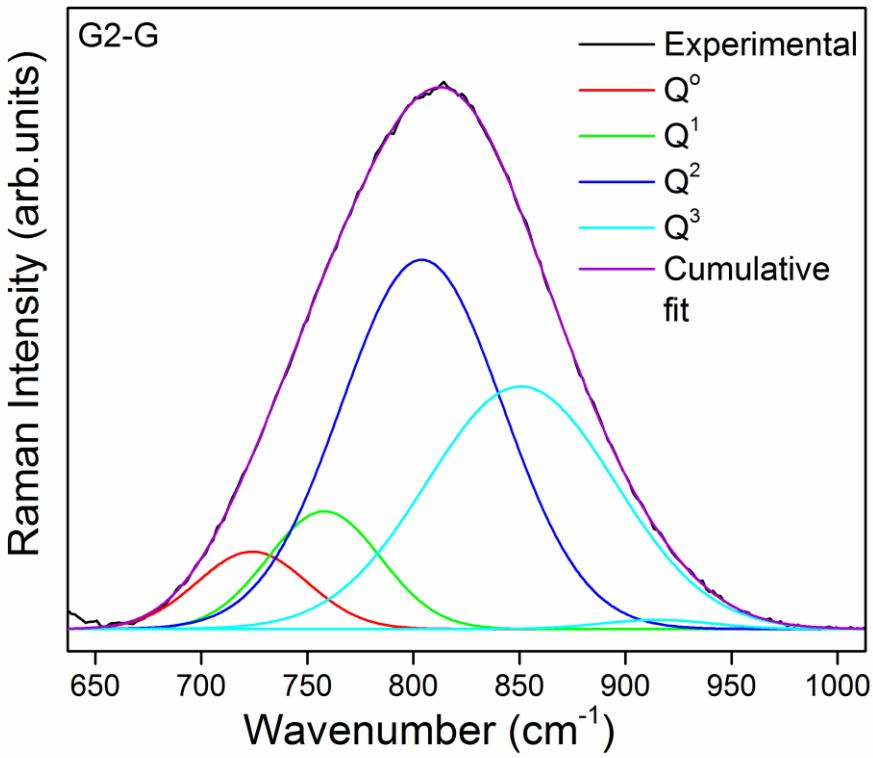

Figure 5.11 : Deconvoluted Raman band for glass G2-G.

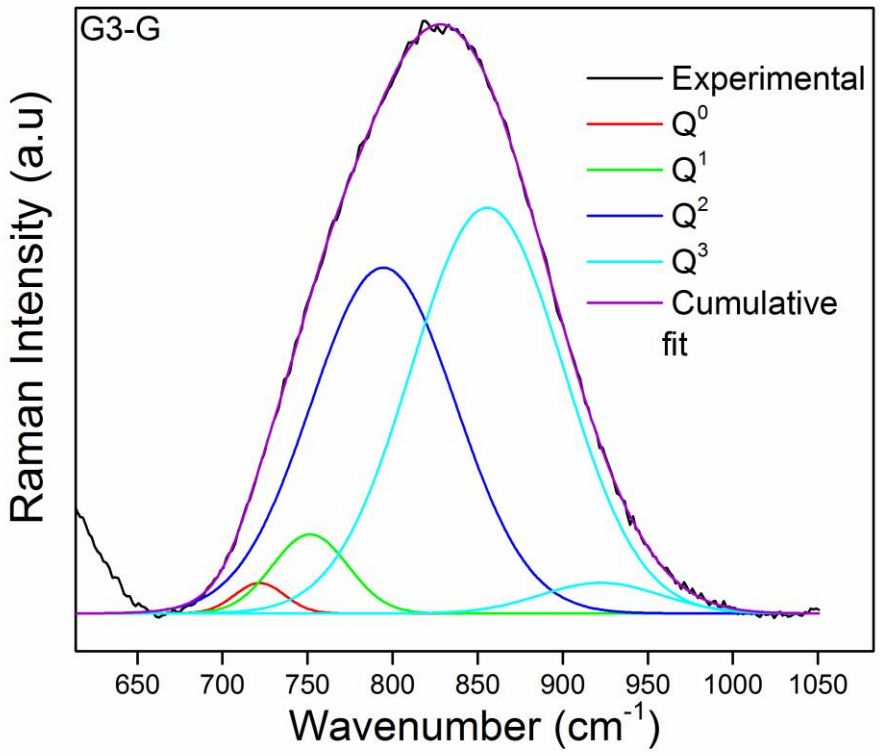

Figure 5.12 : Deconvoluted Raman band for glass G3-G.

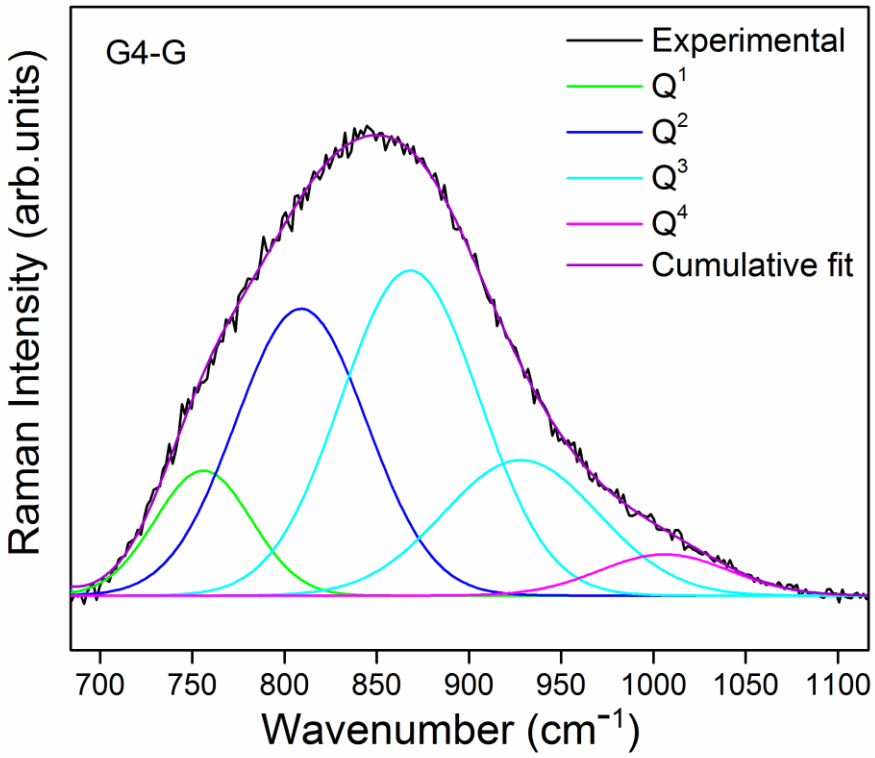

Figure 5.13: Deconvoluted Raman band for glass G4-G.

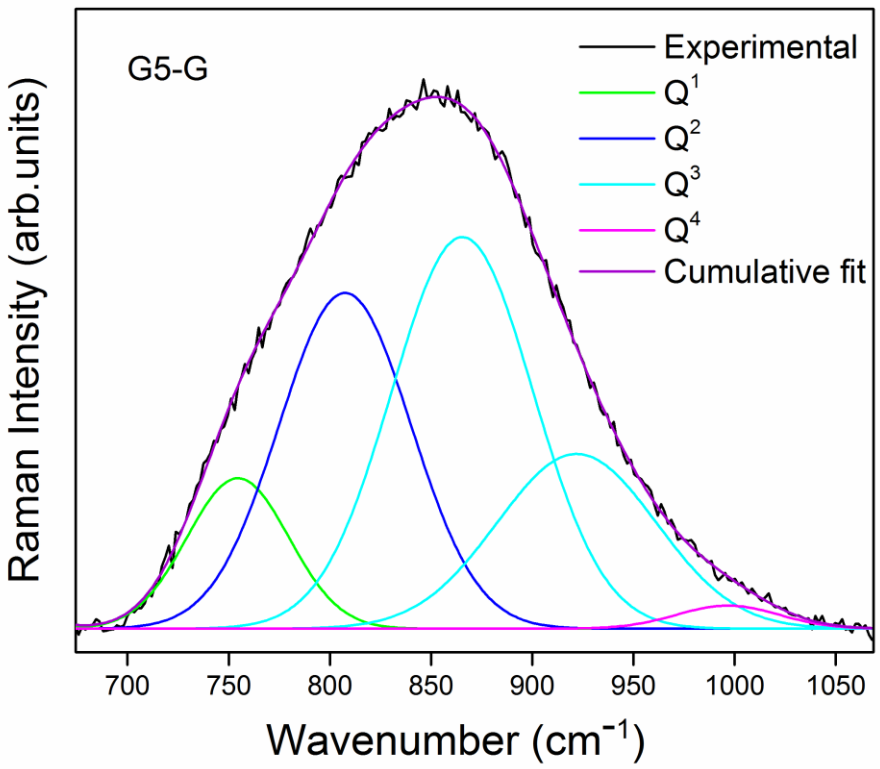

Figure 5.14 : Deconvoluted Raman band for glass G5-G.

Several authors (Table 5.5) have assigned the Raman bands in the deconvoluted region shown in table 5.6 for the respective Q^n based on which the assigned peak positions are listed in Table 5.6

Table 5.5: Raman band assignments

Q^n	Peak position(cm^{-1})	References
Q^o	~ 720	D. D. Martino (2001),V. N. Sigaev (2001), G. S. Henderson (2010), L. Peng and J. F. Stebbins (2007) and R. Xu (2011)
Q^1	~ 755	E. I. Kamitsos (1996), D. D. Martino (2001), G. S. Henderson (2010) and L. Baia(2001)
Q^2	~ 800	J. Alvarado-Rivera (2014), D. D. Martino (2001), P. Lottici (1983), V. Dimitrov (2017) and W. J. Zhang (1994)
Q^3	~ 855	E. I. Kamitsos (1996), D. D. Martino (2001), G. S. Henderson (2010), P. Lottici (1983), V. Dimitrov (2017) and W. J. Zhang(1994)
Q^4	~ 1000	E. I. Kamitsos (1996), D. D. Martino (2001), G. S. Henderson (2010), L. Baia (2001) and R. Xu (2011)

Table 5.6: Raman peak positions and relative areas of the deconvoluted peaks relating to the different Q^n vibrations.

Glass	Assigned positions	Q^0	Q^1	Q^2	Q^3	Q^4
G1-G	Position(cm^{-1})	---	753	793	857	---
	Area	0.0000	0.1131	0.2220	0.6649	0.0000
G2-G	Position(cm^{-1})	723	758	803	850	---
	Area	0.0664	0.1036	0.4658	0.3642	0.0000
G3-G	Position	721	751	794	855	---
	Area	0.0124	0.0485	0.4075	0.5117	0.0000
G4-G	Position(cm^{-1})	---	755	809	868	1006
	Area	0.0000	0.0995	0.3104	0.5459	0.0443
G5-G	Position(cm^{-1})	---	754	807	865	996
	Area	0.0000	0.1056	0.3053	0.5729	0.0163

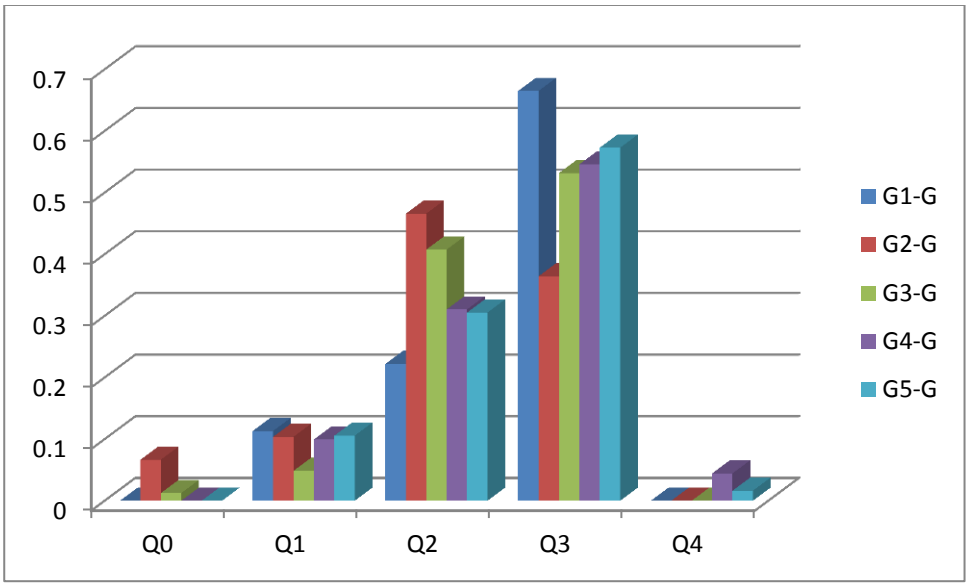

Figure 5.15 : Bar graph showing comparative area ratio of the different structural units in the glasses studied.

5.8 Extended X-ray absorption fine structure

Extended X-ray Absorption Fine Structure **(**EXAFS) experiments (Poswal et al. (2014), Basu et al. (2014)) were performed on the G1-G, G2-G and G3-G germanate glass samples using the Ge K, Nd L_3 and Pr L_3 edges of the BL-09 -Scanning EXAFS Beamline of the INDUS-2 Synchrotron Source (2.5 GeV, 100 mA) at RRCAT, Indore.

The measurements were made in the transmission mode by placing each sample of thickness x between two ionization chamber detectors one at a time. The incident flux (I_0) is measured by the first ionization chamber and the transmitted intensity (I_t) by the second ionization chamber. Thus the absorption coefficient or absorbance($\mu x = -\ln\left(\frac{I_t}{I_0}\right)$) of the samples was obtained.

Figure 5.16 shows the experimental EXAFS ($\mu(E)$ versus E) spectra of the alumino-germanate glass samples measured at and beyond the Ge K-edge. The analysis of the EXAFS data have been carried out using the normal procedure of data reduction and Fourier transformation absorption spectral data in the k range of 2-10 $Å^{-1}$ to obtain the χ(r) v/s r plots (Konigsberger and Prince (1988)), assuming a crystallographic structure (Ge-O shell) to generate the theoretical EXAFS spectra (Kelly et al. (2008)), and fitting of these

theoretical data with the experimental χ(r) v/s r graphs (Newville et al. (1995)) from 1-2 Å using the IFEFFIT software package (FEFF 6.0 code).

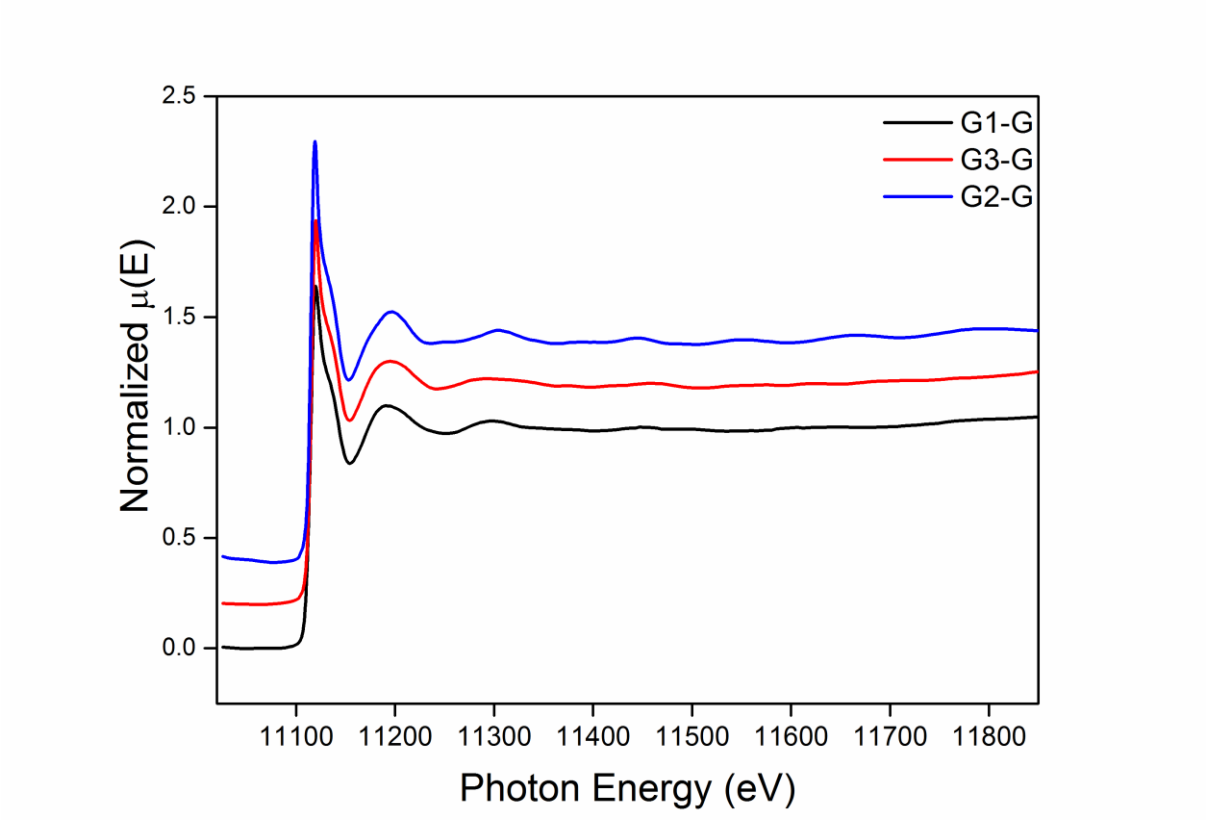

Figure 5.16 Experimental EXAFS spectra at the Ge-K edge

The experimental $\chi(r)$ versus r plots of the germanate glass samples at Ge K edge is shown in the Figure 5.17 along with best fit theoretical plots. The Ge-O bond length and the coordination numbers of oxygen around Ge obtained from the fitting results for the glasses G1, G2 and G3 are listed in Table 5.7. The Ge-O bond length is found to be about 1.74 Å for the glass samples G1 and G3 and 1.75 Å for the glass G2 with the coordination number of approximately 4. This indicates that Ge ions are in tetrahedral structure which is similar to the α-quartz-type GeO_2 structure (Zhao et al (2015)). However the G2 glass sample shows a higher coordination of 4.8 for the Ge-O bond. This increase in coordination number can be attributed to the germanate anomaly. The germanate anomaly is the change of tetrahedral environment of Ge ions to octahedral environment in germanate glasses doped with heavy metal oxide (Witkowska et al. (2006)). Thus for the G2 glass, the average bond length of 1.75 Å and the average coordination of 4.8 would suggest existence of both tetrahedral and octahedral Ge environments.

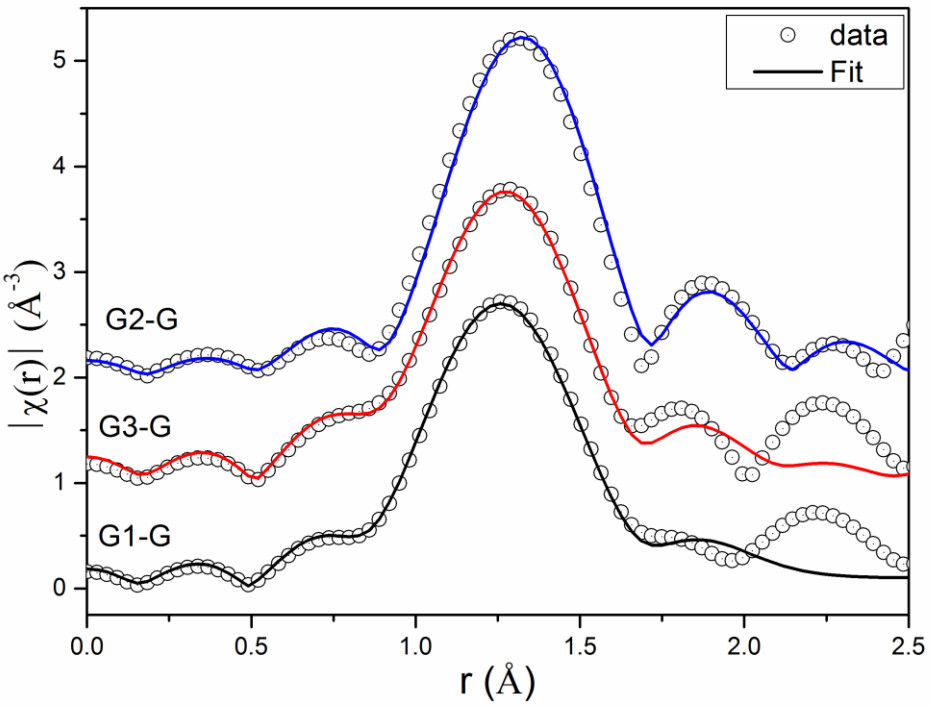

Figure 5.17: $\chi(r)$ versus r plots for the glasses G1-G, G2-G and G3-G.

Table 5.7: Ge-O bond length and coordination numbers for the glasses G1-G, G2-G and G3-G.

Sample	Ge-O		
	r (Å) **±0.02**	N	σ^2
G1-G	1.74(1)	4.0(2)	0.0025(8)
G2-G	1.75(2)	4.8(5)	0.0027(5)
G3-G	1.74(1)	3.9(3)	0.0023(9)

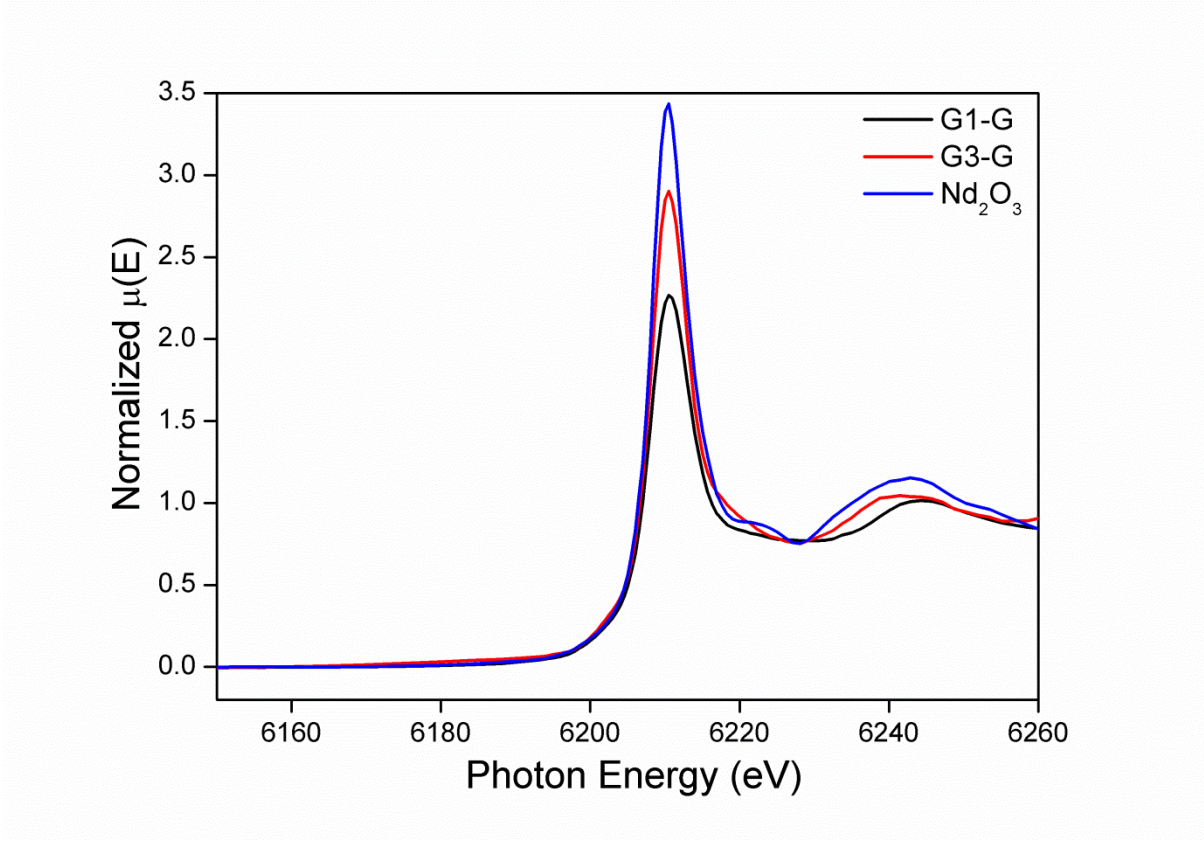

Figure 5.18: XANES spectra of the glasses G1-G and G3-G at the Nd L_3 edge.

As seen from the XANES spectra at Nd L_3 edge for the germanate glasses and the Nd_2O_3 standard shown in Figure 5.18, the absorption edges of the samples G1-G and G3-G lie close to the Nd_2O_3 standard. This indicates that the oxidation state (+3) of the Nd_2O_3 standard and the Nd cations in the samples is the same. A white line appears at ~ 6210 eV for both the samples due to $2p_{3/2}$ to 5d transition, the intensities of which are lower than that of Nd_2O_3 standard.

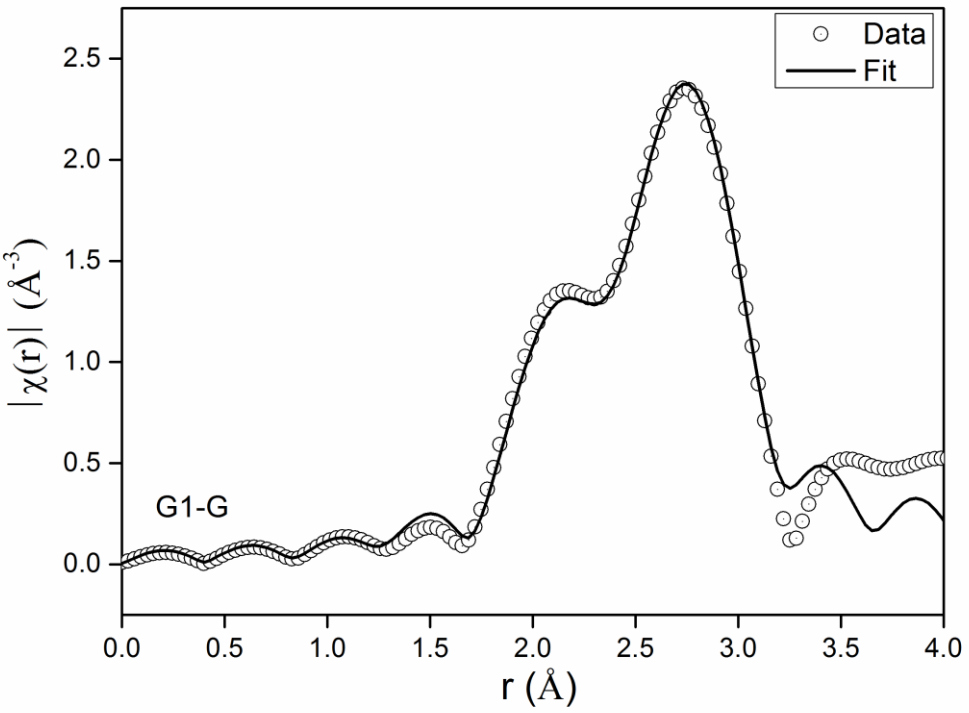

Figure 5.19: $\chi(r)$ versus r plots for the glass G1-G at the NdL_3 edge

The experimental $\chi(r)$ versus r plotsof the G1-G glass sample at Nd L_3 edge shown in the Figure 5.19 shows a strong peak at around 2.73 Å along with a peak at approximately 2.15 Å. The peak at ~ 2.15 Å is due to the Nd-O contribution (Mountjoy et al. (2001), Bowron et al. (1996)).The peak at 2.73 Å may corresponds to Nd-Al or Nd-Ge contributions. Frenkel et al. (1996) reported La-Al bond distance of ~ 3.1 Å in glasses. Therefore the data have been fitted from 1.8Å to 3Å assuming a Nd-O bond at 2.34Å and a Nd-Al bond at 3.1Å. The best fit theoretical plot along with the experimental data are shown in Figure 5.19 and the fitting results are tabulated in Table 5.8.

Table 5.8. Correlation length (Nd-O) and coordination number of O around Nd in glass G1-G.

Sample	Nd-O		
	r (Å) ± 0.002 Å	N	σ^2
G1-G	2.53(3)	8.7(8)	0.004(2)

From the fitting results it can be concluded that 9 oxygen atoms surround the Nd cation at a distance of 2.53 Å. These values are in agreement with reported values in the literature (Mountjoy (2007), Quintas (2008)).

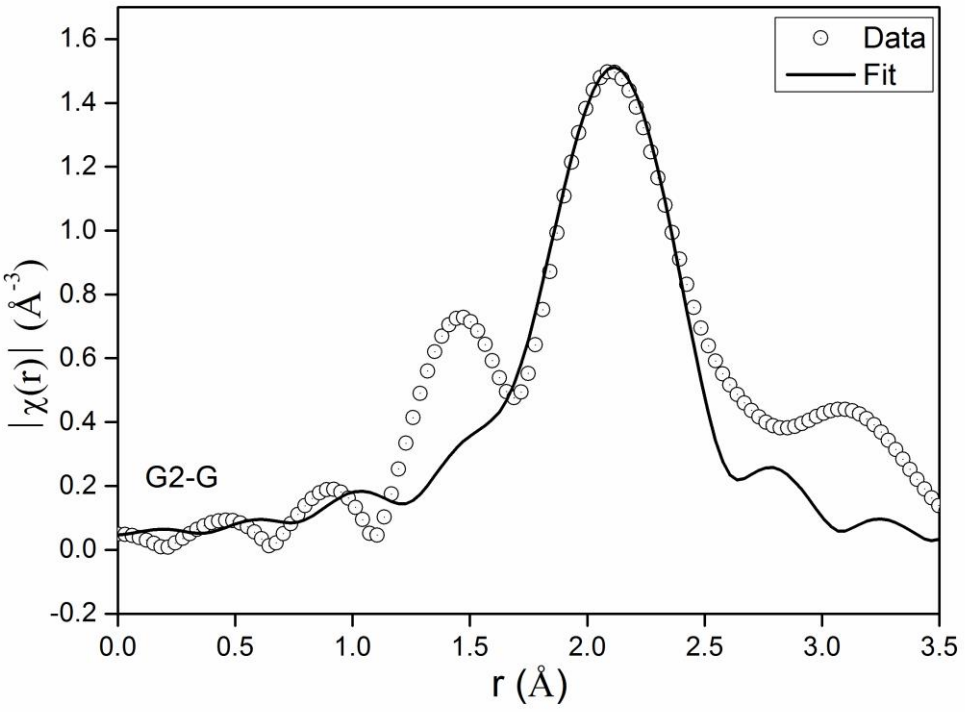

Figure 5.20 : $\chi(r)$ versus r plots for the glass G2-G at the PrL_3 edge

Table 5.9 : Correlation length and coordination number of O around Pr in glass G2-G

Sample	Pr-O		
	r (Å) $\pm$ 0.002 Å	N	σ^2
G2-G	2.58(1)	8.9(9)	0.006(2)

Figure 5.20 shows the experimental $\chi(r)$ versus r plots of the G2-G glass sample at the Pr L_3 edge along with the best fit theoretical plots found from assuming a Pr-O shell at 2.37 Å and the data fitted in the *r* range of 1.5Å to 2.5Å. From the fitting results shown in Table 5.9 it can be concluded that 9 oxygen atoms surround the Pr cation at a distance of 2.58 Å. These values are also in agreement with reported values in the literature (Mountjoy et al (2007)).

5.9 Neutron diffraction

The structure factors for the glasses are shown in Figure 5.21, obtained from the measured intensities after the usual experimental corrections and normalization as detailed in Chapter 2. The pair correlation function and the total correlation functions are obtained from the structure factor and displayed in Figures 5.22 and 5.23 respectively.

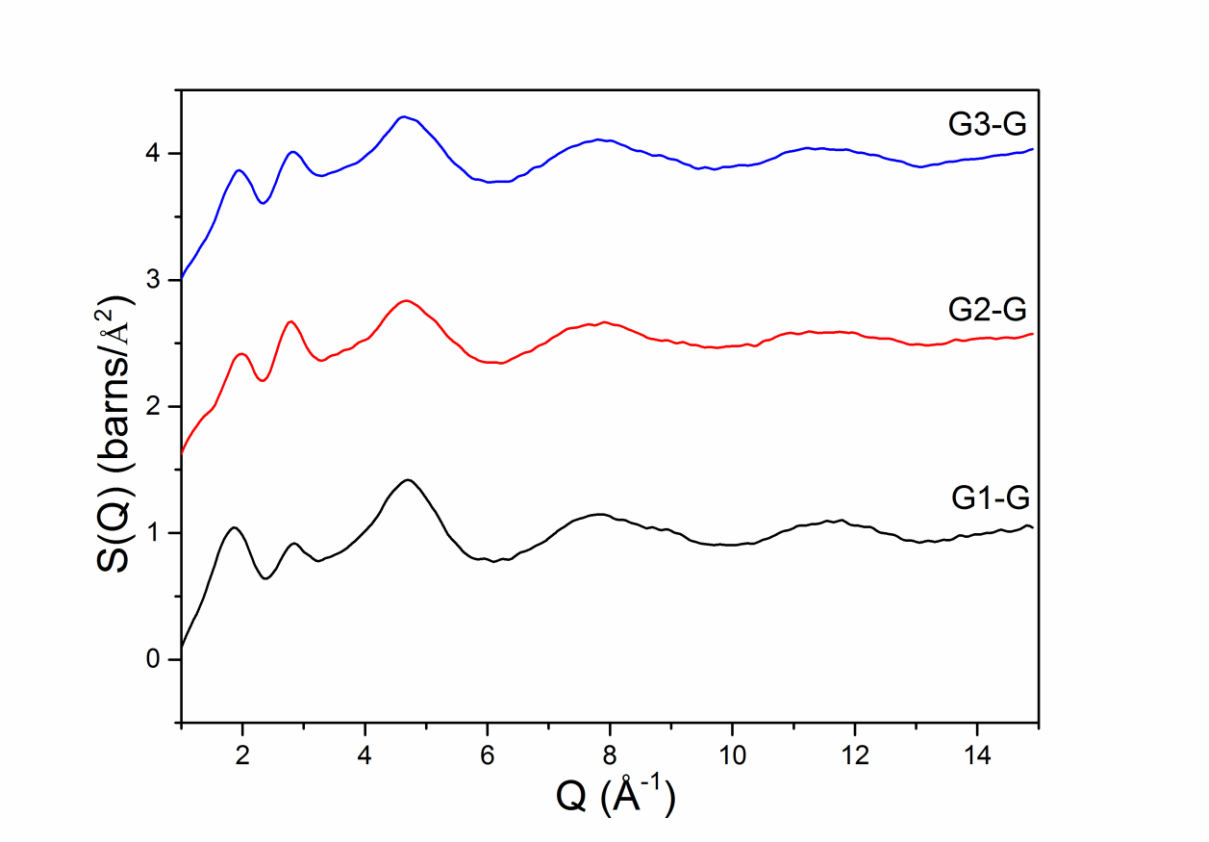

Figure 5.21: The structure factors S(Q) v/s the momentum transfer Q for the glasses G1-G, G2-G and G3-G.

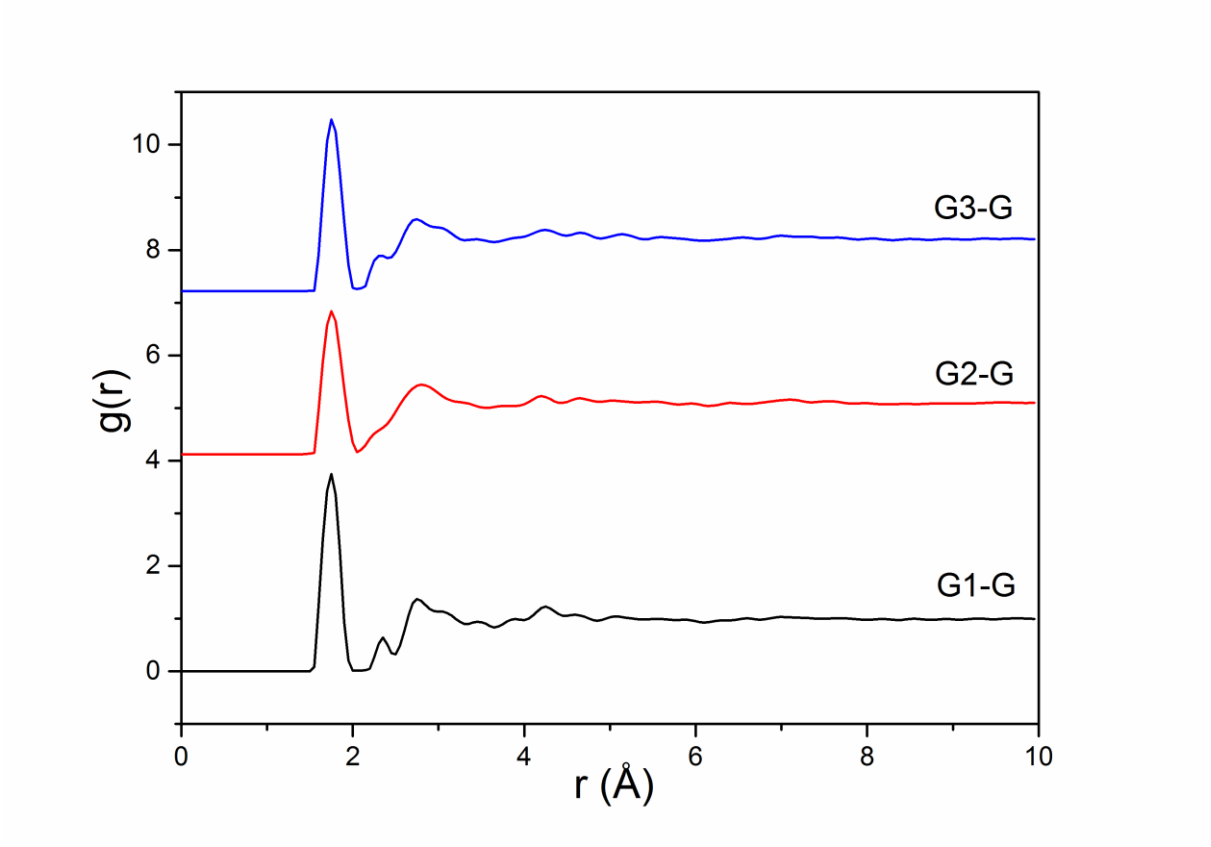

Figure 5.22 : The pair correlation functions g(r) for the glasses G1-G, G2-G and G3-G.

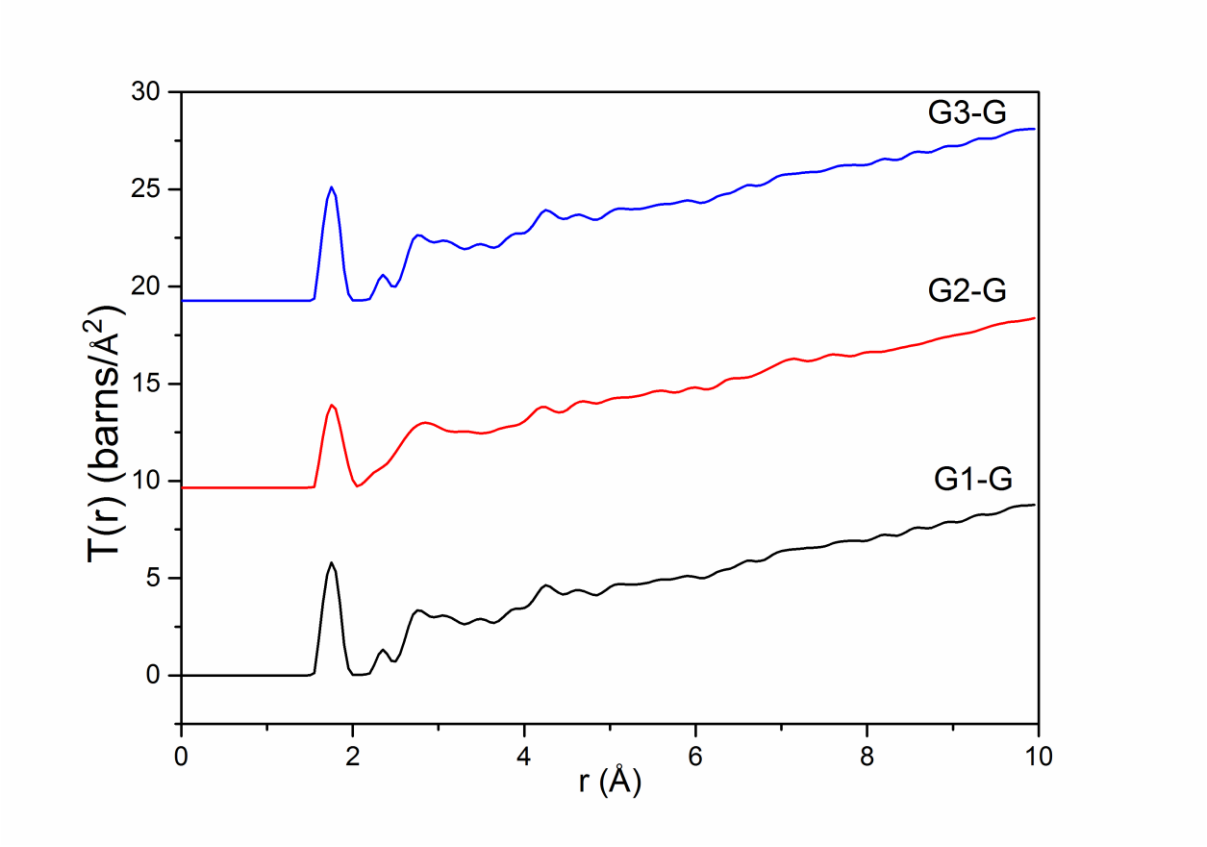

Figure 5.23 : The comparative display of the total correlation function T(r) for the glasses G1-G, G2-G and G3-G.

The correlation lengths and the coordination numbers were obtained by Gaussian peak fitting. The first peak was fitted with two Gaussian functions one for the Ge-O correlation and the other for the Al-O correlation. The area of the smaller peak was chosen according to the expected coordination number of oxygen around Al as 4 and the remainder area of the first peak constituted the Ge-O Peak. Two Gaussian functions were needed to fit the RE-O correlations in these glasses while the O-O peak was fitted with a single Gaussian peak with the area chosen according to the expected value of coordination number equal to 4. The radial distribution function for glass G1-G is fitted with Gaussian peaks up to 4Å is shown in Figure 5.24. The results of the fitting are displayed in Table 5.11.

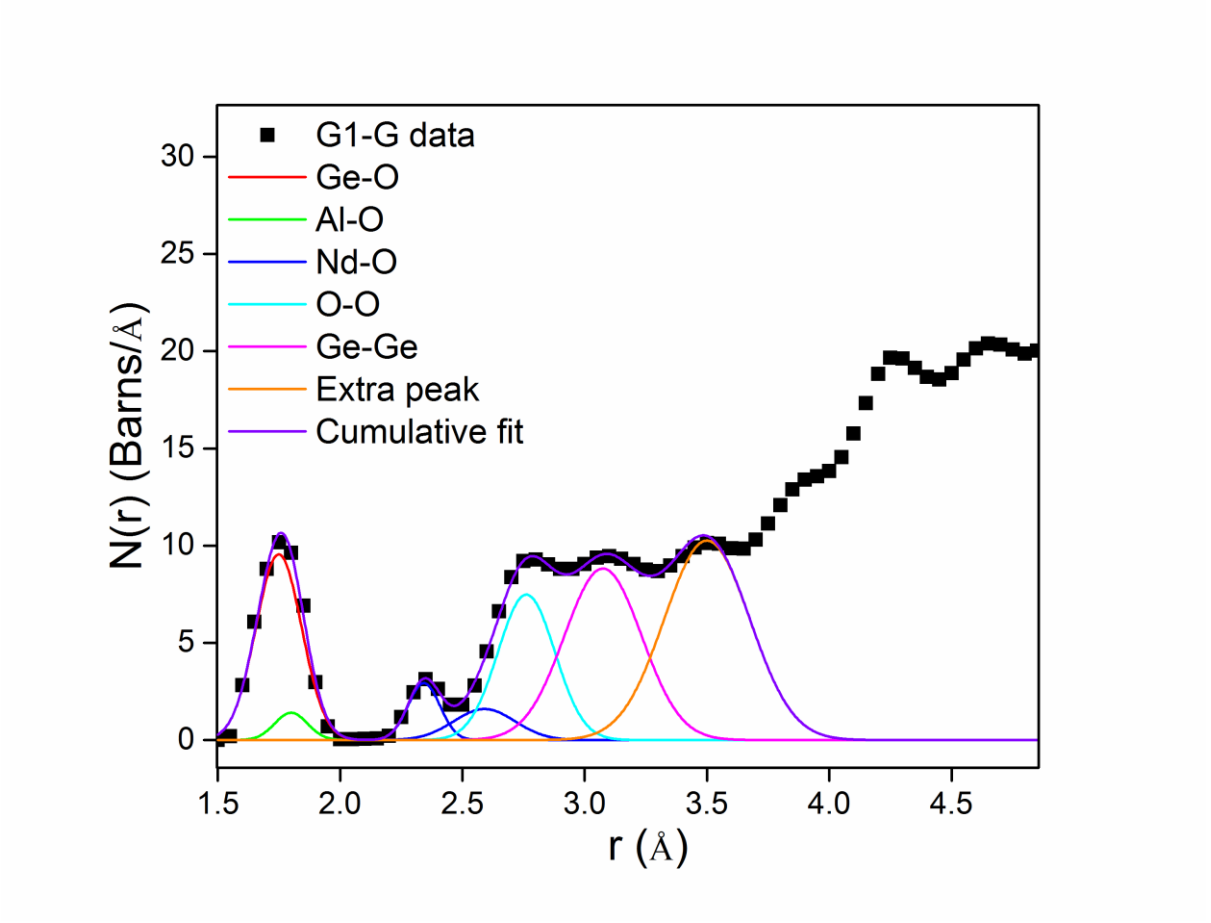

Figure 5.24 : The Gaussian peak fits to the radial distribution function N(r) of the glass G1-G.

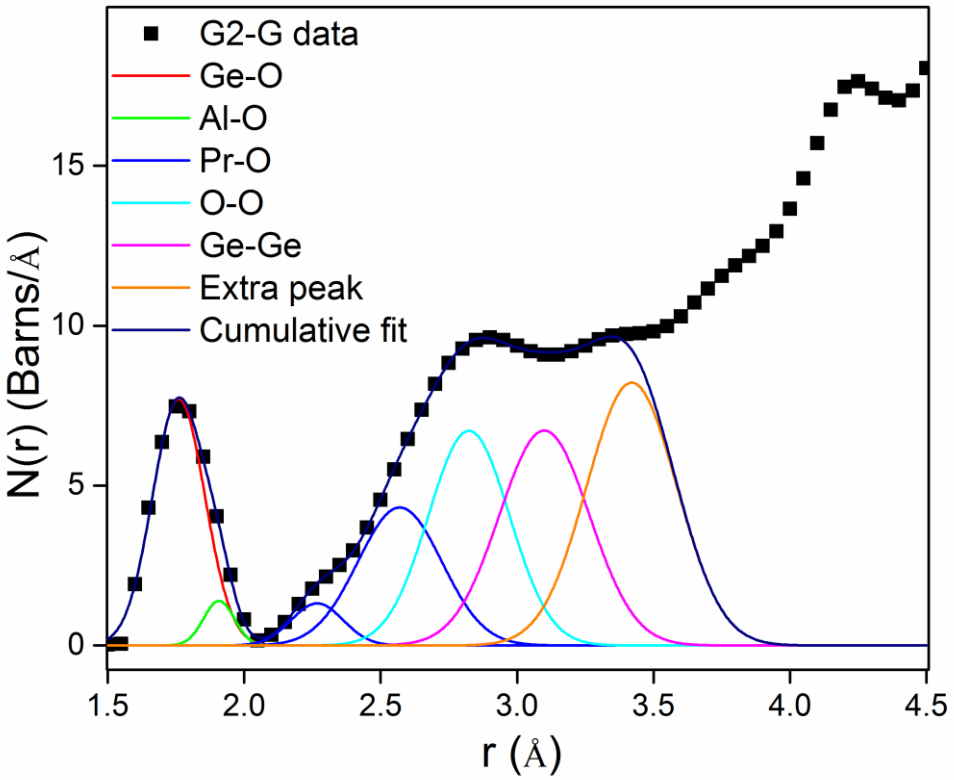

Figure 5.25 : The Gaussian peak fits to the radial distribution function N(r) of the glass G2-G.

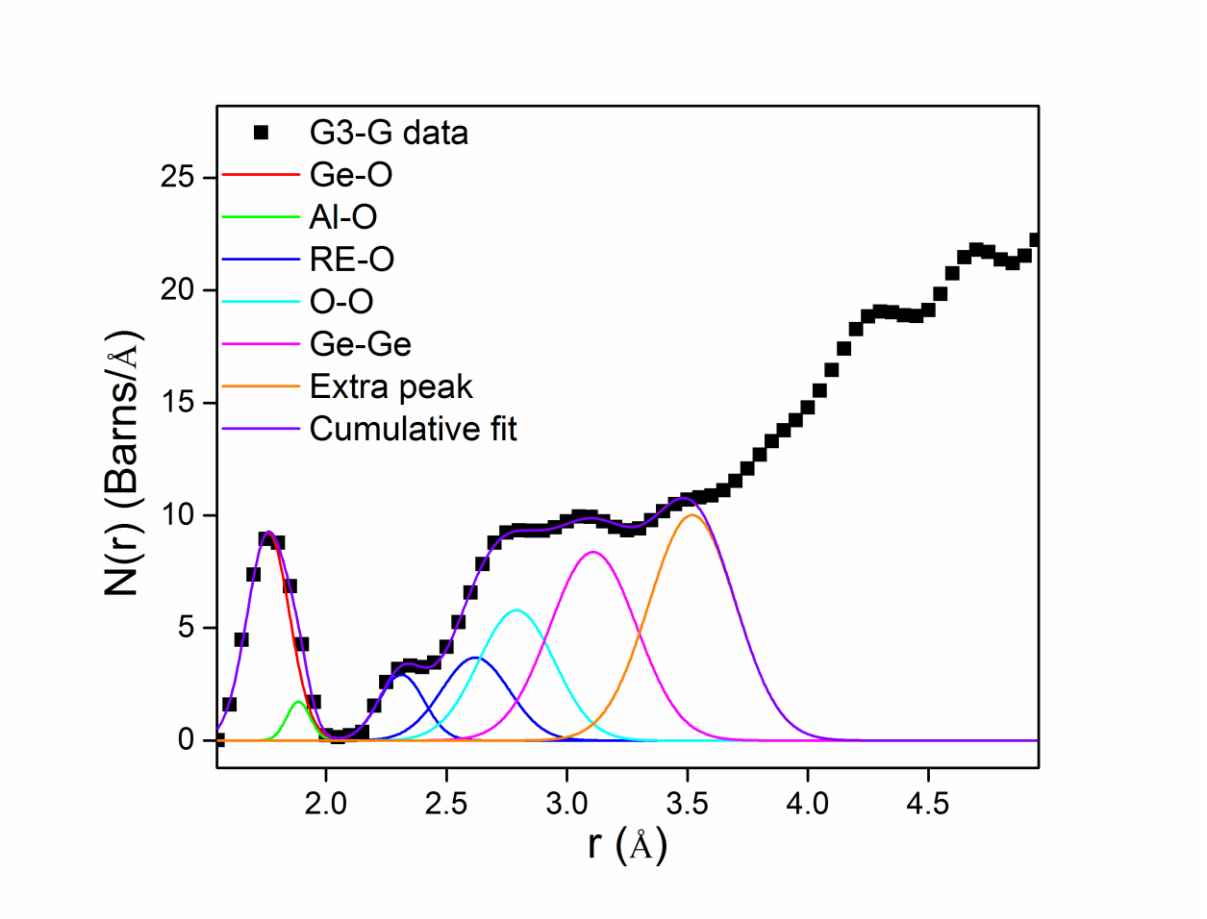

Figure 5.26 : The Gaussian peak fits to the radial distribution function N(r) of the glass G3-G.

Table 5.10 : Correlation length (r) and coordination number (N) of the different correlations in the glases G1-G, G2-G and G3-G.

Correlation	G1-G		G2-G		G3-G	
	r (Å) ±0.02 Å	N	r (Å) ±0.02 Å	N	r (Å) ±0.02 Å	N
Ge-O	1.75	4.0	1.76	4.0	1.76	4.1
Al-O	1.8	4.0	1.9	4.0	1.89	4.0
RE-O	2.47	7.5	2.42	10.1	2.47	10.7
O-O	2.76	4.0	2.82	4.0	2.79	4.0

5.10 Conclusions

A set of five rare-earth alumino-germanate glasses consisting of 10 mol% Al_2O_3 , 80 mol% GeO_2 and the remaining 10 mol% being either singly Nd_2O_3 , Pr_6O_{11} , La_2O_3 or in pairs were prepared by the melt quenched method in air. Glass transition temperatures by DTA gave values between 812^oC and 867^oC, with densities by fluid displacement being from 4.19 g/cc to 4.88 g/cc and the relative trend of both these parameters being the same.

X-ray diffraction confirmed the glassy nature of the samples and showed the devitrified glasses to comprise the crystalline phases of either or both rare-earth constituents.

FTIR spectra on the glass samples showed the presence of GeO_4 tetrahedra, GeO_6 octahedra and three and four-membered rings of GeO_4 tetrahedra with the exception of the Pr containing glasses.

UV-Visible spectra showed absorption peaks due to 4f electronic transitions in ions of Nd and Pr. For samples in which both Nd and Pr were present, the observed spectrum appeared as a superposition of the spectra due to individual ion type. The optical band gaps were estimated from the Tauc plots and found to be 5% to 6% lower for the two Pr included glasses as compared to the other members of this set. However, for the latter samples, it was found that the calculated refractive index, dielectric constant and electronic polarizability were slightly higher than for the other glasses. This would be an indication of the larger number of non-bridging oxygen (NBO) atoms in the network tetrahedra of those glasses containing Pr.

Raman spectroscopy applied to these glasses found that the Nd containing glasses had distributions of Q^n which peaked at Q^3 while those with Pr included in the network had distributions which peaked at Q^2 – again indicative of a less-continuous network for the Pr containing glasses.

EXAFS data on the samples showed the presence of both tetrahedral coordination of oxygen around Ge with the Ge-O distance as 1.74 Å for the Nd included glasses. For the two Pr containing glasses, the presence of GeO_6 octahedra was indicated. The Nd-O distance was found to be 2.53 Å with the coordination of Nd(O) of 8.8 while for the Pr containing glasses the Pr-O was 2.58 Å with the Pr(O) of 8.9. Thus the coordination of oxygen around the rare-earth was found to be about 9.

Neutron diffraction measurements found Ge-O to be 1.75 Å with tetrahedral coordination of Ge(O) and the presence of an Al-O correlation between 1.8 to 1.9 Å for an assumed coordination of 4 oxygen atoms around Al. The rare-earth correlation was 2,47 Å with a coordination of 7.5 for the Nd included glass and 2.42 Å and a Pr(O) of about 10. These findings are in broad agreement with those from EXAFS and also point to a less well connected network for the Pr containing glasses.

References:

1. Alvarado-Rivera J., Rodriguez-Carvajal D. A., Del C. M., Costa-Enriquez. A., Manzanares-Martinez M. B., Alvarez E,. Lozada-Morales R., Diaz G. C., De Leon A., Zayas M. E., J. Am. Ceram. Society, 97(2014)3494-3500
2. Baia L., Iliescu T., Simon S., Kiefer W., J. Molec. Structure, 599 (2001) 9-13
3. Balda R., Fernandez J., Sanz M., De Pablon A., Navarro J. M. F., Mugnier J., Phys. Rev. B 61 (2000) 3384-3390
4. Basu S., Nayak C., Yadav A. K., Agrawal A., Poswal A. K., Bhattacharyya D.,. Jha S. N. and Sahoo N. K., J. Phys.: Conf. Ser. 493 (2014) 012032.
5. Bowron D. T., Saunders G. A., Newport R. J., Rainford B. D., and Senin H. B., Phys. Rev. B 53 (1996) 5268- 5274.
6. Carnall W. T., Fields P. R., Rajnak K., J. Chem. Phys. 49 (1968) 4412-4423
7. Chanshetti U. B., Shelke V. A., Jadhav S. M., Shankarwar S. G., Chondhekar T. K., Shankarwar A. G., Sudarshan V., Jogad M. S., Phys., Chem. and Tech. vol. 9, (1) (2011) 29-36
8. Chen Y., Nie Q., Xu T., Dai S., Wang X., Shen X., J. Non-Cryst. Solids 354 (2008) 3468-3472
9. Culea E., Pop L., Bosca M., J. Alloys Cmpounds 505 (2010) 754-757
10. Davis E.A., Mott N. F., Phil. Mag. 22(1970) 903-927
11. Desa J. A. E., Wright A. C., Wong J., Sinclair R. N., J. Non-Cryst. Solids 51 (1982) 57
12. Desa J. A. E., Wright A. C., Sinclair R. N., J. Non-Cryst. Solids, 99 (1988) 276-288
13. Desa J. A. E., Wong J., Sinclair R. N., AERE- R 10186 report, Harwell, United Kingdom (1981).
14. Dimitrov V., Sakka S., J. Appl. Phys.79(1996)1736-1740

15. Dimitrov V., Dimitriev Y., Montenero A., J. Non-Cryst. Solids 180 (1994) 51-57
16. Frenkel A., Stern E. A., Voronel A., Rubshtein A., Ben-Ezra Y.and Fleurov V., Phys. Rev. B 54 (1996) 884- 892.
17. Greenwood N. N., Earnshaw A., Chemistry of the elements (2nd edition) Butterworth-Heinemann (1997)
18. Hannon A. C., Martino D. D., Santos L. F.,. Almeida R. M, J. Phys. Chem. B 111(13) (2007) 3342-3354
19. Henderson G. S., Fleet M. E., J. of Non-Cryst. Solids 134 (1991) 259-269
20. Henderson G.S., Soltay L.G., Wang H. M., J. non-Cryst. Solids, 356 (2010) 2480-2485
21. Hill R., J. Mater. Sci. Lett. 15 (1996) 1122-1125
22. Kamitsos E. I., Yiannopoulos Y. D., Karakassides M. A., Chryssikos G. D., Jain H., J. Phys. Chem. 100 (1996) 11755-11765
23. Karunakaran R .T ., Marimuthu K., Arumugam S., Babu S. S., Leon-Luis S. F. and Jayasankar C. K., Opt. Mater.32 (2010) 1035 – 1041
24. Kelly S.D., Hesterberg D. and Ravel B., Analysis of soils and minerals using X-ray absorption spectroscopy (2008) 387-464; Methods of Soil Analysis - Part 5.
25. Kim Y., Saienga J., Martin S. W., J. Non-Cryst. Solids 351 (2005) 3716-3724
26. Klonkowski A., J. Non-Cryst. Solids, 72(1985)117-137
27. Konigsberger D.C., and Prince R., X ray Absorption: Principles, Applications, Techniques of EXAFS, SEXAFS and XANES. Wiley, New York, 1988.
28. Kutub A., Osman A. M., Hogarth C. A., Mater. Sci. 21 (1986) 3571
29. Leadbetter A. J., Wright A.C., J. Non-cryst. Solids 7 (1972) 23
30. Lorch E., J. Phys. C : Sol. State Phys. C 2 (1969) 229-237
31. Lottici P., Manzini I., Antonioli G., Gnappi G., Montenero A., J. Non-Cryst. Solids 159 (1983) 278
32. Margaryan A.A., Pilavin M. A., Germanate glasses: structure, spectroscopy and properties, Artech House Inc., Press, Boston, London (1993)
33. Martino D.D., Santos L. F., Marques A.C., Almeida R.M., J.Non-Cryst. Solids 293-295(2001) 394-401
34. Mountjoy G., Cole J.M., Brennan T., Newport R.J., Saunders G.A. and Wallidge G.W., Journal of Non-Cryst. Solids 279 (2001) 20-27.
35. Mountjoy G., J. of Non-Cryst. Solids 353 (2007) 2029–2034.
36. Murthy M. K., Kirby E. M., Phys. Chem. Glasses 5 (1964) 144-146

37. Newville M., Ravel B., Haskel D., Rehr J.J., Stern E.A. and Yacoby Y. Physica B 154 (1995) 208.
38. Peng L., Stebbins J. F., J. Non-Cryst. Solids, 353(2007) 4732-4742
39. Polukhin V. N., Khim Fiz., Stekla 8 (1982) 338-342
40. Poswal A. K., Agrawal A., Yadav A. K., Nayak C., Basu S., Kane S. R., Garg C. K., Bhattachryya D., Jha S. N.and Sahoo N. K., AIP Conf. Proc. 1591 (2014) 649-651.
41. Quintas A., Majerus O., Lenoir M., Caurant D., Klementiev K. and Webb A. J.of Non-Cryst. Solids 354 (2008) 98–104.
42. Rachkovskaya G. E., Zakharevich G. B., J. of Appl. Spect. Vol. 74 Issue 1 (2007) 86-89
43. Rada S., Chelcea R., Culea E., J. Mater. Sci. 45 (2010) 6025- 6029.
44. Rada S., Chelcea R., Culea E., J. Mater. Sci. 45 (2010) 6025- 6029.
45. Rao K. J., Structural chemistry of glasses, Elsevier, North Holland (2002)
46. Rossignol S., Descorme C., Kappenstein C., Duprez D., J. Mater. Chem. 11 (2001) 2587
47. Sahnoun M., Daul C., Khenata R., Baltache H., Eur. Phys. J. B 45 (2005) 455.
48. Shelby J. E., Introduction to Glass Science and Technology, second edition , Royal Soc. Chem. (2005)
49. Sigaev V. N., Gregora I., Pernice P., Champagnon B., Smelyanskaya E. N., Aronne A., Sarkisov P. D., J. Non-Cryst. Solids 279 (2001) 136-144
50. Simon S., Ardelean I., Filip S., Bratu I., Cosma I., Solid State Commun.11[2] (2000) 683-686
51. Stone C.E., Hannon A.C., Ishihara T., Kitamura N., Shirakawa Y., Sinclair R. N., Umesaki N., Wright A. C., J. Non-Cryst. Solids 293-295 (2001) 769-775
52. Umesaki N., Brunier T. M., Wright A. C., Hannon A. C., Sinclair R. N., Physica B 213&214 (1995) 490-492
53. Velli L.L.,Varsamis P.E., Kamitsos E. I., Monche D., Ehrt D., Phys.Chem. Glasses, 46 (2005) 178-181
54. Witkowska, A., Sikora B., Trzebiatowski K.and Rybicki J., J. of Non-Cryst. Solids 352 (2006) 4356-4361.
55. Xiao Z. Z. H., Lu A. X., Zuo C. G., 108 (2009) 325-331
56. Xu R., Xu L., Hu L., Zhang J., J. Phys. Chem. A, 115 (2011) 14163-14167
57. Zarzycki J., Verres et Refractaires 11 (1957) 3-8

58. Zhang W. J., Wang W. C., Zang Q. Y., Jiang Z. H., J. Non-Cryst. Solids, 475 (2017) 108-115
59. Zhao J., Yang L., McLeod J. A. and Liu L.., Sci. Rep. 5 (2015) 17779.

CHAPTER 6

STRUCTURAL STUDIES OF ALUMINO-GERMANO-PHOSPHATE GLASSES DOPED WITH La AND Nd IONS

In this Chapter, the rare earth ions neodymium (Nd) and lanthanum (La) both singly and in pairs have been included in alumino germanate, alumino phosphate and alumino germano-phosphate host glassy networks. The objective here was to study the structural effects of rare-earth inclusions on the mixed formers GeO_2 and P_2O_5. These glasses were prepared using the melt quench technique. Several different experimental techniques have been employed in these studies such as X-ray diffraction, Differential Thermal Analysis, and spectroscopic techniques such as UV- Visible spectroscopy, Fourier Transform Infrared spectroscopy and Raman spectroscopy.

6.1 Introduction

Germano-phosphate glasses are special type of vitreous materials which has a combination of two primary network formers GeO_2 and P_2O_5. In principle, the combined properties of each of the individual glass types may be imparted to the mixed glass former and could result in some new or interesting properties and possibly new applications.

An EXAFS study of several glass compositions of silico- germanate glass (Greegor et al. (1987) found that SiO_4 and GeO_4 tetrahedra are interconnected to form the continuous network in this mixed glass . Bernard et al (2001). using molecular dynamics confirmed that the silico germante glass structure consists of interconnected tetrahedral of SiO_4 and GeO_4.

Li et al. (1987) in their study of silico phosphate glass found evidence that the coordination of oxygen around silicon is six- fold. In a spectroscopic study of sodium containing silico phosphate glass doped with neodymium oxide (Abdelghany et al. (2016)) vibrational modes due to both silicate and phosphate groups was observed with the rare earth having effect on the compactness of the glass structure .

Raman and FTIR spectroscopic studies on ytterbium doped phosphate glasses by introducing a second network former GeO_2 in it (Zhang et al.(2017)) indicated that structural modifications were induced in these glasses with improvement in thermal and spectroscopic properties.

Study of germano - phosphate glass (Takahashi et al.(1976)), by varying the P_2O_5 content suggested the presence of GeO_6 in the network.

Henderson and Amos (2003) used Raman spectroscopy to study the structure of alkali included germano phosphate glass. They observed separate phosphate and germanate components in the glass structure caused by depolymerisation of the glass network due to the alkali cations.

Behrends et al. (2014) works on germano phosphate studies concluded that GeO_2 added to phosphate glass can exist as Ge-O-Ge linkages or get connected to the P-O-P linkages forming P-O-Ge bonds

Fourier transform infrared and Raman spectroscopic data have been obtained on all the glasses studied in this Chapter in order to understand the role of a second glass former in the presence of the first and also to understand the role of a second glass modifier along with the first in these glasses.

6.2 Sample preparation

The glass samples studied in this chapter were prepared using the melt quenching technique as detailed in Chapters 4 and 5. The appropriate molar percentages and the corresponding weights of the constituent oxide powders are shown in the Table 6.1 Ammonium dihydrogen orthophosphate was used as the source of P_2O_5 while GeO_2 was used in crystalline powder form as supplied by Sigma Aldrich (99.9% purity).

The alumino phosphate glass samples P1-G and P5-G described in chapter 4 are coded as NdAlP and NdLaAlP respectively while the alumino germanate glass samples G1-G and G5-G described in chapter 5 are coded as NdAlGe and NdLaAlGe respectively. These glass samples are studied along with the germanophosphate glasses prepared.

Table 6.1: Composition of germano-phosphate glasses.

Glass code	compound	Mol. Wt. (gram-mole)	Mole %	Correspond-ing weight	For 1 gm ±0.0005 gm	For 8 grams ±0.0005 gm
NdAlGeP	Nd_2O_3	336.48	5	16.824	0.0941	0.7527
	Al_2O_3	101.96	5	5.098	0.0285	0.2281
	GeO_2	104.64	40	41.856	0.2341	1.8727
	$NH_4H_2PO_4$ (*2)	230.06	50	115.03	0.6433	5.1465
			100	178.808	1	8
NdLaAlGeP	Nd_2O_3	336.48	2.5	8.412	0.0471	0.3769
	La_2O_3	325.81	2.5	8.14525	0.0456	0.3650
	Al_2O_3	101.96	5	5.098	0.0286	0.2284
	GeO_2	104.64	40	41.856	0.2344	1.8755
	$NH_4H_2PO_4$ (*2)	230.06	50	115.03	0.6443	5.1542
			100	178.5413	1	8

6.3 Differential thermal analysis and density

The values of the densities measured using the liquid displacement method (xylene) and the glass transition temperatures found by differential thermal analysis are displayed in Table 6.2. The densities of the phosphate and germanate glasses were found to decrease when La was added to Nd as compared to the density when only Nd was included in the glass. Also, the density of germanate glass was found to be higher than phosphate glass. On introducing a second glass former GeO_2 , the phosphate glass density values were

found to have been improved from 3.22 gm/cc to 3.26 gm/cc for the single Nd containing glass and from 3.14 gm/cc for both rare-earths in a phosphate to 3.24 gm/cc when GeO_2 was added. Similarly, by adding a second glass former GeO_2 to the phosphate glass, the glass transition temperature values are also found to be improved from 697^oC to 776^oC when only Nd was included in this glass and from 688 ^oC to 755^oC when both rare-earths were included. Thus the phosphate glass network gets modified with decreased density and decreased glass transition temperature on adding a second rare earth La while it gets modified with improved density and increased glass transition temperature on adding a second glass former GeO_2.

Table 6.2 : Density and glass transition temperature

	Density gm/cc $\pm$ 0.00(25) gm/cc	Tg in ^oC $\pm$ 2 ^oC
NdAlP	3.22	697
NdLaAlP	3.14	688
NdAlGe	4.33	830
NdLaAlGe	4.26	817
NdAlGeP	3.26	776
NdLaAlGeP	3.24	755

6.4 X-Ray diffraction

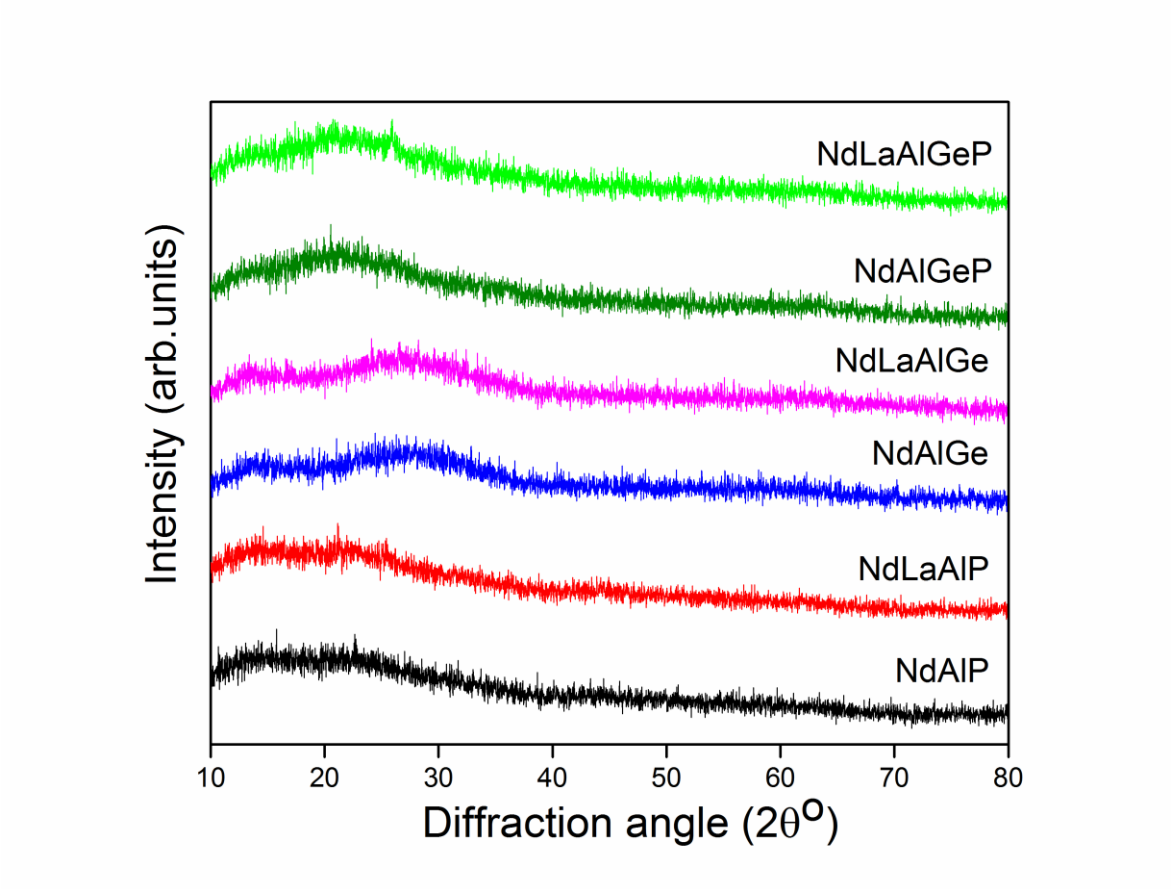

Figure 6.1: X-ray diffraction spectra of the phosphate, germanate and germano-phosphate glasses

The X-ray diffraction patterns of the Nd and Nd &La included in germanate, phosphate and germano-phosphate glasses are shown in the figure 6.1. The presence of diffused diffraction patterns and the absence of sharp Bragg peaks indicate that the glass samples were amorphous. The patterns of broad undulations also appear to be different for the individual phosphate or germanate hosts as compared to the patterns for the mixed phosphate and germanate hosts.

6.5 Fourier Transform Infrared Spectroscopy

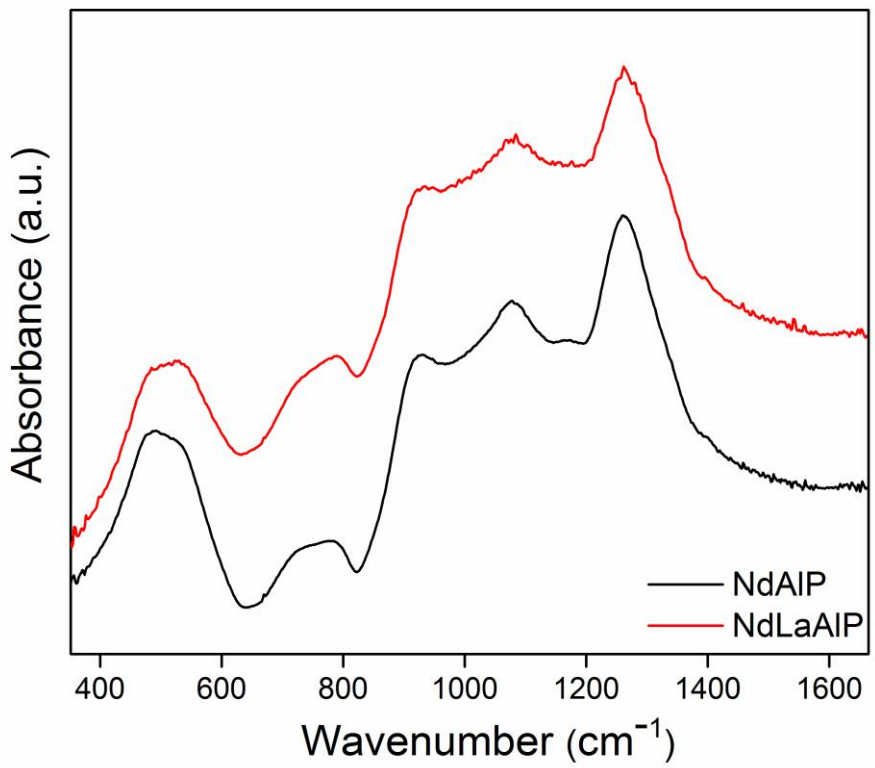

Figure 6.2: Fourier Transform Infra-red Spectra of phosphate glasses NdAlP and NdLaAlP

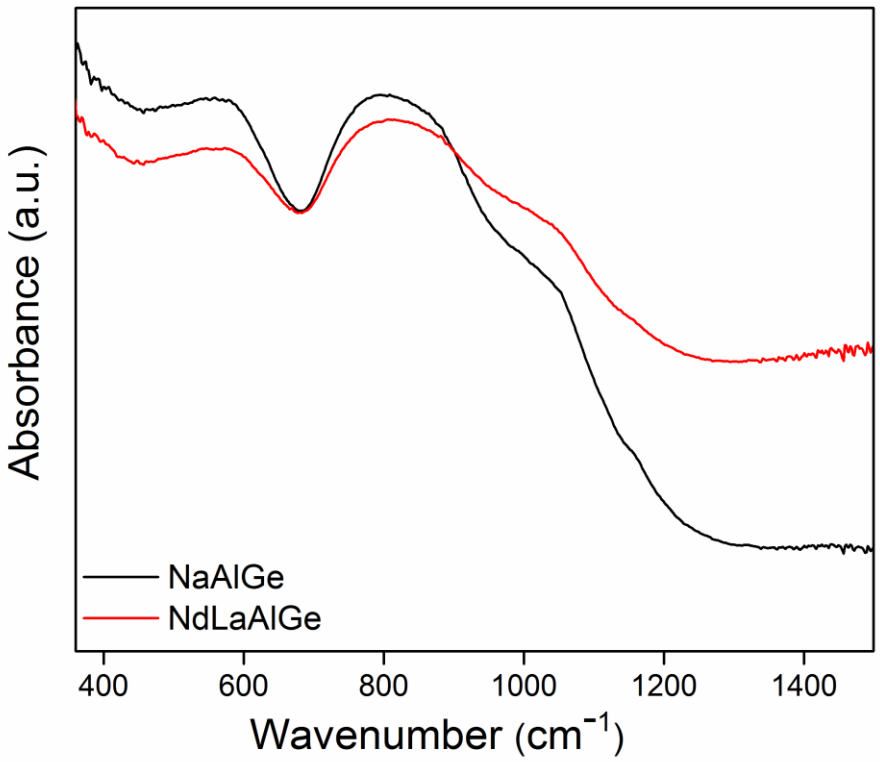

Figure 6.3 : Fourier Transform Infra-red Spectra of Germanate glasses NdAlGe and NdLaAlGe

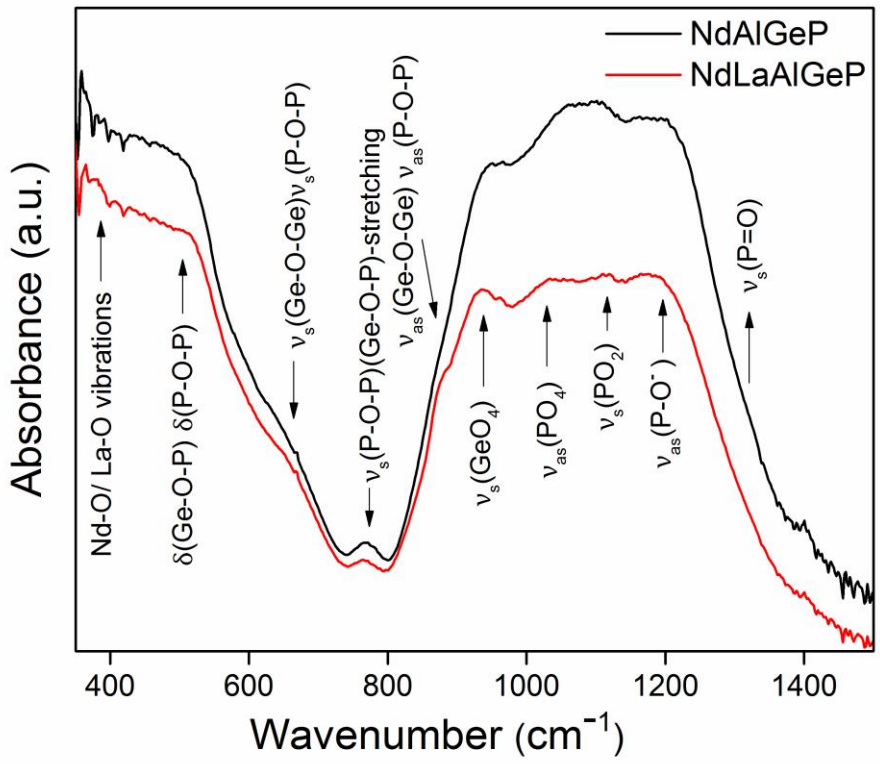

Figure 6.4 : Fourier Transform Infra-red Spectra of germano-phosphate glasses NdAlGeP and NdLaAlGeP

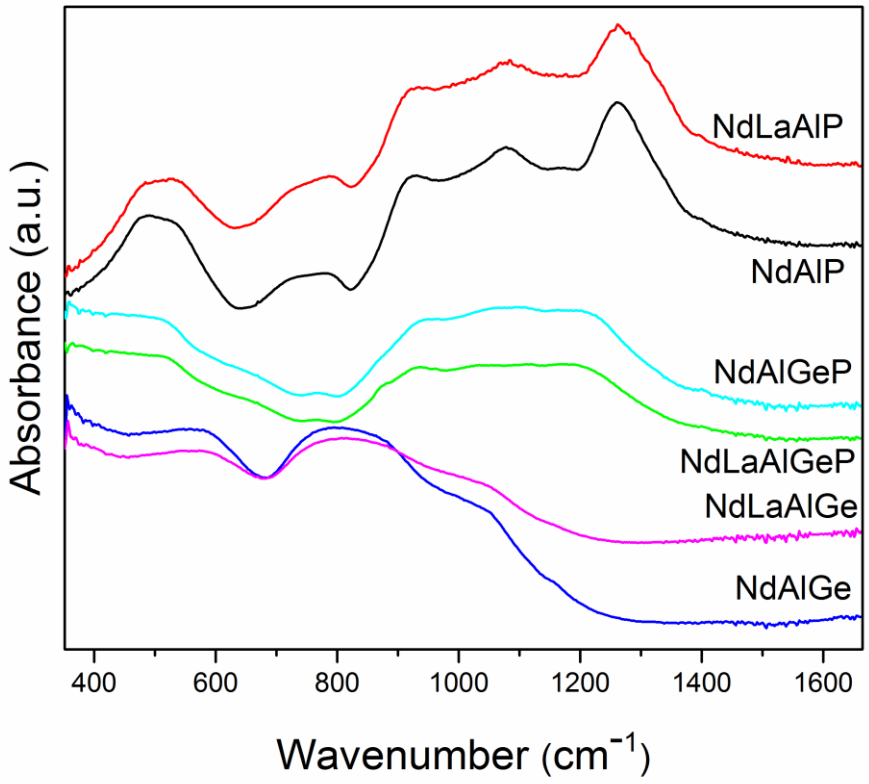

Figure 6.5: Comparative display of Fourier Transform Infra-red Spectra of phosphate, germanate and germano phosphate glass

The Fourier transform infrared (FTIR) spectra of the glass of each each type of host glass former phosphate, germanate and the mixed former with the inclusion Nd and La singly and together in each type of host glass are displayed in Figure 6.5. The Figure 6.2 shows the broad band at about 500cm^{-1} due to the O-P-O vibrations, the band between 650 cm^{-1} to 850 cm^{-1} is due to vibrations in the P-O-P links while the band between 850 cm^{-1} to 1400 cm^{-1} is due to the network structural units having different number of non bridging oxygens(NBO) for the phosphate glass (Kader et al(1991), Pavic et al (2014), Rai et al(2011)). FTIR spectra for the germanate glass are displayed in figure 6.3 showing symmetric vibrations of GeO6 at 590 cm^{-1}, Vibrations of Ge-O-Ge and O-Ge-O in the band between 680 cm^{-1} to 1100 cm^{-1} ((Rachkovskaya et al. (2007), Xiao et al.(2009),

Simon et al. (2000)). FTIR spectra due to vibrations in the germano-phosphate glass are shown in the figure 6.4 (Ilieva et al.(2001), Sahar et al. (2007) , Henderson, Amos (2003), Kamitsos et al.(1996), Kumar et al.(2001)). The modifiers i.e. Nd and La are likely to disrupt the phosphate chains so that the phosphate network gets modified. It may also be observed that there is modification of the fragile phosphate glass network on the addition of another strong glass former i.e. GeO_2 to the matrix

6.6 UV-Visible spectroscopy

The absorption spectra of the germano- phosphate glass is shown in the figure 6.6 below the absorption peaks in both the germano phosphate glasses NdAlGeP and NdLaAlGeP are due to the transitions from the 4f electronic levels of Neodymium. There is no contribution from Lanthanum to the absorption in the visible region as it does not have any f electron (Kutub et al. (1986), Karunakaran (2010)). As in the case of the germanate and phosphate glasses, the absorption spectrum of Nd remains essentially the same whatever be the host glassy network.

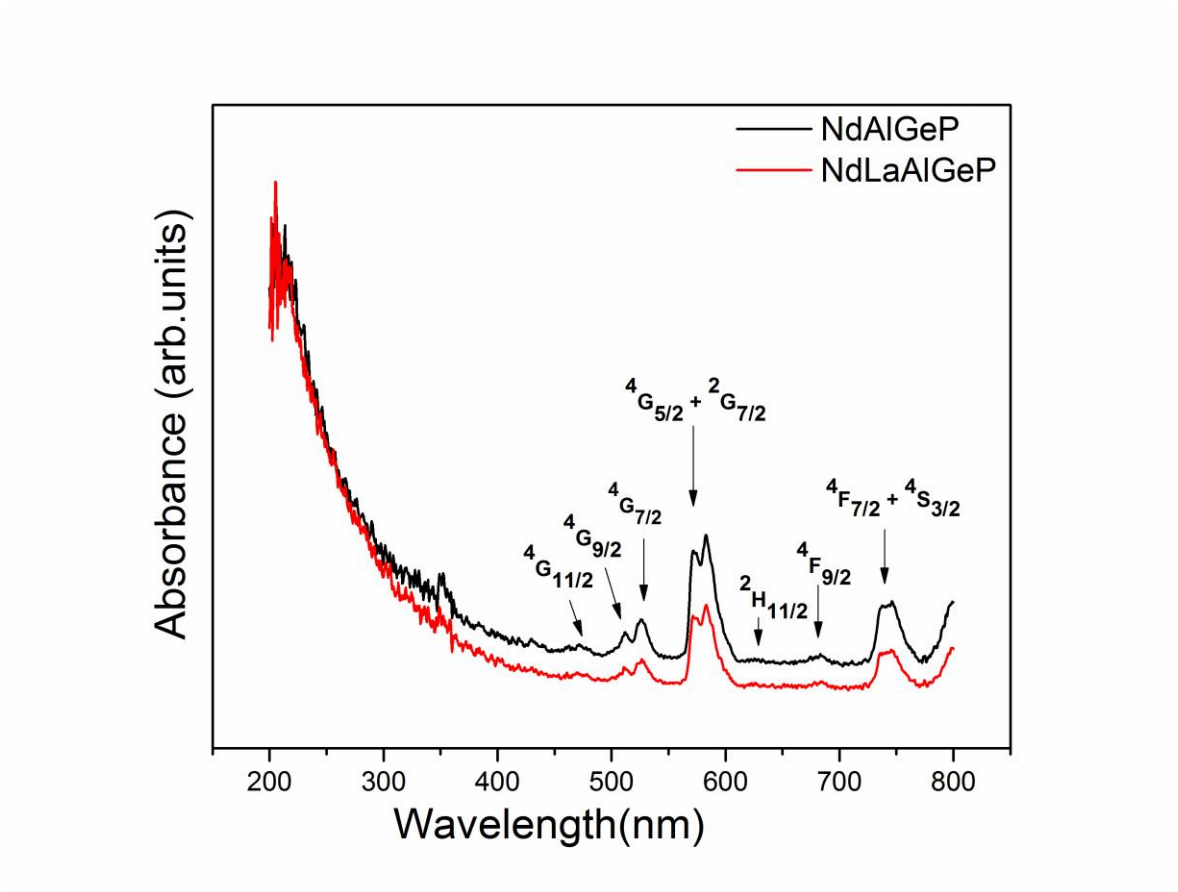

Figure 6.6: Absorption spectra of NdAlGeP and NdLaAlGeP germano-phosphate glasses

6.6.1 Tauc Plots

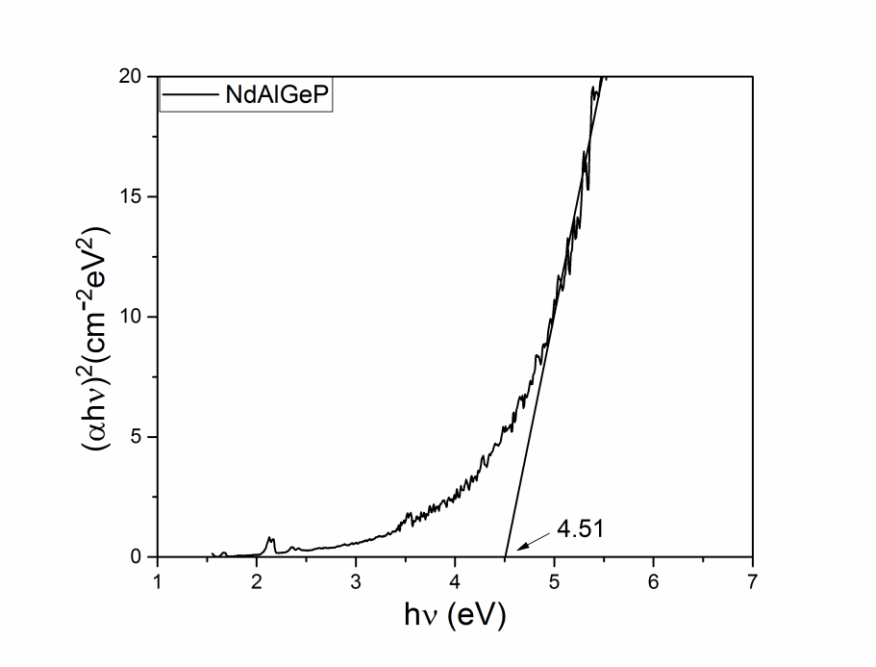

6.7 (a)

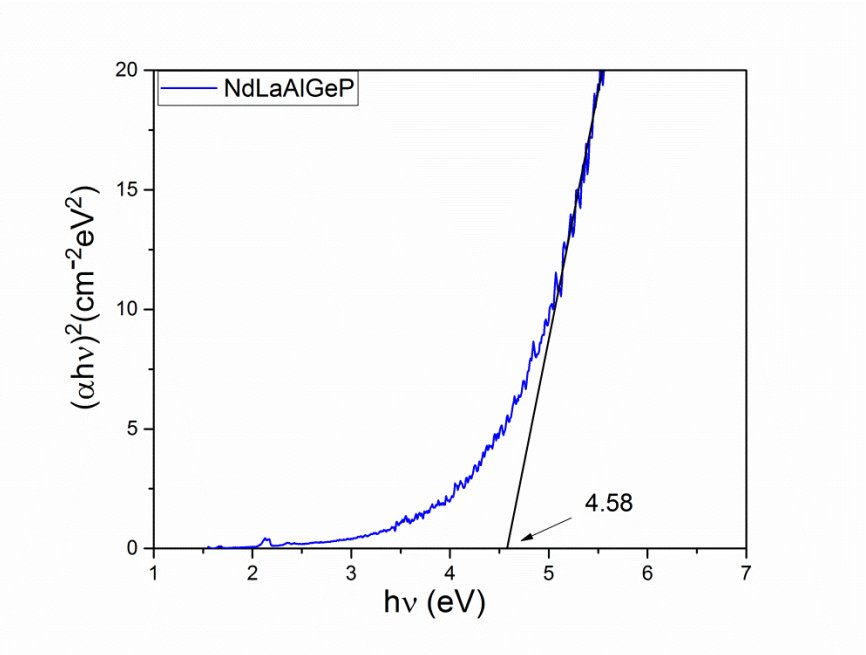

6.7 (b)

Figure 6.7: Tauc plots for the germano-phosphate glasses (a) NdAlGeP (b) NdLaAlGeP

Tauc plots for the two germano-phosphate glasses were plotted according to the procedure detailed in Chapters 4 and 6, and are shown in Figure 6.7(a) for NdAlGeP glass and in 6.7(b) for NdLaAlGeP glass. The values of the optical band gap energy were obtained by interpolating the linear portion of the curve to the hν axis. These were found to be 4.51 eV for NdAlGeP and 4.58 eV for NdLaAlGeP. It appears that the less compacted and lower density glass (~3%) resulting when both rare-earths are present in the germano-phosphate host. This glass also results in a slightly higher (~2%) value of the optical band gap.

6.7 Raman Spectroscopy

The Raman spectra were obtained on all six samples prepared here using the Linkam TS1500 spectrometer whose details are given in Chapter 2 according to the method and parameters of measurement stated in Chapters 4 and 5 in the wavenumber range of 100 cm^{-1} to 1500 cm^{-1}.

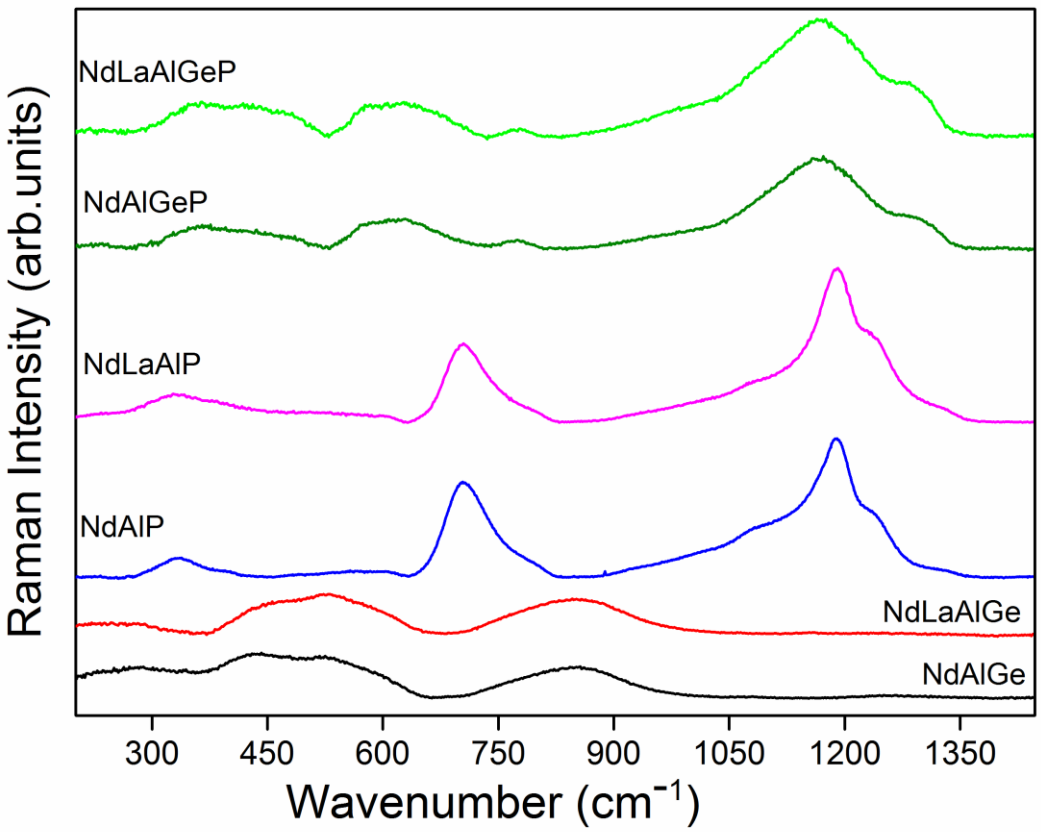

Figure 6.8 : Comparative display of the Raman spectra of the phosphate, germante and germano-phosphate glasses

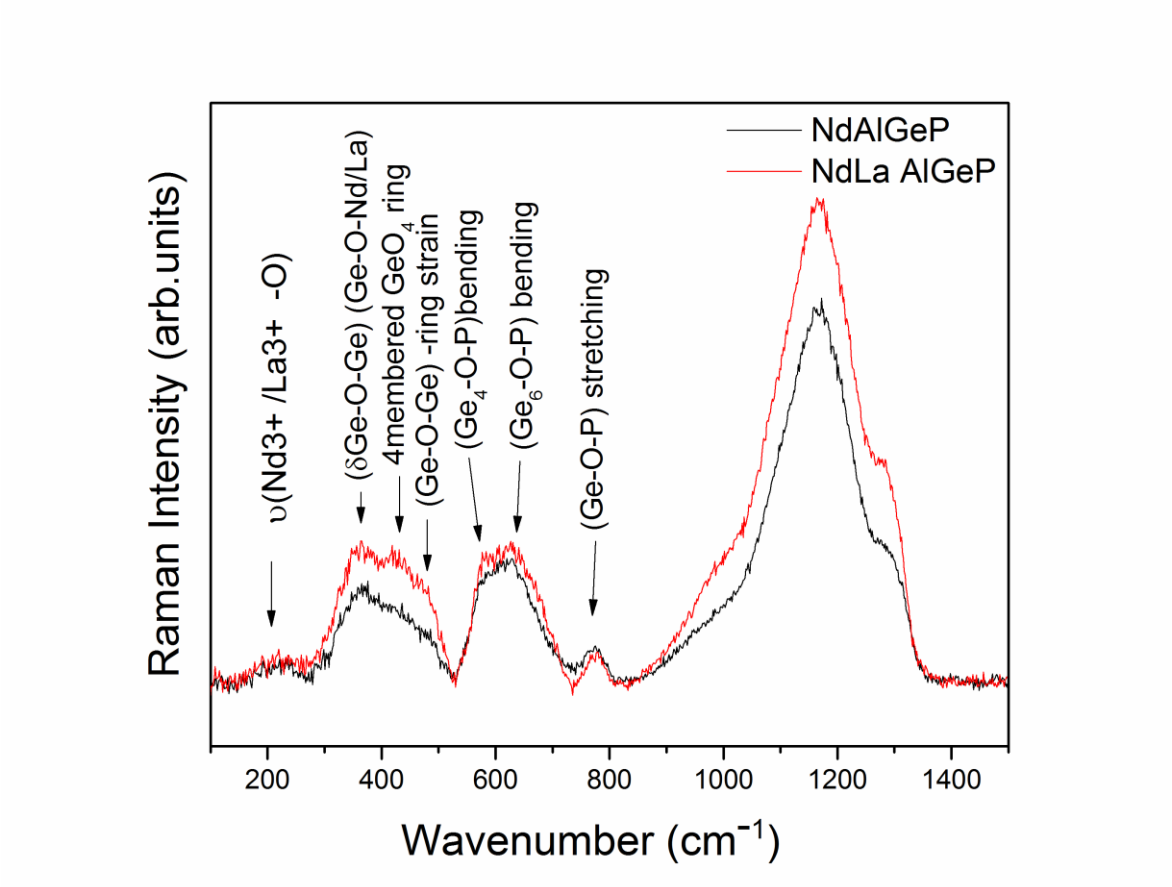

Figure 6.9 : Comparison of the Raman spectra from the two samples having germano-phosphate host networks

The figure 6.9 shows the Raman spectroscopic data for the NdAlGeP and NdLaAlGeP germanophosphate glasses. The band from 140 -270 cm^{-1} is due to the combined vibrational (RE - O) modes associated with phosphate and germanate network structures (Koo et al.(1997)). The peak at 365 cm^{-1} arises due to the combined vibrational modes of Ge-O-RE vibrations and δ(Ge-O-Ge) modes where RE is (Nd^{3+}, La^{3+}) (Meyer (1997), Hudgens et al.(1998). The symmetric stretching Ge-O-Ge vibrations associated with the 4 membered GeO_4 rings appear at 425 cm^{-1} (Galeener et al.(1983) while δ(Ge-O-Ge) from ring strain arises at 480 cm^{-1} (Zhang et al.(2017). The vibrations at 580 cm^{-1} gives a peak which is assigned to Ge_4-O-P bending modes, the peak at 640 cm^{-1} is assigned to Ge_6-O-P bending modes and the small band at 775cm^{-1} is due to the stretching of the Ge-O-P bridges (Kamitsos et al.(1996).

The band between 630 cm^{-1} to 830 cm^{-1} which is due to the P-O-P vibrations in the phosphate glass is modified on adding GeO_2 and gets shifted to the left with a small band

at 775 cm^{-1} showing the mixed Ge-O-P bridges. The higher frequency band from 825 to 1400 cm^{-1} is seen to have been modified with the development of prominent shoulders at around 1278 cm^{-1}. The band relates to the total range of vibrational energies of the basic structural unit in each glass type. This band has been deconvoluted and compared with the constituent deconvoluted peaks of the corresponding phosphate and germanate glasses as detailed in Figures 6.10 to 6.15 below. The relative area ratios of Q^n in these glasses are listed in table 6.3.

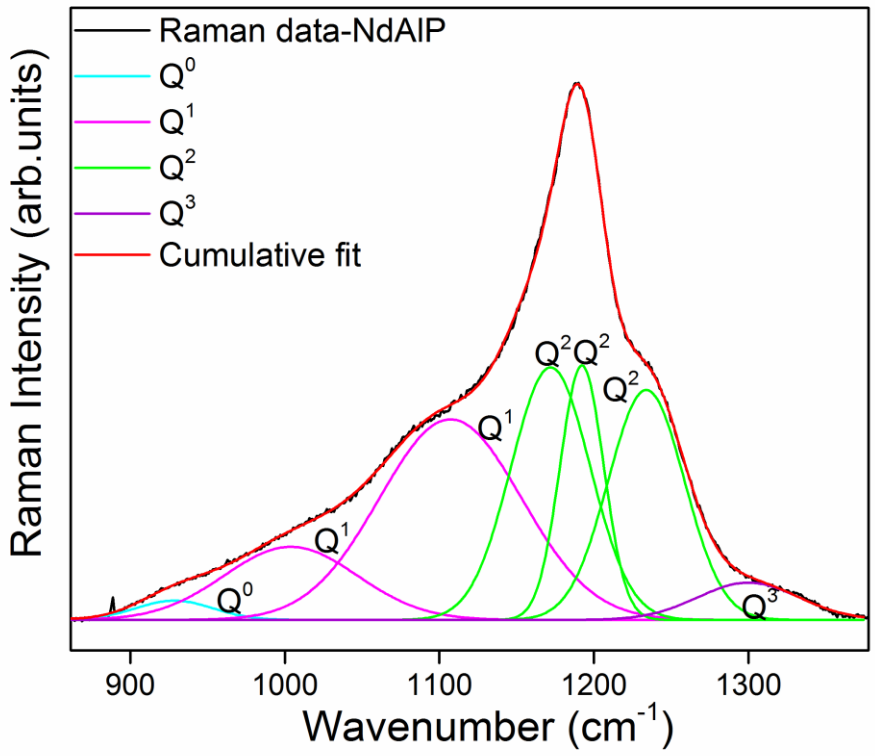

Figure 6.10: Deconvoluted Raman peaks of vibrations of the basic structural units for NdAlP phosphate glass.

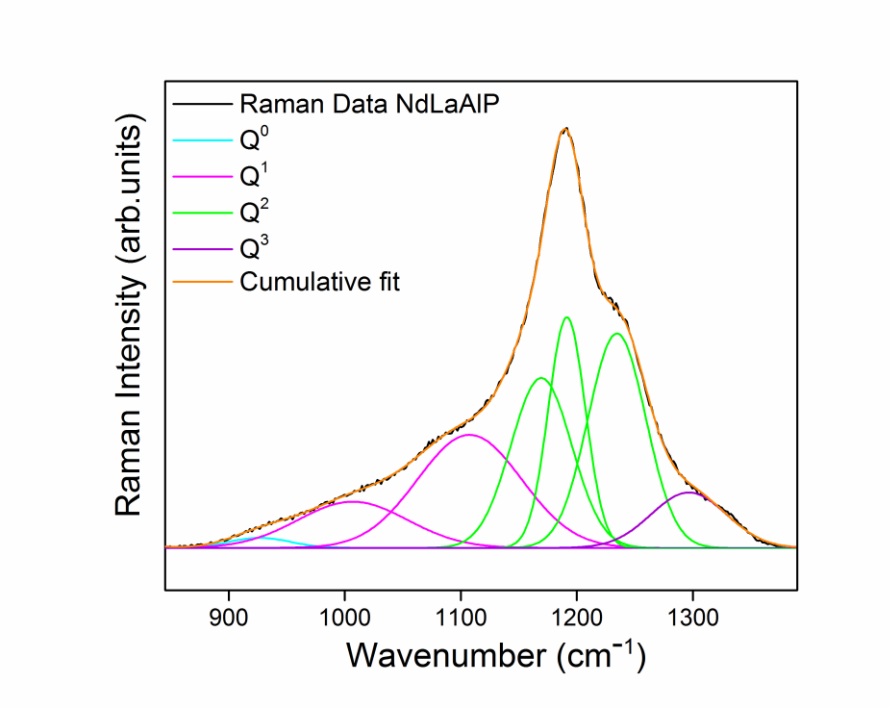

Figure 6.11: Deconvoluted Raman peaks of vibrations of the basic structural units for NdLaAlP phosphate glass.

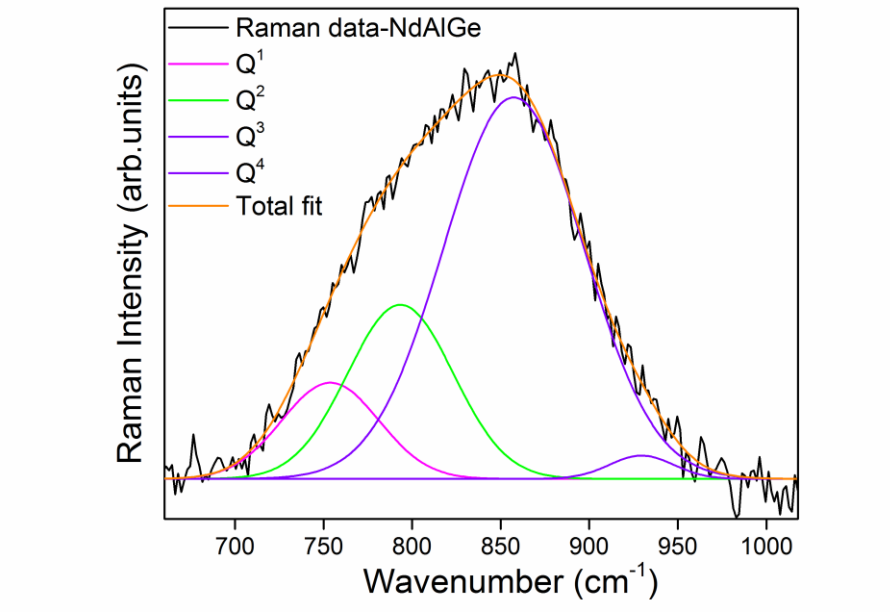

Figure 6.12: Deconvoluted Raman peaks of vibrations of the basic structural units for NdAlGe germanate glass.

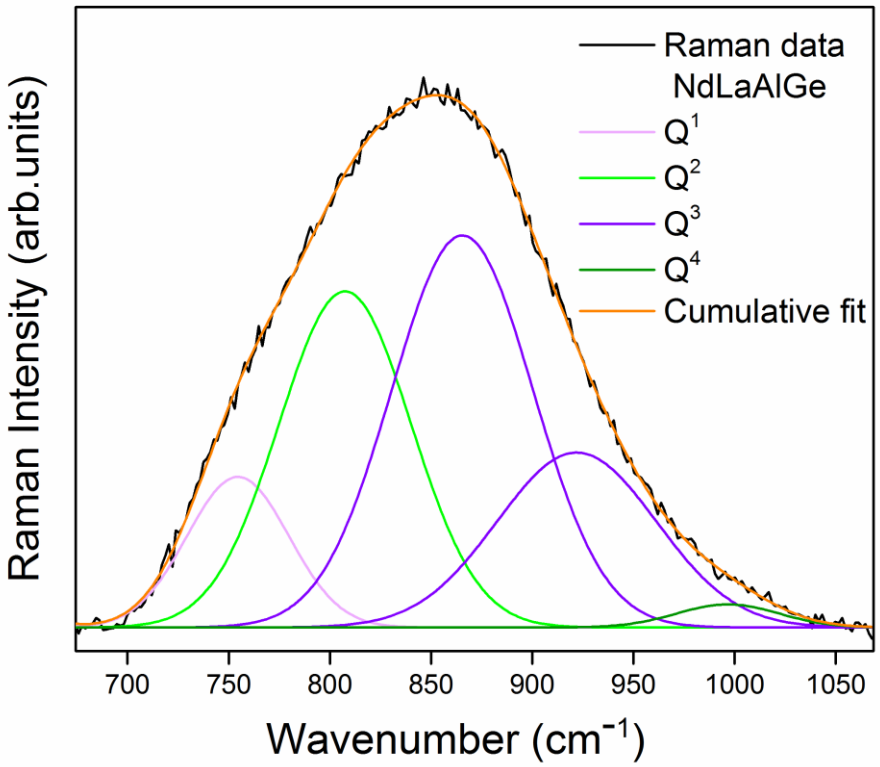

Figure 6.13 : Deconvoluted Raman peaks of vibrations of the basic structural units for NdLaAl Ge germanate glass.

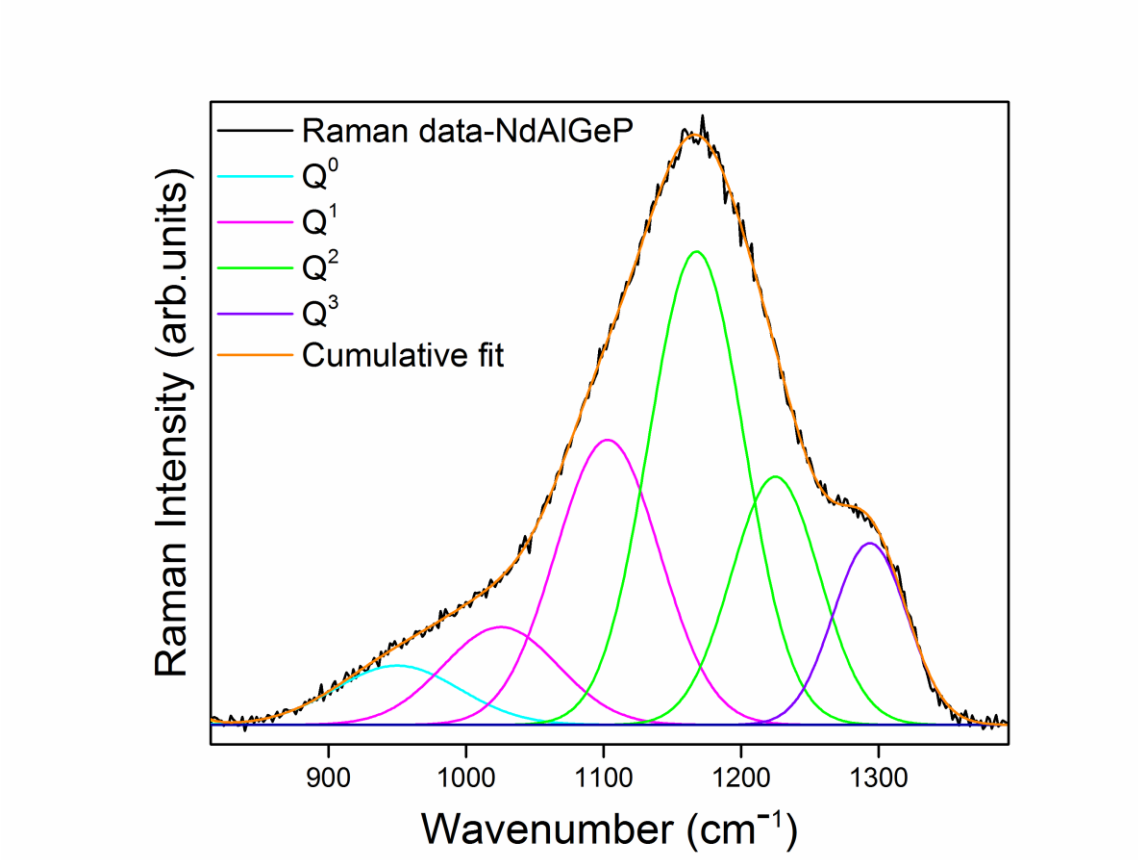

Figure 6.14 : Deconvoluted Raman peaks of vibrations of the basic structural units for NdAlGeP germano-phosphate glass.

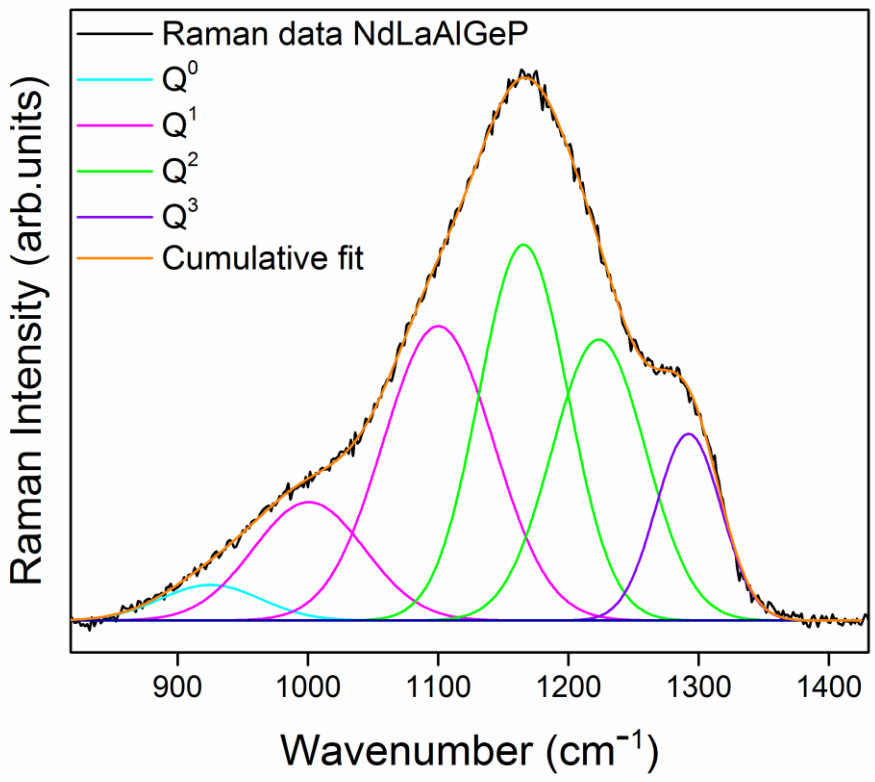

Figure 6.15 : Deconvoluted Raman peaks of vibrations of the basic structural units for NdLaAlGeP germano phosphate glass.

Table 6.3: Relative area ratios of Q^n of the different structural units in the phosphate, germanate and germano-phosphate glasses

Q^n	NdAlP	NdLaAlP	NdAlGe	NdLaAlGe	NdAlGeP	NdLaAlGeP
Q0	0.0161	0.0117	0.0000	0.0000	0.0575	0.0296
Q1	0.4149	0.3183	0.1131	0.1058	0.3182	0.3772
Q2	0.5281	0.5910	0.2220	0.3052	0.5197	0.4926
Q3	0.0409	0.0790	0.6648	0.5727	0.1046	0.1005
Q4	0.0000	0.0000	0.0000	0.0163	0.0000	0.0000
Normal.Areas	1	1	1	1	1	1

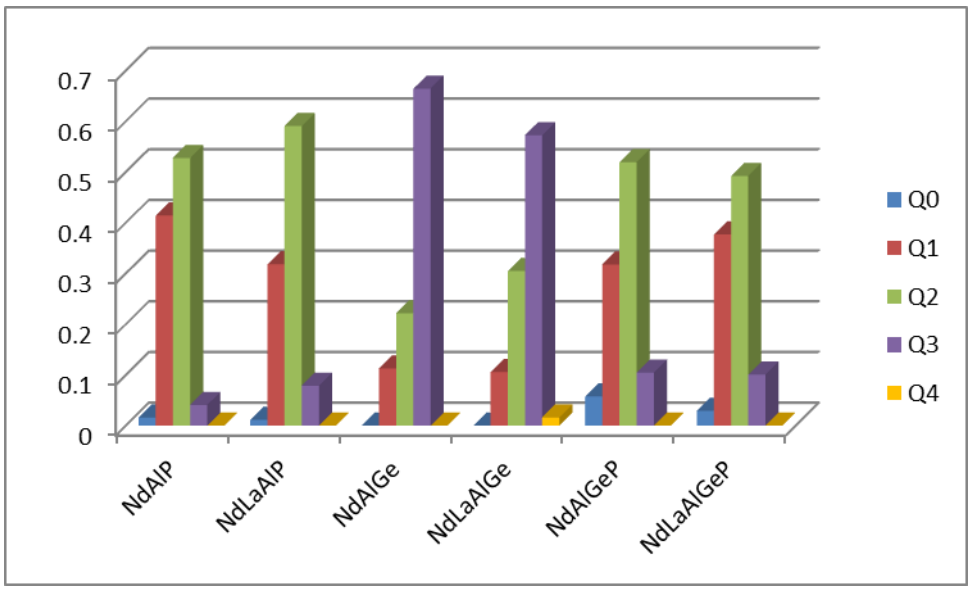

Figure 6.16 : Bar graph display of relative area ratios of Q^n of the phosphate, germanate and germano-phosphate glasses.

Figure 6.16 shows a comparison of the relative ratios of the areas of the constituent Q^n from the deconvoluted peak fits to the vibrations of the structural units of the phosphate, germanate and germano-phosphate glasses. It may be observed that in the two phosphate glasses, the role of La is to increase the network connectivity by increasing the number of Q^2 and Q^3 while decreasing the number of Q^1 structural units. Thus, the number of non-bridging oxygens decreases while the number of bridging oxygens increases suggesting better connectivity. However in the two germanate glasses, the addition of lanthanum causes the fraction of Q^3 to decrease but the fraction of Q^2 to increase. Thus in these germanates, on adding La connectivity decreases. In the mixed host germano-phosphate glasses, on adding La the number of Q^1 increases while the number of Q^2 structural units decreases, and the fraction of Q^3 structural units remaining the same.Thus there will be net increase in the number of non-bridging oxygens and a net resultant loss of connectivity. It may be noted that in the phosphate and germano-phosphate glasses, the main connectivities are Q^1 and Q^2, while in the germanate glasses the principal connectivities are Q^2 and Q^3

Alternately, it be noted that for the Nd phosphate glass, the introduction of GeO_2 as the second glass former, decreases Q^1 and increases Q^2 and Q^3 - thus resulting in a better connected glass. However, for the NdLa phosphate glass, introduction of GeO_2 as the second former causes Q^2 to decrease and Q^1 to increase - thus lowering the connectivity of the glass. For the Nd germanate and NdLa germanate glasses, when phosphate is added as the second former, Q^3 substantially decreases while Q^2 and Q^1 substantially increase - thus resulting in a net decrease of connectivity in both these glass types.

6.8 Conclusions

Two germano phosphate glasses were prepared, one with a single rare earth Nd and the other with a second rare earth La along with Nd. These glasses were studied along with two phosphate glasses and two germanate glasses each with a single rare earth Nd and Nd with La in pairs. The XRD spectra of the glasses confirmed that proper glasses were formed.

Density measurements showed that the density of the phosphate glasses improved on adding a second network former GeO_2 to it, however the density of the glasses decreased on adding a second rare earth La to the glass having a single type Nd.

FTIR spectra showed the presence of Ge in the phosphate glass network indicating that the phosphate network structure is modified.

UV- Visible spectral data show 4f electronic transitions due only to the Nd modifier ions in the glass network as La does not possess these electronic levels. Tauc plots were plotted and the electronic band gap energy for the Nd germano-phosphate glass was 4.51 eV which was slightly lower than the band gap of 4.58 eV for NdLa germano-phosphate glass which may be related to the lower density of the latter glass.

The Raman spectral data analyses showed that the major connectivies of the phosphate glass change from Q^1 and Q^2 to those having a small percent of Q^0 and Q^3 structural unitsin addition. Structurally GeO_2 is a stronger network former compared to the more fragile P_2O_5. Also the higher acidity of P_2O_5 makes it compete with GeO_2 and take up most of the oxygen from the modifier. Thus in the germano-phosphate glass, the phosphate part of the network would be modified due to the presence of the modifier rare earth while the GeO_2 part remains almost unaffected. The presence of Lanthanum seems to increase the network connectivity of the glass when it is added to it along with the first rare earth. When germania is added as a second former to the Nd phosphate, the glass connectivity is improved while when germania is added to the NdLa phosphate the connectivity becomes worse. In the case of phosphate being added to Nd or to NdLa germanate glasses, in both cases the connectivity substantially worsens.

References:

1. Abdelghany A. M.,. Zeyada H. M,. ElBatal H. A, Fetouh R.. Silicon, 8 (2016) 325-330
2. Alvarado-Rivera J., Rodriguez-Carvajal D. A., del M., Acosta-Enriquez C., Manzanares-Martinez M. B., Alvarez E., Lozada-Morales R., Diaz G C., de Leon A., Zayas M. E., J. Am. Ceram. Society, 97 (2014) 3494-3500
3. Behrends F., Eckert H., J. Phys. Chem. C,118 (2014) 10271-10283
4. Bernard C., Chaussedent S., Monteil A., Balu N., Obriot J., Duverger C., Ferrari M., Bouazaoui M., Kinowski C., Turrell S., J. Non- Cryst. Solids 284 (2001) 68
5. Galeener F. L., Leadbetter A. J., Stringfellow M.W., Phys. Rev. B 27 (1983) 1052
6. Greegor R. B., Lytle F. W., Kortright J., Fischerkolbrie A., J. Non. Cryst. Solids, 89 (1987) 311

7. Henderson G. S., Amos R. T., J. Non-Cryst. Solids 328 (2003) 1-19
8. Henderson G. S., Amos R. T., J. of Non-Cryst. Solids 328 (2003) 1-19
9. Hudgens J. J., Brow R. K., Tallant D. R., Martin S. W., J. Non-Cryst. Solids 223 (1998) 21-31
10. Ilieva D., Jivov B., Kovacheva D., J. Non-Cryst. Solids 293-295 (2001) 562-568
11. Kader A. A., Higazy A. A., Elkholy M.M., J. Mater. Sci.: Mater. Electron 2 (1991) 157- 63
12. Kamitsos E. I., Yiannopoulos Y. D., Karakassides M. A., Chryssikos G. D., Jain H., J. Phys. Chem. 100 (1996) 11755-11765
13. Karunakaran R .T ., Marimuthu K., Arumugam S., Babu S. S., Leon-Luis S. F. and Jayasankar C. K., Opt. Mater.32 (2010) 1035 – 1041
14. Koo J., Bae Byeong-Soo, Na Hoon-Kyun, J. Non-Cryst. Solids 212 (1997) 173-179
15. Kumar S., Murugavel S., Rao K. J., J. Phys. Chem. B 105 (2001) 5873
16. Kutub A., Osman A. M., Hogarth C. A., Mater. Sci. 21 (1986) 3571
17. Li D., Bankroft G. M., Fleet M. E., Am. Miner. 81 (1986) 111
18. Meyer K., J. Non- Cryst. Solids 209 (1997) 227-239
19. Pavic L., Milankovic A. M., Rao P. R., Santic A., Kumar V.R., Veeraiah N., J. Alloys Comp. 604 (2014) 352-362
20. Rachkovskaya G. E., Zakharevich G. B., J. of Appl. Spect. Vol. 74 (1) (2007) 86-89
21. Rai V.N., Rajasekhar B. N., Tiwari P., Kshirsagar R. J., Deb S. K., J. Non-Cryst. Solids 357 (2011) 3757-3764
22. Sahar M. R., Wahab A., Hussein M. A., Hussin R., J. Non-Cryst. Solids,353 (2007) 1134-1140
23. Simon S., Ardelean I., Filip S., Bratu I., Cosma I., Solid State Commun.11[2] (2000) 683-686
24. Takahashi K., Mochida N., Matsui H., Takeuchi S., Gohshi Y., J. Cer. Soc. 84 (1986) 482
25. Zhang L. Y., Li H., Hu L. L., J. Alloys and compounds 698 (2017) 103-113
26. Zhang L. Y., Xue T. F., Hee D. B., Guzik M., Boulon G., Opt. Express 23 (2015) 1505-1511

CHAPTER 7

CONCLUSIONS

Rare earth alumino-phosphate glasses were prepared by the melt quenching method. Rare earth ions, La, Pr, Nd and combinations of these in pairs were included in the host glass. Three of these glasses were suitably heat treated and devitrified.

The vitreous nature of the glass samples and the crystalline nature of the devitrified samples were confirmed from the X-ray diffraction spectra. The devitrified samples were found to exhibit higher densities than the corresponding glasses that were devitrified. Fourier Transform Infra-red Spectra of the devitrified samples show better resolved sharper peaks as compared to the glass samples indicating that the tetrahedra are better linked in the devitrified samples.

Similarities in the FTIR spectra of the glasses indicate that the rare-earth ions play-the role of modifiers in the glass network. UV-Visible spectroscopy data show optical absorption peaks for the glasses included with Nd or Pr or both Nd and Pr ions due to the 4f electronic transitions. This indicates that the rare-earth ions would be preferably occupying positions in the phosphate glass network to balance the negative charge of the terminal or non-bridging oxygen of the PO_4 structural units without actually bonding to bridging oxygen atoms i.e. the rare-earth ions would have network modifier roles.

Raman vibrational spectra of the devitrified samples show better resolved modes than those of the corresponding glasses. Fitting of the Raman band in the 850 cm^{-1} to 1400 cm^{-1} range with Gaussian peaks corresponding to the vibrational modes of the Q^n structural units, resulted in the finding that the main connectivities for the Nd, La and Nd-La included glasses as well as their devitrified states had the Q^1 and Q^2 linkages as the most frequently occurring ones. The Nd-La containing glass and its devitrified state shows the presence of Q^0 linkages without any Q^3 or Q^4 connectivities. As expected, the calculated connectivity was also seen to be lower when both Nd and La were present suggesting a more open structure of the Nd-La containing glass system. Analysis of the Raman data for the structural units for a simple alumino-phosphate host glass (without included ions) shows Q^2 as the prominent linkage but with the presence of Q^1 and Q^3. On adding Pr to the host glass, there is an increase in the fraction of Q^1structural units with a decrease in the fraction of Q^2 while the fraction of Q^3 structural units remains the same. This indicates the metaphosphate network of Q^2 structures gets modified to a less connected network on adding Pr. The Pr_6O_{11} which was used in the preparation consists of network modifier Pr^{3+}

as well as network former Pr^{2+}. Hence the resultant connectivity of the alumino-phosphate gets modified with the addition of Pr ions. There is some conversion of Q^2 units to Q^1 units suggesting an increase in the number of non-bridging oxygen atoms on adding Pr to the host network.

EXAFS data for the three glasses having Nd , La and both Nd, La together shows that the coordination of oxygen around Nd is slightly less than octahedral in the glass. This coordination becomes approximately 8 for the devitrified states. The variation in Nd-O and La-O bond lengths is found to be in the range 2.36 Å to 2.40 Å for these glasses. These values are in good agreement with the neutron results showing the rare-earth to oxygen correlation length varying between 2.35Å to 2.38 Å and coordination numbers of 6 to 8.5 thereby confirming the network modifier role of rare-earth ions in the continuous random network of PO_4 tetrahedra.

Rare-earth alumino-germanate glasses were prepared by the melt quenched method in air and consisting of 10 mole% Al_2O_3 , 80 mole% GeO_2 and the remaining 10 mole% being rare-earth oxides included either singly as Nd_2O_3 , Pr_6O_{11} or La_2O_3 and in pairs. Glass transition temperature and density were found to be the maximum for the glass with singly included Pr while these values were the lowest for the glass with singly included La. X-ray diffraction confirmed the glassy nature of the samples and showed the crystalline phases of either or both rare-earth constituents in the devitrified state.

FTIR spectra on the devitrified samples except the glass containing only Pr showed the presence of GeO_4 tetrahedra, GeO_6 octahedra and three and four-membered rings of GeO_4 tetrahedra. These structural units are also present in the respective glasses prior to devitrification. The 4f electronic transitions in ions of Nd and Pr gave rise to the absorption peaks in the UV-Visible absorption spectra. For samples in which both Nd and Pr were present, the measured spectrum was a linear superposition of the spectra due to each ion type. The Tauc plots yielded the values of optical band gaps about 5% to 6% lower for the two Pr included glasses as compared to the other glasses while the calculated values of refractive index, dielectric constant and electronic polarizability were 2% to 4% higher for the latter samples than for the other glasses. These figures would be related to the larger number of non-bridging oxygen atoms in the network tetrahedra of those glasses containing Pr.

Raman spectral studies indicate that only the singly included Pr glass have the highest fraction of Q^2 structural units while all other glasses have the maximum in the

number of Q^3 structural units - with the Nd included glass being the highest. Thus the singly included Nd glass has the most continuous network while the singly included Pr glass has a less continuous network.

EXAFS data on the samples showed the presence of both tetrahedral coordination of oxygen around Ge with the Ge-O distance as 1.74 Å for the Nd included glasses. The singly included Pr glass shows a higher coordination number of Ge-O indicating a probable presence of GeO_5 units in this glass as also suggested by FTIR analysis. The coordination of oxygen around the rare-earth was found to be approximately 9 rather than merely octahedral. Neutron diffraction measurements found Ge-O to be 1.75 Å with tetrahedral coordination of Ge(O) and the presence of an Al-O correlation between 1.8 to 1.9 Å and an assumed coordination of Al(O) of 4. The coordination number of oxygen around the rare-earth is 7.5 for the singly included Nd glass and about 10 for the singly included Pr glass.

Two alumino germano-phosphate glasses were prepared, one with a single rare earth Nd and the other with two rare earths La and Nd. Comparative study of these germano-phosphates was carried out along with phosphate and germanate glasses with the same rare-earth inclusions. The XRD spectra of the glasses indicated proper glass formation. Density and glass transition temperatures are found to improve on adding a second network former GeO_2 to P_2O_5. However in each type of host glasses, the density of the glasses decreased on adding the another rare earth La to the only Nd containing glass .

FTIR spectra results that Ge is present in the phosphate glass network indicates that the phosphate network structure gets modified on adding a second glass former. UV-Visible spectral data show 4f electronic transitions due only to the Nd modifier ions in the glass network as La does not possess these electronic levels. Tauc plots were plotted and the electronic band gap energy for the NdLa germano-phosphate glass was 4.58 eV eV which was higher than the band gap of 4.51 for the Nd germano-phosphate glass - which may be due to the higher density of the Nd included glass.

The Raman spectral data analyses showed that on adding GeO_2 the major structural units of the phosphate glass change from being Q^1 and Q^2 to those having a small percentage of Q^0 and Q^4 structural units along Q^1 and Q^2 structural units the fraction of which slightly decreases. Thus in the germano-phosphate glass, P_2O_5 being a more fragile network former compared to GeO_2 which is structurally stronger, the phosphate part

of the network would be affected more by the presence of the modifier rare earth. The network connectivity of the phosphate glass seems to increase due to the presence of Lanthanum when it is added along with the first rare-earth Nd. When germania is added as a to the Nd phosphate as second glass former, the glass connectivity is found to improve while in case of NdLa phosphate the connectivity becomes worse. In the case of phosphate being added to germanate glasses with Nd or NdLa, in both cases the connectivity substantially decreases in both these glasses.

Future Scope

Further insights into the structures of the glass systems that have been studied in this thesis are necessary. For this, high momentum transfer neutron diffraction studies (such as at the pulsed neutron source of RAL) on representative members of these glasses and their devitrified states would be of much value. Monte Carlo simulation studies which would be guided by such high resolution neutron diffraction data can then be used to construct three dimensional structural models of these systems.

The computer simulation studies – particularly on the devitrified states – would be of special aid to the development of quasi crystalline models of the structures of the glasses that have been studied in this work and would be of much relevance to mixed glass former systems and their optimal ratios of mixing. Several industrially useful glasses use mixed glass formers to improve the physical and chemical properties of the single formers.

BIBLIOGRAPHY

1. Abdelghany A. M., Zeyada H. M., ElBatal H. A., Fetouh R., Silicon, 8 (2016) 325
2. Abo-Naf S.M.,.El-Amiry M.S., Abdul-Khalik A.A.,Opt.Mater.30(2008)900
3. Alben R. and Boutron P., Science, 187 (1975) 430
4. Alvarado-Rivera J., Rodriguez-Carvajal D. A., Del C. M., Costa-Enriquez. A., Manzanares-Martinez M. B., Alvarez E,. Lozada-Morales R., Diaz G. C., De Leon A., Zayas M. E., J. Am. Ceram. Society, 97(2014)3494-3500
5. Baert K., Meulebroeck W., Wouters H., Cosyns P, Nys K., Thienponttb H. and Terryna G., J. Raman Spect.42 (2011) 1789
6. Baia L., Iliescu T., Simon S., Kiefer W., J. Molec. Structure, 599 (2001) 9-13
7. Balda R., Fernandez J., Sanz M., De Pablon A., Navarro J. M. F., Mugnier J., Phys. Rev. B 61 (2000) 3384-3390
8. Banwell C. N., Fundamentals of molecular spectroscopy, 3rd edition, May 1983 University of Sussex
9. Basu S., Nayak C., Yadav A. K., Agrawal A., Poswal A. K., Bhattacharyya D., Jha S. N. and Sahoo N. K., J. Phys.: Conf. Ser. 493 (2014) 012032.
10. Behrends F., Eckert H., J. Phys. Chem. C,118 (2014) 10271-10283
11. Bernard C., Chaussedent S., Monteil A., Balu N., Obriot J., Duverger C., Ferrari M., Bouazaoui M., Kinowski C., Turrell S., J. Non- Cryst. Solids 284 (2001) 68
12. Besancon R. M., The encyclopedia of Physics, (second edition) Van Nostrand Reinhold (1974)
13. Beveridge P., Domènech I. and Pascual E., Warm Glass, Lark Books (2005) 66
14. Bionducci M., Bellisent R., Messa M. P., Piccaluga G., Pinna G., Bettinelli M., J. Non- Cryst. Solids 36 (1995) 192
15. Blech L.A. and Averbach B. L., Phys. Rev. 137 (1965) 1113
16. Bowron D. T., Saunders G. A., Newport R. J., Rainford B. D. and Senin H. B., Phys. Rev. B 53 (1996) 5268.
17. Boyd R. W., Non linear Optics, Academic press (1992).
18. Bragg W. L., Proceedings of the Cambridge Philosophical society, 17 (1913) 43-57
19. Brow R. K., J. Non-Cryst. Solids 194 (1996) 267
20. Brow R. K., J. Non-Cryst. Solids 263&264 (2000) 1-28.

21. Brow R. K., Kirkpatrick R. J. and Turner G. L., J. Amer. Cer. Soc 76 (1993) 919-928
22. Campbell J. H., Suratwala T. I., J. Non-cryst. Sol., 263 & 264 (2000) 318-341.
23. Carnall W. T., Fields P. R., Rajnak K., J. Chem. Phys. 49 (1968) 4412-4423
24. Carvalho E. A., Frietas A. M., Silva G. H,. Bell M. J. V. Kassab, L. R. P., Anjos V., Vibrational Spectroscopy 87 (2016) 147-148
25. Chahine A., Et-Tabirou M., Pascal J. L.,Mater.Lett.58 (2004) 2776-2778
26. Chakraborty I. N., Condrate Sr R .A., Phys. Chem. Glasses 26 (1985) 68
27. Chakraborty I. N., Day D. E., Lapp J.C., Shelby J. E., J. Am. Ceram. Soc.,68 (1985) 368
28. Chanshetti U. B., Shelke V. A., Jadhav S. M., Shankarwar S. G., Chondhekar T. K., Shankarwar A. G., Sudarshan V., Jogad M. S., Phys., Chem. and Tech. vol. 9, (1) (2011) 29-36
29. Chen Y., Nie Q., Xu T., Dai S., Wang X., Shen X., J. Non-Cryst. Solids 354 (2008) 3468-3472
30. Clark C. M., Dutrow B. L. (Geochemical Instrumentation)
31. Cole J. M., VanEck E. R. H., Mountjoy G., Anderson R.,Brennam T., B-Wye G., Newport R. J. and Saunders G. A., J. Physics; condens. matter 13 (2001) 4105-4122.
32. Cole J. M., VanEck E.R.H., Mountjoy G., Newport R.J., Brennam T., Saunders G.A., J. Phys: Condens. Matter II (1999) 9165-9178.
33. Colomban P., Milande V. and Lucas H., J. Raman Spect. 35 (2004) 68
34. Culea E., Pop L., Bosca M., J. Alloys Cmpounds 505 (2010) 754-757
35. Davis E.A., Mott N. F., Phil. Mag. 22(1970) 903-927
36. Debenedetti P. G., Stillinger F. H., Nature 410 (2001) 259-267
37. Desa J. A. E., Wong J., Sinclair R. N., AERE- R 10186 report, Harwell, United Kingdom (1981).
38. Desa J. A. E., Wright A. C., Sinclair R. N., J. Non-Cryst. Solids, 99 (1988) 276-288
39. Desa J. A. E., Wright A. C., Wong J., Sinclair R. N., J. Non-Cryst. Solids 51 (1982) 57
40. Dimitrov V., Dimitriev Y., Montenero A., J. Non-Cryst. Solids 180 (1994) 51-57
41. Dimitrov V., Sakka S., J. Appl. Phys.79(1996)1736-1740
42. Dixon M., Wright A. C., P. Hutchinson, U.K.A.E.A. Harwell report R 8619 (1976)
43. Durville F. M., Behrens E. G., Powell R. C., Phys. Rev. 34 (1986) 4213

44. Fisher H. E., Barnes A. C., Salmon P. S., Rep. Prog.Phys.69 (2006) 233
45. Frenkel A., Stern E. A., Voronel A., Rubshtein A., Ben-Ezra Y. and Fleurov V., Phys. Rev. B 54 (1996) 884- 892.
46. Galeener F. L., Leadbetter A. J., Stringfellow M.W., Phys. Rev. B 27 (1983) 1052
47. Gibbons P. C., Physics, Barron Educational Series (2008)
48. Greaves G. N., Glass, Science and Technology, Academic Press London (1990)
49. Greegor R. B., Lytle F. W., Kortright J., Fischerkolbrie A., J. Non. Cryst. Solids, 89 (1987) 311
50. Greenwood N. N., Earnshaw A., Chemistry of the elements (2nd edition) Butterworth-Heinemann (1997)
51. Hagg G., J. Chem. Phys. 3 (1935) 42- 49
52. Hannon A. C., Martino D. D., Santos L. F.,. Almeida R. M, J. Phys. Chem. B 111(13) (2007) 3342-3354
53. Hannon A. C., Sinclair R.N., Wright A.C., Physica A, 201 (1993) 375
54. Harani R., Hograth C. A., Ahmed M.M., J. Mater. Sci. Lett. 3 (1984) 843
55. Hee P., Christensen R., Ledemi Y., Wren J. E. C., Dussauze M., Cardinal T., Fargin E., Kroekar S., Messaddeq Y., J. Mater. Chem. C 2 (2014) 7906
56. Hellwarth R. W., Phys. Rev. 130 (1963) 1850
57. Henderson G. S. and Fleet M. E., J. of Non-Cryst. Solids 134 (1991) 259-269
58. Henderson G. S., Amos R. T., J. Non-Cryst. Solids 328 (2003) 1-19
59. Henderson G.S., Soltay L.G., Wang H. M., J. non-Cryst. Solids, 356 (2010) 2480-2485
60. Hill R., J. Mater. Sci. Lett. 15 (1996) 1122-1125
61. Hitachi high Technologies, America, manual.
62. Holand W., Rheinberger V. and Schweiger M., Phil. Trans. R. Soc. Lond. A 361 (2003) 575-589
63. Hong H Y P , Act. Crysta. B ,(24 (1968) 38, 30 (1974) 468-474)
64. Hoppe U., Brow R. K., Wyckoff N. P., Schops A., Hannon A. C., J. Non- Cryst. Solids 354 (2008) 3572-3579
65. Hoppe U., Heidepriem H. E., Neuefeind J., Bowron D. T., Z. Naturforsch 56a (2001) 237 – 243
66. Hoppe U., Walter G., Kranold R., Stachel D., Z. Naturforsch, 53a, (1998) 93-104.
67. Howrath O., Theory of spectroscopy, Halsted printing press (1973)

68. Hudgens J. J., Brow R. K., Tallant D. R., Martin S. W., J. Non-Cryst. Solids 223 (1998) 21-31
69. Ilieva D., Jivov B., Kovacheva D., J. Non-Cryst. Solids 293-295 (2001) 562-568
70. Ivanov A.O., Evstropiev K. S., Dokl. Akad. Nauk. SSSR 145 (1962) 797
71. Jones G. O., Glass, Methuen, London (1956) 119
72. Jouni A., Ferid M., Gacon J.C., Grosvalet L., Thozet A., TrabelsiAyadi M., Mat. Res. Bull., 38 (2003) 1613-1622
73. Judd B. R., Phys. Rev. 127 (1962) 750
74. Kader A.A., Higazy A.A., Elkholy M.M., J. Mater.Sci.: Mater. Electron. 2 (3) (1991) 157-163
75. Kamitsos E. I., Yiannopoulos Y. D., Karakassides M. A., Chryssikos G. D., Jain H., J. Phys. Chem. 100 (1996) 11755-11765
76. Karabulut M., Marasinghe G.K., Metwalli E.,.Witteenauer A.K, Brow R. K., Booth C. H., Shuk D. K., Phys. Rev. B, 65 (2002) 104206.
77. Karunakaran R .T ., Marimuthu K., Arumugam S., Babu S. S., Leon-Luis S. F. and Jayasankar C. K., Opt. Mater.32 (2010) 1035-1041
78. Kauzmann W., Chem. Rev. 43 (1948) 219
79. Kelly S.D., Hesterberg D. and Ravel B., Analysis of soils and minerals using X-ray absorption spectroscopy (2008) 387-464; Methods of Soil Analysis - Part 5.
80. Khan M.N., Harani R., Ahmed M.M., Hograth C. A., J. Mater. Sci. 20 (1985) 2207
81. Kim Y., Saienga J., Martin S. W., J. Non-Cryst. Solids 351 (2005) 3716-3724
82. Kittel C., Introduction to Solid State Physics, New York, John Wiley and Sons (1976)
83. Klonkowski A., J. Non-Cryst. Solids, 72(1985)117-137
84. Konigsberger D.C., and Prince R., X ray Absorption: Principles, Applications, Techniques of EXAFS, SEXAFS and XANES. Wiley, New York, 1988.
85. Koo J., Bae Byeong-Soo, Na Hoon-Kyun, J. Non-Cryst. Solids 212 (1997) 173-179
86. Koroleva O. N., Shtenberg M. V., Ivanova T. N., J. Non- Cryst. Solids 510 (2019) 143
87. Krogh-Moe J., ActaCryst. 9 (1956) 551
88. Kumar S. and Rao K. J., Solid State ionics 170 (2004)191
89. Kumar S., Murugavel S., Rao K. J., J. Phys. Chem. B 105 (2001) 5873
90. Kutub A., Osman A. M., Hogarth C. A., Mater. Sci. 21 (1986) 3571

91. Lai Y.M., Liang X. F., Yang S. Y., Wang J. X., Cao L. H., Dai B., 992 (2011) 84-88
92. Leadbetter A. J., Wright A. C., J. Non-Cryst. Sol., 7, (1972) 23-36
93. Li D., Bankroft G. M., Fleet M. E., Am. Miner. 81 (1986) 111
94. Liang X., Yin G., Yang S, Lai Y. and Wang J., Spectroscopy letters 44 (2011) 418-423.
95. Lide D. R., Hand book of chemistry and Physics (87ed), Boca Raton, Florida; CRC Press(1998) pp 4-40
96. Liebau F., Keefe M. O., Novrotsky A., Structure and Bonding in Crystals, Academic Press New York (1981) 197
97. Long D. A., The Raman effect, John Wiley and Sons Press (2002)
98. Lorch E. A., Thesis, Univ. of Birmingham (1967)
99. Lorch E. A., J. Phys. C : Sol. State Phys. C 2 (1969) 229-237
100. Lottici P., Manzini I., Antonioli G., Gnappi G., Montenero A., J. Non-Cryst. Solids 159 (1983) 278
101. Luo Z., Lu A., Hu X. and Liu W., J. Non-Cryst. Solids 368 (2013) 79-85
102. Macmillan P. W., Glass Ceramics, Academic Press London, (1964) 229
103. Magdas D. A., Cozar O., Chis V., Ardelean I., Vedeanu N., Vib. Spectrosc. 48 (2008) 251-25
104. Margaryan A.A., Pilavin M.A., Germanate glass: Structure ,Spectroscopy and Properties, Publisher Artech House Boston, London (1993)
105. Martin R. A., Salmon P. S., Fisher H. E., Cuello G. J., J. Non- Cryst. Solids 345 (2004) 208
106. Martin S. W., Eur. J. Solid State Chem. 28 (1991)163
107. Martino D.D., Santos L. F., Marques A.C., Almeida R.M., J.Non-Cryst. Solids 293-295(2001) 394-401
108. Matuszewski J., Kropiwnicka J., Znamierowska T., Jour. of Sol. State Chem., 75 (1988) 285-290
109. McGreeevy R. L., Pusztai L., Mol. Simu. Vol.1 (1988) 359-367.
110. Meyer K., J. Non- Cryst. Solids 209 (1997) 227-239
111. Mollazadeh S., Yekta B. E., Javadpour J., Yusefi A. and Jafarzadeh T. S., J.Non-cryst. Solids 361 (2013) 70-77
112. Morey G. W., J. Am. Ceram. Soc 17 (1934) 315-328
113. Morgan S. H., Magruder R. H., Silberman E., J. Am. Ceram. Soc. 70 (1987) 70

114. Mountjoy G., Cole J.M., Brennan T., Newport R.J., Saunders G.A. and Wallidge G.W., Journal of Non-Cryst. Solids 279 (2001) 20-27.
115. Mountjoy G., J. of Non-Cryst. Solids 353 (2007) 2029–2034.
116. Muraoka Y., Kihara K., Phys. and Chem. of Minerals 24 (1997) 243-253
117. Murthy M. K., Kirby E. M., Phys. Chem. Glasses 5 (1964) 144-146
118. Murthy M.K., Ip J., Nature 201(1964) 285
119. Nelson B. N. and Exarhos G. J., J.Chem. Phys. 71 (1979) 2739
120. Neutron Beam Research Facility manual, BARC,
121. Newville M., Ravel B., Haskel D., Rehr J.J., Stern E.A. and Yacoby Y., Physica B 154 (1995) 208.
122. Norman N., Actacryst. 10 (1957) 370
123. Ofelt G. S., J. Chem. Phys. 37 (1962) 511
124. Paalman N. H. and Pings C. J., J. Appl. Phys. 33 (1962) 2635
125. Pavic L., Milankovic A. M., Rao P. R., Santic A., Kumar V.R., Veeraiah N., J. Alloys Comp. 604 (2014) 352-362
126. Pemberton J. E., Latifzadeh L., Fletcher J.P., Rishbud S.H., Chem. Mater. 3 (1991) 195-200
127. Peng L., Stebbins J. F., J. Non-Cryst. Solids, 353(2007) 4732-4742
128. Placzek G., Phys. Rev. 86(3) (1952) 377-388
129. Polukhin V. N., Khim Fiz., Stekla 8 (1982) 338-342
130. Porai-Koshits E. A., The structure of Glass Consultants Bureau, New York (1953) 25
131. Poswal A. K., Agrawal A., Yadav A. K., Nayak C., Basu S., Kane S. R., Garg C. K., Bhattachryya D., Jha S. N. and. Sahoo N. K., AIP Conf. Proc. 1591 (2014) 649.
132. Pusztai L., McGreevy R. L., J. Neutron Research, 8 (1999) 17-35.
133. Quintas A., Majerus O., Lenoir M., Caurant D., Klementiev K. and Webb A. J.of Non-Cryst. Solids 354 (2008) 98–104.
134. Rachkovskaya G. E., Zakharevich G. B., J. of Appl. Spect. Vol. 74 Issue 1 (2007) 86-89
135. Rada S., Chelcea R., Culea E., J. Mater. Sci. 45 (2010) 6025- 6029.
136. Rai V.N., Rajasekhar B. N., Tiwari P., Kshirsagar R. J., Deb S. K., J.Non-Cryst. Solids 357 (2011) 3757-3764
137. Randall J. T., Rooksby H. P., Cooper B. S., Nature 125 (1930) 458
138. Rao K. J., Structural chemistry of glasses, Elsevier, North Holland (2002)

139. Rao N. R., Krishna P.S.R., Basu S., Dasannacharya B.A., Sangunni K.S., Gopal E.S.R., J. Non-Cryst. Sol., 240 (1998) 221-231.
140. Rawson H., Inorganic glass forming systems, University of Sheffield, Department of glass technology, Sheffield , England, (1967) Academic Press, London and New York
141. Rossignol S., Descorme C., Kappenstein C., Duprez D., J. Mater. Chem. 11 (2001) 2587
142. Rouse Jr G. B., Miller P. J. and Risen W.M., J. Non-Cryst. Solids 28 (1978) 193
143. Roy A.P., Dev S. K.,. Rekha M. A, and Sinha A. K., J. Pure and Appl. Phys. 30 (1992) 724
144. RRCAT, Indore, BL-09 facility, website.
145. Sahar M. R., Wahab A., Hussein M. A., Hussin R., J. Non-Cryst. Solids,353 (2007) 1134-1140
146. Sahnoun M., Daul C., Khenata R., Baltache H., Eur. Phys. J. B 45 (2005) 455.
147. Sales B.C., Mater. Res. Soc. Bull. 12 (1987)32
148. Sammons R. L., Thackray A. C., Ledo H. M., Marquis P. M., Jones I. P., Yong P. and Macaskie L. E., J. Physics: Conference series 93(2007) 012048 :1-7)
149. Saout L.G., Simon P., Fayon F., Blin A., Vaills Y., J.Raman Spec. 33(2002)740-746
150. Scholes S. R., Glass Ind., 26 (1945) 417-438
151. Scholze H., Glass nature , Structure and Properties, Springer -Verlag, Berlin (1991)
152. Schrader B., Infrared and Raman Spectroscopy: Methods and applications VCH (1995)
153. Shaim A., Et-Tabirou M., Pascal J.L., Mater. Chem. Phys. 80 (2003) 63-67
154. Sharaf El-Deen L. M., Al Salhi M. S., Elkholy M. M., J. of Alloys and Compounds 465 (2008) 333-339
155. Shelby J. E., Introduction to Glass Science and Technology, second edition , Royal Soc. Chem. (2005)
156. Shelby J. E., J. Am. Ceram. Soc., 68 (1985) 368
157. Shi Q., Kang J., Qu Y., Liu S., Khater G. A., Li S., Wang Y. and Yue Y., J. Non-Cryst. Solids 491 (2018) 71-78
158. Shikerkar A. G., Desa J. A. E, Krishna P. S. R., Chitra R., J. Non-Cryst. Solids., 270 (2000) 234-246.
159. Shimadzu FTIR-8900 manual

160. Shimadzu UV-2401 manual
161. Shriver D. F., Atkins P. W., Inorganic Chemistry, 4th edition, Oxford University Press, Oxford (2006) 189-190
162. Sigaev V. N., Gregora I., Pernice P., Champagnon B., Smelyanskaya E. N., Aronne A., Sarkisov P. D., J. Non-Cryst. Solids 279 (2001) 136-144
163. Simon S., Ardelean I., Filip S., Bratu I., Cosma I., Solid State Commun.11[2] (2000) 683-686
164. Smekal A., J. Soc. Glass Technol. 35 (1951) 411-420
165. Smith H., Cohen H., Phys. Chem. Glasses 4 (1963) 173
166. Soper A. K.and Egelstaff P. A., Nucl. Instrum. Meth. (1980) 415
167. Stocker T.and Cobean R. C., National Geographic (1981)
168. Stone C.E., Hannon A.C., Ishihara T., Kitamura N., Shirakawa Y., Sinclair R. N., Umesaki N., Wright A. C., J. Non-Cryst. Solids 293-295 (2001) 769-775
169. Sugiyama K., Waseda Y., Ashizuka M., Mater. Trans. JIM 32(1991)1030
170. Sun K. H., J. Am. Ceram. Soc. 30 (1947) 277
171. Takahashi K., Mochida N., Matsui H., Takeuchi S., Gohshi Y., J. Cer. Soc. 84 (1986) 482
172. Tammann G., Glaszustand Der, Leipzig: L. Vob (1933)
173. Teledyne Princeton instrument manual.
174. Thomas D. G., Staveley L. A. K., J. Chem. Soc. (1952) 4569
175. Turnbull D., Cohen M. H., J. Chem. Phys.29 (1958) 1049
176. Turnbull D., Seitz F., Solid State Physics,Academic Press, New York, 3 (1956) 223-306
177. Umesaki N., Brunier T. M., Wright A. C., Hannon A. C., Sinclair R. N., Physica B 213&214 (1995) 490-492
178. Van Hove L., Phys. Rev. 95 (1954)249
179. VanWazer J. R., Phosphorus and its compounds, vol 1&2, Interscience, New York 1958
180. Velli L. L., Varsamis P. E., Kamitsos E. I., Moncke D., Ehrt D., Phys. Chem. Glasses, 46 (2005) 178-181
181. Warren B. E., J. Appl. Phys., 8 (1937) 645
182. Weeks R. A., Nastrallah M., Arafa S. and Bishay A., J. Non-Cryst. Solids 38,39 (1980) 129-134

183. West A. R., Basic Solid State Chemistry, 2nd Edition, Wiley, London (2001) 203-210
184. Witkowska A., Sikora B., Trzebiatowski K. and Rybicki J., J. of Non-Cryst. Solids 352 (2006) 4356-4361.
185. Wong J. and Angell C. A., Glass: Structure by spectroscopy (1976)
186. Wright A. C., Advances in Structure Research by Diffraction Methods, 5 (1974) 1-84
187. Wright A. C., Conell G. A. N., Allen J. W., J. Non-Cryst. Solids 42 (1980) 69
188. Wright A. C., University of Reading publication (1981)
189. Xiao Z. Z. H., Lu A. X., Zuo C. G., 108 (2009) 325-331
190. Xu R., Xu L., Hu L., Zhang J., J. Phys. Chem. A, 115 (2011) 14163-14167
191. Yarnel J. L., Kartz M. J., Wenzel R. G., Koenig S. H., Phys. Rev. A7 (1973) 2130
192. Yiannopoulos Y. D., Varsamis C.P.E., Kamitsos E. I., J. Non-Cryst. Solids 293-295 (2001) 244-249
193. Yifen J., Dehua J., Xiangsheng C., Behya B., Xihuai H., J.Non-Cryst.Solids 80(1-3) (1986)147-151
194. Ylanen H., Comb. And Mat. Chem. (2000)
195. Zachariasen W. H., J. Am. Chem. Soc. 54 (1932) 3841-3851
196. Zanotto E. D., Cassar D. R., Scientific reports (2017)
197. Zarzycki J., Glass And The Vitreous State, Cambridge Univ. Press 220 (1991)
198. Zarzycki J., Glass structure, J. Non-Cryst. Solids 52 (1982) 31- 43
199. Zarzycki J., Verres et Refractaires 11 (1957) 3-8
200. Zhang L. Y., Li H., Hu L. L., J. Alloys and compounds 698 (2017) 103-113
201. Zhang L. Y., Xue T. F., Hee D. B., Guzik M., Boulon G., Opt. Express 23 (2015) 1505-1511
202. Zhang W. J., Wang W. C., Zang Q. Y., Jiang Z. H., J. Non-Cryst. Solids, 475 (2017) 108-115
203. Zhao J., Yang L., McLeod J. A. and Liu L.., Sci. Rep. 5 (2015) 17779
204. Zwanziger J., Shaw J .L., Zwanziger U. W., Aitken B. G., J. Phys. Chem. B 110 (2006) 20123

APPENDIX

Publications

1. B. P. Soares. J. A. E. Desa, C. Nayak, D. Bhattacharyya and S. N. Jha, "Effect of Neodymium and Lanthanum oxides on alumino phosphate vitreous and devitrified states" Mater. Res. Express 6 (2019) 075202

2. B. P. Soares, J. A. E. Desa, C. Nayak, D. Bhattacharyya and S. N. Jha, "Raman and EXAFS study of Neodymium and Praseodymium included alumino-germanate glass" Mater. Res. Express 6 (2019) 095205

3. Benedict P. Soares, J. A. Erwin Desa and P. S. R. Krishna, "Influence of Praseodymium on alumino- germanate glasses containing Nd and La inclusions" AIP Conference Proceedings 2115 (2019) 030247

Conference Presentations

1. Participated in the School of 'Neutrons as Probes of condensed Matter' at BARC, Mumbai from Feb. 4-8, 2014.

2. Attended Conference of Neutron Scattering at IISER, Pune from Feb.10-12, 2014.

3. Poster presentation made at the 2nd Asia Oceania Conference on Neutron Scattering (AOCNS 2015) under the auspices of the Asia-Oceania Neutron Scattering Association (AONSA) held in Sydney, Australia between July 19-23, 2015.

4. Poster presentation at National Conference On Thermophysical Properties (NCTP-2015) at MNIT Jaipur from December 14-16, 2015

5. Poster presentation at 6^{th} Conference on Neutron Scattering (CNS-2016) at BARC, Mumbai, Maharashtra, from Nov. 21- 23, 2016

6. Oral presentation at International Conference on Functional Oxides and Nanomaterials at Saurashtra University, Rajkot, Gujarat from November 11-13, 2016

7. Poster Presentation at 63^{rd} DAE-Solid State Physics Symposium at Guru Jambheshwar University of Science and Technology , Hisar, Haryana from December 18-22, 2018